

SYNTHESIS, CHARACTERIZATION AND THERMAL DECOMPOSITION OF
HYBRID AND REVERSE FLUOROSILICONES

by

Michael Perry Cyrus Conrad

A thesis submitted in conformity with the requirements
for the degree of Doctor of Philosophy
Graduate Department of Chemical Engineering and Applied Chemistry
University of Toronto

© Copyright by Michael Perry Cyrus Conrad, 2009



Library and Archives
Canada

Published Heritage
Branch

395 Wellington Street
Ottawa ON K1A 0N4
Canada

Bibliothèque et
Archives Canada

Direction du
Patrimoine de l'édition

395, rue Wellington
Ottawa ON K1A 0N4
Canada

Your file *Votre référence*
ISBN: 978-0-494-60937-8
Our file *Notre référence*
ISBN: 978-0-494-60937-8

NOTICE:

The author has granted a non-exclusive license allowing Library and Archives Canada to reproduce, publish, archive, preserve, conserve, communicate to the public by telecommunication or on the Internet, loan, distribute and sell theses worldwide, for commercial or non-commercial purposes, in microform, paper, electronic and/or any other formats.

The author retains copyright ownership and moral rights in this thesis. Neither the thesis nor substantial extracts from it may be printed or otherwise reproduced without the author's permission.

AVIS:

L'auteur a accordé une licence non exclusive permettant à la Bibliothèque et Archives Canada de reproduire, publier, archiver, sauvegarder, conserver, transmettre au public par télécommunication ou par l'Internet, prêter, distribuer et vendre des thèses partout dans le monde, à des fins commerciales ou autres, sur support microforme, papier, électronique et/ou autres formats.

L'auteur conserve la propriété du droit d'auteur et des droits moraux qui protègent cette thèse. Ni la thèse ni des extraits substantiels de celle-ci ne doivent être imprimés ou autrement reproduits sans son autorisation.

In compliance with the Canadian Privacy Act some supporting forms may have been removed from this thesis.

While these forms may be included in the document page count, their removal does not represent any loss of content from the thesis.

Conformément à la loi canadienne sur la protection de la vie privée, quelques formulaires secondaires ont été enlevés de cette thèse.

Bien que ces formulaires aient inclus dans la pagination, il n'y aura aucun contenu manquant.


Canada

Synthesis, Characterization and Thermal Decomposition of
Hybrid and Reverse Fluorosilicones

Doctor of Philosophy, 2009

Michael Perry Cyrus Conrad

Department of Chemical Engineering and Applied Chemistry

University of Toronto

Abstract

Traditional fluorosilicones contain a siloxane backbone and pendant fluorinated group leading to low temperature ductility and excellent thermal stability. However, acidic or basic catalysts can reduce the thermal stability from a potential 350 °C to 150 °C. The predominant decomposition mechanism is through chain scission and it is hypothesized that preventing this will result in polymers with higher thermal stability. Three approaches were taken to prevent chain scission.

First, a series of hybrid fluorosilicones based on (trifluorovinyl)benzene were synthesized through condensation polymerization with initial decomposition temperatures of approximately 240 °C. These were compared to similar aromatic polyethers and removal of the ether oxygen lowered the initial decomposition temperature by approximately 190 °C demonstrating the importance of this oxygen to the stability of polyethers.

Second, reverse fluorosilicone (fluorinated backbone and pendant siloxane) terpolymers of chlorotrifluoroethylene (CTFE), vinyl acetate (VAc) and methacryloxypropyl-terminated polydimethylsiloxane (PDMSMA) were synthesized in supercritical CO₂ (scCO₂) or by emulsion polymerization. Chain scission was prevented as initial decomposition occurred between 231 and 278 °C. In both the

emulsion and scCO₂ cases, VAc was essential in facilitating cross-propagation between CTFE and PDMSMA and the branching was similar suggesting polymerization media does not affect polymer structure. Emulsion-based polymers had higher molar masses and thermal stability whereas comparable scCO₂ polymers had higher yields and incorporated more PDMSMA.

Third, a series of homo-, co-, and terpolymers of CTFE, VAc and methacryloxypropyl-terminated silsesquioxane (POSSMA) were synthesized representing the first synthesis of POSSMA containing polymers in scCO₂ and demonstrating reverse fluorosilicones can be synthesized without VAc. Chain scission was prevented as initial decomposition occurred from 244 to 296 °C with thermal stability increasing with CTFE content to a limit. Decomposition of the polymers was examined and mechanism elucidated. In air, the copolymers give 40 to 47 wt% char since the silsesquioxane oxidizes to SiO₂ while in N₂, no residue is seen. In contrast, the terpolymers give a carbonaceous residue of approximately 20 wt% in N₂. The flammability and surface properties of the polymers were examined with the terpolymers having flammability similar to p(CTFE) and surface properties comparable to p(POSSMA) giving a low-flammability, hydrophobic polymer.

Acknowledgements

I would like to thank the following people:

Patrizia, without whose unwavering support this thesis would have been impossible,

Adamo, for being a constant reminder of the need to finish,

My family for all their encouragement over the many years,

Karyn Ho, Doug Baumann, Catherine Kang, and Ryan Wylie for being a sounding board to many of my ideas both Ph.D. related and otherwise and being my on campus support team during the final year of my thesis,

Drs. Bilal Baradie, Jordan Wosnick and Naum Naveh for their assistance and expertise in the various aspects of this thesis,

Drs. Peter Brodersen and David McNally at the University of Toronto for their help in obtaining the XPS spectra and solid state ^{13}C NMR, respectively,

Dr. SungCheal Moon and Professor Richard Farris at the University of Massachusetts, Amherst for help in obtaining the PCFC data,

Profs. Mark Kortschot and Mitchell Winnik for their guidance through an eventful thesis, and

Prof. Molly Shoichet for giving me the space to find my own path to the completion of this thesis.

Table of Contents

Abstract.....	ii
Acknowledgements	iv
List of Tables.....	ix
List of Figures	xi
List of Schemes	xvii
1 Introduction	1
1.1 Thermal Stability	1
1.1.1 Effect of Polymer Composition	4
1.1.2 Effect of Polymer Structure	5
1.1.3 Effect on Other Polymer Properties.....	7
1.2 Traditional Fluorosilicones	8
1.2.1 Structure.....	8
1.2.2 Synthesis.....	10
1.2.3 Properties.....	13
1.2.3.1 <i>Thermal Stability</i>	13
1.2.3.2 <i>Surface Energy</i>	16
1.2.4 Potential Improvements.....	17
1.3 Hybrid Fluorosilicones	18
1.3.1 Structure.....	19
1.3.2 Synthesis.....	21
1.3.3 Properties.....	22
1.3.4 Potential Improvements.....	26
1.4 Reverse Fluorosilicones	27
1.4.1 Synthesis.....	28
1.4.2 Properties.....	29
1.4.2.1 <i>Thermal</i>	29
1.4.2.2 <i>Surface</i>	31

1.4.3	Potential Improvements.....	32
1.5	Hypotheses	40
1.6	Objectives	42
1.7	References	44
2	Synthesis and Thermal Stability of a Perfluorocyclobutane based Aromatic Hybrid Fluorosilicone.....	49
2.1	Abstract.....	49
2.2	Introduction.....	50
2.3	Experimental.....	53
2.3.1	Modeling.....	53
2.3.2	Materials.....	53
2.3.3	Characterization	54
2.3.4	Synthesis of Monomers.....	55
2.3.5	Synthesis of Polymers.....	57
2.4	Results and Discussion	60
2.4.1	Modeling.....	60
2.4.2	Polymerization.....	62
2.4.3	Thermal Properties.....	69
2.5	Conclusion	78
2.6	References	79
3	Synthesis of Fluorosilicone Terpolymers through Emulsion or Supercritical Carbon Dioxide.....	82
3.1	Abstract.....	82
3.2	Introduction.....	82
3.3	Experimental	87
3.3.1	Materials.....	87
3.3.2	Characterization	88
3.3.3	Synthesis of Poly(CTFE- <i>ter</i> -VAc- <i>ter</i> -PDMSMA) by Emulsion	89

3.3.4	Synthesis of Poly(CTFE- <i>ter</i> -VAc- <i>ter</i> -PDMSMA) by Supercritical CO ₂	90
3.3.5	Polymer Purification	90
3.3.6	Calculation of Reactivity Ratios	95
3.4	Results and Discussion	97
3.4.1	Polymer Synthesis	97
3.4.2	Terpolymer Composition	100
3.4.3	Reactivity Ratios	103
3.4.4	Terpolymer Yield	107
3.4.5	Terpolymer Molar Mass	109
3.4.6	Terpolymer Branching	111
3.4.7	Terpolymer Viscosity	118
3.4.8	Thermal Analysis	121
3.5	Conclusions	125
3.6	References	126
4	Synthesis and Decomposition of Fluorocarbon-Silsesquioxane	
	Polymers	130
4.1	Abstract	130
4.2	Introduction	131
4.3	Experimental	134
4.3.1	Materials	134
4.3.2	Polymerization	134
4.3.3	Bulk Analysis	135
4.3.4	Surface Analysis	141
4.3.5	Thermal Analysis	141
4.3.6	Decomposition Product Analysis	142
4.3.7	Flammability Analysis	143
4.4	Results and Discussion	144
4.4.1	Polymer Structure	144
4.4.2	Surface Properties	148

4.4.3	Thermal Properties.....	152
4.4.4	Polymer Decomposition	155
4.4.5	Flammability	166
4.5	Conclusions	169
4.6	References	170
5	Conclusions and Recommendations	174
5.1	Thermal Stability.....	174
5.1.1	Hybrid Fluorosilicones	176
5.1.2	Reverse Fluorosilicones	177
5.1.3	Comparison of Hybrid and Reverse Fluorosilicones	180
5.2	Hypotheses Tested.....	182
5.3	Recommendations	186
5.4	References	188
	Appendix A: Nuclear Magnetic Resonance (NMR) Spectra.....	190
	Appendix B: Fourier-Transform Infrared (FT-IR) Spectra	214
	Appendix C: Gas Chromatography (GC) and Mass Spectroscopy (MS) Spectra	215
	Appendix D: Gel Permeation Chromatography (GPC) Curves	224
	Appendix E: Differential Scanning Calorimetry (DSC) Traces	236
	Appendix F: Thermal Gravimetric Analysis (TGA) Traces	243
	Appendix G: X-ray Photoelectron Spectroscopy (XPS) Spectra	252

List of Tables

Table 1.1: Defining temperatures for commodity polymers.	1
Table 1.2: Mean bond enthalpies	4
Table 1.3: Effect of thermally stable moiety location on polymer thermal decomposition temperature	6
Table 1.4: Hybrid fluorosilicones	20
Table 1.5: Effect of fluoroalkyl link on glass transition and decomposition temperature	23
Table 1.6: Thermal properties of hybrid fluoroether-siloxane polymers compared with fluoroalkyl-siloxane polymers	25
Table 1.7: Comparison of surface tension for poly(trifluoropropylmethylsiloxane), poly(tetrafluoroethylene), and poly(dimethylsiloxane)	31
Table 1.8: Reactivity ratios for fluoromonomer (1) and vinyl acetate (2)	40
Table 2.1: Effect of oxygen on ΔH_f	61
Table 2.2: Summary of molar mass and thermal properties for hybrid fluorosilicones ..	62
Table 3.1: Composition, molar mass and yield of CTFE-Vac-PDMSMA terpolymers ...	92
Table 3.2: Assignments of the ^1H and ^{19}F NMR for a representative CTFE-VAc-PDMSMA terpolymer (emA) in CDCl_3	94
Table 3.3: Literature mole fractions used to determine reactivity ratios.....	96
Table 3.4: Mark-Houwink Parameters for CTFE-VAc-PDMSMA terpolymers	114
Table 3.5: Decomposition ($T_{1\%}$, $T_{50\%}$) and glass transition temperatures (T_g).....	123
Table 3.6: Effect of pendant group on methacrylate glass transition temperature.....	124
Table 4.1: Molar mass and yield of polymers.	145
Table 4.2: Compositional drift of CS polymers	148
Table 4.3: Calculation of mol% POSSMA at polymer film surface for CS(33-67).....	149
Table 4.4: Surface properties of CS and CVS polymers	150
Table 4.5: Triad composition of CVS polymers.	153
Table 4.6: Calculation of decomposition products for CS(33-67).	159
Table 4.7: Calculation of decomposition products of CVS(46-52-02).....	160
Table 4.8: Percentage of POSSMA lost due to sublimation.	162

Table 4.9: Flammability of CS and CVS polymers as determined by PCFC analysis	166
Table 4.10: Comparison of experimental (DOT/FAA/AR-01/31) [43] and calculated h^0_c values for various polymers.....	168
Table 5.1: Comparison of the thermo-oxidative stability of reverse fluorosilicones with the same nominal feed composition and molar mass	178

List of Figures

Figure 1.1: Typical effect of temperature on tensile modulus for an amorphous polymer .	2
Figure 1.2: Poly(3,3,3-trifluoropropylmethylsiloxane) – PTFPMS	9
Figure 1.3: Thermal intrachain rearrangement of siloxanes	14
Figure 1.4: Schematic of thermodynamic adhesion process	38
Figure 2.1: Perfluorocyclobutane aromatic ether thermoset	52
Figure 2.2: Perfluorocyclobutane-based aromatic units	53
Figure 2.3: Mass spectra of P2c at 344 °C	66
Figure 2.4: Gel permeation chromatography trace of P2b	68
Figure 2.5: Comparison of experimental (◆) to calculated glass transition temperatures according to Equation (2.6)	73
Figure 2.6: Thermal gravimetric analysis of hybrid fluorosilicones, P2a to P2c	74
Figure 2.7: Mass spectra of P2c at 239 °C	75
Figure 2.8: π -Electron density of carbon para to functional group on substituted benzenes	77
Figure 3.1: Repeat unit of the generic P(CTFE-VAc-PDMSMA) terpolymer	87
Figure 3.2: NMR spectra of CTFE-VAc-PDMSMA terpolymer emA	93
Figure 3.3: Effect of CTFE to VAc ratio of polymer composition	101
Figure 3.4: NMR spectra of VAc methine region	103
Figure 3.5: Equivalent CH ₂ groups in (a) p(VAc) and (b) CTFE-VAc-PDMSMA terpolymer	113
Figure 3.6: Mark-Houwink plot for CTFE-VAc-PDMSMA terpolymers	116
Figure 3.7: Effect of F_{PDMSMA} on intrinsic viscosity	119
Figure 3.8: Effect of $\log(F_{PDMSMA})$ on intrinsic viscosity	120
Figure 3.9: Typical TGA traces for scCO ₂ and emulsion terpolymers	122
Figure 3.10: Typical DCS traces for scCO ₂ and emulsion terpolymers	123
Figure 4.1: Effect of feed composition (f_i) on polymer composition (F_i)	145
Figure 4.2: Effect of F_{CTFE} on initial decomposition temperature	153
Figure 4.3: Decomposition of polymers by DSC	155
Figure 4.4: TGA traces of a select group of polymers under (a) N ₂ , and (b) air.	156

Figure 4.5: Decomposition mechanisms for: (a) V(100) and (b) CVS polymers.	165
Figure 5.1: Initial thermo-oxidative decomposition temperature for all synthesized polymers.....	175
Figure 5.2: Effect of fluorocarbon on percentage of AAA triads	179
Figure A.1: ^1H NMR of I2.....	190
Figure A.2: ^{19}F NMR of I2.....	190
Figure A.3: ^1H NMR of M2.....	191
Figure A.4: ^{19}F NMR of M2.....	191
Figure A.5: ^1H NMR of P2a	192
Figure A.6: ^{19}F NMR of P2a	192
Figure A.7: ^{29}Si NMR of P2a	193
Figure A.8: ^1H NMR of P2b	193
Figure A.9: ^{19}F NMR of P2b	194
Figure A.10: ^{29}Si NMR of P2b	194
Figure A.11: ^1H NMR of P2c	195
Figure A.12: ^{19}F NMR of P2c.....	195
Figure A.13: ^{29}Si NMR of P2c.....	196
Figure A.14: ^1H NMR of emA	197
Figure A.15: ^{19}F NMR of emA	197
Figure A.16: ^1H NMR of emB	198
Figure A.17: ^{19}F NMR of emB	198
Figure A.18: ^1H NMR of emC	199
Figure A.19: ^{19}F NMR of emC	199
Figure A.20: ^1H NMR of emD	200
Figure A.21: ^{19}F NMR of emD	200
Figure A.22: ^1H NMR of scA.....	201
Figure A.23: ^{19}F NMR of scA.....	201
Figure A.24: ^1H NMR of scB.....	202
Figure A.25: ^{19}F NMR of scB.....	202
Figure A.26: ^1H NMR of scC	203
Figure A.27: ^{19}F NMR of scC.....	203

Figure A.28: ^1H NMR of scD	204
Figure A.29: ^{19}F NMR of scD.....	204
Figure A.30: ^1H NMR of S(100)	205
Figure A.31: ^{19}F NMR of CS(02-98)	205
Figure A.32: ^1H NMR of CS(10-90).....	206
Figure A.33: ^{19}F NMR of CS(10-90)	206
Figure A.34: ^1H NMR of CS(20-80).....	207
Figure A.35: ^{19}F NMR of CS(20-80)	207
Figure A.36: ^{19}F NMR of CS(33-67)	208
Figure A.37: ^1H NMR of CS(81-19).....	208
Figure A.38: ^{19}F NMR of CS(81-19)	209
Figure A.39: ^1H NMR of CVS(40-59-01).....	209
Figure A.40: ^{19}F NMR of CVS(40-59-01).....	210
Figure A.41: ^1H NMR of CVS(46-52-02).....	210
Figure A.42: ^{19}F NMR of CVS(46-52-02).....	211
Figure A.43: ^{19}F NMR of CS(50-50), Reaction Time = 0 h	211
Figure A.44: ^{19}F NMR of CS(50-50), Reaction Time = 3 h	212
Figure A.45: ^{19}F NMR of CS(50-50), Reaction Time = 8 h	212
Figure A.46: ^{19}F NMR of CS(50-50), Reaction Time = 24 h	213
Figure B.1: FT-IR of I2.....	214
Figure B.2: FT-IR of M2.....	214
Figure C.1: MS of M2	215
Figure C.2: MS of P2b at T = 238 °C.....	215
Figure C.3: MS of P2b at T = 308 °C.....	216
Figure C.4: MS of P2b at T = 450 °C.....	216
Figure C.5: MS of P2b at T = 450 °C.....	217
Figure C.6: MS of P2c at T = 194 °C.....	217
Figure C.7: MS of P2c at T = 239 °C.....	218
Figure C.8: MS of P2c at T = 334 °C.....	218
Figure C.9: MS of P2c at T = 450 °C.....	219
Figure C.10: GC of CS(02-98).....	219

Figure C.11: MS of CS(02-98) at T = 310 °C	220
Figure C.12: GC of CS(10-90).....	220
Figure C.13: MS of CS(10-90) at T = 337 °C	221
Figure C.14: GC of CS(20-80).....	221
Figure C.15: MS of CS(20-80) at T = 349 °C	222
Figure C.16: GC of CS(33-67).....	222
Figure C.17: MS of CS(33-67) at T = 367 °C	223
Figure D.1: P2a	224
Figure D.2: P2b	224
Figure D.3: P2c	225
Figure D.4: emA	225
Figure D.5: emB	226
Figure D.6: emC	226
Figure D.7: emD	227
Figure D.8: scA	227
Figure D.9: scB	228
Figure D.10: scC	228
Figure D.11: scD	229
Figure D.12: S(100).....	229
Figure D.13: CS(02-98).....	230
Figure D.14: CS(10-90).....	230
Figure D.15: CS(20-80).....	231
Figure D.16: CS(33-67).....	231
Figure D.17: CS(81-19).....	232
Figure D.18: CVS(40-59-01)	232
Figure D.19: CVS(46-52-02)	233
Figure D.20: CS(50-50), Reaction Time = 0 h.....	233
Figure D.21: CS(50-50), Reaction Time = 3 h.....	234
Figure D.22: CS(50-50), Reaction Time = 8 h.....	234
Figure D.23: CS(50-50), Reaction Time = 24 h.....	235
Figure E.1: P2a	236

Figure E.2: P2b	236
Figure E.3: P2c	237
Figure E.4: emD	237
Figure E.5: scD	238
Figure E.6: S(100).....	238
Figure E.7: CS(02-98).....	239
Figure E.8: CS(10-90).....	239
Figure E.9: CS(20-80).....	240
Figure E.10: CS(33-67).....	240
Figure E.11: CS(81-19).....	241
Figure E.12: CVS(40-59-01).....	241
Figure E.13: CVS(46-52-02).....	242
Figure F.1: P2a in air.....	243
Figure F.2: P2b in air.....	243
Figure F.3: P2c in air.....	244
Figure F.4: emD in air.....	244
Figure F.5: scD in air.....	245
Figure F.6: S(100) in N ₂	245
Figure F.7: CS(02-98) in N ₂	246
Figure F.8: CS(10-90) in N ₂	246
Figure F.9: CS(20-80) in N ₂	247
Figure F.10: CS(33-67) in N ₂	247
Figure F.11: C(100) in N ₂	248
Figure F.12: CVS(40-59-01) in N ₂	248
Figure F.13: CVS(46-52-02) in N ₂	249
Figure F.14: V(100) in N ₂	249
Figure F.15: S(100) in air	250
Figure F.16: CS(33-67) in air.....	250
Figure F.17: C(100) in air	251
Figure F.18: CVS(46-52-02) in air	251
Figure G.1: CS(02-98) at 90° take-off angle.....	252

Figure G.2: CS(10-90) at 90° take-off angle.....	252
Figure G.3: CS(20-80) at 90° take-off angle.....	253
Figure G.4: CS(33-67) at 90° take-off angle.....	253
Figure G.5: CS(33-67) char prepared at 300 °C, 90° take-off angle.....	254
Figure G.6: CS(33-67) char prepared at 380 °C, 90° take-off angle.....	254
Figure G.7: CS(33-67) char prepared at 460 °C, 90° take-off angle.....	255
Figure G.8: CVS(40-59-01) at 90° take-off angle	255
Figure G.9: CVS(46-52-02) at 90° take-off angle	256
Figure G.10: CVS(46-52-02) char prepared at 300 °C, 90° take-off angle	256
Figure G.11: CVS(46-52-02) char prepared at 375 °C, 90° take-off angle	257
Figure G.12: CVS(46-52-02) char prepared at 450 °C, 90° take-off angle	257

List of Schemes

Scheme 1.1: Thermal rearrangement of α - and β -trifluorosilanes	9
Scheme 1.2: Hydrosilylation.....	11
Scheme 1.3: Polymerization of PTFPMS, (a) Anionic ring-opening polymerization and (b) Equilibrium polymerization.	12
Scheme 1.4: Condensation of dihalosilanes to high molecular weight linear siloxanes.	13
Scheme 2.1: Synthesis of monomers.....	57
Scheme 2.2: Synthesis of polymers.....	59
Scheme 2.3: Two-step hybrid fluorosilicone condensation.....	64

1 Introduction

1.1 Thermal Stability

Thermal stability can be defined as the ability of a substance to resist permanent physical or chemical change at elevated temperatures. To determine whether a substance has high thermal stability it is necessary to understand this definition. The thermal component conveys that the material is heated in an inert atmosphere. This differs from thermo-oxidative stability where the material is heated in air. The elevated temperature considered to be the threshold for thermal stability will depend on the material class; ceramics will have a higher thermal stability than metals which will have a higher thermal stability than polymers. Elevated temperature with respect to polymers is taken to mean a temperature greater than those typically reached by unmodified commodity polymers, including polyethylene (PE), polypropylene (PP), polystyrene (PS), poly(methyl methacrylate) (PMMA), and poly(vinyl chloride) (PVC). These polymers all have operating temperatures below 100 °C, exhibit melting temperatures between 110° and 240 °C, and decomposition temperatures between 200° and 387 °C as shown in Table 1.1 below.

Table 1.1: Defining temperatures for commodity polymers

Material	Maximum Operating Temperature¹ (°C)	Crystalline Melting Temperature² (°C)	Decomposition Temperature³ (°C)	Reference
PE	55	110-140	387	[1]
PP	100	165-176	350	[2]
PS	50	240	280	[3]
PMMA	50	160	200	[4]
PVC	50	212	220	[5]

^{1,2} [6]

³ Inert atmosphere

The definition of thermal stability also describes a permanent physical or chemical change in the material. To describe these changes, the words degradation and decomposition have been used interchangeably. However, to avoid confusion they have been defined as follows for the purposes of this thesis. Thermal *degradation* is a change in the *physical* properties, typically in a negative manner, of a polymer as temperature increases. This is illustrated in Figure 1.1 by a plot of tensile modulus versus temperature for a typical amorphous polymer where the modulus decreases with increased temperature. If it is assumed that the end-use application requires a baseline tensile modulus (e.g., 10^8 Pa) and an increase in temperature reduces the tensile modulus below that baseline (e.g., from 10^8 to 10^6 Pa) then the tensile modulus was affected in a negative manner for this particular application. Thermal *decomposition*, in contrast, is a permanent *chemical* change in the material resulting in both gaseous and solid decomposition products.

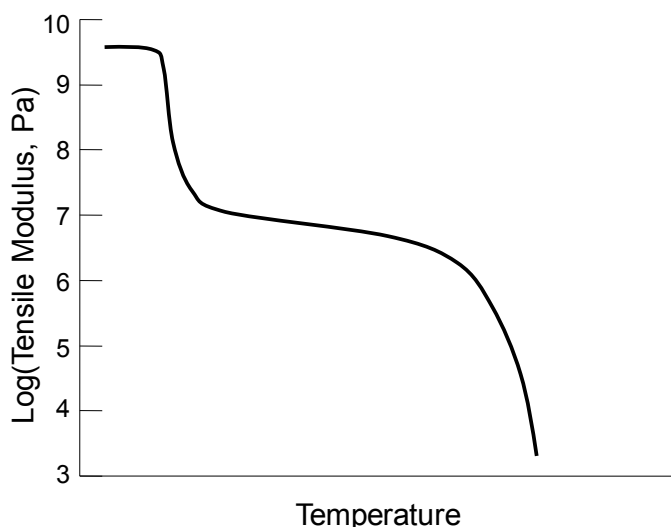


Figure 1.1: Typical effect of temperature on tensile modulus for an amorphous polymer (adapted from Sperling [7])

Thermal degradation does not necessarily arise from thermal decomposition but potentially the disruption of meso-scale order within the polymer as seen at the glass transition (T_g) or crystalline melting (T_m) temperature of the polymer. This suggests that thermal degradation of a material as defined above may not be permanent, yet to achieve the identical starting properties the identical thermal history must be experienced by the polymer. In contrast, if thermal decomposition occurs, thermal degradation typically follows. The properties examined for the polymers synthesized herein are chemical in nature (e.g., flammability) and can depend directly on the decomposition products of the polymer. Therefore, the focus of this thesis was thermal decomposition, a *chemical* change, rather than thermal degradation, a *physical* change.

Thermal decomposition is rate dependant and subsequently affected by the heating rate of the instrument used to determine the onset temperature, T_d . As an example, the T_d of powdered PVC increases by approximately 45 K when the heating rate is increased from 2 K/min to 20 K/min [8]. Therefore, where possible the heating rate associated with the onset temperature has been given. As well, temperatures other than the onset temperature are reported, typically some percentage of mass loss as recorded by the instrument when the sample is heated. These are denoted $T_{x\%}$ where x is the percentage of mass loss. For example, $T_{5\%}$ is the temperature at which 5% of the polymer mass has been lost due to thermal decomposition.

1.1.1 Effect of Polymer Composition

The onset of thermal decomposition is determined by the breaking of the chemical bonds which form the polymer structure. Once a sufficient number of bonds have broken (i.e., at least 2), gaseous products may be released and recorded as decomposition. Therefore, preventing bond scission will lead to high thermal stability. By incorporating functionalities into the polymer that are thermodynamically stable, the polymer will likely decompose at high temperatures. As can be seen from Table 1.2, which shows typical bond strengths (a measure of thermodynamic stability), incorporating the following functionalities into a polymer will likely give high thermal stability: Aromatic C-C, C-F, Si-O. This hypothesis is borne out by the fact that polymers containing aromatic structures, perfluorinated polymers, and siloxanes are known to have high thermal stability; noticeable decomposition of polyphenylene-based polymers and poly(tetrafluoroethylene), PTFE, requires temperatures above 400 °C [9, 10] with polydimethylsiloxanes degrading above 350 °C in the absence of acid or base catalysts [11].

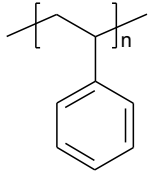

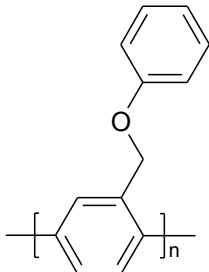
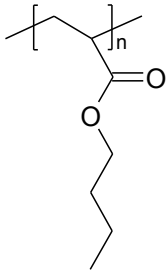
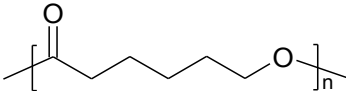
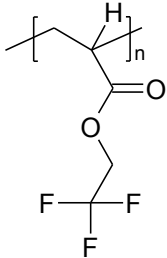
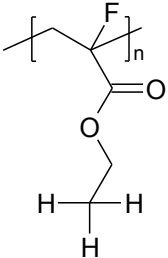
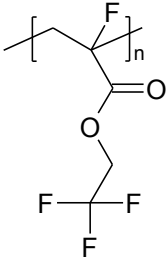
Table 1.2: Mean bond enthalpies [12]

Bond	Mean bond enthalpy (kJ/mol)
C-C (aromatic)	518
C-F	484
Si-O	466
C-H	436
C-O (single)	360
C-C (single)	348
C-Cl	338
C-Br	276

1.1.2 Effect of Polymer Structure

Selecting an appropriate location for these thermodynamically stable moieties can also enhance thermal stability; an inappropriate choice may lead to a reduction in stability. The two locations for a functional group within a polymer are the backbone or pendant locations. In many instances, the initial decomposition of a polymer is driven by loss of a pendant group as elimination and rearrangement reactions such as the elimination of acetic acid in poly(vinyl acetate) [13] or the thermal rearrangement of fluoromethylsilanes [14] can occur. Therefore, the chemistry used to attach the pendant group to the polymer backbone should be selected to avoid such reactions. Furthermore, the attachment should be through a thermally stable functionality although this may not be possible due to synthetic constraints. Due to the potential for undesired reactions when locating the thermally stable moiety in the pendant group, the preferred location is the backbone unless another specific property, such as low surface energy, drives a pendant location. Incorporating the thermally stable moiety in the backbone can lead to significantly enhanced thermal stability; however, it should be noted that this is not necessarily the case for all polymers as can be seen in the series of acrylic polymers in Table 1.3.

Table 1.3: Effect of thermally stable moiety location on polymer thermal decomposition temperature

Pendant	Backbone	Both
		
Polystyrene 280 °C Nitrogen, 40 °C/min [3]	Poly(<i>p</i> -phenylene) 700 °C Nitrogen, 10°C/min [15]	Poly(benzoyl-1,4-phenylene) 500 °C Nitrogen, 10 °C/min [10]
		
Poly(<i>n</i> -butyl acrylate) 300 °C Nitrogen, 10 °C/min [16]	Polycaprolactone 386 °C Nitrogen, 20 °C/min [17]	
		
Poly(fluoroethylacrylate) 334 °C Air, T _{5%} [18]	Poly(ethyl fluoracrylate) 323 °C Air, T _{5%} [18]	Poly(fluoroethyl fluoracrylate) 362 °C Air, T _{5%} [18]

1.1.3 Effect on Other Polymer Properties

Incorporating thermally stable groups is not without drawbacks. In many cases, rotation around the bonds within the thermally stable group is reduced. This inhibits the mobility of the polymer chains and increases the glass transition temperature leading to polymers that are brittle at room temperature. This effect may be mitigated in applications where the operating temperature exceeds the glass transition temperature. However, for those applications that require a broad operating temperature range, the brittle nature of some thermally stable polymers can render them unusable. Processing also becomes difficult as the viscosity likely also rises due to decreased chain mobility and the temperatures required for significant flow can represent an inhibitory engineering cost. Much research has gone into the modification of high thermal stability polymers to improve flow and processing characteristics. For example, to improve the processing characteristics of homopolymeric PTFE a copolymer of trifluorovinyl ether with tetrafluoroethylene was synthesized [19]. Other authors have added phenylether side groups [15] to poly(1,4-phenylene) to obtain a soluble derivative, poly(benzoyl-1,4-phenylene). A similar process will likely occur for other thermally stable polymers as the optimum between thermal stability and processability is sought.

Of the many thermally stable polymers available, fluorosilicones retain excellent low temperature capabilities (i.e., they maintain ductility at low temperatures) while providing for enhanced thermal stability [20]. For example, typical commercial fluorosilicone elastomers¹ have operating temperatures from -68 to 232 °C. Thus, this class of high thermal stability polymers does not display the

¹ An elastomer is a cross-linked, amorphous polymer above its glass transition temperature.

brittle behaviour exhibited by thermally stable polymers with glass transition temperatures above room temperature as discussed above.

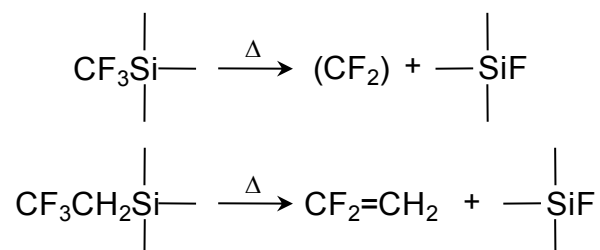
In comparison with other thermally stable polymers, fluorosilicones exhibit hydro- and oleophobicity, a specific property which may be desirable for a given application such as electrophotographic printing. This combination of low temperature capabilities, high thermal stability and hydro- and oleophobicity has led to the examination, synthesis and characterization of fluorosilicones presented in this thesis. The predominant focus has been the effect structure has on these properties.

1.2 Traditional Fluorosilicones

1.2.1 Structure

Traditional fluorosilicones consist of a backbone that contains alternating Si and O atoms joined by single bonds; this configuration is termed a siloxane or silicone. Silicon is a tetravalent atom, leaving two locations for subsequent attachment. Fluorosilicones, by definition, contain the silicone group as well as a fluorinated component. Based on the above definition the simplest fluorosilicone consists of a siloxane backbone with a fluorine atom attached directly to the silicon. However, the reactivity of this combination makes these compounds useful only as intermediates [20]. Moving the fluorine farther from the silicon by attaching a fluorinated methyl group results in a similar reaction as the Si-C bond can still be hydrolytically cleaved; the electron withdrawing nature of the CF_3 group enhances the electropositive nature of the silicon. Additionally, the formation of SiF is possible through thermal rearrangement, Scheme 1.1. Shifting the CF_3 group to the beta

position results in similar hydrolytic cleavage and thermal rearrangement with an olefin eliminated, Scheme 1.1 [14].



Scheme 1.1: Thermal rearrangement of α - and β -trifluorosilanes [14]

To prevent rearrangement, a hydrocarbon spacer with a minimum length of two carbons must be placed between the fluorinated group and the siloxane backbone if a polymer with high thermal stability is desired; this results in the use of a 3,3,3-trifluoropropyl (TFP) group ($-\text{CH}_2\text{CH}_2\text{CF}_3$). The first fluorosilicone, Poly(3,3,3-trifluoropropylmethylsiloxane) (PTFPMS), Figure 1.2, synthesized by Pierce et al. [21] contains this requisite structure.

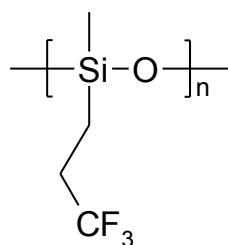
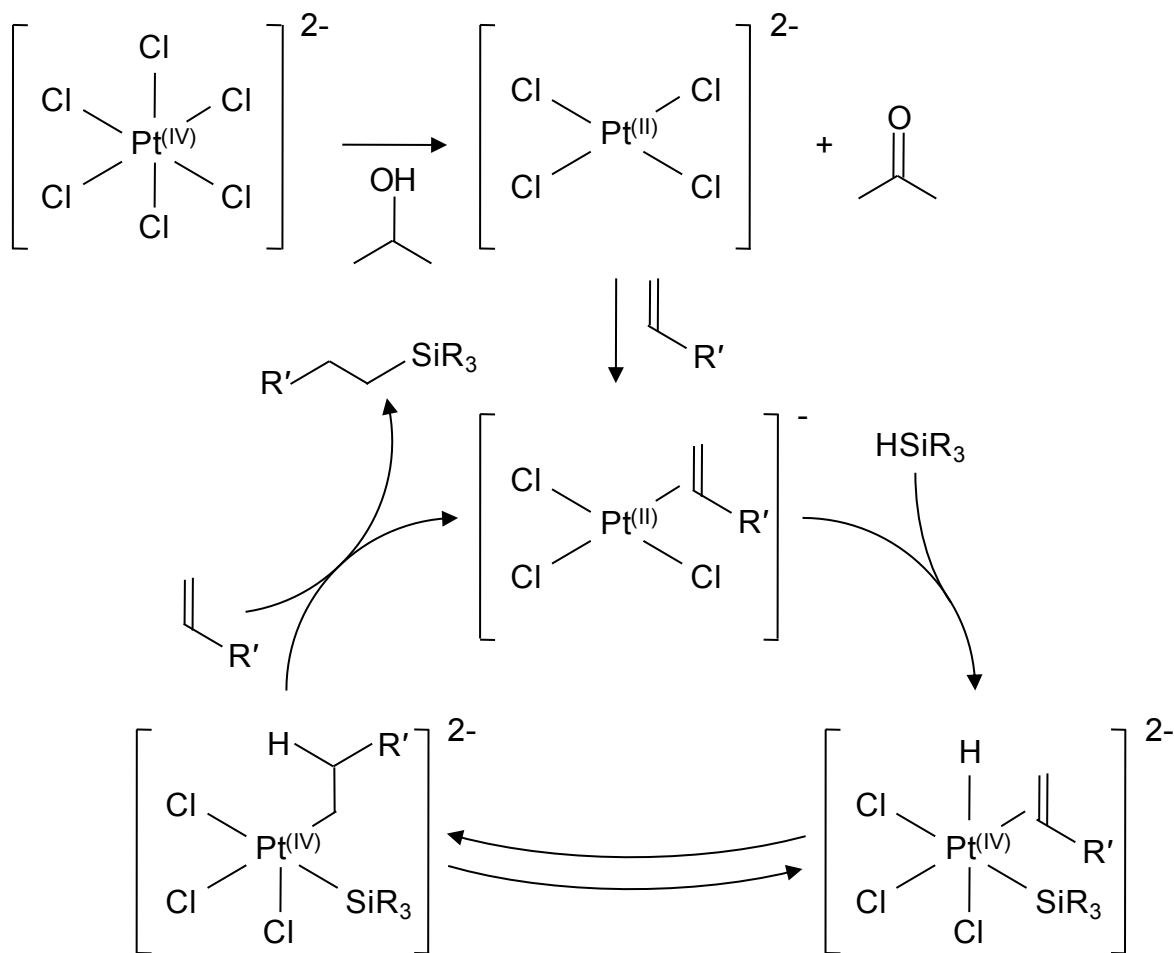


Figure 1.2: Poly(3,3,3-trifluoropropylmethylsiloxane) – PTFPMS

1.2.2 Synthesis

To prepare a typical fluorosilicone the fluorinated moiety must be attached to the silicon of the siloxane backbone and the polymer formed. Both fluorination followed by polymerization and polymerization followed by fluorination have been used to produce fluorosilicones depending on the nature of the fluorinated group, the hydrocarbon link between the fluorine and silicon and the desired polymerization method.

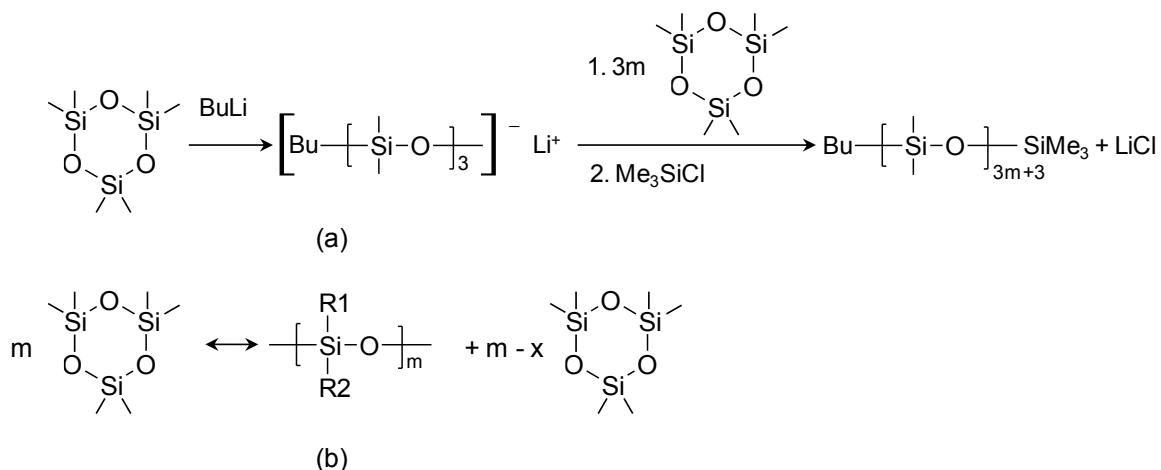
Hydrosilylation chemistry, whereby a vinyl group bonds to a hydrosilane, is the most common route used to add a fluorinated group, which contains a terminal vinyl group, to the silicon. Typically this is accomplished through a platinum catalyst as shown in Scheme 1.2 [11]. This method has been used to synthesize both fluorosilicone monomers for subsequent polymerization (e.g., in the formation of PTFPMS) as well as joining any number of fluorinated groups to siloxane backbones post-polymerization as evidenced by a review on fluorosilicones by Boutevin and Pietrasanta [22]. This review predominantly focuses on the synthesis of vinyl-containing fluorinated groups. The alternative to hydrosilylation, which typically leads to an ethyl link between the silicon and the fluorinated group, is to use Grignard chemistry [23]. This chemistry widens the possible number of linking groups with aromatic rings most often utilized due to facility with which they undergo Grignard reactions.



Scheme 1.2: Hydrosilylation. Adapted from [11]

The fluorosilicone described by Pierce et al. [21] was produced through the ring-opening polymerization of a tricyclosiloxane containing one TFP group and one methyl group on each silicon with current ring opening polymerization methods using either anionic or cationic initiation, Scheme 1.3a. Typically ring-opening polymerization is preferred over equilibration methods, Scheme 1.3b, as the polydispersity is reduced and the molar masses achieved are much higher [11]. Both methods require the removal of cyclics, for example tricyclosiloxanes, through heating and any residual acidic or basic catalyst or initiator will likely reduce the thermal stability of the final polymer as will be discussed in Section 1.2.3.1 Thermal

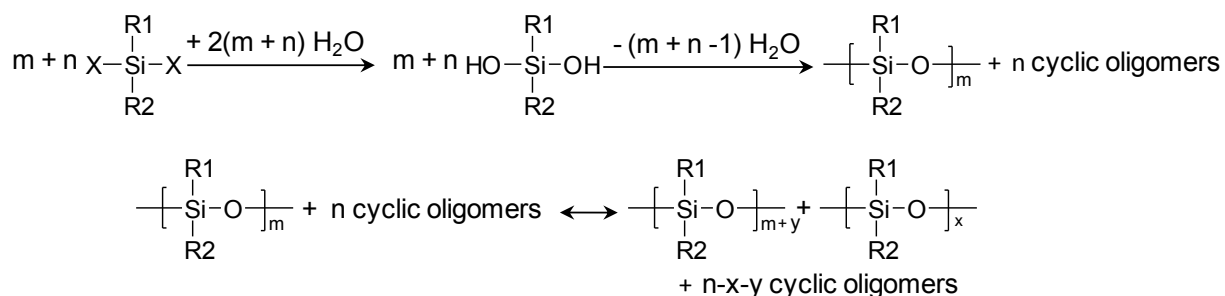
Stability. As well, both polymerization methods constrain the size of the fluorinated component; groups larger than CF_3 may hinder the polymerization as shown by Furukawa [24] with a cyclotrisiloxane substituted with three 1H, 1H, 2H, 2H-nonafluorohexyl groups. This leads to the use of post-polymerization attachment, which will reduce the number of fluorinated repeat units unless the attachment yield is 100%.



Scheme 1.3: Polymerization of PTFPMS, (a) Anionic ring-opening polymerization and (b) Equilibrium polymerization. R1 = methyl, R2 = trifluoropropyl

Condensation chemistry has also been examined as an alternative to ring-opening polymerization for PTFPMS [25-27], Scheme 1.4. However, this method of synthesis is not typically used for short-chain fluorinated groups since the above ring opening polymerization, particularly with the advent of living systems, provides more control over the final molar mass without the issues of reactant purity associated with condensation polymerizations. Yet using condensation polymerization to form fluorosilicones still has some utility. As mentioned, if the desired pendant group is bulky, a fluorosilicone can be synthesized through the condensation of siloxane oligomers. Most often the condensed polymers have silanol or chlorosilane termini

[25, 28] and the method of condensation is the same as for non-fluorinated siloxane polymers, Scheme 1.4. Hydrosilylation has also been used as the linking reaction [29, 30]. Where condensation and other step growth polymerization methods have found significant use is in the synthesis of hybrid fluorosilicones discussed in Section 1.3 Hybrid Fluorosilicones.



Scheme 1.4: Condensation of dihalosilanes to high molecular weight linear siloxanes

1.2.3 Properties

1.2.3.1 Thermal Stability

The acid or base catalyst in equilibration or ring-opening polymerization methods used to form traditional fluorosilicones can reduce the thermal stability of the end polymer compared to the potential achievable thermal stability ($T_d > 350$ °C versus 150 °C in the presence of 5% KOH, [11]). The decomposition of the siloxanes, and fluorosilicones, occurs primarily through intrachain reactions that result in the thermodynamically stable tricyclo- and tetracyclo-siloxanes, Figure 1.3. These types of reaction occur more easily with uncapped siloxanes, i.e. those linear chains that are not terminated with a trimethylsilane. Thus, the catalysts such as KOH enhance depolymerization by cleaving the siloxane chain leaving reactive silanol or silanolate end groups.

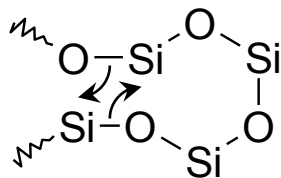


Figure 1.3: Thermal intrachain rearrangement of siloxanes (adapted from Guida-Pietrasanta [28])

As stated in Section 0 Synthesis, the majority of the hydrocarbon linkers in traditional fluorosilicones are ethyl due to the use of hydrosilylation chemistry. However, incorporation of an aromatic ring as the linking group will likely lead to polymers with greater thermal stability for two reasons. First, as the bond strength within the ring is greater than that of an ethyl link [12] this will prevent the potential loss of the pendant fluorinated group through cleavage of the ethyl C-C bond. Second, the bulkiness of the aromatic group will likely hinder the intrachain rearrangement in Figure 1.3, although Patwardhan et al. [23] did note that the bulky aromatic group does not prevent the fluorinated attachment from migrating to the surface. Having the aromatic group in the polymer backbone will likely raise the thermal stability further. This is seen in Section 1.3 Hybrid Fluorosilicones.

An alternative method to enhance the thermal stability (specifically thermal degradation) of fluorosilicones is to synthesize a polymer that incorporates a functional group for post-polymerization crosslinking or chain extension. This group, typically vinyl, is found either as end groups [29, 31-34], or on a repeat unit [30, 35-37], each location having associated advantages and disadvantages. Making the reactive group part of each repeat unit provides the greatest number of potential reactive sites. However, each site is likely adjacent to a TFP group, which sterically hinders the reactive group and will reduce the rate of crosslinking. To prevent this,

the two functionalities can be separated. Placing the reactive group at the end of each fluorosilicone chain reduces the steric hindrance of the TFP group, but also reduces the degree of crosslinking that can be achieved.

A vinyl group allows for both hydrosilylation and radical crosslinking methods, such as peroxide based cures. The focus has been on hydrosilylation due to the specificity of the reaction. As a reminder, this specificity is also used for the attachment of different fluorinated pendant groups (Section 1.2.2 Synthesis). Importantly, radical crosslinking requires the incorporation of hydrocarbon chains in the fluorosilicone, which may cause decreased thermal stability. Another disadvantage of using crosslinking to enhance mechanical properties at elevated temperature is the loss of low temperature flexibility, which arises from the mobility of the siloxane backbone. Crosslinking will reduce this flexibility, resulting in a higher T_g and a higher temperature at which the ductility associated with polymers is lost. Takita [38] attempted to resolve this issue by incorporating low molecular weight fluorosilicones as plasticizers. However, this iterative process of crosslinking to enhance properties, and subsequently, adding oligomers to improve low temperature properties appears unnecessarily complicated.

1.2.3.2 Surface Energy

The thermal stability of PTFPMS is mainly derived from the siloxane backbone. Other desired properties, such as solvent resistance² and low surface energy³, which lead to the application of fluorosilicones as release coatings and sealants in jet-fuel lines, are derived in part from the mobility of this siloxane backbone. This allows the polymer to rearrange such that the TFP group is oriented to the surface. However, the major contributor to these effects is the chemical nature of the CF₃ group at the end of the trifluoropropyl pendant moiety since based on chemical composition, the CF₃ group has the lowest surface energy of all functional groups [39].

In the synthesis of PTFPMS, Pierce et al. [21] found that the solvent resistance of the material was greater than that of polydimethylsiloxane. This led to the examination of longer pendant fluorinated groups, including -CH₂CH₂CF₂CF₃ and -CH₂CH₂CF₂CF₂CF₃, in the same article likely based on the hypothesis that incorporating a longer fluorinated chain would enhance the solvent resistance. However, Pierce et al. found that the longer chains did not increase solvent resistance further and PTFPMS was chosen for commercialization. Later work on the extension of the short trifluoropropyl group to longer fluorinated alkyl chain yielded similar results [24, 40-45].

Pierce et al. and others discovered solvent resistance is not enhanced by a sufficient degree to offset the greater synthetic cost due to the increased amount of

² Solvent resistance describes the ability of the polymer to resist physical and chemical changes when immersed in a given solvent.

³ A low surface energy means that liquids do not easily wet the surface of the polymer.

fluorine for fluorinated groups longer than CF_3 . This leaves the remaining reason for incorporating long fluorinated chains: a reduction in the surface energy of the polymer. Research by Owen and Groh [46] shows that longer fluorinated alkyls may not be advantageous as the CF_3 coordinates to the silicon of the polymers leading to a looped structure and a surface that consists of CF_2 groups, which have a higher surface energy. However, later research by Owen and Kobayahshi [41] found that a $-(\text{CH}_2)_2(\text{CF}_2)_7\text{CF}_3$ group had the lowest surface energy although the most efficient fluorosilicone (i.e. the fluorosilicone that had the greatest decrease in surface energy relative to PDMS with the least incorporation of fluorine) contained a $-(\text{CH}_2)_2(\text{CF}_2)_3\text{CF}_3$ pendant group. Therefore, longer fluorinated chains may lead to the lowest surface energy fluorosilicones attainable, but as is the case with solvent resistance this must be balanced against the efficiency and increased cost of fluorine incorporation.

1.2.4 Potential Improvements

The structure of traditional fluorosilicones, a siloxane backbone with a pendant fluorinated group, leads to polymers with excellent low temperature properties, enhanced solvent resistance and low surface energy. In combination with crosslinking to enhance the retention of mechanical properties at elevated temperatures, this gives a class of polymers that appears to be unparalleled and is used in applications as diverse as: lubricants, surfactants, and gels, electrical devices; release coatings; and elastomers, typically in the presence of harsh chemicals and/or environments [47]. However, despite the excellent characteristics above, the siloxane backbone is still prone to depolymerization at elevated

temperature (as low as 150 °C in the presence of impurities) due to chain scission [11].

Designing a fluorosilicone where the silicon and fluorine are in the alternate locations will result in prevention of this chain scission and potentially greater thermal stability. Hybrid fluorosilicones, where both the siloxane and the fluorine are located in the backbone, have been synthesized through step growth polymerizations and are discussed in the following section. This class of fluorosilicone prevents chain scission by blocking the rearrangement of the backbone. Reverse fluorosilicones, where the siloxane moiety is in the pendant location, eliminate the chain scission mechanism completely and are discussed in Section 1.4. While each of these classes of fluorosilicones may not have the same properties as traditional fluorosilicones, they potentially represent an avenue to similar applications as lubricants and release coatings yet at higher operating temperatures. Thus, hybrid and reverse fluorosilicones have been examined in this thesis.

1.3 Hybrid Fluorosilicones

As introduced above, hybrid fluorosilicones contain both the siloxane and fluorinated components in the backbone. Inserting a hydrocarbon between the siloxane components, and more specifically a fluorinated hydrocarbon in the case of hybrid fluorosilicones, prevents the chain scission and subsequent unzipping of the siloxane chain exhibited by traditional fluorosilicones.

1.3.1 Structure

Similar to traditional fluorosilicones, the fluorinated block is limited only in that it has a functionality which can react with the siloxane component leading to the synthesis of hybrid fluorosilicones with linear and branched fluoroalkyl, fluoroether, or fluoroaromatic blocks, Table 1.4. An excellent review on hybrid silicones by Guida-Pietrasanta and Boutevin [28] also contains a section on fluorinated silicones.

From the structures in Table 1.4, it can be seen that hybrid fluorosilicones have an alternating structure where the fluorinated component is sandwiched between a siloxane consisting of two silicon atoms. By limiting the length of the siloxane joining the hydrocarbon group to less than four siloxane repeat units, the intrachain thermal rearrangement that causes the decomposition of traditional fluorosilicone at elevated temperatures can be prevented. However, siloxane links containing two silicon atoms do not appear to be sufficient to prevent crystallization of the resulting hybrid fluorosilicones limiting their use as elastomers [48], one of the applications for fluorosilicones. Additionally, an argument may be made that many of these hybrid fluorosilicones should not be classed as fluorosilicones as the fraction of siloxane is minimal. Yet the incorporation of a siloxane bridge containing only two silicon atoms as the link between the fluorinated components reduces the glass transition temperature significantly implying that little siloxane incorporation is required. For example, the aromatic polyether that is equivalent to the aromatic hybrid fluorosilicones synthesized by Smith and Babb [49] and Rizzo and Harris [50] exhibits a T_g of 170 °C [51]. By comparison, the aromatic polyether which contains a two silicon link has a T_g of 24 °C (calculated from [52] and [50]).

Table 1.4: Hybrid fluorosilicones

Fluorinated Linker		x	y	R ₁	R ₂	Reference
Alkyl	$\left[\begin{array}{c} R_1 \\ \\ \text{Si}(\text{CH}_2)_x(\text{CF}_2)_y(\text{CH}_2)_x\text{SiO} \\ \\ R_2 \end{array} \right]_n$	2 or 3	6	CH ₃	CH ₃	[14, 53, 54]
		2	1,2,4,6,8,10	CH ₃	C ₂ H ₄ CF ₃	[14, 54]
		2 or 3	6	CH ₃	CH ₃	[14, 53, 54]
		2	6	CH ₃	C ₂ H ₄ (CF ₂) ₃ CF ₃	[55]
		2	6	C ₂ H ₄ CF ₃	C ₂ H ₄ CF ₃	[14]
Ether	$\left[\begin{array}{c} R_1 \\ \\ \text{Si}(\text{CH}_2)_2(\text{CF}_2)_x\text{O}(\text{CF}_2)_y(\text{CH}_2)_2\text{SiO} \\ \\ R_2 \end{array} \right]_n$	2 or 3	2	CH ₃	C ₂ H ₄ CF ₃	[56, 57]
	$\left[\begin{array}{c} R_1 \\ \\ \text{Si}(\text{CH}_2)_2(\text{CF}_2)_x\text{O}(\text{CF}_2)_y\text{O}(\text{CF}_2)_x\text{CH}_2)_2\text{SiO} \\ \\ R_2 \end{array} \right]_n$	2	2 or 5			
	$\left[\begin{array}{c} \text{CH}_3 \quad \text{CF}_3 \quad \text{CF}_3 \quad \text{CH}_3 \\ \quad \quad \quad \\ \text{SiC}_2\text{H}_4\text{CFO}(\text{CF}_2)_5\text{OCFC}_2\text{H}_4\text{SiO} \\ \quad \\ \text{C}_2\text{H}_4\text{CF}_3 \quad \text{C}_2\text{H}_4\text{CF}_3 \end{array} \right]_n$	and	$\left[\begin{array}{c} \text{CH}_3 \quad \text{CF}_3 \quad \text{CF}_3 \quad \text{CH}_3 \\ \quad \quad \quad \\ \text{SiC}_2\text{H}_4(\text{CF}_2)_4\text{OCFCF}_2\text{OCFC}_2\text{H}_4\text{SiO} \\ \quad \\ \text{C}_2\text{H}_4\text{CF}_3 \quad \text{C}_2\text{H}_4\text{CF}_3 \end{array} \right]_n$			
Aromatic		1 to 6				[49, 50, 52, 58, 59]

1.3.2 Synthesis

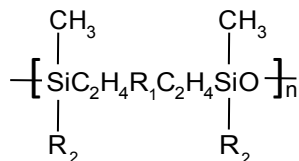
The fluoroalkyl and fluoroether hybrid fluorosilicones are typically synthesized through hydrosilylation between an α,ω -divinylfluorinated group and chlorodimethylsilane [14, 53, 55, 57]. The result is a hybrid fluorosilicone precursor end-capped with Si-Cl bonds. This is subsequently hydrolyzed to form the resultant hybrid fluorosilicone which must have the alternating structure seen in Table 1.4 and a siloxane component that contains two silicon atoms. Thus, the structure is derived from the synthetic method used for these polymers. The length of the siloxane component could be increased by using an α,ω -dichlorosiloxane, yet this reintroduces the possibility of intrachain rearrangement.

An alternative shown by Smith and coworkers [49, 52, 58, 60] is to synthesize a hybrid fluorosilicone precursor with a polymerizable fluorinated group rather than using siloxane condensation to form the polymer. By using the thermocyclodimerization of a trifluorovinyloxybenzene as the polymerization method they also incorporated a living aspect into their system. However, this polymerization scheme is constrained by low molar masses ($M_n < 20$ kg/mol) although Rizzo and Harris [50, 59] increased the molar mass three-fold by reverting back to the typical silanol condensation method. Despite the potential for chain scission, Smith and coworkers incorporated longer siloxane chains into the polymer structure, affecting the thermal properties as described in the following section 1.3.3 Properties.

1.3.3 Properties

The hypothesis that led to the synthesis of hybrid fluorosilicones is that a block, in this case a fluorinated block, situated in the backbone of a siloxane will prevent the depolymerization of traditional silicones and fluorosilicones. This hypothesis is confirmed in Table 1.5 where all of the fluoroalkyl hybrid fluorosilicones have thermal stabilities greater than PTFPMS ($> 440^{\circ}$ versus 245°C [54]). Of note, these polymers all have an alternating structure which will lead to the highest thermal stability for a hybrid siloxane as seen in work by Dvornic and Lenz [61] on siloxanes. Although the incorporation of the linker increases the overall operating temperature for the hybrid fluorosilicone and prevents depolymerization, the glass transition temperature also increases, thereby reducing the low temperature applicability of the polymer (Table 1.5). This is likely due to the stiffening of the flexible siloxane backbone by the fluorinated component.

Table 1.5: Effect of fluoroalkyl link on glass transition and decomposition temperature; all polymers are of the structure below with the exception of PTFPMS in the first line of the table



R ₁	R ₂	T _g (°C)	T _{50%} in inert atmosphere (°C)	Reference
PTFPMS		-67	245	[54]
CF ₂ [†]	(CH ₂) ₂ CF ₃	-38	N/A	[14]
C ₂ F ₄	(CH ₂) ₂ CF ₃	-27	493	[14, 54]
C ₄ F ₈	(CH ₂) ₂ CF ₃	-25	N/A	[14]
C ₆ F ₁₂ [†]	(CH ₂) ₂ CF ₃	-28	490	[14, 54]
C ₈ F ₁₆	(CH ₂) ₂ CF ₃	-28	N/A	[14]
C ₁₀ F ₂₀	(CH ₂) ₂ CF ₃	-11	N/A	[14]
C ₆ F ₁₂	(CH ₂) ₂ C ₄ F ₉	-42	490	[55]
C ₆ F ₁₂ [‡]	CH ₃	-53	470	[53, 54]
CH ₂ C ₆ F ₁₂ CH ₂	CH ₃	-40	N/A	[53]
C ₆ H ₁₂ [‡]	CH ₃	-76	440	[54]

[†] denotes polymers that are compared to one another in the following text

[‡] denotes polymers that are compared to one another in the following text

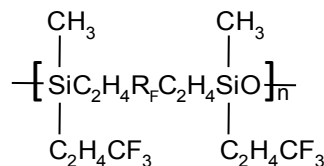
An examination of Table 1.5 also reveals that both a hydrocarbon or fluorocarbon linker can increase the thermal stability nearly to the same extent; compare the polymers with the C₆H₁₂ and the C₆F₁₂ linkers (denoted by ‡ in Table 1.5). This may be expected as polyethylene and PTFE have similar decomposition temperatures of approximately 390 °C in inert atmospheres [1, 9]. Thus, it appears that if the spacer has a high thermal decomposition temperature, the incorporation of fluorine is not necessary. No mention is made of the mechanical properties of these

polymers, but the hydrocarbon-based hybrid would likely degrade prior to the fluorocarbon-based one. As well, the thermal stability in air, (thermo-oxidative stability), should be considered for practical applications. In this case, a linker consisting of a fluorinated hydrocarbon will likely have greater thermo-oxidative stability than a non-fluorinated one. By comparison, the thermo-oxidative stability of PE (240 °C [1]) is less than PTFE (475 °C [62]). Additionally, Table 1.5 shows that a polymer containing two CF₂ linking units has the same thermal stability as one with six CF₂ units (denoted by † in Table 1.5) suggesting that minimal incorporation of the fluorinated group is necessary to enhance the thermal stability. Combined, these points suggest that the disruption of siloxane depolymerization can be effected with a minimal incorporation of fluorine. As a reminder, this type of effect where minimal incorporation of fluorine is necessary to achieve the desired result has been seen previously with the surface properties of traditional fluorosilicones, Section 1.2.3.2 Surface Energy.

As mentioned in Section 1.1.3 Effect on Other Polymer Properties, an iterative process is usually required to obtain high thermal stability while maintaining the other desired polymer properties. To prevent the loss of low temperature capabilities seen by the incorporation of a fluoroalkyl link, Riley and Kim [56, 57] examined the use of a fluoroether as the linking component. Their studies demonstrated that incorporating oxygen increases the free volume of the fluorinated group, and subsequently, reduce the glass transition temperature. Their hybrid fluoroether-siloxane polymers exhibited lower glass transition temperatures than

comparable fluoroalkyl-siloxanes while maintaining a high thermal stability as seen in Table 1.6.

Table 1.6: Thermal properties of hybrid fluoroether-siloxane polymers compared with fluoroalkyl-siloxane polymers; all polymers are of the structure



R_F	T_g (°C)	$T_{50\%}$ in inert atmosphere (°C)	Reference
C_2F_4	-27	493	[14, 54]
C_6F_{12}	-28	490	[14, 54]
C_8F_{16}	-28	N/A	[14]
$(CF_2)_3O(CF_2)_2$	-39	N/A	[57]
$(CF_2)_2O(CF_2)_2O(CF_2)_2$	-40	497	[57]
$(CF_2)_2O(CF_2)_5O(CF_2)_2$	-52	502	[57]

An alternative method to decrease the glass transition temperature, and subsequently increase the operating range of the polymer is to increase the length of the siloxane component. Due to the bulky nature of the aromatic perfluorocyclobutane as the linker, the T_g (24 °C [50]) is greater than a comparable fluoroether siloxane (T_g = -39 to -52 °C) synthesized by Riley and Kim [56, 57]. By incorporating longer siloxane chains the T_g of the fluoroaromatic hybrid can be reduced to -60 °C [50]. This includes siloxane links that contain more than four silicon atoms, the requisite number for intrachain depolymerization. However, decomposition equivalent to traditional fluorosilicones, suggesting a similar decomposition mechanism, is not seen in the fluoroaromatic hybrids, likely due to the extremely bulky nature of the fluorocarbon component.

1.3.4 Potential Improvements

As mentioned, the use of a fluoroether link has been shown to extend the usable temperature range of hybrid fluorosilicones by enhancing low temperature properties while maintaining high thermal stability. Additionally, aromatics are known to enhance thermal stability when incorporated into the backbone as seen in Table 1.3 of Section 1.1 Thermal Stability. Therefore, it is expected that the aromatic fluoroether polymers of Smith and Babb [49, 52, 58, 60] should exhibit some of the highest thermal stabilities of hybrid fluorosilicones, yet work by Kennedy et al. [63] suggests that the oxygen may be the initial location for thermal decomposition. This implies that removal of the oxygen may increase the thermal stability further albeit potentially increasing the T_g as well. The synthesis and comparison of such polymers is examined in Chapter 2.

The dependence of the chain scission mechanism on the number of siloxane repeat units was also examined in Chapter 2 where polymers with linkers containing two, four, and four to seven silicon atoms are discussed. The last example contains a range in the number of silicon atoms due to the variability in the starting siloxane as discussed further in Chapter 2. Hypothetically, the thermal stability of the polymers containing more than two silicon atoms in the linker should be reduced relative to the first as the polymers contain a potential avenue for the thermal intrachain rearrangement, although this may not be true as shown by Rizzo and Harris [50] who synthesized a hybrid fluorosilicone containing six siloxane repeat units with a thermal decomposition temperature ($T_{5\%}$) of 445 °C in air. This will allow confirmation as to the capacity of a bulky fluorinated component to prevent chain

scission while retaining low temperature ductility through a low T_g and provide an alternative to the fluoroether-siloxane hybrids.

1.4 Reverse Fluorosilicones

Reverse fluorosilicones have been coined as they are the opposite of traditional fluorosilicones; rather than a siloxane backbone with a pendant fluorinated group, the backbone consists of a fluoropolymer with a pendant siloxane component. This change must prevent the depolymerization by chain scission seen in traditional fluorosilicones. Additionally, this will allow for radical polymerization methods that are more robust than the equilibration or ring-opening polymerizations used in traditional fluorosilicone synthesis and the condensation polymerization used in hybrid fluorosilicone synthesis. Moving to a fluorinated backbone gives a wider range of potential starting monomers and polymer backbones; any double-bonded fluorocarbon is a potential candidate, suggesting the properties of the final polymer may be tailored more easily to the application. For example, the incorporation of chlorotrifluoroethylene may result in a polymer with lower flammability than traditional fluorosilicones.

Reverse fluorosilicones may not be considered true fluorosilicones by virtue of eliminating the siloxane backbone and pendant fluorine group from which traditional fluorosilicones derive many of their characteristics. However, naming them fluorosilicones implies that the polymer must contain a fluorinated component as well as one based on silicon-oxygen bonds. Fluoropolymers with any other pendant group do not fall into this category. Furthermore, there is no apparent reason that reverse fluorosilicones cannot attain some of the properties associated

with traditional fluorosilicones given a judicious selection of the fluorinated and silicon-containing components.

1.4.1 Synthesis

Reverse fluorosilicones are typically synthesized by attaching a siloxane graft to a fluoropolymer post-polymerization [64-66]. However, in all cases this graft is to the hydrocarbon component of a fluorocarbon-hydrocarbon copolymer. Using acid catalysts, Suzuki, Takeishi and Narisawa [64], grafted siloxanes of varying molecular weight ($M_n = 1230, 2670, \text{ and } 4440 \text{ g/mol}$) to terpolymers of CTFE-(*tert*-butylacrylate)-(propenoxybutanol). This method allows for the grafting of relatively long siloxane chains.

Alternatively, direct copolymerization of a polymerizable siloxane moiety with a fluorocarbon monomer can be used to achieve a reverse fluorosilicone [62]. This will limit the size of the siloxane group which can be incorporated, yet as discussed in the above section on thermal stability chains with greater than four siloxane repeat units may be prone to depolymerization, and thus, this limit may not be detrimental. In these cases, the number of siloxanes incorporated will depend on the initial monomer concentration and reactivity ratios of the respective monomers. Using copolymerization as a methodology also allows for a rapid assessment of the feasibility of various fluoromonomers and polymerizable siloxane combinations.

The copolymerization of fluoromonomers and polymerizable siloxanes is subject to the same synthetic constraint as other copolymerizations. Namely, the reactivity of the two components must be similar enough in the polymerization media chosen that a copolymer will form. Work by Baradie and Shoichet [62] as well as

unpublished research has shown that the selection of the copolymer components is crucial. Without the addition of a linking monomer, vinyl acetate (VAc), a copolymer between TFE and monomethacryloxypropyl-terminated polydimethylsiloxane (PDMSMA) cannot be synthesized under the conditions studied, i.e., in supercritical CO₂ using AIBN initiation. This is due to the 1000-fold difference in the reactivity ratios between TFE and PDMSMA.

1.4.2 Properties

1.4.2.1 Thermal

The two synthetic methods lead to two different concerns with regards to the thermal stability of the resulting polymers. In the case of the reverse fluorosilicones synthesized by post-polymerization attachment, the length of the siloxane graft (greater than four siloxane repeat units) and amount of the siloxane (grafting ratios as high as 73% were obtained) in the resulting polymers, suggest that these polymers will have a thermal stability more similar to traditional fluorosilicones than the fluoropolymer backbone although this property was not examined by Suzuki et al. [64]. Similar polymers [65] with a urethane link will likely yield similar results.

The second issue is the use of a hydrocarbon component in the polymers. Unless this component consists of thermodynamically stable groups as discussed in Section 1.1.1 Effect of Polymer Composition, thermal decomposition will likely initiate at this hydrocarbon. This is seen in the work by Baradie and Shoichet [62] where they hypothesize that the initial step in the decomposition pathway of their TFE-VAc-PDMSMA terpolymer is loss of the acetate group by VAc. Removing or minimizing the VAc component will likely enhance the thermal stability of the

terpolymer. Furthermore, the VAc has the highest surface tension of the three components (CTFE = 30.9 dyn/cm; VAc = 36.5 dyn/cm; and PDMS, which is considered to be the equivalent of the PDMSMA pendant group and the surface active component = 20 dyn/cm) [39], suggesting the VAc provides little value to the functionality of the terpolymer although it may have benefit in other unexamined areas such as mechanical properties. A more thermally stable siloxane-containing component is also desirable as the decomposition temperature of p(PDMSMA) is relatively low (226 °C).

Traditional fluorosilicones are also known for their low temperature capabilities with the low temperature flexibility derived from the mobility of the siloxane backbone. Reversing the structure such that the fluorinated component is in the backbone will reduce this flexibility and the glass transition temperature will rise. Again, work by Baradie and Shoichet confirms this as the T_g of their terpolymer is 28 °C [62]. However, this effect may be mitigated by selecting an appropriate monomer, or combination of monomers for the fluorinated component. For example, a terpolymer of tetrafluoroethylene, perfluoromethyl vinyl ether (PMVE) and vinylidene fluoride, has an operating temperature as low as -35 °C compared to -67 °C for PTFPMS [47]. This highlights the advantage of using a one-pot radical polymerization technique over a post-polymerization grafting method. The latter requires a fluorocarbon monomer with a reactive functionality whereas the former can use any available fluorocarbon monomer and the low temperature properties may be tailored through copolymerization.

1.4.2.2 Surface Properties

The low surface energy in traditional fluorosilicones, specifically PTFPMS, is derived from the pendant CF_3 group, which has the lowest surface energy of all functional groups, and due to its location in the polymer migrates to the surface. However, reverse fluorosilicones can incorporate a much broader range of fluorocarbon monomers which will have surface energies greater than PTFPMS. Thus, the siloxane component becomes the surface active species particularly due to its location as a pendant group. Furthermore, if the polymer is to be used in a liquid or semi-solid form, (e.g., as a lubricant) siloxanes such as PDMS have lower surface energies than PTFPMS, refer to Table 1.7.

Table 1.7: Comparison of surface tension for poly(trifluoropropylmethylsiloxane), poly(tetrafluoroethylene), and poly(dimethylsiloxane)

Polymer	Equilibrium Liquid Surface Tension (mN/m)	Solid Surface Tension (mN/m)
PTFPMS	24	14-15 ^a
PTFE	26	14 ^a
Polytrifluoroethylene	-	24 ^b
Poly(vinylidene fluoride)	-	30 ^b
Poly(vinyl fluoride)	-	37 ^b
PCTFE	-	27 ^a
PDMS	21	19-25 ^a

^a Data was obtained by Owen [67] using the Owens-Wendt technique.

^b [47]

A surface composed of a siloxane component may also have advantages for other polymer properties, such as flammability. Upon being exposed to flame, the siloxane may oxidize to a silsesquioxane, where each silicon atom is bonded to three oxygen atoms as opposed to two, and subsequently silicon dioxide. This will form a layer that will inhibit further oxidation of the bulk polymer, much the same as

carbonaceous char formation inhibits the burning of wood. With a fluorinated surface, char formation will be reduced as the main contributor to the low flammability of fluorinated compounds is the formation of HF.

1.4.3 Potential Improvements

Of the two synthetic methods discussed, the radical copolymerization scheme affords the widest potential for enhancing and tailoring the properties of reverse fluorosilicones. The current work in the area suggests that for the terpolymer synthesized by Baradie and Shoichet [60] to be improved, the following criteria must be met. The first two potentially eliminate the hydrocarbon component of the terpolymer by reducing the 1000-fold difference in reactivity whereas the last will improve the component with the second lowest thermal stability.

1. Increase the reactivity of the fluororadical,
2. Decrease the reactivity of the siloxane-containing radical, and
3. Increase thermal stability of the siloxane-containing component.

One method to modify reactivity ratios is to change the polymerization media. The change in reactivity ratios can arise due to a shift in the heterogeneity of the system. For example the reactivity ratios for the methyl methacrylate (MMA) / N-vinylcarbazole (NVC) system are $r_{MMA} = 1.80$ and $r_{NVC} = 0.06$ in benzene versus $r_{MMA} = 0.57$ and $r_{NVC} = 0.75$ in methanol [68] where the change in reactivity ratios is due to a change from a homogeneous polymerization in benzene to a heterogeneous precipitation polymerization in methanol. In methanol, the radical is trapped within the precipitated polymer and is less accessible to NVC relative to the

polymerization in benzene. This reduces the amount of NVC that is incorporated into the copolymer and modifies the reactivity ratios.

The reactivity ratios for a pair of monomers may also change with other characteristics of the reaction medium including viscosity, pH and polarity. The effect of viscosity is shown by Johnson et al. [69] who polymerized styrene and MMA by bulk polymerization and in benzene. Less styrene is incorporated into the polymer in the first case as its transport to the reactive site is decreased relative to MMA due the gel effect.

The pH of the solvent will affect acidic monomers such as acrylic acid (AA). Ponratnam and Kapur [70] show that the reactivity ratios between acrylic acid and N-vinylpyrrolidone depend on the degree of ionization of the acrylic acid. As pH (and the ionization) of the acrylic acid increases, the reactivity ratio decreases due to the difference in reactivity between the ionized and unionized form. Interestingly, the authors also found a minimum r_{AA} at pH 5, which they attribute to a lowering of the concentration of ionized acrylic acid at the reactive site. Therefore, in all three examples (heterogeneity, viscosity and pH), the effect of the solvent is to modify the transport of one of the monomers to the reactive propagating site. This is also the case when one monomer is more soluble in the polymerization media than the other. The local concentration of the monomers at the reactive site will be modified by the solvent and results in an apparent modification in reactivity ratios.

The polarity of the solvent will affect the reactivity of the monomer itself rather than monomer transport. The copolymerization of VAc with ethylene [71] shows that an increase in hydrogen bonding and dipole-dipole interactions between the VAc

and the solvent reduces the VAc activity through modification of the electron density at the double bond. A similar effect may be present for the polymers synthesized by Baradie and Shoichet [72] as their collaboration with others [73] showed that the supercritical CO₂ interacts with the carbonyl of the VAc. Moving from supercritical CO₂ to an aqueous medium will modify this interaction and potentially the reactivity ratios although the effect may be minimal as work by Baradie and Shoichet [72] and Murray et al. [74] show similar reactivity ratios for the same fluoromonomer-VAc combination.

An examination of the shift from supercritical CO₂ to an aqueous medium is also important because while supercritical CO₂ is an environmentally benign solvent and leads to reduced post synthesis purification, the pressures required are on the order of 300 bar suggesting that the potential for industrial applicability may be limited. The formation of these polymers using a polymerization at lower pressures and a well-known industrial process is, therefore, desired. Furthermore, synthesis of VAc-containing reverse fluorosilicones by emulsion will allow for a comparison of the branching between this medium and supercritical CO₂. At present, the molar masses of polymers synthesized in the two media fall on either side of the molar mass cutoff for significant long-chain branching due to VAc show by Grcev et al. [75]. If polymers of similar molar mass and composition are achieved a direct comparison can be made.

Chapter 3 describes the polymerization of CTFE, VAc and PDMSMA by emulsion in an attempt to modify the reactivity ratios seen in the TFE, VAc, PDMSMA system. The TFE was substituted with CTFE as chlorine is less

electronegative than fluorine leading to increased reactivity of the fluororadical, meeting the first criterion, although this may be offset due to the greater steric hindrance of the chlorine. The reactivity ratios of TFE and CTFE with VAc can be used to estimate the relative reactivity of the two fluoromonomers. From work by Baradie and Shoichet [72], $r_{TFE} = -0.009 \pm 0.61$ and $r_{VAc} = 0.95 \pm 0.08$ and $r_{CTFE} = 0.014 \pm 0.05$ and $r_{VAc} = 0.44 \pm 0.03$ for the TFE-VAc and CTFE-VAc systems, respectively. The range of r_{TFE} (-0.619 to 0.601) and r_{CTFE} (-0.036 to 0.19) overlap suggesting that TFE and CTFE have nearly equivalent affinities for VAc and subsequently, similar reactivity. A comparison of the reactivity ratios of TFE and CTFE to one another, $r_{TFE} = 1.0$ and $r_{CTFE} = 1.0$, confirms potentially similar reactivity for the two fluoromonomers [68]. Additionally, the use of CTFE enhances the safety of the polymerization since TFE can polymerize explosively and the mitigating effect of the supercritical CO₂ with which it forms a pseudo-azeotrope [76] is not available in the emulsion system.

The effect of shifting from polymerization in scCO₂ to an aqueous medium on the reactivity of PDMSMA is unknown. However, the solubility of the PDMSMA in the aqueous medium is likely reduced. This will lead to a reduction in the PDMSMA concentration at the reactive site (in an emulsion polymerization) as transport of the monomer through the aqueous phase is decreased and a subsequent change in the reactivity ratios between CTFE and PDMSMA is likely. Therefore, the second criterion is potentially fulfilled. This criterion may also be filled if the reactivity of the PDMSMA is reduced. An alternative monofunctional polymerizable PDMS-based fluid, monovinyl-terminated PDMS, is available; however, the molar mass of

62 kg/mol and the length of the siloxane chain will likely sterically hinder the polymerization.

These CTFE-VAc-PDMSMA terpolymers will likely find application as high temperature lubricants or release agents. For example, the fuser roller system used in electrophotographic printing uses reactive silicone oil that coats a fluoroelastomer. The reactive silicone oil, which prevents the ink from depositing on the heated fuser roller, decomposes at 150 °C, yet the operating temperature of the fusing system is between 200° and 260 °C [77]. Therefore, obtaining a release agent that is capable of operating at 200° to 260 °C is desired.

A polymer that meets all three criteria above has been synthesized and characterized in Chapter 4. Maintaining the use of CTFE, as in the emulsion polymerizations in Chapter 3, fulfills the first criteria of increasing the fluorocarbon reactivity. Replacing the PDMSMA with monomethacryloxypropyl-terminated polyhedral oligomeric silsesquioxane (POSSMA), a cage structure where each silicon atom is bonded to three oxygen atoms versus the linear structure of the siloxane in PDMSMA, fulfills the second as the bulk of the pendant group is closer to the propagating radical, increasing the steric hindrance and reducing the reactivity. Furthermore, polyhedral oligomeric silsesquioxane (POSS) structures have higher thermal stability than comparable linear siloxanes [78] fulfilling the third criterion. In addition to the thermal stability, the flammability of these polymers was also examined as both CTFE and POSS are known for being low flammability compounds [79-83]. As will be seen this approach also eliminates the hydrocarbon component, VAc. The elimination of VAc is beneficial as it is the point of initial

thermal decomposition [62] and its removal may lead to polymers of greater thermal stability. The VAc also has the highest surface energy of the three components [39] suggesting it provides little value with respect to this property. The POSS-containing polymers may find similar applications to the PDMSMA based terpolymers as lubricants and release coatings with the added benefit of low flammability. The low flammability may allow the polymers to find alternative applications, such as additives to paint formulations.

These applications, release coatings and additives to paint formulations, also drive the selection of CTFE as the comonomer for the reverse fluorosilicones. In these applications, adhesional wetting is important. Adhesional wetting is the wetting of a solid by a liquid that was not previously in contact with said solid [84]. This can be described by the decrease in Gibbs free energy per unit area when two dissimilar bodies (e.g., a release coating and the object to be released) are brought together as shown in Figure 1.4 and described by Equations (1.1) through (1.3) [85] where γ_{sl} , γ_{sv} and γ_{lv} denote the surface free energy of the solid-liquid, solid-vapour and liquid-vapour interfaces, respectively; ΔG_{sl}^a denotes the Gibbs free energy associated with the process; and θ denotes the contact angle.

$$\Delta G_{sl}^a = \gamma_{sl} - \gamma_{sv} - \gamma_{lv} \quad (1.1)$$

$$\gamma_{sv} = \gamma_{sl} + \gamma_{lv} \cos \theta \quad (1.2)$$

$$\Delta G_{sl}^a = -\gamma_{lv} (1 + \cos \theta) \quad (1.3)$$

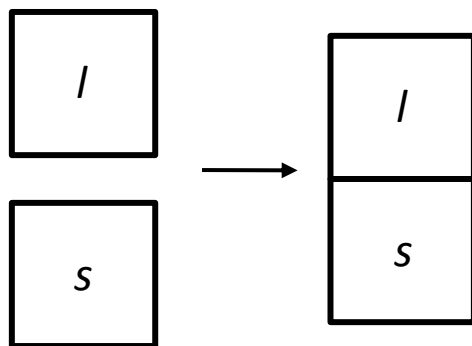


Figure 1.4: Schematic of thermodynamic adhesion process (adapted from [85])

From Equation (1.3), it can be seen that as the contact angle increases (i.e., the surface energy of the coating reduces), the reduction in Gibbs free energy that occurs when the bodies are brought together is smaller. Therefore, the barrier that must be overcome to separate the two bodies is also reduced and the low surface energy coating releases the object more easily. A similar situation applies for those release coatings where the coating itself is separated to allow release although it is the energy associated with cohesion rather than adhesion that is important. A contact angle of 180° implies zero reduction in the Gibbs free energy and no adhesion, a perfect release coating.

For a release coating to function, the solid or liquid must be withdrawn from the coating. Therefore, the receding contact angle is important. The receding contact angle is determined by the highest surface energy component that is found at the surface of the coating. Therefore, to optimize the performance of the coating the receding contact angle should be as great as possible with the maximum receding contact angle being equal to the advancing contact angle (i.e., no contact angle hysteresis). Based on the definition of reverse fluorosilicones, a fluorinated backbone and pendant siloxane group, there are two methods to minimize the

contact angle hysteresis. The first method is to select fluorinated and siloxane-containing components that have identical surface energy. The surface tension of PDMS is approximately 20 mN/m [39] and the fluoromonomers with the most similar surface tensions are TFE and HFP at 23.9 and approximately 14.9 mN/m, respectively [39]. As the surface tension is not identical, both cases will lead to contact angle hysteresis and potentially poor coating performance.

The second method is to select a fluoromonomer that has a higher surface energy than the siloxane-containing component. This will drive the siloxane-component to the surface, particularly as in reverse fluorosilicones the siloxane is in the pendant location. This method was chosen as it is believed that it will have a greater likelihood of preventing the undesired contact angle hysteresis. Thus fluoromonomers such as CTFE, vinyl fluoride (VF) and vinylidene fluoride (VDF) are potential candidates. However, both VF and VDF will form more random copolymers with VAc than CTFE. As r_1 , r_2 and r_1r_2 reduce to zero for a monomer pair, there is a greater tendency for alternation in the polymer backbone. Table 1.8 shows that r_1r_2 equals 0.87, 0.48 and 0.01 for VDF, VF and CTFE, respectively, based on literature values [39]. The alternation of the fluoromonomer and VAc in the polymer backbone increases from VDF to VF to CTFE. For this to occur, the probability of CTFE reacting with VAc and vice versa is greater than for the other fluoromonomers. This is confirmed for the VDF-VAc system where Baradie and Shoichet [72] show no alternating triads for this combination of monomers. Therefore, the reaction of CTFE and VAc is likely to proceed more easily than for VDF and VF. Furthermore, the yields of VDF-VAc copolymers are reduced relative

to CTFE-VAc copolymers [72] and VF is a Group 2A carcinogen [86]. This designation states that VF is probably carcinogenic to humans.

Table 1.8: Reactivity ratios for fluoromonomer (1) and vinyl acetate (2)

Fluoromonomer	r_1	r_2	$1/r_1$	r_1r_2
VDF*	3.5	0.25	0.29	0.87
VF*	6.0	0.08	0.16	0.48
CTFE [†]	0.024	0.43	41.0	0.01

* r_1 and r_2 values obtained from [39]

[†] r_1 and r_2 values calculated in this work

1.5 Hypotheses

Traditional fluorosilicones are prone to depolymerization at elevated temperatures due to chain scission. This chain scission is enhanced by the presence of acid or base catalysts that may remain from reactions used to functionalize the siloxane backbone. For example, a reactive silicone oil found in the fuser roller system for electrophotography degrades at 150 °C [77] whereas a non-functional pure silicone decomposes at temperatures greater than 350 °C [11]. While methods such as crosslinking between siloxane chains have been used to enhance this thermal stability, these are not without drawbacks. One alternative to these methods is to reposition the thermally stable components, Si and F, forming hybrid and reverse fluorosilicones. In hybrid fluorosilicones, fluorine moves from a pendant location in traditional fluorosilicones to one within the polymer backbone. In reverse fluorosilicones, the fluorine is in the backbone whereas the silicon is located in the pendant group.

Each class of fluorosilicones, hybrid and reverse, has been examined by others; however, there is room for improvement. For hybrid fluorosilicones,

fluoroalkyl, fluoroether and fluoroaromatic hybrids have been synthesized. Of these the fluoroaromatic hybrid demonstrated the most flexibility as the incorporation of siloxane links with greater than two silicon atoms is possible. However, these fluoroaromatic hybrids degrade at the ether oxygen linking the fluorinated and aromatic components suggesting that removal of this oxygen link will enhance the thermal stability. Reverse fluorosilicones of TFE-VAc-PDMSMA have been synthesized previously in supercritical CO₂. To improve the thermal stability, it appears that the removal of the hydrocarbon component, VAc, is desired. Two methods were examined to achieve this.

Based on the above, one general and three more specific hypotheses were proposed in this thesis. They are as follows:

1. the hybrid and reverse fluorosilicones synthesized herein will have higher thermal stability, as measured by the initial thermo-oxidative decomposition temperature, than traditional fluorosilicones;
2. removal of the ether oxygen (i.e., directly linking the fluorinated and aromatic component) will increase the thermal stability, as measured by the initial thermo-oxidative decomposition temperature, of the resulting hybrid;
3. moving from a supercritical CO₂ polymerization medium to an aqueous-based medium and changing from TFE to CTFE will modify the reactivity ratios between the fluorocarbon and siloxane-containing monomers such that a copolymer can be synthesized;
4. changing the fluoromonomer from TFE to CTFE and the silicon-containing monomer from PDMSMA to POSSMA will modify the reactivity ratios such

that a copolymer of CTFE and POSSMA can be synthesized using supercritical CO₂.

1.6 Objectives

To confirm the above hypotheses the following main objectives were set:

1. synthesize a hybrid fluorosilicone based on a fluorinated component consisting of the thermocyclodimerized product of 1-bromo-4-(trifluorovinyl)benzene;
2. synthesize a series of CTFE-PDMSMA copolymers by emulsion polymerization and CTFE-VAc-PDMSMA terpolymers by emulsion and in supercritical CO₂;
3. synthesize a series of CTFE-POSSMA copolymers in supercritical CO₂;
4. compare the thermo-oxidative decomposition temperatures of the above synthesized polymers to traditional fluorosilicones.

The above objectives will not only confirm the four hypotheses, but also allow for the study of other parameters associated with the formation of the polymers.

Completing objective 1 will allow for an examination into the effect of removing the ether oxygen on the synthesis and glass transition temperature. Additionally, the synthesis of such a polymer will confirm the effect of siloxane length on decomposition temperature and the low temperature capabilities of fluoroaromatic hybrid fluorosilicones.

Completing objective 2 will allow for direct comparison as to the effect of polymerization media on branching as current comparisons are confounded by

differing molar masses. The polymers were also characterized with respect to composition, molar mass, and viscosity.

Completing objective 3 will allow for the homopolymerization of POSSMA in scCO₂ as a basis of comparison, providing an environmentally responsible polymerization method for this polymer. The composition, reactivity ratios, molar mass, surface properties, glass transition temperature, thermal decomposition, and flammability of these polymers were also determined.

1.7 References

1. McNeill IC and Mohammed MH. *Polymer Degradation and Stability* 1995;48:175-187.
2. Chatterjee A and Deopura BL. *Journal of Applied Polymer Science* 2006;100:3574-3578.
3. Kokta BV, Valade JL, and Martin WN. *Journal of Applied Polymer Science* 1973;17:1-19.
4. Amir N, Levina A, and Silverstein MS. *Journal of Polymer Science Part A: Polymer Chemistry* 2007;45:4264-4275.
5. McNeill IC and Memetea L. *Polymer Degradation and Stability* 1994;43:9-25.
6. Maier C and Calafut T. *Polypropylene: The Definitive User's Guide and Databook*. Norwich, NY: Willam Andrew Inc., 1998.
7. Sperling LH. *Introduction to Physical Polymer Science*, 2nd ed. Toronto: John Wiley & Sons, Inc., 1992.
8. Hatakeyama T and Quinn FX. *Thermal Analysis: Fundamentals and Applications to Polymer Science*, 2nd ed. Toronto: John Wiley & Sons, 1999.
9. Conesa JA and Font R. *Polymer Engineering and Science* 2001;41(12):2137-2147.
10. Edwards A, Blumstengel S, Sokolik I, Yun H, Okamoto Y, and Dorsinville R. *Synthetic Metals* 1997;84:639-640.
11. Brook MA. *Silicon in Organic, Organometallic, and Polymer Chemistry*. Toronto: John Wiley & Sons, Inc., 2000.
12. Atkins PW. *Physical Chemistry*, 5th ed. New York: W.H. Freeman and Company, 1994.
13. Holland BJ and Hay JN. *Polymer* 2002;43(8):2207-2211.
14. Pierce OR and Kim YK. *Rubber Chemistry and Technology* 1971;44(5):1350-1362.
15. Wang Y and Quirk RP. *Macromolecules* 1995;28(10):3495-3501.
16. Grassie N and Speakman JG. *Journal of Polymer Science Part A-1* 1971;9:919-929.
17. Ishida H and Lee Y-H. *Polymer* 2001;42:6971-6979.

18. Shimizu T. Fluorinated Acrylic Ester Polymers. In: Scheirs J, editor. Modern Fluoropolymers. Chichester, New York: Wiley, 1997. pp. 507-523.
19. Lousenberg RD and Shoichet MS. Journal of Polymer Science Part A-Polymer Chemistry 1999;37(16):3301-3308.
20. Maxson MT, Norris AW, and Owen MJ. Fluorosilicones. In: Scheirs J, editor. Modern Fluoropolymers. Toronto: John Wiley & Sons, 1997. pp. 359-372.
21. Pierce OR, Holbrook GW, Johansson OK, Saylor JC, and Brown ED. Industrial and Engineering Chemistry 1960;52(9):783-784.
22. Boutevin B and Pietrasanta Y. Progress in Organic Coatings 1985;13(5):297-331.
23. Patwardhan DV, Zimmer H, and Mark JE. Journal of Inorganic and Organometallic Polymers 1997;7(2):93-109.
24. Furukawa Y, Shin-Ya S, Miyake H, Kishino H, Yamada M, Kato H, and Sato M. Journal of Applied Polymer Science 2001;82:3333-3340.
25. Razzano JS. United States Patent 3997496, 1976
26. Bluestein BA and Evans ER. United States Patent 4317899, 1982
27. Kobayashi H. United States Patent 5371155, 1994
28. Guida-Pietrasanta F and Boutevin B. Advanced Polymer Science 2005;179:1-27.
29. Ikeno M, Tanaka M, Hara H, Fujiki H, Sato S, and Inomata H. United States Patent 5292848, 1994
30. Maxson MT. United States Patent 4732931, 1988
31. Blizzard JD and Swihart TJ. United States Patent 4465805, 1984
32. Elias JL, Lee C-L, and Maxson MT. United States Patent 4332368, 1989
33. Fujiki H. United States Patent 5236997, 1993
34. Evans ER. United States Patent 4355121, 1982
35. Bush RB and Evans ER. United States Patent 4525528, 1985
36. Evans ER and Matsumoto M. United States Patent 4585848, 1986
37. Evans ER. United States Patent 4960811, 1990
38. Takita K. United States Patent 6369155, 2002

39. Brandrup J, Immergut EH, and Grulke EA. Polymer Handbook, 4th ed. Toronto: John Wiley & Sons Inc., 1999.
40. Boutevin B and Youssef B. *Macromolecules* 1991;24(3):629-632.
41. Owen MJ and Kobayashi H. *Macromolecular Symposia* 1994;82:115-123.
42. Boutevin B, Guida-Pietrasanta F, and Ratsimihety A. *Journal of Polymer Science Part A-Polymer Chemistry* 2000;38(20):3722-3728.
43. Mera AE and Wynne KJ. *Abstracts of Papers of the American Chemical Society* 1998;216:806-807.
44. Miyake H, Shin-Ya S, and Furukawa Y. United States Patent 4814418, 1989
45. Furukawa Y and Yoneda T. *Journal of Polymer Science Part A-Polymer Chemistry* 2003;41:2704-2714.
46. Owen MJ and Groh JL. *Journal of Applied Polymer Science* 1990;40:789-797.
47. Scheirs J. *Modern Fluoropolymers: High Performance Polymers for Diverse Applications*. Toronto: John Wiley & Sons, 1997.
48. Longuet C, Ratsimihety A, Guida-Pietrasanta F, Ganachaud F, and Boutevin B. *E-Polymers* 2005:1-10.
49. Smith DW and Babb DA. *Macromolecules* 1996;29(3):852-860.
50. Rizzo J and Harris FW. *Polymer* 2000;41(13):5125-5136.
51. Ford LA and DesMarteau DD. *Chemical Communications* 2003:2596-2597.
52. Smith DW, Ji J, Narayan-Sarathy S, Neilson RH, and Babb DA. Fluorosilicones containing the perfluorocyclobutane aromatic ether linkage. In: Clarson SJ, editor. *Silicones and Silicone-Modified Materials*, vol. 729. Washington, D.C.: American Chemical Society, 2000. pp. 308-321.
53. Ameduri B, Boutevin B, Guida-Pietrasanta F, Manseri A, Ratsimihety A, and Caporiccio G. *Journal of Polymer Science Part A-Polymer Chemistry* 1996;34(15):3077-3090.
54. Boutevin B, Caporiccio G, Guida-Pietrasanta F, and Ratsimihety A. *Macromolecular Chemistry and Physics* 1998;199(1):61-70.
55. Boutevin B, Guida-Pietrasanta F, Ratsimihety A, and Caporiccio G. *Main Group Metal Chemistry* 1997;20(2):133-136.

56. Kim YK, Pierce OR, and Bourrie DB. *Journal of Polymer Science: Part A-1* 1972;10(3):947-953.
57. Riley MO, Kim YK, and Pierce OR. *Journal of Fluorine Chemistry* 1977;10(2):85-110.
58. Smith DW, Narayan-Sarathy S, Ji JM, Neilson RH, Traiphol R, and Perahia D. *Abstracts of Papers of the American Chemical Society* 2001;221:86-87.
59. Rizzo J, Harris F, and Meng HH. *Abstracts of Papers of the American Chemical Society* 1999;217:86-87.
60. Smith DW, Babb DA, Shah HV, Hoeglund A, Traiphol R, Perahia D, Boone HW, Langhoff C, and Radler M. *Journal of Fluorine Chemistry* 2000;104(1):109-117.
61. Dvornic PR and Lenz RW. *Macromolecules* 1992;25(14):3769-3778.
62. Baradie B and Shoichet MS. *Macromolecules* 2005;38:5560-5568.
63. Kennedy AP, Babb DA, Bremmer JN, and Pasztor AJ. *Journal of Polymer Science Part A-Polymer Chemistry* 1995;33(11):1859-1865.
64. Suzuki H, Takeishi M, and Narisawa I. *Journal of Applied Polymer Science* 2000;78(11):1955-1963.
65. Suzuki H, Kobayashi T, and Takeishi M. *Polymer Journal* 2000;32(5):447-451.
66. Baradie B, Lai PHM, and Shoichet MS. *Canadian Journal of Chemistry- Revue Canadienne De Chimie* 2005;83(6):553-558.
67. Owen MJ. *Journal of Applied Polymer Science* 1988;35:895-901.
68. Odian G. *Principles of Polymerization*, 4th ed. Hoboken, NJ: John Wiley & Sons, Inc., 2004.
69. Johnson M, Karmo TS, and Smith RR. *European Polymer Journal* 1978;14:409-414.
70. Ponratnam S and Kapur SL. *Journal of Polymer Science* 1976;14:1987-1992.
71. van der Meer R, Aarts MWAM, and German AL. *Journal of Polymer Science: Polymer Chemistry Edition* 1980;18:1347-1357.
72. Baradie B and Shoichet MS. *Macromolecules* 2002;35(9):3569-3575.

73. Baradie B, Shoichet MS, Shen Z, McHugh MA, Hong L, Wang Y, Johnson JK, Beckman EJ, and Enick RM. *Macromolecules* 2004;37(20):7799-7807.
74. Murray DL, Harwood HJ, Shendy SMM, and Piirma I. *Polymer* 1995;36(20):3841-3848.
75. Grcev S, Schoenmakers P, and Iedema P. *Polymer* 2004;45(1):39-48.
76. Jones CW. United States Patent 5723556, 1998
77. O'dell P. Mississauga, 2004. Meeting at Xerox Research Centre Canada.
78. Mantz RA, Jones PF, Chaffee KP, Lichtenhan JD, Gilman JW, Ismail IMK, and Burmeister MJ. *Chemistry of Materials* 1996;8(6):1250-1259.
79. Lyon RE and Janssens ML. Polymer Flammability. In: Administration USDoTFA, editor., 2005. pp. 58.
80. Schwab JJ and Lichtenhan JD. *Applied Organometallic Chemistry* 1998;12(10-11):707-713.
81. Bourbigot S, Duquesne S, and Jama C. *Macromolecular Symposia* 2006;233:180-190.
82. Devaux E, Rochery M, and Bourbigot S. *Fire and Materials* 2002;26(4-5):149-154.
83. Liu L, Hu Y, Song L, Nazare S, He SQ, and Hull R. *Journal of Materials Science* 2007;42(12):4325-4333.
84. Shaw DJ. *Introduction to Colloid and Surface Chemistry*. Boston, USA: Butterworth-Heinemann, 1992.
85. Good RJ. Contact Angle, Wetting and Adhesion: A Critical Review. In: Mittal KL, editor. *Contact Angle, Wettability and Adhesion*. Utrecht, The Netherlands: VSP, 1993. pp. 3-36.
86. Grosse Y, Baan R, Straif K, Secretan B, El Ghissassi F, Bouvard V, Altieri A, and Cogliano V. *Lancet Oncology* 2007;8:679-680.

2 Synthesis and Thermal Stability of a Perfluorocyclobutane-based Aromatic Hybrid Fluorosilicone¹

2.1 Abstract

Aromatic hybrid fluorosilicones, such as perfluorocyclobutane aromatic polyethers, have higher thermal stability than typical polysiloxanes. While these polyethers decompose by homolytic cleavage of the oxygen-perfluorocyclobutane bond, the enhanced thermal stability of the polyethers may, in part, arise from this oxygen through the anomeric effect. To determine the effect of the ether oxygen on thermal stability, two perfluorocyclobutane aromatic units, one with and one without the oxygen, were modeled. To confirm the results experimentally, a series of hybrid fluorosilicones based on the latter were synthesized by thermocyclodimerization of 1-bromo-4-(trifluorovinyl)benzene, silicon-halogen exchange, and condensation with one of: 1,3-dichlorotetramethyldisiloxane; 1,7-dichlorooctamethyltetrasiloxane; or chlorine-terminated poly(dimethylsiloxane). The decomposition temperature ($T_{1\%}$) was lower (~ 240 °C) than the comparable polyethers (~ 430 °C). These results demonstrate the importance of the ether oxygen to the stability of perfluorocyclobutane aromatic polyethers through a number of effects including the anomeric effect and enhancing the strength of the silicon-aromatic bond.

¹ Conrad, MPC and Shoichet MS. Polymer 2007;48(18):5233-5240.

2.2 Introduction

Polysiloxanes are known for excellent low temperature capabilities as well as chemical and thermal stability. Despite this thermal stability, polysiloxanes are prone to depolymerization at elevated temperatures due to random chain scission [1]. To prevent chain scission, various polysilalkylene and polysilarylene siloxanes (hybrid silicones) have been synthesized. As described in a review by Guida-Pietrasanta and Boutevin [2], higher decomposition temperatures can be achieved with alternating polymers. Additionally, aromatic polymers generally have greater thermal stability than their linear counterparts [3]. Thus, an exactly alternating polysilarylene siloxane should have the highest decomposition temperature of the hybrid silicone class.

Fluoropolymers also have excellent thermal stability. Numerous authors [2, 4-8] have synthesized hybrid fluorosilicones, wherein the fluorinated moiety is incorporated into the polymer backbone, to take advantage of this fact. Research by Boutevin and coworkers [4-6] demonstrated that linear perfluorinated groups resulted in elevated decomposition temperatures ($T_{10\%} \sim 285 \text{ }^\circ\text{C}$). Moreover, hybrid fluorosilicones based on a perfluorocyclobutane aromatic ether showed even higher decomposition temperatures ($T_{1\%} \sim 430 \text{ }^\circ\text{C}$) [7, 8], likely due to the incorporation of an aromatic versus a linear spacer between the siloxane repeats of the copolymer.

The high thermal stability of the perfluorocyclobutane-based polymers arises despite the potential for cycloreversion due to the equilibrium nature of the $2\pi + 2\pi$ cycloaddition. Atkinson and Trenwith [9] examined the pyrolysis of tetrafluoroethylene and octafluorobutane and calculated activation energies for the

forward and reverse reactions at 25.4 kcal/mol and 74.1 kcal/mol, respectively. The overall dimerization reaction is exothermic (-48.7 kcal/mol) reflecting the stability of the perfluorocyclobutane ring with temperatures on the order of 500 °C required before the rate of reversion is significant. Smith and Babb [7] saw a similar heat of reaction in the formation of their hybrid fluorosilicones with a ΔH of -57 kcal/mol. Combined, these results suggest that despite the reversible nature of the $2\pi + 2\pi$ cycloaddition, the cycloreversion will be negligible for the perfluorocyclobutane group prior to thermal decomposition.

The thermal and oxidative decomposition of a thermoset based on the perfluorocyclobutane aromatic polyether was also studied (see Figure 2.1) [10]. Kennedy et al. postulate that the mechanism for decomposition includes chain scission at either the benzylic carbon or oxygen and subsequent decomposition of the resulting perfluorocyclobutene to hexafluorobutadiene. Thus, the oxygen appears to be one of the weak links in the polymer structure. However, further examination of the perfluorocyclobutane aromatic ethers reveals that these polymers have the requisite structure, R-X-A-Y, to exhibit the anomeric effect [11]. In R-X-A-Y, R is a hydrogen or alkyl group (aromatic ring), X is an element with lone pairs (oxygen), A has an intermediate electronegativity (carbon), and Y is more electronegative than A (fluorine). The group or element in parentheses denotes the corresponding moiety in the perfluorocyclobutane aromatic ethers. In the case of these polyethers, the stereoelectronic interpretation of the anomeric effect is relevant. The lone pair on oxygen mixes with the antibonding C-F σ orbital, resulting

in a lower energy molecular orbital. This, in turn, lowers the overall energy of the structure, giving greater stability to the polymer.

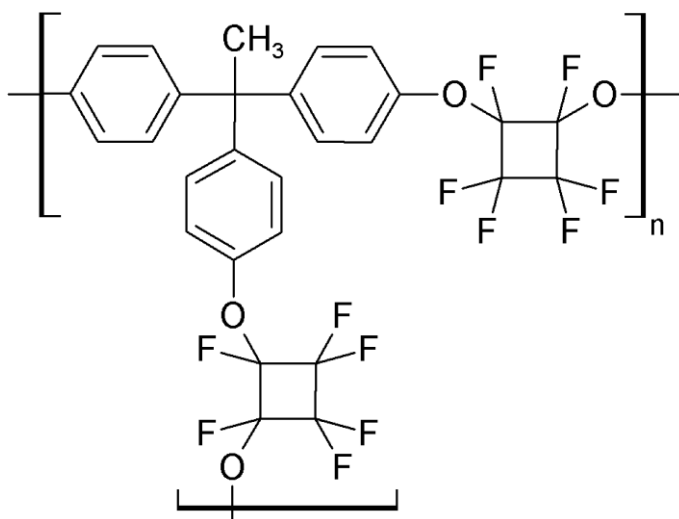


Figure 2.1: Perfluorocyclobutane aromatic ether thermoset (adapted from Kennedy et al. [10])

It was unclear whether removal of the ether oxygen would result in improved stability, due to prevention of homolytic cleavage, or reduced stability, due to elimination of the anomeric effect. This phenomenon was investigated because materials based on perfluorocyclobutane aromatic polyethers show promise in numerous applications: optical waveguides [12]; proton exchange membranes [13]; liquid crystals [14]; and coatings [15]. Two perfluorocyclobutane-based aromatic units, one with and one without oxygen (Figure 2.2), were modeled and compared experimentally by synthesizing a series of hybrid fluorosilicones based on **M2**.

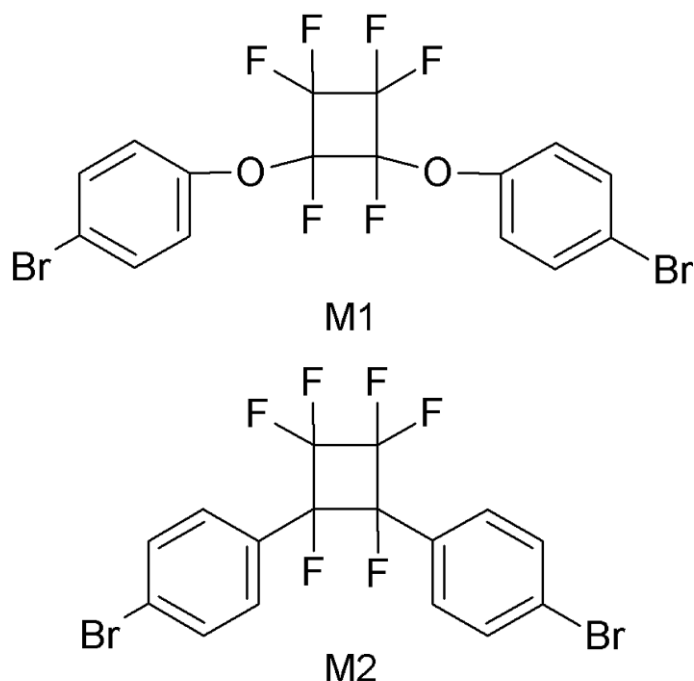


Figure 2.2: Perfluorocyclobutane-based aromatic units, **M1** was synthesized by Ligon et al. [16], **M2** was synthesized herein

2.3 Experimental

2.3.1 Modeling

Compounds **M1** and **M2** were optimized for geometry in mechanics using augmented Allinger molecular mechanics force field (MM3) [17] parameters. Subsequently, the heat of formation for each of the molecules was calculated based on this optimized geometry in the CAChe semi-empirical molecular orbital package (MOPAC 2002 Version 6.1.1.0) using parametric method 3 (PM3) [18] parameters.

2.3.2 Materials

4-Bromiodobenzene, *n*-butyl lithium, diethyl ether, anhydrous dimethylformamide, tetrakis(triphenylphosphine) palladium(0), and zinc dust were purchased from Sigma-Aldrich (Ontario, Canada). Isopropanol, methanol, pentane,

concentrated hydrochloric acid, and magnesium sulfate were purchased from Caledon (Ontario, Canada). Diethyl ether was dehydrated by passing over a neutral alumina column under an inert atmosphere. Inhibited bromotrifluoroethylene was purchased from SynQuest Laboratories Inc. (Alachua, Florida). The inhibitor was removed by inline filtration through chromatographic silica gel (200-425 mesh, Fisher Scientific, Ontario, Canada) prior to use. 1,3-dichlorotetramethyldisiloxane, 1,7-dichlorooctamethyltetrasiloxane, and chlorine-terminated polydimethylsiloxane (425-600 g/mol) were purchased from Gelest Inc. (Tullytown, Pennsylvania). Zinc dust was activated using a literature procedure [19].

2.3.3 Characterization

^1H NMR at 400MHz, ^{19}F NMR at 376MHz and ^{29}Si NMR at 79MHz spectra were obtained with a Varian Mercury 400-MHz system with chloroform-d as the solvent. Infrared spectra were obtained of neat liquids placed on a Harrick Split Pea™ system equipped with a Si window attached to a Nicolet Avatar 370 MCT FTIR spectrophotometer. The gas chromatography/mass spectrometry (GC/MS) data were obtained from an HP5890 II gas chromatograph coupled with a VG Trio 1000 mass spectrometer. The method used was electron ionization at an energy level of 70 eV. For the polymer samples, only the mass spectra were obtained. An aliquot of polymer was placed into a small glass capillary tube, heated from 100° to 450 °C at 0.5 °C/s and the decomposition products analyzed. Polymer molar mass was measured by gel permeation chromatography (GPC, Viscotek VE2001 GPCmax) using a Viscotek TDA302 detector for refractive index. Using THF as the

mobile phase at a flow rate of 1 mL/min, polymer molar mass was calculated relative to polystyrene standards using two ViscoGEL™ columns (I-MBHMW-3807 and I-MBLMW-3807) in series.

Glass transition temperature (T_g) was measured using a TA Q1000 differential scanning calorimeter (DSC), under a nitrogen atmosphere, at a heating rate 10 °C/min and scanning range of -90° to 125 °C. Thermogravimetric analysis (TGA) was performed using a TA Q50 instrument under a compressed air atmosphere at a heating rate of 5 °C/min and scanning range of 25° to 600 °C. See the following Appendices for detailed spectra and curves: NMR (A), FT-IR (B), GC/MS (C), GPC (D), DSC (E), and TGA (F).

2.3.4 Synthesis of Monomers

1-bromo-4-(trifluorovinyl)benzene (**12**) was synthesized as shown in Scheme 2.1, based on work by Burton and others [20-23] and specifically the method outlined by Heinze and Burton [20] involving bromotrifluoroethylene was used. In an inert atmosphere, activated zinc powder (9.3 g, 142 mmol) and a magnetic stir bar were placed in a 250 mL, three-neck round-bottom flask. This was connected to a dry ice/isopropanol condenser. Anhydrous dimethylformamide (DMF) (99.4 g) was added by cannula. A gas cylinder containing bromotrifluoroethylene was connected to both the flask and a vacuum line through a series of Swagelok® fittings. The gas line was evacuated and purged with nitrogen. Bromotrifluoroethylene (**2**) (34.4 g, 207 mmol) was slowly added while maintaining the temperature of the flask between 0° and 10°C with an ice bath; a brown mixture resulted. The amount of gas added

was determined by weight difference. After the full amount of gas was added, the mixture was brought to room temperature and stirred for an additional 4 h.

In an inert atmosphere, a second 250 mL, three-neck, round-bottom flask with a magnetic stir bar was charged with 4-bromoiodobenzene (24.8 g, 88 mmol) and tetrakis(triphenylphosphine) palladium ($\text{Pd}(\text{PPh}_3)_4$, 2.0 g, 2 mol% based on the aryl iodide). The zinc reagent formed in the previous step was transferred to this flask under inert atmosphere by cannula. The reaction was stirred overnight under an inert atmosphere at 30 °C.

The mixture was extracted with 25 mL of pentane five times (total of 125 mL). The resulting yellow solution was washed with 25 mL of 5% HCl three times and subsequently dried over magnesium sulfate. The solution was filtered through a silica gel column and concentrated. The residue was distilled under high-vacuum (25 mm Hg and 45 °C) to yield **12** (16.4 g, 79% - based on the aryl iodide). The synthesis was confirmed by ^1H and ^{19}F NMR, FT-IR spectroscopy and GC/MS.

^1H NMR (400 MHz, CDCl_3) δ : 7.54 (d, 2H, Ar), 7.32 (d, 2H, Ar).

^{19}F NMR (375 MHz, CDCl_3) δ : -99.0 (dd, F_{cis}), -113.8 (dd, F_{trans}), -177.5 (dd, F_{α});

$J_{\text{cis-trans}} = 69$ Hz, $J_{\text{trans-}\alpha} = 110$ Hz, $J_{\text{cis-}\alpha} = 33$ Hz. IR (neat) 1759 (vs, $\text{CF}_2=\text{CF-}$),

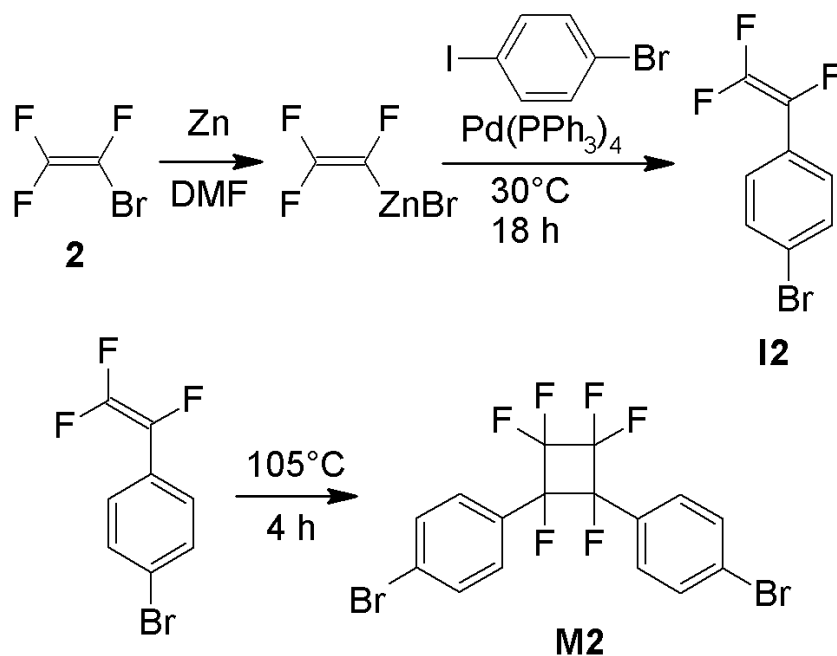
1593 (m), 1491 (m), 1402 (m), 1290 (vs, C-F), 1151 (s), 1072 (m), 983 (s), and

825 (s) cm^{-1} . Mass spectrum: $\text{C}_8\text{F}_3\text{H}_4^{81}\text{Br}^+$, 238 (100); $\text{C}_8\text{F}_3\text{H}_4^{79}\text{Br}^+$, 236 (100);

$\text{C}_8\text{F}_3\text{H}_4^+$, 157 (71); $\text{C}_8\text{F}_2\text{H}_3^+$, 137 (65); C_7FH_4^+ , 107(62).

1,1'-(1,2,3,3,4,4-hexafluorocyclobutane-1,2-diyl)bis(4-bromobenzene) (**M2**) was synthesized according to Scheme 2.1. A three-neck, 100 mL round-bottom flask was charged with 2.8 g (12 mmol) of **12**, sealed, purged with nitrogen, and

heated to 105 °C for 4 hours. Any remaining **I2** was removed through vacuum evaporation (50 °C, 30 mm Hg). This resulted in a *trans:cis* ratio of 56:44 (according to Ligon et al. [16]), as determined by comparing the integration of the aromatic peaks in ^1H NMR, and a yield of 86%. The synthesis of **M2** was confirmed by ^1H and ^{19}F NMR, FT-IR spectroscopy and GC/MS. ^1H NMR (400 MHz, CDCl_3) δ : 7.62 (d, 2H, Ar), 7.46 (d, 2H, Ar), 7.41 (d, 2H, Ar), 7.10 (d, 2H, Ar). ^{19}F NMR (375 MHz, CDCl_3) δ : -125.1 (m, 4 F_a), -164.1 (d, 2 F_b). IR (neat) 1593 (m), 1494 (s), 1369 (s), 1254 (m), 1185 (vs), 1076 (m), 1011 (m), 879 (m), 857 (s), 820 (m), and 794 (m) cm^{-1} . Mass spectrum: $\text{C}_8\text{F}_3\text{H}_4^{81}\text{Br}^+$, 238 (100); $\text{C}_8\text{F}_3\text{H}_4^{79}\text{Br}^+$, 236 (98); $\text{C}_8\text{F}_3\text{H}_4^+$, 157 (45); $\text{C}_8\text{F}_2\text{H}_3^+$, 137 (30); C_7FH_4^+ , 107 (48).



Scheme 2.1: Synthesis of monomers

2.3.5 Synthesis of Polymers

The hybrid fluorosilicones are synthesized by reacting *n*-BuLi with **M2** and subsequently forming a condensation polymer by adding a dichlorosiloxane as

shown in Scheme 2.2. A typical experiment is as follows. In a three-neck 100 mL round-bottom flask fitted with two equalizing addition funnels 1.94 g (4.1 mmol) of **M2** was dissolved in 3.6 g of anhydrous diethyl ether. This mixture was cooled to -78°C using an acetone/liquid nitrogen bath. The addition funnels were charged with 2.27 g (8.7 mmol) of *n*-BuLi (2.5M in hexanes) and 0.85 g (4.2 mmol) of 1,3-dichlorotetramethyldisiloxane (**a**), respectively. The *n*-BuLi was added dropwise to **M2** while maintaining the temperature at -78°C . The reaction mixture turned orange and was held at -78°C for approximately 1 h. The siloxane was then added dropwise. Afterwards, the mixture was brought to room temperature and stirred for at least 1 h. Any precipitate was removed by filtration and solvent was removed through rotary evaporation. The crude product was dissolved in ether and precipitated in methanol. The polymer was redissolved in ether, dried over MgSO_4 , filtered and any remaining ether was removed by vacuum drying. This resulted in 166 mg (0.3 mmol, 9%) of a tacky, orange solid (**P2a**). The synthesis of **P2a** was confirmed through ^1H , ^{19}F , and ^{29}Si NMR.

^1H NMR (400 MHz, CDCl_3) δ : 7.47 (m, 8H, Ar), 0.21 (m, 12H, $\text{OSi}(\text{Me}_2)\text{Ar}$).

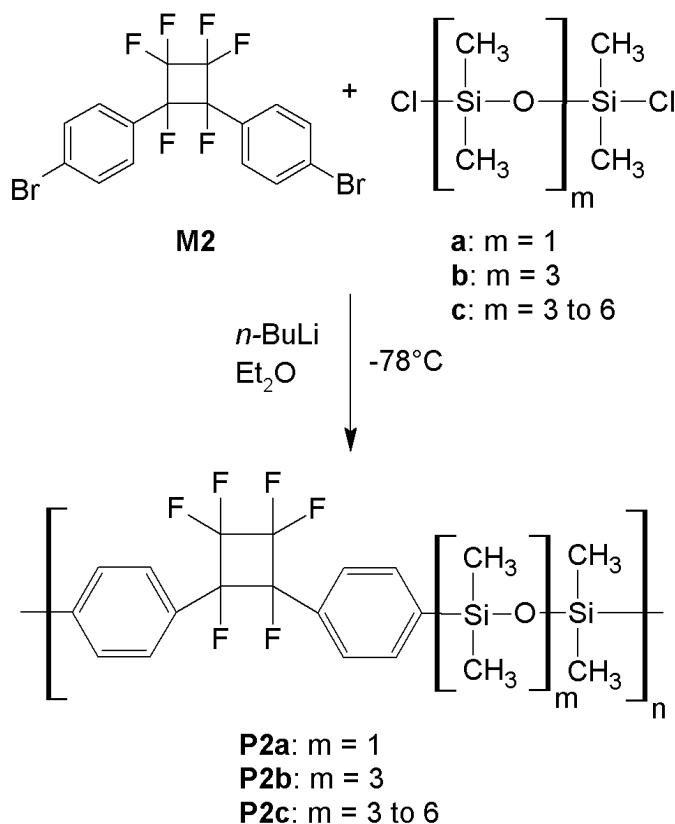
^{19}F NMR (375 MHz, CDCl_3) δ : -125.6 (m, 4F), -163.5 (d, 2F).

^{29}Si NMR (79 MHz, CDCl_3) δ : -0.64 (s, 2Si, $\text{OSi}(\text{Me}_2)\text{Ar}$).

The above reaction was also completed using 3.5 g (7.4 mmol) of **M2**, 4.9 g (18.9 mmol) of *n*-BuLi (2.5M in hexanes) and 2.7 g (7.7 mmol) of 1,7-dichlorotetramethyldisiloxane (**b**), yielding 990 mg (1.7 mmol, 23%) of a tacky, orange solid (**P2b**). The synthesis of **P2b** was confirmed through ^1H , ^{19}F , and ^{29}Si NMR. ^1H NMR (400 MHz, CDCl_3) δ : 7.63 (d, 2H, Ar), 7.55 (d, 2H, Ar),

7.44 (d, 2H, Ar), 7.20 (d, 2H, Ar), 0.28 (m, 12H, OSi(Me₂)Ar),
 0.02 (m, 12H, OSi(Me₂)O). ¹⁹F NMR (375 MHz, CDCl₃) δ: -124.9 (m, 4F),
 -163.3 (d, 2F). ²⁹Si NMR (79 MHz, CDCl₃) δ: -2.53 (s, 2Si, OSi(Me₂)Ar),
 -20.22 (s, 2Si, OSi(Me₂)O).

The synthesis of **P2c** is similar to that of **P2a** using 4.75 g (10 mmol) of **M2**, 5.37 g (21 mmol) of *n*-BuLi (2.5M in hexanes), and 5.13 g (10 mmol) of chlorine-terminated polydimethylsiloxane (**c**) yielding 2.42 g (3.2 mmol, 32%) of a tacky, orange solid (**P2c**). The synthesis of this polymer was also confirmed through ¹H, ¹⁹F, and ²⁹Si NMR. The NMR results for **P2c** are indistinguishable from those for **P2b**.



Scheme 2.2: Synthesis of polymers

2.4 Results and discussion

2.4.1 Modeling

The heats of formation for **M1** and **M2** are -1140 kJ/mol and -815 kJ/mol, respectively. These were calculated based on the optimized geometry in MOPAC using PM3 parameters. Therefore, 1,1'-[(1,2,3,3,4,4-hexafluorocyclobutane-1,2-diyl)bis(oxy)]bis(4-bromobenzene) (**M1**) is more stable by 325 kJ/mol. The majority of this stability arises from the inclusion of oxygen in **M1**. As shown in Table 2.1, the average decrease in ΔH_f is 150 kJ/mol per oxygen, which results in a difference of 300 kJ/mol between **M1** and **M2**. This would seem to suggest that the experimental work (i.e., the synthesis of polymers containing **M2** as the fluorinated component) discussed in the remainder of this Chapter is not justified as modeling demonstrates a significantly greater stability for **M1** and by extension polymers containing **M1**. However, work in Chapter 4 shows that the thermal stability of a polymer is not necessarily derived from the thermal stability of the constituent monomers but rather the decomposition mechanism. It is hypothesized that polymers with **M2** will have a different decomposition mechanism than those based on **M1** as the initial decomposition point (the ether oxygen) demonstrated by Kennedy et al. [10] is removed. Since the decomposition mechanism cannot be determined prior to experimentation, the experimental component of this Chapter is necessary.

Table 2.1: Effect of oxygen on ΔH_f taken from [24, 25]

Compounds	ΔH_f (kJ/mol)	$\Delta\Delta H_f$ (kJ/mol)	ΔH_f per oxygen added (kJ/mol)
Methane / Methanol	-75 / -201	126	126
Ethane / Ethanol	-85 / -235	150	150
Ethane / Ethylene glycol	-85 / -390	305	153
Propane / Propanol	-104 / -269	165	165
Propane / Glycerol	-104 / -586	482	161
Butane / Diethyl ether	-126 / -253	109	109
Benzene / Phenol	83 / -96	179	179

Compound **M1** also displays the requisite structure for the anomeric effect and should be stabilized by an additional 5 to 10 kJ/mol. Interestingly, Ligon et al. [16] show the dihedral angle of the cyclobutane ring for *trans*-**M1** to be 16° and for *cis*-**M1** to be 4° . The dihedral angle for perfluorocyclobutane is $20 \pm 4^\circ$ [26]. Thus, while the dihedral angle for the *trans*-**M1** falls within this range, *cis*-**M1** has additional ring strain from adopting the planar form. Modeling of **M2** suggests that both the *cis* and *trans* forms adopt the puckered conformation and should be present in nearly equal amounts, yet the ratio of *trans*:*cis* is 56:44 compared with 53:47 for **M1**. The relative increase in the *cis* isomer for **M1** may be due to stabilization of the planar form by the anomeric effect as the barrier between the planar and puckered conformation is 6 kJ/mol [26].

There is also the potential for compounds **M1** and **M2** to form 1,2-disubstituted (as shown in Figure 2.2) or 1,3-disubstituted products. Ligon et al. [16] showed that the 1,3-disubstituted product was formed in minor amounts. This formation and amount of 1,3-disubstituted product was not confirmed for **M2** since the focus of this

work was on the condensation polymerization of the hybrid fluorosilicone and the presence of the 1,3-disubstituted product will not detrimentally affect this reaction.

2.4.2 Polymerization

A family of hybrid fluorosilicones was synthesized by a condensation polymerization between **M2** and dichlorosiloxanes of varying lengths. Results are summarized in Table 2.2.

Table 2.2: Summary of molar mass and thermal properties for hybrid fluorosilicones, P2a to P2c.

Polymer	M _w ^a (kg/mol)	M _n ^a (kg/mol)	M _w /M _n	T _g ^b (°C)	T _{1%} ^c (°C)
P2a	1.9	1.5	1.3	-7	237
P2b	9.3	2.8	3.3	-55	236
P2c	18	7.3	2.5	-77	241

^a Determined by GPC using polystyrene standards in THF at 35 °C.

^b Mid-point in change in slope in DSC thermogram obtained with a heating rate of 10 °C/min.

^c Temperature at which 1% weight loss was seen during TGA under air at a heating rate of 5 °C/min.

The synthetic scheme used in this work is similar to that demonstrated by Smith and Babb [7] and Rizzo and Harris [8]. Smith and Babb performed the condensation of the dichlorosiloxane with the 1-bromo-4-(trifluorovinyl)benzene prior to thermocyclopolymerization. While this gives a large degree of control over the final molar mass of the product, it leads to a somewhat reduced molar mass of 12 to 20 kg/mol depending on the siloxane linker. However, this method is unsuitable for polymers based on α,β,β -trifluorostyrene. The condensation cannot occur prior to thermocyclopolymerization because the reaction between the styrene and lithium-based nucleophiles leads to the formation of a stilbene [27]. Rizzo and Harris reverse the order of the condensation and thermocyclopolymerization

achieving higher molar mass of 52 to 58 kg/mol by using silanol self-condensation as the polymerization mechanism. Yet they also attach the silicon to the aromatic ring prior to thermocyclodimerization, which will lead to the formation of a stilbene for fluorinated styrene monomers. Stilbene formation can be completely avoided by the thermocyclodimerization of the styrene [28] prior to the addition of the nucleophile, removing the reactive fluorinated alkene.

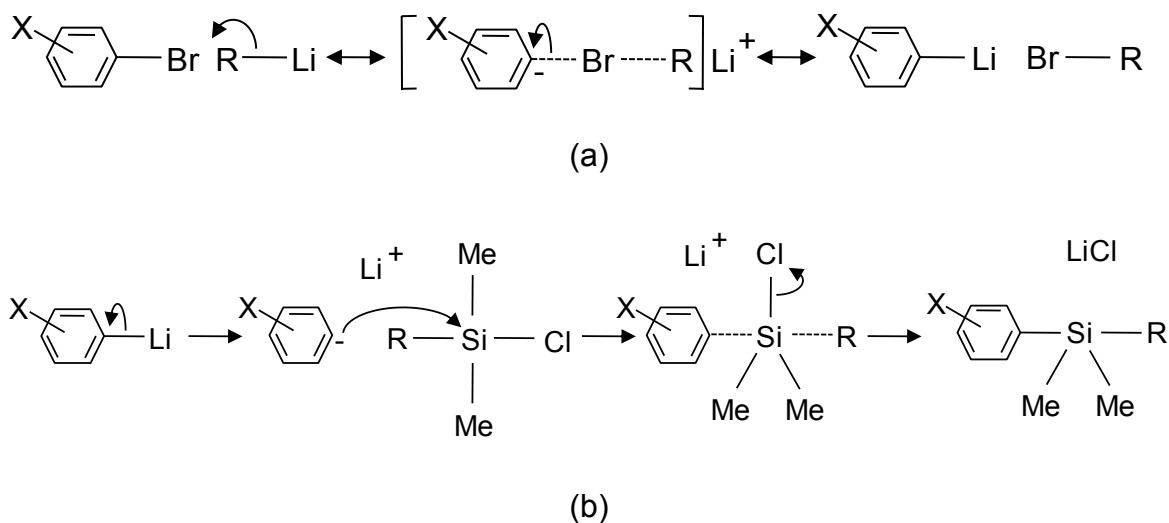
Rizzo and Harris also demonstrate that the effect of changing the condensation mechanism can be substantial. Moving from thermocyclodimerization to silanol self-condensation increases the molar mass by a factor of 3. However, they use chlorodimethylsilane to form their Si to aromatic attachment. While the Si-H is a less reactive leaving group than Si-Cl [29], the possibility exists for premature polymerization. Particularly since the hydrogen most readily reacts when attached to an arylsilane [29]. This was avoided herein by using dichlorosiloxanes and thus forming the desired polymer in one step. A drawback to changing the condensation mechanism is a severe reduction in molar mass which can be seen by comparing **P2b** ($M_n = 2.8$ kg/mol) to the equivalent perfluorocyclobutane aromatic polyether ($M_n = 58$ kg/mol) [8].

This reduction in molar mass is due to the change in condensation mechanism from the self-condensation of a disilanol to an overall silicon-halogen exchange reaction (lithium-halogen exchange followed by nucleophilic substitution at silicon). In the former, as well as the work by Smith and Babb [7], an A-B monomer is used and the molar mass of the polymer is dependent only upon the extent of reaction, p . However, in the latter (the work herein), the chain-forming reaction

occurs between two monomers: A-A and B-B. The molar mass depends on both the extent of reaction and the ratio of the monomers, r , as seen in Equation (2.1). An imbalance in the molar concentration of the starting reactants will reduce the degree of polymerization. Since Rizzo and Harris [8] form high molar mass polymer through the condensation of a dichlorosiloxane and disilanol, the inability to form high molar mass polymer likely results from either low efficiency of the metal-halogen exchange reactions as shown in Scheme 2.3 or competing side reactions that reduce the molar mass of the polymers synthesized herein.

$$\overline{DP}_n = \frac{1+r}{1+r-2rp} \quad (2.1)$$

There are two reactions that occur in Scheme 2.2: the exchange between n -BuLi and **M2** and the nucleophilic substitution between lithiated **M2** (Li-**M2**) and a dichlorosiloxane. These reactions are shown below in Scheme 2.3.



Scheme 2.3: Two step hybrid fluorosilicone condensation: (a) metal-halogen exchange and (b) nucleophilic substitution. X denotes an electron withdrawing group. Adapted from [29, 30].

Poor efficiency, ε_1 , of the first reaction will result in a reduction of r as it is not the ratio of **M2** to the dichlorosiloxane but rather the ratio of Li-**M2** to dichlorosiloxane that determines r . This also minimizes the impact of monomer purity on the degree of polymerization. Typically, high purity monomers are required to achieve a high degree of polymerization in condensation polymerizations. However, only those impurities in the monomer (**M2**) that can undergo lithium-halogen exchange will interfere with the desired condensation reaction. Furthermore, of those impurities that undergo lithium-halogen exchange only those that are mono-functional with respect to this reaction are of concern as they represent a capping reaction. Difunctional impurities will be incorporated into the polymer.

The minimum r value, r_{min} , can be calculated by setting $p = 1$ in Equation (2.1), i.e. the reaction between Li-**M2** and the dichlorosiloxane is quantitative. This results in r_{min} values of 0.74, 0.80 and 0.90 for **P2a**, **P2b**, and **P2c**, respectively, which are lower than the r values calculated from the monomer masses (0.98, 0.96, and 0.996). The difference is the efficiency of the lithium-metal exchange, since $r_{min} = r\varepsilon_1$, and the calculated ε_1 is between 76 and 92%. This corresponds well with similar reactions between *t*-BuLi and brominated trifluorovinyloxybenzene where yields of 58 to 78% are seen [31]. Additionally, mass spectroscopy of **P2b** and **P2c** show equal intensity peaks at 235.9 and 237.9 m/z , which arise due to the ratio of ^{79}Br to ^{81}Br , indicating the presence of bromine in the structure suggesting that all of the bromine in **M2** was not fully exchanged with lithium. A representative spectrum is shown in Figure 2.3.

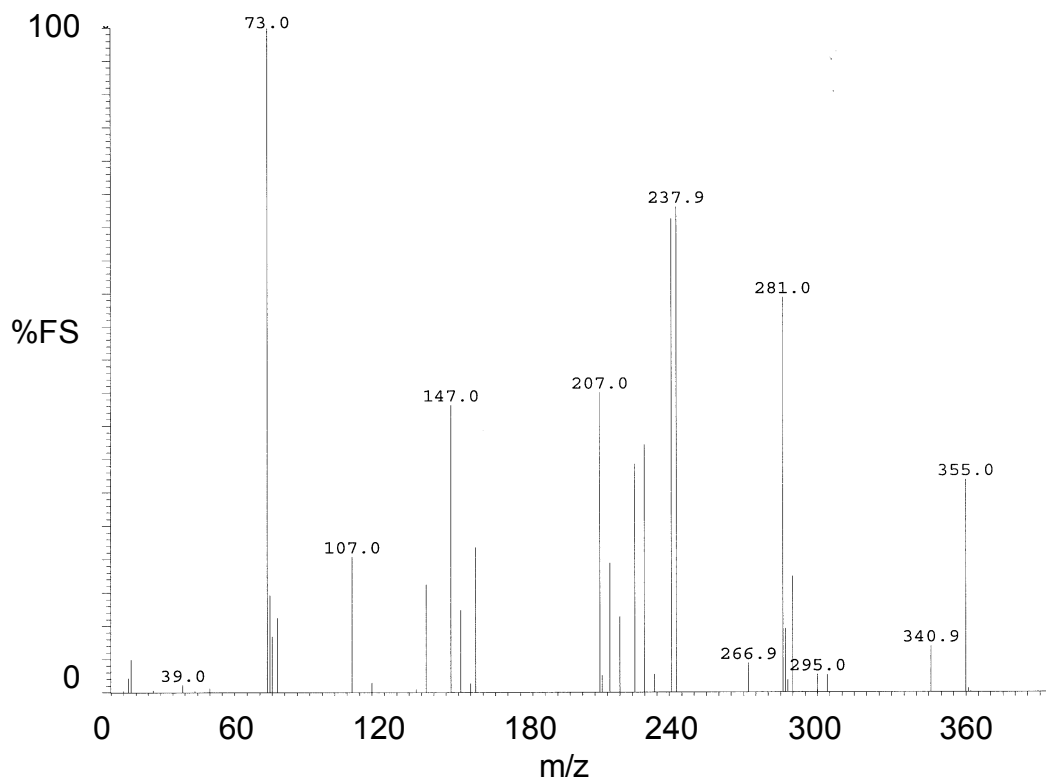


Figure 2.3: Mass spectra of P2c at 344 °C

The r value may also be reduced if the metal-halogen exchange only occurs at one of the bromines on **M2**. However, work by Larsen and Jørgensen [32] on calixarenes show that the number of bromines substituted corresponds to the number of equivalents of n -BuLi used, and thus, a molar ratio of **M2**: n -BuLi of 1:2 should result in a dilithium product. In contrast, Beak and Liu [33] show a mix of dibromo, monobromo and bromine-free products for a metal-halogen exchange, yet this occurs with t -BuLi. They add only one equivalent of t -BuLi whereas due to the equilibrium nature of the metal-halogen exchange reaction a second equivalent of t -BuLi is required to make the reaction irreversible [30].

Poor yield of the second reaction between Li-**M2** and the dichlorosiloxane will affect the extent of reaction, p . The minimum extent of reactions, p_{min} , which is

calculated by setting $r = 1$, is 0.85, 0.89, and 0.95 for **P2a**, **P2b**, and **P2c**. While these extent of reactions would be satisfactory for a wide variety of chemical reactions, for condensation polymerizations p is typically greater than 98 to 99% to achieve high molar mass polymers [34].

The alternative to poor lithium-halogen exchange efficiency is the presence of side reactions which can reduce both r and p . This possibility was examined by running the polymerization without one of the monomers (i.e., one reaction with only **M2** and one reaction with only the dichlorosiloxane). There appears to be no side reaction in the lithium-halogen exchange between n -BuLi and **M2** although there is evidence of leftover **M2**. This is not unexpected as it is unlikely that the reaction is quantitative as seen by both calculations of the lithium efficiency and the results of Ji et al. [31].

The second reaction results in the formation of a butyl-substituted siloxane, likely α,ω -butylsiloxane. This will reduce the expected amount of dichlorosiloxane available for reaction; however, this does not necessarily reduce r for the overall reaction. As less **M2** undergoes the lithium-halogen exchange, giving a lower ε_1 , r for the reaction will be reduced. Yet a similar reduction in the amount of dichlorosiloxane by side reactions will increase r since it is determined by the ratio of the reactive groups rather than their absolute number. A more detrimental effect of this side reaction is substitution of the chlorine by the butyl group which represents an end-capping reaction. This will reduce the molar mass of the polymers and may also affect the polydispersity.

The classical polydispersity index (PDI) for condensation polymerizations is 2.0. However, none of the polymers synthesized herein have PDIs which approach this number. Low polydispersities have previously been seen by Rizzo and Harris [8] and were attributed to fractionation during the methanol precipitation. This is likely the case for **P2a**. The high polydispersity for **P2b** is attributed to a low molar mass tail, which may arise from two sources: cyclic oligomers and a capping reaction. No evidence of cyclics was found in the GPC data, which suggests the latter is contributing to the broader molar mass distribution. Variation in the extent of reaction at which the capping reaction occurs will lead to broadening of the molar mass distribution. This also likely gives rise to the multiple peaks within the spectra of **P2b**, Figure 2.4. For example, higher molar mass peaks result from polymers where the capping reaction did not occur or was delayed relative to the lower molar mass peak. Polymer **P2c** most closely approaches the theoretical PDI value. In this case, the difference from theoretical is accredited to the dichlorosiloxane having a molar mass range rather than a specific molar mass.

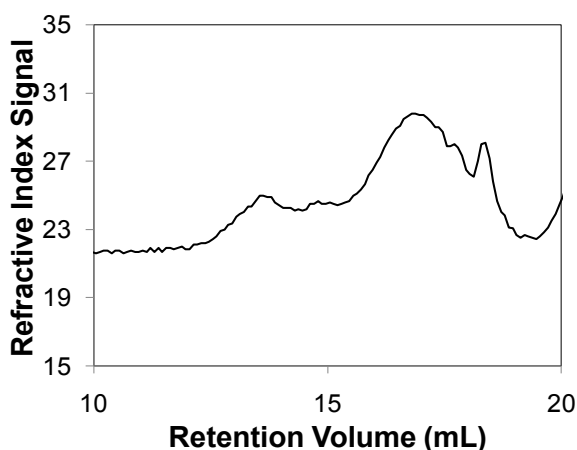


Figure 2.4: Gel permeation chromatography trace of P2b

While the polymerization scheme presented herein prevents the formation of a stilbene and potential premature polymerization, using lithium-halogen exchange as the condensation mechanism appears unsuitable for this particular combination of monomers. The efficiency of the reaction as well as potential side reactions results in a significantly lowered molar mass. However, this does not preclude an examination of the thermal properties of the oligomers formed.

2.4.3 Thermal Properties

The T_g of a polymer is affected by polymer chain flexibility, with increased flexibility resulting in a lower T_g . Similarly for copolymers, increasing the weight percent of the more flexible component yields a decrease in T_g . This effect has been observed in polysilarylene-siloxanes [35] and perfluorocyclobutane aromatic polyethers [8, 36]. The glass transition temperatures of the hybrid fluorosilicones synthesized herein follow the expected pattern of decreasing T_g with increasing weight percentage of siloxane, from **P2a** (-7 °C / 30 wt%) to **P2b** (-55 °C / 47 wt%) to **P2c** (-77 °C / 58 wt%), as shown in Figure 2.5. These results are tempered by the low molar mass of the three polymers. Rizzo and Harris [8] show that for a polymer similar to **P2a**, a molar mass of 50 kg/mol is required before T_g is independent of molar mass. This molar mass independent T_g (T_g^∞) can be calculated based on Equation (2.2) [34]:

$$T_g = T_g^\infty - \frac{K}{M}, \quad (2.2)$$

where T_g is the glass transition temperature of the polymer at molar mass M , and K is a constant. The K for the polymers synthesized herein is unknown, but can be

determined using work by Boyer [37]. Since the T_g of the polymers is known for a given M , there is only one point on the curve presented by Boyer, which relates T_g^∞ and K , that will satisfy Equation (2.2). This results in K values of 80, 20, and 10 kg·K/mol for **P2a**, **P2b**, and **P2c**, respectively. Using the same methodology gives $K = 60$ kg·K/mol for the polymer synthesized by Rizzo and Harris, which corresponds with their reported experimental value of 50 kg/mol. The corrected glass transition temperatures still follow the expected pattern of decreasing T_g with increasing weight percent siloxane, from **P2a** (46 °C) to **P2b** (-48 °C) to **P2c** (-76 °C); however the T_g values are higher than those measured experimentally.

The effect of copolymer composition on T_g can be determined through a number of equations. The base equation, Equation (2.3), from Couchman and Karasz [38] arises from a thermodynamic treatment where the T_g of a two component system is derived from the entropy of mixing due to conformational changes. This may be simplified through a number of assumptions. If the Simha-Boyer rule [39], which states that $T_g \times \Delta C_p$ is constant is applied, then Equation (2.3) simplifies to Equation (2.4). This is further reduced to Equation (2.5), the Fox equation, if $T_{g1} \sim T_{g2}$. Alternatively, if $\Delta C_{p1} \sim \Delta C_{p2}$ then Equation (2.3) reduces to Equation (2.6), which can be converted to a simple rule of mixtures, Equation (2.7), if $T_{g1}/T_{g2} \sim 1$.

$$\ln\left(\frac{T_g}{T_{g1}}\right) = \frac{w_2 \Delta C_{p2} \ln(T_{g2}/T_{g1})}{w_1 \Delta C_{p1} + w_2 \Delta C_{p2}} \quad (2.3)$$

$$\ln\left(\frac{T_g}{T_{g1}}\right) = \frac{w_2 \ln(T_{g2}/T_{g1})}{w_1 (T_{g2}/T_{g1}) + w_2}, \quad (2.4)$$

$$\frac{1}{T_g} = \frac{w_1}{T_{g1}} + \frac{w_2}{T_{g2}}, \quad (2.5)$$

$$\ln T_g = w_1 \ln T_{g1} + w_2 \ln T_{g2}, \quad (2.6)$$

$$T_g = w_1 T_{g1} + w_2 T_{g2}, \quad (2.7)$$

where T_g is the T_g of the copolymer; w_1 and w_2 are the weight percents of the respective components; and T_{g1} and T_{g2} are the T_g s of the respective components.

These equations can be used to obtain a value for T_{g2} , since the perfluorocyclobutane aromatic homopolymer is unavailable. Based on the structure of the fluorinated component and the known T_g of PDMS of -127°C (PDMS is the equivalent of the siloxane linker), the assumption that $T_{g1} \sim T_{g2}$ or $T_{g1}/T_{g2} \sim 1$ is likely invalid. Therefore, only Equations (2.4) and (2.6) will apply for these copolymers. Equation (2.3) is not used as a second unknown, the molar heat capacity of the perfluorocyclobutane aromatic homopolymer, is introduced.

For the series of copolymers based on **M1**, the T_g of the fluorinated homopolymer is 160 to 165°C [40]. The removal of the ether oxygen in **M2** is expected to raise this T_g slightly. Additionally, for each series of polymers (based on **M1** or **M2**) the T_g of a number of copolymers is known. By minimizing the sum of the squares of the error for each of Equations (2.4) and (2.6) an estimate of T_{g2} is determined with the results shown in Figure 2.5. Based on the known T_g for the

homopolymer of **M1**, the logarithmic rule of mixtures given in Equation (2.6) returns the best estimate with T_g s of **M1** and **M2** of 111° and 115 °C, respectively. This methodology underestimates the true T_g of the perfluorocyclobutane component. However, without the homopolymer available this represents the best estimate for T_{g2} . The T_g of the polyethers is on the order of the polymers without the ether oxygen. Therefore, the incorporation of the ether oxygen does not appear to enhance the flexibility of the polymer backbone as is typically the case, but rather has little effect. Interestingly, an increase in T_g for the polyether is seen when comparing the T_g of **P2b** at -48 °C (47 wt% siloxane) with an equivalent polyether at -12 °C and 45 wt% siloxane [8].

This may be explained by the anomeric effect, which provides enhanced stability to certain molecular conformations over others, for example, the preference for the axial rather than the equatorial position for alkoxy substituted pyranose rings [11]. As mentioned, the perfluorocyclobutane aromatic polyethers have the requisite structure to exhibit the anomeric effect. Thus, some conformations of these polymers will be preferred over others. The stabilization of these conformations represents an additional barrier to molecular movement, which increases the T_g of the polyethers above that of polymers without the ether oxygen.

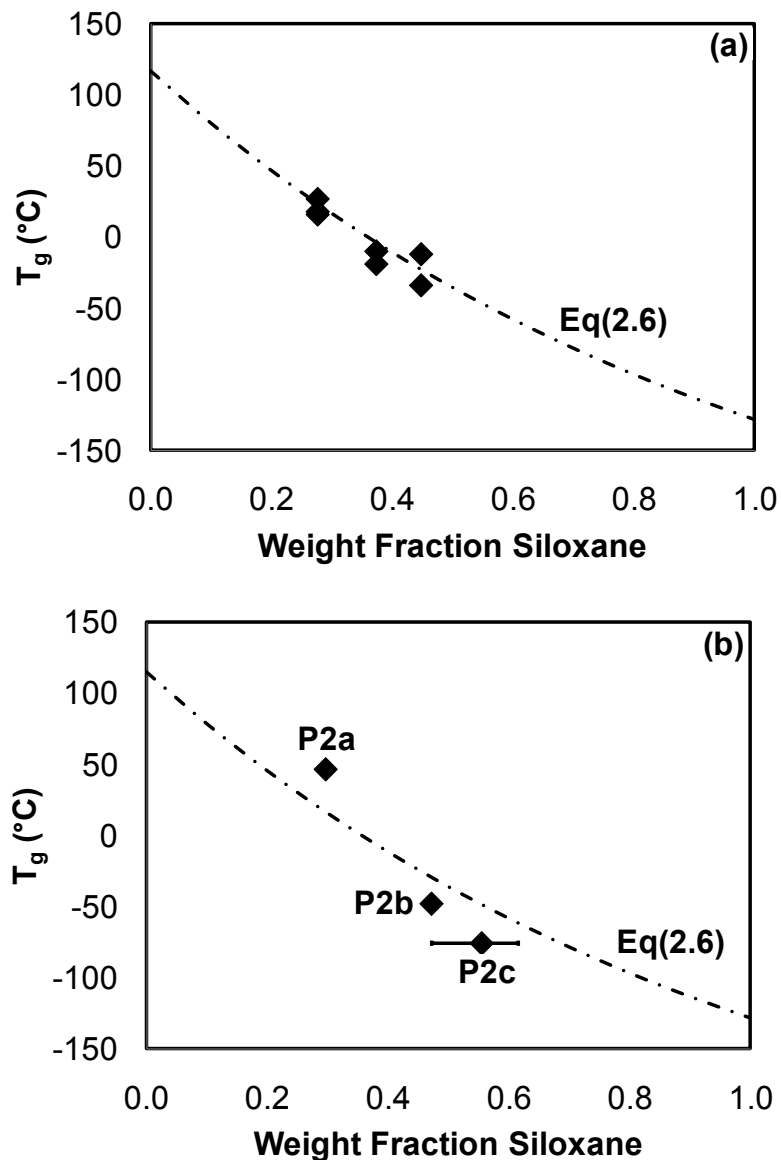


Figure 2.5: Comparison of experimental (◆) to calculated glass transition temperatures according to Equation (2.6): (a) Perfluorocyclobutane aromatic polyethers based on M1 [7,8,15], (b) Perfluorocyclobutane aromatic polymers based on M2, synthesized herein. The T_g values were calculated using a T_{g1} of -127 °C for polydimethylsiloxane

The greater thermal stability of the perfluorocyclobutane aromatic polyethers [36] was confirmed experimentally. The polymers based on **M1** degraded at much higher temperatures ($T_{1\%} \sim 432\text{ °C}$ in N_2) than those in this work ($T_{1\%} \sim 240\text{ °C}$ in air). This comparison is valid, despite the change in atmosphere, as research has shown

little to no difference in the onset decomposition temperature when the atmosphere is changed from air to N₂ [10]. Additionally, **P2b** was run in N₂ and gave T_{1%} of 212 °C. Air was considered the more industrially relevant of the two and all subsequent thermal analyses were run in this atmosphere.

While the length of siloxane linkage affected T_g, it had little to no effect on the T_{1%} as shown in Figure 2.6.

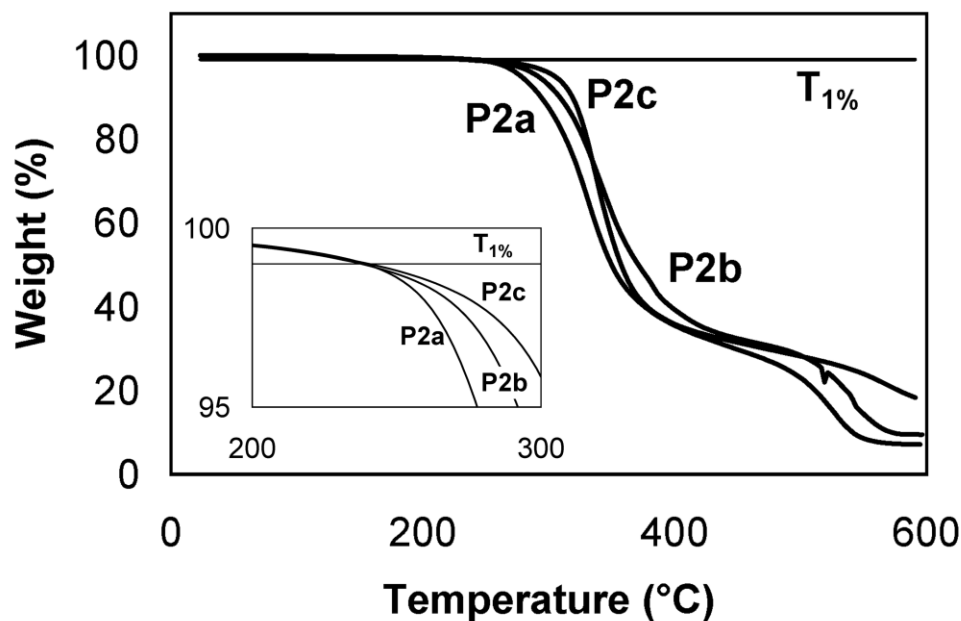


Figure 2.6: Thermal gravimetric analysis of hybrid fluorosilicones, P2a to P2c (5°C/min in air)

The lack of effect on T_{1%} for varying siloxane weight percent was also seen for perfluorocyclobutane aromatic polyethers [36]. Additionally, T_{1%} is independent of molar mass for the polymers in this work as shown in Table 2.2. A replicate of **P2b** was completed giving a T_{1%} of 243 °C, suggesting that for polymers examined under the same conditions variations in the T_{1%} of 7 °C may be observed. The difference in T_{1%} between **P2a**, **P2b** and **P2c**, which have differing molar masses, falls within this 7 °C error. This is contrary to the results for a series of linear polysiloxanes where a

reduction in molar mass led to a reduction in $T_{1\%}$, which suggests that the lower decomposition temperature measured for the hybrid fluorosilicones herein is due to the polymeric structure rather than the lower molar mass. It should be noted that trace amounts of $MgSO_4$ may catalyze the decomposition [29], but this was removed during purification and would unlikely result in nearly identical decomposition temperatures.

To determine the initial decomposition mechanism, polymers **P2b** and **P2c** were heated at $0.5\text{ }^\circ\text{C}/\text{min}$ from 100° to $450\text{ }^\circ\text{C}$, and the products were analyzed by mass spectrometry. Figure 2.7 was used as a basis for the determination of the volatile decomposition compounds with the peak assignments given in the associated table.

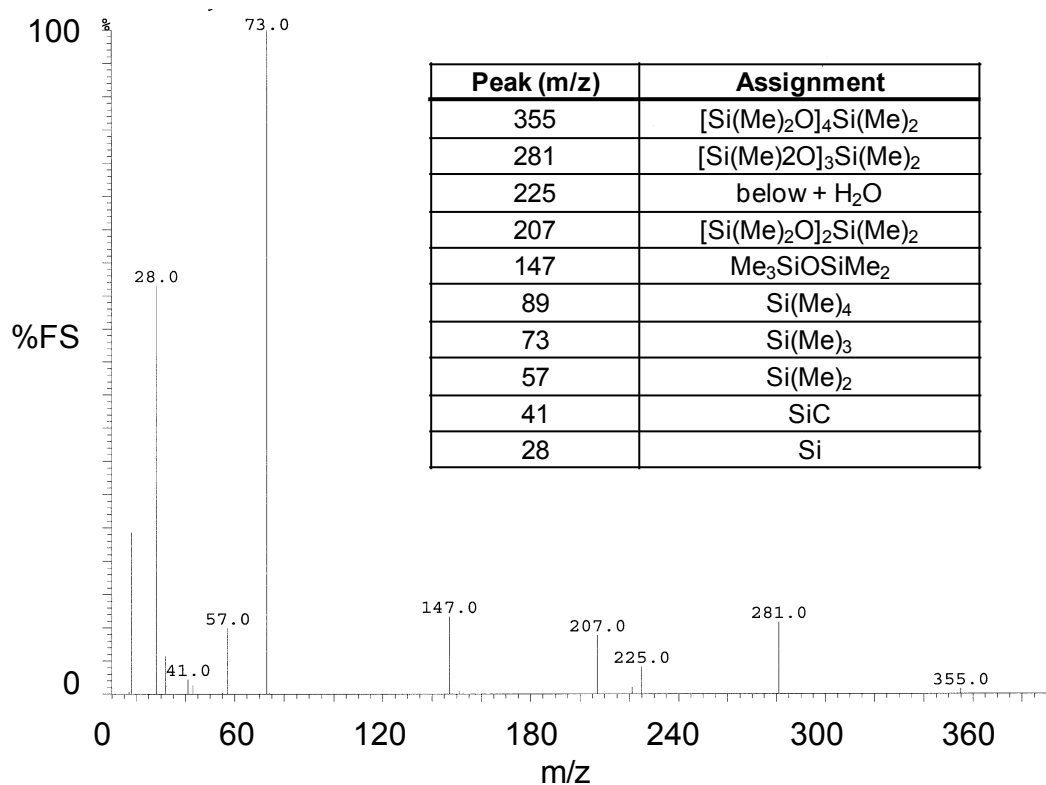


Figure 2.7: Mass spectra of P2c at $T = 239\text{ }^\circ\text{C}$

In the case of **P2c**, the first decomposition product observed at 322 °C is $[\text{Si}(\text{Me})_2\text{O}]_4\text{Si}(\text{Me})_2$ and lower order siloxanes, i.e. with 3 and 2 $[\text{Si}(\text{Me})_2\text{O}]$ units. This suggests that the initial decomposition step is cleavage of the Si-Ar bond. This is confirmed by the decomposition of **P2b** where $[\text{Si}(\text{Me})_2\text{O}]_3\text{Si}(\text{Me})_2$ is the only product observed until 299 °C. The lack of higher molar mass siloxanes, as seen in **P2c**, suggests that this decomposition is also the result of Si-Ar bond cleavage since the siloxane linker in **P2b** consisted of a linear tetrasiloxane. The Si-Ar bond cleaved is likely that associated with the end groups. The lack of higher molar mass siloxanes also suggests that linear siloxanes are not formed during polymerization.

At higher temperatures, the presence of a butyl siloxane provides experimental evidence for the postulated capping mechanism, where unreacted *n*-BuLi reacts with the growing chain, reducing the polymer molar mass. Above 330 °C, the first indication of a trifluorostyrene resulting from the cleavage of the perfluorocyclobutane ring is found. This includes traces of the brominated starting product, **M2**, confirming the likelihood of less than 100% efficiency for the lithium-halogen exchange reaction. At temperatures greater than 440 °C, the bond between the aromatic and perfluorocyclobutane rings is broken. Therefore, the postulated mechanism for decomposition is cleavage of the Si-Ar bond, followed by splitting of the perfluorocyclobutane ring, and breaking of the aromatic / perfluorocyclobutane C-C bond.

If the Si-Ar cleavage is the initial decomposition step, one would expect the decomposition temperature of the polymers synthesized herein to be comparable to

the aromatic polyethers. This is not the case, which implies that the Si-Ar bond in the polyethers must be stronger. Work by Hehre et al. [41] supports this hypothesis. They show that the π -electron density on the aromatic carbon para to an oxygen substituent is greater than the electron density for one opposite an alkyl fluoride (see Figure 2.8). This increased electron density on the carbon strengthens the Si-Ar bond, and the incorporation of oxygen has led to a second possible stabilization effect for these polymers.

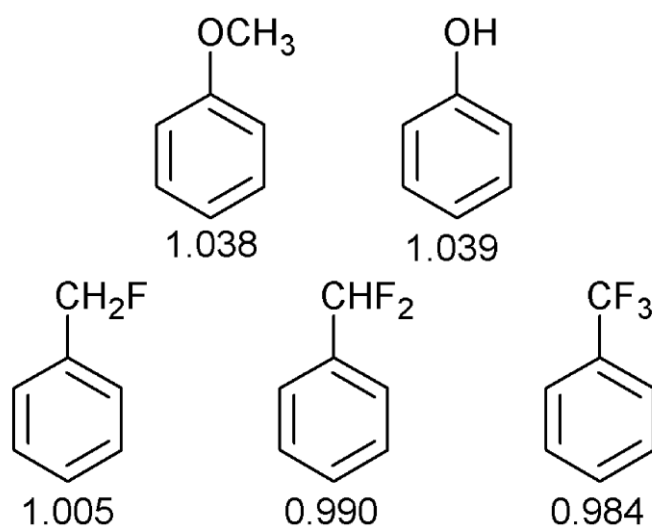


Figure 2.8: π -Electron density of carbon para to functional group on substituted benzenes (adapted from Hehre [41])

2.5 Conclusion

The effect of the ether oxygen on the stability of perfluorocyclobutane aromatic polyethers has been determined. Molecular modeling shows that an oxygen link between the perfluorocyclobutane and phenyl rings results in a more stable structure versus one with a direct perfluorocyclobutane to phenyl bond, with heats of formation of -1140 kJ/mol and -815 kJ/mol, respectively. This was confirmed experimentally by synthesizing a series of new fluorosilicones by the thermocyclodimerization of 1-bromo-4-(trifluorovinyl)benzene followed by condensation with a number of dichlorosiloxanes and comparing the thermal stability of these polymers to perfluorocyclobutane aromatic polyethers [8, 36]. In both modeling and experimental results, the polymers without the ether oxygen have lower thermal stability. This decrease in thermal stability does not arise from either an increased weight percent of the siloxane component or a decrease in molar mass. The reduced thermal stability is due to the removal of the ether oxygen. While the removal of this oxygen eliminates a possible decomposition pathway, it also eliminates the anomeric effect and the greater stability of the silicon-aromatic bond.

2.6 References

1. Dvornic PR and Lenz RW. High Temperature Siloxane Elastomers. New York: Huthig & Wepf Verlag Basel, 1990.
2. Guida-Pietrasanta F and Boutevin B. Advanced Polymer Science 2005;179:1-27.
3. Conley RT. Molecular Structure and Stability Criteria. In: Conley RT, editor. Thermal Stability of Polymers. New York: Marcel Dekker, Inc., 1970. pp. 21-45.
4. Boutevin B, Guida-Pietrasanta F, Ratsimihety A, and Caporiccio G. Main Group Metal Chemistry 1997;20(2):133-136.
5. Ameduri B, Boutevin B, Guida-Pietrasanta F, Manseri A, Ratsimihety A, and Caporiccio G. Journal of Polymer Science Part A-Polymer Chemistry 1996;34(15):3077-3090.
6. Boutevin B, Caporiccio G, Guida-Pietrasanta F, and Ratsimihety A. Macromolecular Chemistry and Physics 1998;199(1):61-70.
7. Smith DW and Babb DA. Macromolecules 1996;29(3):852-860.
8. Rizzo J and Harris FW. Polymer 2000;41(13):5125-5136.
9. Atkinson B and Trenwith AB. Journal of the Chemical Society 1953;July:2082-2087.
10. Kennedy AP, Babb DA, Bremmer JN, and Pasztor AJ. Journal of Polymer Science Part A-Polymer Chemistry 1995;33(11):1859-1865.
11. Juaristi E and Cuevas G. The Anomeric Effect. Ann Arbor: CRC Press, 1995.
12. Wong S, Ma H, Jen AKY, Barto R, and Frank CW. Macromolecules 2003;36(21):8001-8007.
13. Perpall MW, Smith DW, DesMarteau DD, and Creager SE. Polymer Reviews 2006;46(3):297-313.
14. Jin JY, Smith DW, Glasser S, Perahia D, Foulger SH, Ballato J, Kang SW, and Kumar S. Macromolecules 2006;39(14):4646-4649.

15. Smith DW, Babb DA, Shah HV, Hoeglund A, Traiphol R, Perahia D, Boone HW, Langhoff C, and Radler M. *Journal of Fluorine Chemistry* 2000;104(1):109-117.
16. Ligon SC, Krawiec M, Kitaygorodskiy A, and Smith DW. *Journal of Fluorine Chemistry* 2003;123(1):139-146.
17. Allinger NL, Yuh YH, and Lii JH. *Journal of the American Chemical Society* 1989;111(23):8551-8566.
18. Stewart JJP. *Journal of Computational Chemistry* 1989;10(2):209-220.
19. Tran-Van F, Garreau S, Louarn G, Froyer G, and Chevrot C. *Journal of Materials Chemistry* 2001;11(5):1378-1382.
20. Heinze PL and Burton DJ. *Journal of Fluorine Chemistry* 1986;31(1):115-119.
21. Heinze PL and Burton DJ. *Journal of Organic Chemistry* 1988;53(12):2714-2720.
22. Anilkumar R and Burton DJ. *Tetrahedron Letters* 2002;43(15):2731-2733.
23. Raghavanpillai A and Burton DJ. *Journal of Organic Chemistry* 2004;69(21):7083-7091.
24. Winnick J. *Chemical Engineering Thermodynamics: An Introduction to Thermodynamics for Undergraduate Engineering Students*. New York: Wiley, 1997.
25. Smith JM, Van Ness HC, and Abbott MM. *Introduction to Chemical Engineering Thermodynamics*, 5th ed. Toronto: The McGraw-Hill Companies, Inc., 1996.
26. Cotton FA and Frenz BA. *Tetrahedron* 1974;30(12):1587-1594.
27. Souzy R, Ameduri B, and Boutevin B. *Progress in Polymer Science* 2004;29(2):75-106.
28. Tellier F, Sauvetre R, Normant JF, Dromzee Y, and Jeannin Y. *Journal of Organometallic Chemistry* 1987;331(3):281-298.
29. Brook MA. *Silicon in Organic, Organometallic, and Polymer Chemistry*. Toronto: John Wiley & Sons, Inc., 2000.
30. Clayden J. *Organolithiums: Selectivity for Synthesis*. New York: Pergamon, 2002.

31. Ji J, Narayan-Sarathy S, Neilson RH, Oxley JD, Babb DA, Rondan NG, and Smith DW. *Organometallics* 1998;17(5):783-785.
32. Larsen M and Jørgensen M. *Journal of Organic Chemistry* 1996;61(19):6651-6655.
33. Beak P and Liu C. *Tetrahedron* 1994;50(20):5999-6004.
34. Odian G. *Principles of Polymerization*, 4th ed. Hoboken, NJ: John Wiley & Sons, Inc., 2004.
35. Dvornic PR and Lenz RW. *Macromolecules* 1992;25(14):3769-3778.
36. Smith DW, Ji J, Narayan-Sarathy S, Neilson RH, and Babb DA. Fluorosilicones containing the perfluorocyclobutane aromatic ether linkage. In: Clarson SJ, editor. *Silicones and Silicone-Modified Materials*, vol. 729. Washington, D.C.: American Chemical Society, 2000. pp. 308-321.
37. Boyer RF. *Macromolecules* 1974;7(1):142-143.
38. Couchman PR and Karasz FE. *Macromolecules* 1978;11(1):117-119.
39. Simha R and Boyer RF. *The Journal of Chemical Physics* 1962;37(5):1003-1007.
40. Babb DA, Ezzell BR, Clement KS, Richey WF, and Kennedy AP. *Journal of Polymer Science: Part A: Polymer Chemistry* 1993;31:3465-3477.
41. Hehre WJ, Radom L, and Pople JA. *Journal of the American Chemical Society* 1972;94(5):1496-1504.

3 Synthesis of Fluorosilicone Terpolymers through Emulsion or Supercritical Carbon Dioxide

3.1 Abstract

Terpolymers of chlorotrifluoroethylene (CTFE), vinyl acetate (VAc) and methacryloxypropyl-terminated polydimethylsiloxane (PDMSMA) were synthesized in supercritical CO₂ (scCO₂) or by emulsion polymerization. For the emulsion polymerizations, an organic soluble initiator and fluorosurfactant were required. In both cases, VAc was essential in facilitating cross-propagation between CTFE and PDMSMA. The terpolymers had M_ws between 1700 and 4900 kg/mol with polydispersities between 2.8 and 5.4. The terpolymers exhibited one T_g between 48° and 54 °C, and initial thermo-oxidative decomposition occurred between 231° and 278 °C. The emulsion system gave polymers with higher molar masses and thermal stability whereas comparable scCO₂ polymerizations had higher yields and incorporated more PDMSMA into the terpolymer. The branching between the two polymerization media, emulsion and supercritical CO₂, is similar suggesting little effect on polymer structure between the two methods.

3.2 Introduction

Fluorosilicones are used commercially as high-temperature lubricants and elastomers because of their excellent chemical, thermal, and thermo-oxidative resistance [1, 2]. Most fluorosilicone polymers consist of either polysiloxane macromers grafted onto fluorocarbon backbones or perfluorinated side chains grafted onto polysiloxane backbones [3-5] and have low molar masses (M_w = 20 to 60 kg/mol) [6] relative to those that can be obtained through radical polymerization.

Fluorosilicones resulting from multi-step condensation reactions also exhibit low molar masses ($M_w < 60$ kg/mol) [7, 8]. Fluorocarbon-siloxane copolymers have been synthesized by free radical polymerization [9, 10]; however, both the fluorocarbon and siloxane moieties were pendant to the hydrocarbon main chain, likely limiting overall thermal stability as the siloxane component, poly(methacryloxypropyl-terminated polydimethylsiloxane) [p(PDMSMA)] has a decomposition temperature of 226 °C [11] and the fluorocarbon component has a decomposition temperature on the order of 280 °C [12].

To achieve fluorosilicones with greater thermal stability, for use in electrophotography [13-15] for example, a terpolymer of tetrafluoroethylene (TFE), methacryloxypropyl-terminated poly(dimethylsiloxane) (PDMSMA) and vinyl acetate (VAc) in supercritical carbon dioxide (scCO₂) was synthesized by Baradie and Shoichet [11] who showed that VAc is necessary due to the 1000-fold difference in reactivity ratios between TFE and PDMSMA. However, the incorporation of VAc leads to a lower thermal stability, due to elimination of acetic acid from VAc at 244 °C, than may be achievable despite the use of highly thermally stable TFE. Furthermore, the VAc has the highest surface energy of the three components [16] suggesting it provides little value to the functionality of the terpolymer although it may have benefit in other unexamined areas such as mechanical properties. Thus, a copolymer of only siloxane and fluorine containing components is desired. To accomplish this, the reactivity ratios of the fluorocarbon and siloxane containing moiety must be modified to allow their copolymerization such that the reactivity of

the fluororadical is increased and/or the reactivity of the siloxane-containing radical is decreased.

To increase the reactivity of the fluororadical, the TFE used by Baradie and Shoichet [11] was substituted with CTFE as chlorine is less electronegative than fluorine leading to increased radical reactivity although this will be slightly offset due to the greater steric hindrance of the chlorine. An examination of the reactivity ratios of each of the fluoromonomers with VAc confirms similar reactivities;

$r_{TFE} = -0.009 \pm 0.61$ and $r_{VAc} = 0.95 \pm 0.08$ and $r_{CTFE} = 0.014 \pm 0.05$ and

$r_{VAc} = 0.44 \pm 0.03$ for the TFE-VAc and CTFE-VAc systems [17], respectively.

Coincidentally, the use of CTFE enhances the safety of the polymerization since TFE can polymerize explosively and the mitigating effect of the scCO₂ with which it forms a pseudo-azeotrope [18] is not available in the emulsion system.

One method used to modify reactivity ratios is to change the polymerization media. The change in reactivity ratios may arise from a number of phenomena including a shift in the heterogeneity, viscosity, pH or polarity of the system as discussed in Chapter 1, Section 1.4.3. For the fluoromonomer-VAc-PDMSMA system, it is believed that in moving from a scCO₂ based system to an emulsion polymerization, the heterogeneity, solvent polarity and viscosity will be modified. The effect may be minimal as both the scCO₂ based and emulsion polymerizations are likely heterogeneous and work by Baradie and Shoichet [17] and Murray et al. [19] show similar reactivity ratios between scCO₂ and emulsion for the same fluorocarbon-VAc pair.

From an industrial perspective, while scCO_2 is an environmentally benign solvent, gives enhanced solubility of the fluorinated and siloxane monomers, and leads to minimal post synthesis purification, the pressures required are on the order of 300 bar suggesting that the potential for industrial applicability may be limited. The formation of these fluorosilicones at lower pressures using a well-known industrial process is, therefore, desired; an added benefit to modifying the polymerization media.

Additionally, a comparison of the polymer structure, specifically branching, obtained by the two polymerization methods (emulsion and scCO_2) is of fundamental interest. Moreover, branching with VAc results in polymers with ester groups in the backbone which, upon hydrolysis, can cause a dramatic reduction in molar mass, which would be undesirable in terms of maintaining the polymer's physical properties [20]. Copolymers of TFE-VAc, chlorotrifluoroethylene (CTFE)-VAc, and vinylidene difluoride (VDF)-VAc synthesized by scCO_2 appear to be predominantly linear [17, 21] due to a reduction in the chain transfer to polymer while copolymers of TFE-VAc synthesized by emulsion contain long chain branches [18, 22]. Work by Grcev et al. [23] demonstrates a minimum molar mass threshold for long chain branching in VAc of approximately 1000 kg/mol. The molar mass (M_w) of the copolymers synthesized in scCO_2 is between 110 to 290 kg/mol [17, 21] while the molar mass of the copolymers synthesized by emulsion is between 1000 to 2000 kg/mol [22], falling below and above the threshold described by Grcev, respectively. Therefore, a direct comparison as to the effect of the two different polymerization media cannot be accomplished as it may be confounded by the

different molar masses. To determine the effect of polymerization media on branching, polymers of similar molar mass are required.

While these copolymers [17, 18, 21, 22] do not contain PDMSMA as in the work by Baradie and Shoichet [11], it is hypothesized that the effect of PDMSMA on branching will be minimal with the majority of the branching derived from VAc due to chain transfer to the polymer through the methyl group of VAc and terminal double-bond polymerization [24-27] from chain transfer to the monomer. Thus, the copolymers can be used as a basis of comparison with the terpolymers of Baradie and Shoichet as well as those synthesized in this work.

An examination of the CTFE, VAc, and PDMSMA system in an emulsion polymerization was undertaken in an attempt to modify the reactivity ratios seen in the TFE, VAc, and PDMSMA system. The use of emulsion will also allow for a direct comparison with previous work on the branching of VAc [18, 22] and represents the first emulsion polymerization of reverse fluorosilicones (i.e., a fluorosilicone where the siloxane component is pendant to the fluorinated backbone). Specifically, terpolymers of CTFE, VAc, and PDMSMA (shown in Figure 3.1) were synthesized by a modified-emulsion system and compared to similar polymers synthesized in $scCO_2$. The synthesis of poly(CTFE-*ter*-VAc-*ter*-PDMSMA) from either a $scCO_2$ or an emulsion based system was compared to better understand the effect of the polymerization media on: composition, molar mass, thermal stability, and branching. Assuming polymers of similar molar mass are achieved, the branching will shed further light on the linearity of fluorocarbon-VAc copolymer synthesized in supercritical CO_2 , potentially determining whether the linearity seen in $scCO_2$ is a

property derived from the polymer (i.e., molar mass) or from the polymerization medium.

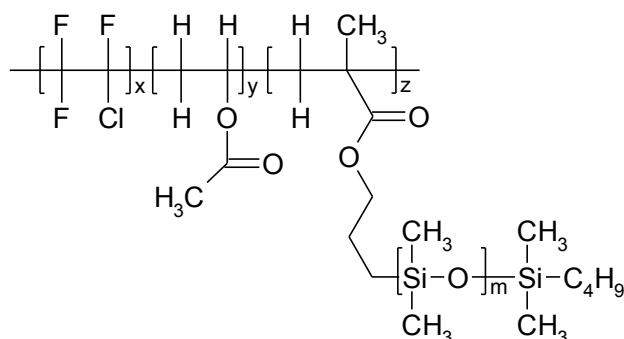


Figure 3.1: Repeat unit of the generic P(CTFE-VAc-PDMSMA) terpolymer, the pendant siloxane tail has $m = 8$ to 10 dimethylsiloxane repeat groups

3.3 Experimental

3.3.1 Materials

All reagents were used as received unless otherwise specified.

Chlorotrifluoroethylene, vinyl acetate, dichloromethane, and the fluorosurfactant Zonyl FSN-100 ($C_nF_{2n+1}CH_2CH_2O(CH_2CH_2O)_xH$ where $n = 3$ to 8 and $x = 20$ to 100) were purchased from Sigma-Aldrich Co. (Ontario, Canada). Azobisisobutyronitrile (AIBN) was supplied by E.I. Du Pont de Nemours as Vazo® 64.

Monomethacryloxypropyl-terminated polydimethylsiloxane (PDMSMA, MW = 800-1000 g/mol) was purchased from Gelest Inc. (Morrisville, PA). Supercritical fluid purity CO_2 was purchased from The Linde Group and contained less than 0.5 ppm of non-specified hydrocarbons, less than 0.001 ppm of non-specified halocarbons, and less than 2 ppm of water. Water was de-ionized and distilled from Millipore Milli-RO 10 Plus and Milli-Q UF Plus (Bedford, MA) systems at 18 M Ω resistance.

3.3.2 Characterization

Polymer molar mass was measured by gel permeation chromatography (GPC, Viscotek VE2001 GPCmax) using a Viscotek TDA302 detector for refractive index and viscosity. Using THF as the mobile phase at a flow rate of 0.6 mL/min; an injection volume of 100 μ L; a detector and column temperature of 22 $^{\circ}$ C; sample concentrations between 2.03 and 2.37 mg/mL; and PS standards between 0.9 and 1800 kg/mol, the polymer molar mass was calculated relative to polystyrene standards through a Universal Calibration using a GMHxl column. 1 H and 19 F NMR spectra (Varian 400 MHz spectrometer) were obtained in CDCl_3 at 399.95 and 376.30 MHz, respectively with α,α,α -trifluorotoluene (TFT) used as a reference. Since both H and F are high field elements, considerable modification of the spectrometer is required to decouple the signals. This was not justified in this thesis as the methine peak associated with the VAc provided sufficient detail of the polymer backbone structure. Glass transition temperatures (T_g) were measured using a TA Instruments Q1000 differential scanning calorimeter (DSC), under an inert nitrogen atmosphere, with a heating rate 10 $^{\circ}$ C/min and scanning range of -90 $^{\circ}$ to 150 $^{\circ}$ C. Thermogravimetric analysis (TGA) was performed using a TA Instruments Q50 Thermogravimetric Analyzer under a compressed air atmosphere, with a heating rate of 5 $^{\circ}$ C/min and scanning range of 25 $^{\circ}$ to 600 $^{\circ}$ C. See the following Appendices for detailed spectra and curves: NMR (A), GPC (D), DSC (E), and TGA (F).

3.3.3 Synthesis of Poly(CTFE-*ter*-VAc-*ter*-PDMSMA) by Emulsion

The free radical initiator, AIBN (2 mol% based on monomer mass), was recrystallized from methanol (0.3 M solution), dried in a vacuum oven for several hours at room temperature and then dissolved in the VAc/PDMSMA monomer mixture. A glass reactor equipped with a magnetic stir bar was fed with the Zonyl FSN-100 surfactant/water solution (1.2 wt% surfactant in 100 g of water) and the initiator/monomer solution and subsequently purged with nitrogen gas for at least 20 min. The reactor was evacuated after which gaseous CTFE was added by mass, for a total monomer mass of approximately 20 g. The accuracy of the scale for CTFE addition was ± 0.1 g. The reactor was then heated to 60 ± 1 °C to initiate polymerization. The estimated pressure of the CTFE in the reactor ranged from 6.9 to 10 bar depending on the volume of CTFE added. This estimation assumes all of the CTFE remained in the headspace. The vapour pressure of CTFE at 60 °C was calculated at 14.5 bar from Equation (3.1).

$$\log(P) = A + \frac{B}{T} + C \log T + DT + ET^2 \quad (3.1)$$

where P is the vapour pressure in mmHg and T is the temperature in K. The values A through E are constants as follows: A is 81.1728, B is -2915.2, C is -30.175, D is 2.3253×10^{-2} and E is 1.1177×10^{-13} [28]. Based on preliminary trials, the agitation rate was set to a speed that prevented coagulation of the polymer during polymerization but was not measured beyond a qualitative assessment of slow versus fast. The reactions were stopped after 24 h by cooling the reactor and venting to atmosphere.

3.3.4 Synthesis of Poly(CTFE-*ter*-VAc-*ter*-PDMSMA) by Supercritical CO₂

Poly(CTFE-*ter*-VAc-*ter*-PDMSMA) was synthesized following a procedure similar to that for p(TFE-*ter*-VAc-*ter*-PDMSMA) [11]. Recrystallized AIBN was added to a 50 mL high-pressure stainless steel CO₂ reactor equipped with a Parr magnetic stirrer. The reactor was evacuated as it was cooled to -65 °C. The VAc and PDMSMA monomers were mixed and added by cannula, and the reactor contents were degassed. The CTFE was then added while ensuring that the reactor temperature did not rise above the boiling point (-28 °C) of liquid CTFE. The amount of CTFE added was determined by measuring the mass lost by the CTFE gas cylinder. The total mass of the monomers was approximately 20 g. Supercritical fluid purity CO₂ was added while the reactor was heated to 10 °C, with a resulting pressure was approximately 55 bar. The reactor was then heated to the reaction temperature of 60 ± 1 °C, which was controlled by a combination of resistive heating and water cooling jackets. This gave an initial pressure of 330 to 350 bar. During the course of the polymerization the pressure reduced to a minimum of approximately 200 bar. The stir rate of the polymerizations was estimated at 550 rpm. Polymerizations were stopped after 24 h by cooling the reactor and slowly venting to atmosphere.

3.3.5 Polymer Purification

For both the emulsion and scCO₂ polymerizations, the resulting terpolymers were dissolved in dichloromethane – the emulsion-based polymers required an initial precipitation in methanol to break the emulsion prior to this step – and precipitated in 1 L of methanol. The polymer was then filtered and dried under vacuum

(10 mm Hg) at 50 °C for 5 h. The feed compositions based on the monomer masses added to the reactor and the terpolymer compositions as determined by quantitative ^1H and ^{19}F NMR are shown in Table 3.1. The incorporation of all monomers into the terpolymer was also confirmed by ^1H and ^{19}F NMR (Figure 3.2 and Table 3.2). The chemical shifts listed in Table 3.2 are for polymer composition **emA** but all emulsion polymers had similar spectra. In this thesis, em denotes emulsion, sc denotes supercritical CO_2 , and the letter denotes a particular feed composition. The chemical shifts for polymers synthesized in scCO_2 were similar to those synthesized by emulsion, yet the scCO_2 polymers do not have any peaks associated with the Zonyl FSN-100 as no fluorosurfactant was used in these polymerizations. The integration of the spectra differed since this will depend on the amount of each monomer incorporated into the terpolymer. Yield was determined by dividing the mass of the final isolated terpolymer by the mass of the feed monomers.

Table 3.1: Composition, molar mass and yield of CTFE-VAc-PDMSMA terpolymers.

ID	Feed*			Polymer**			Triad Sequence [†] (%)			Molar Mass (kg/mol)			Yield (%)
	f _{CTFE}	f _{VAc}	f _{PDMSMA}	F _{CTFE}	F _{VAc}	F _{PDMSMA}	BAB	AAB + BAA	AAA	M _w	M _n	PDI	
emA	0.602	0.370	0.028	0.425	0.554	0.021	34	53	14	2690	800	3.4	27
emB	0.486	0.485	0.028	0.405	0.584	0.011	29	54	17	4120	830	5.0	31
emC	0.372	0.600	0.028	0.327	0.672	0.001	16	54	29	4870	1000	4.9	29
emD	0.582	0.363	0.055	0.458	0.539	0.003	54	41	5	4320	804	5.4	30
scA	0.612	0.360	0.028	0.442	0.511	0.047	50	44	6	1750	459	3.8	44
scB	0.523	0.451	0.026	0.390	0.576	0.034	38	51	11	2180	647	3.4	52
scC	0.405	0.568	0.027	0.368	0.606	0.026	22	57	20	2890	619	4.7	54
scD	0.564	0.378	0.058	0.413	0.474	0.113	41	49	10	1530	543	2.8	40

*f_X denotes the molar fraction of X in the feed

**F_X denotes the molar fraction of X in the polymer

[†]A denotes a VAc monomer repeat unit, B denotes a CTFE or PDMSMA repeat unit

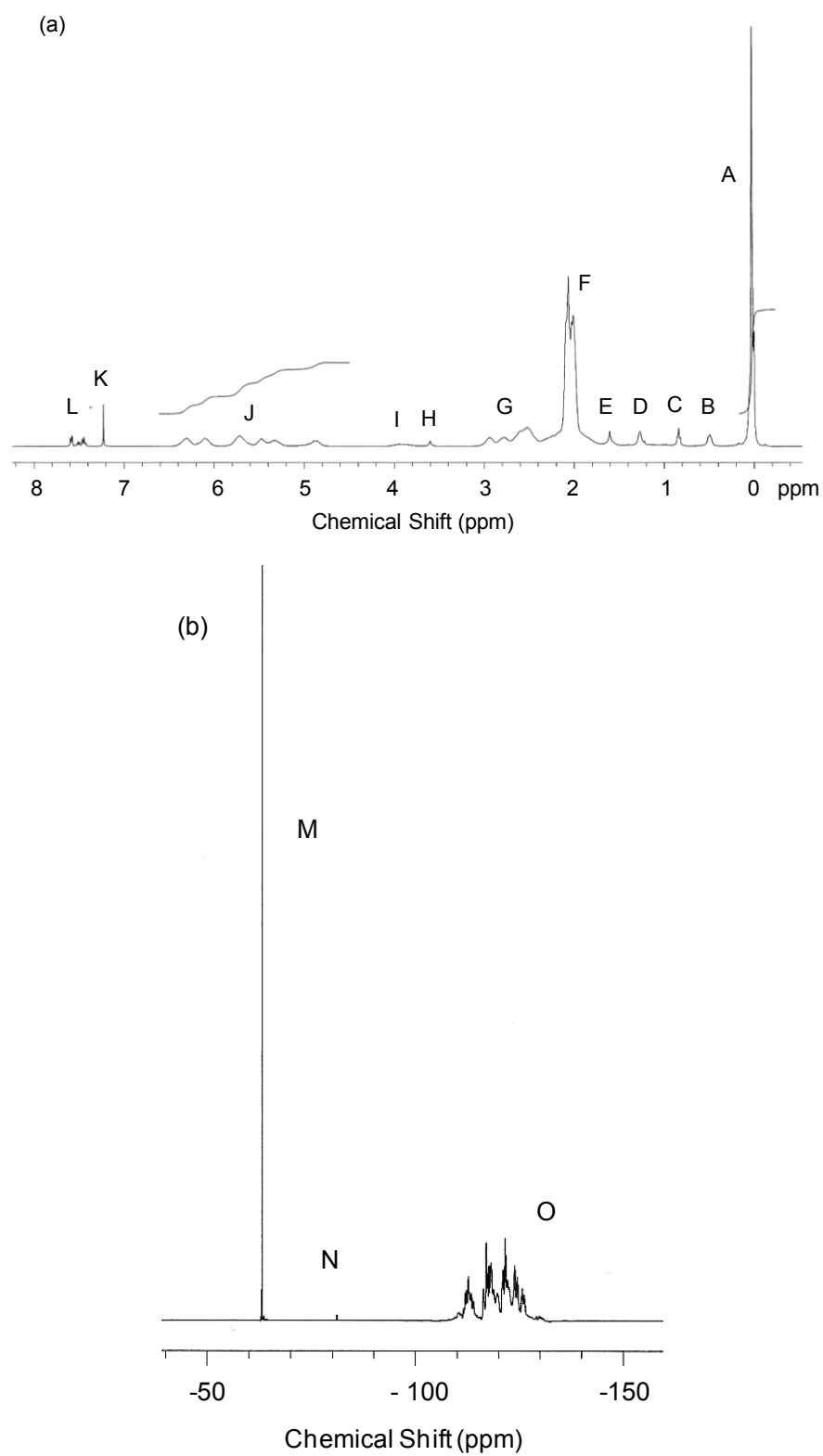


Figure 3.2: NMR spectra of CTFE-VAc-PDMSMA terpolymer emA: (a) ^1H NMR spectrum, (b) ^{19}F NMR spectrum. Assignments of the labelled peaks are given in Table 3.2.

Table 3.2: Assignments of the ^1H and ^{19}F NMR for a representative CTFE-VAc-PDMSMA terpolymer (emA) in CDCl_3 (See Figure 3.2)

Peak	Chemical Shift (ppm)	Assignment
A	0.07	Siloxane CH_3
B	0.53	CH_2 adjacent to Si
C	0.88	Terminal CH_3 of C_4H_9 siloxane cap
D	1.30	CH_2 at center of C_4H_9 siloxane cap; CH_3 of methacrylate
E	1.68	CH_2 at centre of propyl link between siloxane and methacrylate
F	1.82 to 2.25	CH_2 backbone groups for both VAc and PDMSMA; CH_3 group on VAc
G	2.45 to 3.10	CH_2 backbone groups for VAc
H	3.64	Zonyl FSN-100 surfactant
I	3.87 to 4.03	CH_2 adjacent to ester oxygen in PDMSMA
J	4.81 to 6.48	CH group of VAc
K	7.27	CDCl_3
L	7.43 to 7.67	Aromatic H of TFT
M	-63.2	CF_3 of TFT
N	-81.3	CF_3 of Zonyl FSN-100
O	-112.7 to -123.9	CF_2 of CTFE; CF of CTFE; CF_2 of Zonyl FSN-100

3.3.6 Calculation of Reactivity Ratios

The reactivity ratios presented in this chapter were calculated from literature values from work by Baradie and Shoichet [11, 17] and Murray et al. [19] and not the polymers synthesized herein. Reactivity ratios were calculated using the software RREVM Version 2.3 [29], which solves the differential form of the instantaneous copolymer composition equation, shown in Equation (3.2), using the error-in-variables model (EVM) method.

$$F_1 = \frac{r_1 f_1^2 + f_1 f_2}{r_1 f_1^2 + 2f_1 f_2 + r_2 f_2^2}, \quad (3.2)$$

where F_1 is the mole fraction of monomer 1 in the copolymer, f_1 and f_2 are the mole fractions of monomers 1 and 2 in the feed, and r_1 and r_2 are the monomer reactivity ratios for monomers 1 and 2. The use of Equation (3.2) requires negligible compositional drift over the course of the polymerization. All copolymerizations [11, 17, 19] used in the calculation of the reactivity ratios were taken to low conversions (on average 11 wt%) to satisfy this criterion with each set of data containing 7 runs at a minimum of 4 compositions. The mole fractions used from literature to calculate the reactivity ratios are provided in Table 3.3.

Table 3.3: Literature mole fractions used to determine reactivity ratios

Supercritical CO₂ copolymerization of VAc with PDMSMA [11]							
f_{VAc} (mol%)	97.3	95.5	91.3	88.4	93.3	93.3	93.3
F_{VAc} (mol%)	66.7	46.0	33.0	26.2	41.2	40.3	40.4
Supercritical CO₂ copolymerization of CTFE with VAc [17]							
f_{VAc} (mol%)	87.2	76.0	58.8	33.3	67.0	67.0	67.0
F_{VAc} (mol%)	81.7	68.9	61.2	55.6	62.3	64.8	61.7
Emulsion copolymerization of CTFE with VAc [19]							
f_{VAc} (mol%)	9.7	13.7	35.4	39.1	51.5	72.9	81.8
F_{VAc} (mol%)	36.8	39.5	54.2	60.2	63.1	72.4	75.9

To determine reactivity ratios using EVM, an estimate of the error for both the feed and copolymer composition is required. Literature values for the error associated with the scCO₂ polymerizations [11, 17] were considered to be equivalent for the corresponding emulsion polymerization as no data on this latter error was available. This assumes that the techniques used to measure the feed and polymer compositions in both the work by Baradie and Shoichet [11, 17] and the work by Murray et al. [19] yield similar errors. In both cases, the fluoromonomer was added to the reactor by flash distillation from a pressurized cylinder to a cooled reactor suggesting that the equivalent errors in the mass of CTFE added will be seen. Baradie and Shoichet added the VAc to the reactor by pipetting from a flask containing the measured mass of VAc. Murray et al. added the VAc through a syringe. As both additions were conducted at room temperature, (i.e., the density of the VAc was the same in both cases), it is unlikely that a significantly different error

will be achieved for mass versus the volumetric method of addition. The polymer composition in both Baradie and Shoichet [11, 17] and Murray et al. [19] was determined by elemental analysis again suggesting equivalent error. Therefore, the assumption that the error associated with the scCO₂ polymerizations is equivalent to that for the emulsion polymerizations is valid. Using the data in the literature on CTFE-VAc copolymerizations in both scCO₂ [17] and emulsion polymerizations [19] as well as a VAc-PDMSMA copolymerization in scCO₂ [11] 95% confidence ellipses for each set of reactivity ratios was determined.

3.4 Results and Discussion

3.4.1 Polymer Synthesis

A series of CTFE-VAc-PDMSMA terpolymers were synthesized through a modified emulsion polymerization technique and compared to polymers with similar feed ratios synthesized in scCO₂. The ability to synthesize the terpolymers by emulsion polymerization gives a viable alternative to the high-pressure scCO₂ polymerization used previously [11] although the polymers herein contain CTFE rather than TFE. The term modified is used to describe the emulsion polymerization as the initiator, AIBN, is oil soluble rather than water soluble as typically seen in emulsion systems. While the use of an oil-soluble initiator suggests a suspension or dispersion polymerization, it does not preclude an emulsion type of polymerization as seen by numerous authors [30-37]. Furthermore, suspension polymerizations typically use a water-insoluble stabilizer at less than 1 wt% [38] whereas the Zonyl FSN-100 used in this synthesis is a water-soluble ethoxylated non-ionic fluorosurfactant at 1.2 wt% of the overall mixture. Dispersion polymerizations can

be considered a special case of precipitation polymerizations that require a dispersant (on the order of 1 wt% or greater) to aid in the formation of the polymer. In this work, no precipitation was seen during or after the polymerization until the emulsion was broken. Additionally, a typical emulsion polymerization will have a surfactant weight percentage between 1 to 3% such that the critical micelle concentration (CMC) is exceeded by 1 to 3 orders of magnitude [38]. The CMC of Zonyl FSN-100 is 0.011 mM [39] and the concentration in this system is 12 mM, a difference of three orders of magnitude. Thus, despite the modification whereby an oil-soluble initiator is used, the polymerization system likely falls in the regime of an emulsion polymerization rather than suspension or dispersion polymerization.

Azobisisobutyronitrile was used to limit the formation of p(VAc) as was seen with water soluble initiators such as potassium or ammonium persulfate (data not shown). AIBN is essentially insoluble in water. However, the marginal solubility it does have in water allows for a polymerization similar to that achieved by water-based initiators while preventing the runaway polymerization of VAc.

Furthermore, AIBN and Zonyl FSN-100 were selected to limit chain transfer to the initiator or surfactant. Both molecules can be considered quite electron rich. As all of the monomers in the reaction are also electron-rich, the chain transfer will likely be reduced relative to a neutral or electron-poor chain transfer agent [38]. The AIBN also has a chain transfer constant that is approximately half of the chain transfer constants listed for peroxide based systems [16]. The chain transfer to Zonyl FSN-100 can be modelled by the chain transfer constant for ethyl ether (45×10^{-4} at 60°C) [16] and 1H, 1H, 7H-dodecaheptanol (33.3×10^{-4} at 60°C) [16]. Many of the

chain transfer constants for VAc to solvent are an order of magnitude greater [16]. Thus, any chain transfer seen will likely be due to chain transfer to monomer or polymer.

Zonyl FSN-100 is a water-soluble non-ionic surfactant. As the surfactant is non-ionic, it should interfere minimally with the propagation reaction; it will appear as a neutral molecule. The polarity of the Zonyl-FSN 100 was not the main driver in the selection of the surfactant but rather the fluorinated component. This will likely enhance the solubility of the CTFE for the reaction mixture as the CTFE will have a greater affinity for the fluorinated hydrophobic component of the Zonyl FSN-100 relative to other non-fluorinated surfactants, allowing greater incorporation of this monomer into the terpolymer.

The scCO₂ polymerizations are likely precipitation polymerizations. Due to a lack of view port on the reactor, this cannot be stated conclusively, however, a strong inference may be made based on the solubility of similar polymers. Baradie et al. [40], which describes the solubility of TFE-VAc copolymers in scCO₂ shows that a copolymer comprised of 46.7 mol% TFE requires a pressure of 740 bar and 75 °C to be soluble in scCO₂. As well, to achieve a single phase system, although it is in liquid CO₂, copolymers of TFE-VAc with mole percentages of TFE ranging from 11.6 to 26.5% require pressures of 500 bar. Pure p(VAc) requires even higher pressure to achieve solubility [40]. Therefore, it is highly unlikely that the terpolymers in this work remain in solution, resulting in a precipitation polymerization. For the terpolymers in this work 47 to 60 mol% of the polymer is VAc which has low scCO₂ solubility. Also, experiments by Watkins and McCarthy

[41] show that PCTFE swells, but does not dissolve, in scCO₂ at 80 °C and 243 bar, similar conditions to this work. The small difference in structure between the emulsion based and scCO₂ based polymerization also suggests a heterogeneous polymerization in scCO₂.

3.4.2 Terpolymer Composition

The composition of the p(CTFE-*ter*-VAc-*ter*-PDMSMA) samples synthesized by both emulsion and scCO₂ methods are summarized in Table 3.1. Compositions **emA** to **emC** differ in CTFE/VAc feed molar ratio with constant PDMSMA feed content whereas composition **emD** has twice the PDMSMA feed content but a similar CTFE/VAc ratio to composition **emA**. Compositions **scA**, **scB**, **scC** and **scD** were synthesized in scCO₂ and correspond to monomer feed ratios used in **emA** through **emD**, respectively.

For a constant f_{POSSMA} (**emA** through **emC** and **scA** through **scC**), as the ratio of $f_{\text{CTFE}}/f_{\text{VAc}}$ increases, that is, as the feed is enriched with CTFE, F_{CTFE} and F_{POSSMA} increased while F_{VAc} decreased, shown in Figure 3.3. Figure 3.3 also shows that there appears to be no difference in the CTFE or VAc content between the emulsion and scCO₂ based polymers since the error associated with the composition, as determined by quantitative NMR, overlaps. Furthermore, F_{PDMSMA} is much greater for the scCO₂ polymerizations. This corroborates the emulsion character of the aqueous polymerizations. In both the emulsion and scCO₂-based polymerizations, the VAc and PDMSMA are dissolved in one another prior to addition to the reactor. If in the aqueous media, the polymerization is occurring in the monomer droplets which contain PDMSMA (i.e., a suspension polymerization) there would likely not be

a large reduction in PDMSMA content. However, if the polymerization is occurring in the micelles then the transport of the PDMSMA from the monomer droplet through the aqueous medium to the micelle becomes an issue. Since PDMSMA is minimally soluble in water, its transport is likely reduced relative to that of the VAc, a water soluble monomer, and the resulting polymers have a lower PDMSMA content than in the scCO₂ system. The water solubility of VAc is demonstrated by the rapid desorption of the growing VAc radical in the emulsion homopolymerization of VAc, which leads to an average number of particles per radical of approximately 0.1 or lower [38]. Furthermore, the solubility of VAc in water is 25 g/L. This can be compared to styrene which has a solubility of 0.07 g/L [38].

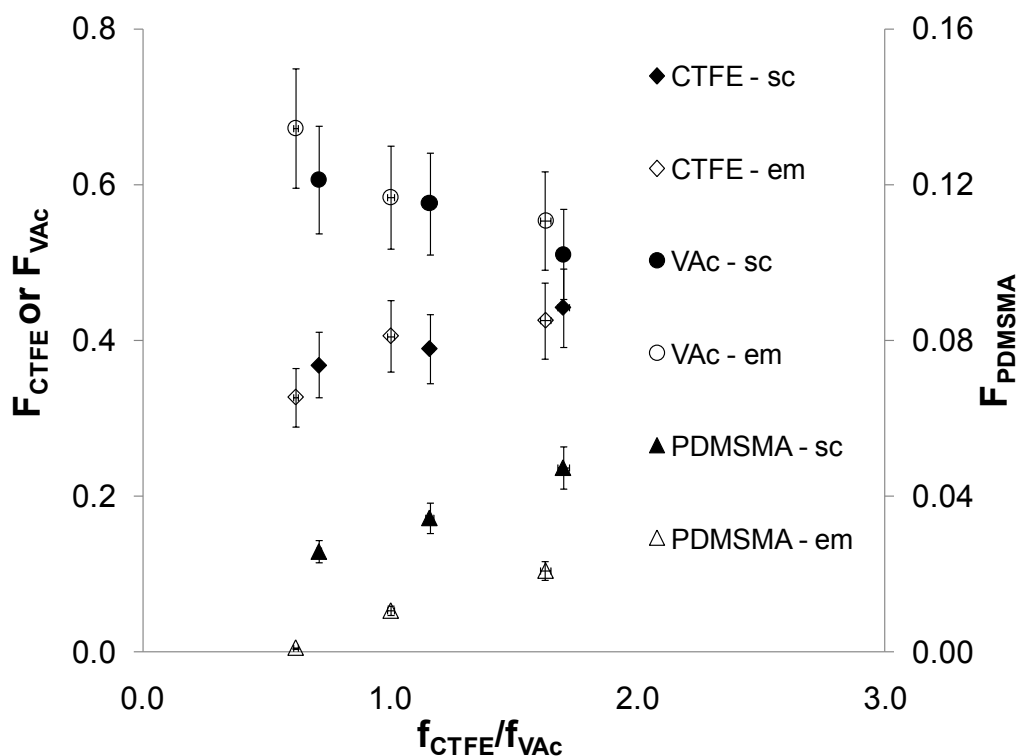


Figure 3.3: Effect of CTFE to VAc ratio of polymer composition

To gain further insight into the molecular configuration in the terpolymer, ^1H NMR was used to track triads of VAc and CTFE. Given the sensitivity of the VAc methine hydrogen peak to the neighbouring repeat units, triad composition was investigated according to the peaks attributed to eight different triad stereochemical structures by Murray et al. [19]. A comparison of the integrated areas under the peaks for the triad sequences, AAA vs. AAB + BAA vs. BAB, where A denotes a VAc unit and B denotes a CTFE unit, shown in Table 3.1 with the NMR spectra shown in Figure 3.4, demonstrates the tendency of VAc to homopolymerize or cross-propagate with CTFE. The BAB triads were considered to be CTFE-VAc-CTFE although the possibility exists for B to represent PDMSMA. However, the percentage of PDMSMA units in the terpolymers falls between 0.3 and 11.3% compared with 32.7 to 45.8% for CTFE, and the probability of the BAB triad consisting of a PDMSMA unit ranges from 1 in 4 for **scD** to 1 in 340 for **emC**. For both polymerization systems, increased f_{VAc} resulted in an increase in AAA triads and a decrease in BAB triads. This suggests that during propagation the VAc terminal radicals preferentially add VAc monomer units irrespective of the amount incorporated into the terpolymer.

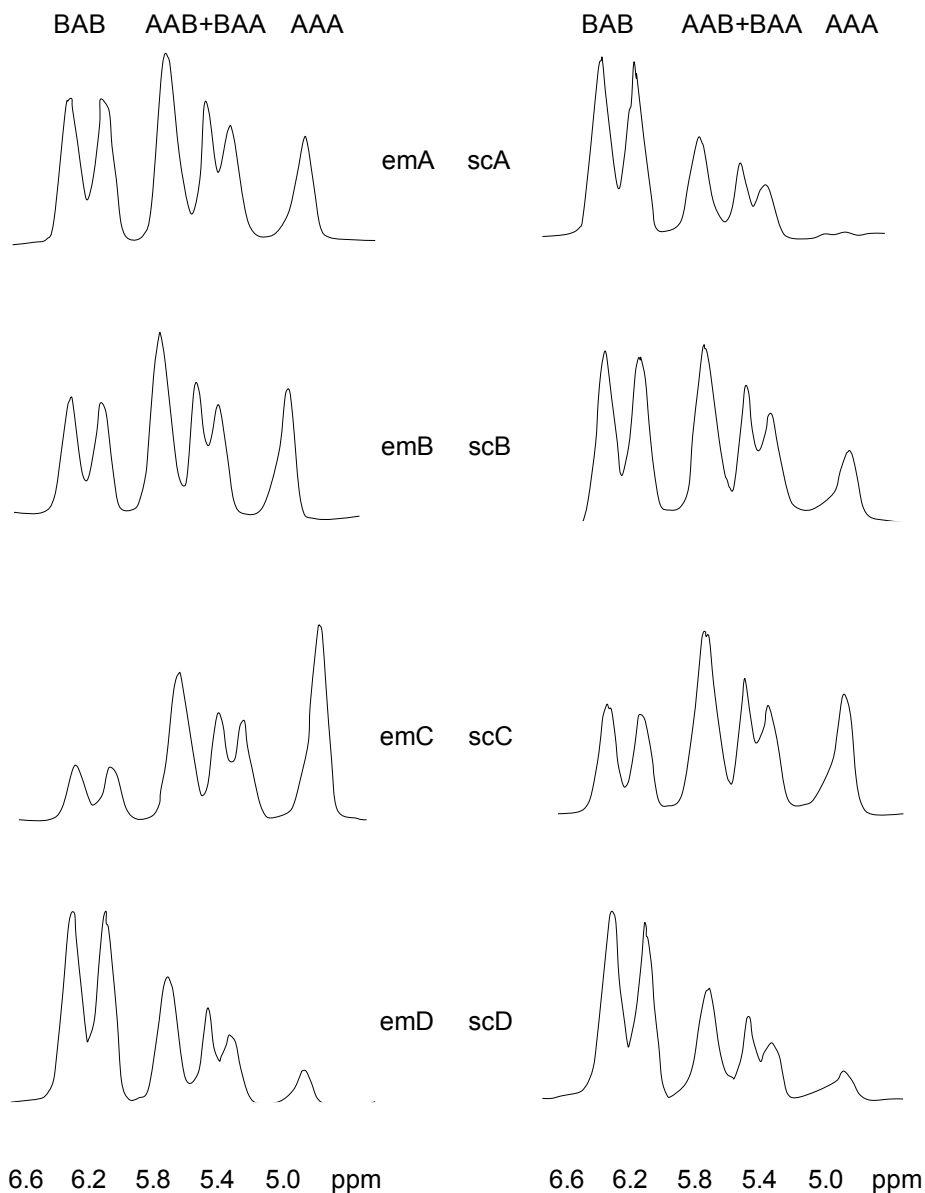


Figure 3.4: NMR spectra of VAc methine region

3.4.3 Reactivity Ratios

Initially the copolymerization of CTFE and PDMSMA was attempted in both emulsion and scCO_2 , yet only PDMSMA homopolymers resulted (data not shown). Previous work [11] with TFE has shown nearly three orders of magnitude difference between TFE reactivity ratios and those of PDMSMA. This necessitated the

inclusion of a third monomer of intermediate reactivity, VAc [11] to obtain copolymers. A similar large difference in reactivity ratios between CTFE and PDMSMA provides an explanation as to why only PDMSMA homopolymers resulted when CTFE-PDMSMA copolymers were attempted. Again, the inclusion of VAc was necessary to form a polymer that incorporated both CTFE and PDMSMA. Since VAc can form copolymers with each of the other monomers (CTFE and PDMSMA), it can act as a link between the two analogous to the manner in which an adhesive can cause two dissimilar materials to bond.

To gain a greater understanding of the necessity of VAc in the polymerization of CTFE and PDMSMA, the CTFE-PDMSMA reactivity ratios (r_{13} and r_{31}) were estimated using the following ratio:

$$\frac{r_{12}}{r_{21}} \times \frac{r_{23}}{r_{32}} = \frac{r_{13}}{r_{31}} \quad (3.3)$$

where monomer 1 is CTFE, monomer 2 is VAc, and monomer 3 is PDMSMA.

Equation (3.3) requires the reactivity ratios of the CTFE-VAc and VAc-PDMSMA systems. The reactivity ratios r_{12} , r_{21} , r_{23} and r_{32} were calculated using the EVM [29] method and are reported as the reactivity ratio \pm the maximum error associated with a 95% confidence ellipse. The 95% confidence ellipse is calculated as per Rossignogli and Duever [42] and provides an indication as to the variability and degree of fit for the reactivity ratios calculated using the EVM method, similar to the R^2 value for a least-squares estimate. Larger values for the maximum error (like lower values for R^2) indicate an estimate for the reactivity ratio that is less accurate. The reactivity ratios in $scCO_2$, using literature values of f_1 , f_2 , and F_1 from Baradie and Shoichet [11, 17] for CTFE-VAc were $r_{12} = 0.024 \pm 0.061$ and $r_{21} = 0.43 \pm 0.036$

and for VAc-PDMSMA were $r_{23} = 0.051 \pm 0.18$ and $r_{32} = 22 \pm 44$. The reactivity ratios for CTFE-VAc for an emulsion polymerization were also calculated based on values of f_1 , f_2 , and F_1 reported by Murray et al. [19] with $r_{12} = 0.076 \pm 0.022$ and $r_{21} = 0.58 \pm 0.052$.

Non-linear regression analysis was not used for the calculation of the reactivity ratios. Work by Rossignoli and Duever [41] shows that a nonlinear regression analysis technique and EVM can result in similar reactivity ratios when the error in the measurement of the feed molar ratios is on the order of 1%. This error is 1.4% for the polymers synthesized herein. Furthermore, the reactivity ratios for the CTFE-VAc copolymerization calculated by Murray et al. [19] are $r_{12} = 0.04 \pm 0.02$ and $r_{21} = 0.68 \pm 0.11$ based on a nonlinear technique. These reactivity ratios overlap those calculated by the EVM in this thesis, suggesting that EVM and nonlinear regression analysis are similar for these polymers. Therefore, EVM was selected for direct comparison to previously synthesized terpolymers by Baradie and Shoichet [11, 17] and the reactivity ratios for the polymerization conducted by Murray et al. [19] were recalculated to maintain a basis for comparison.

Numerous reaction conditions can affect the reactivity ratios of a given polymer pair including the reaction medium, temperature, pressure [38]. The literature polymerizations of Baradie and Shoichet [17] and Murray et al. [19] differ in all of these parameters. Baradie and Shoichet polymerized CTFE and VAc in $scCO_2$ at 45 °C and 230 bar whereas Murray et al. conducted the polymerization in an

emulsion system at 25 °C and 100 bar (the pressure was calculated based on the reactor volume and mass of CTFE added).

Both increasing temperature and pressure, will shift a copolymerization toward an ideal copolymerization where $r_1r_2 = 1$. The effect of temperature on a reactivity ratio is given by Equation (3.4)

$$r_x = \frac{A_{xx}}{A_{xy}} \exp\left[\frac{E_{xx} - E_{xy}}{RT}\right] \quad (3.4)$$

where A_{xx} and A_{xy} are the pre-exponential factors for self-propagation and cross-propagation, E_{xx} and E_{xy} are the activation energies for self- and cross-propagation, R is the gas constant and T is the reaction temperature. As the temperature increases r_x decreases to the limit of A_{xx}/A_{xy} . If the values for A_{xx} and A_{xy} are similar, then A_{xx}/A_{xy} will be approximately 1. Since both r_x and r_y will shift to the value of 1 as temperature increases, their product will also shift to the limit of 1 and a more ideal polymerization. It is known that increasing the pressure reduces the selectivity of the propagating radical for the next monomer [38]. Higher pressures are a more energetic state than lower pressures and to reduce the overall energy of the system, the reaction becomes less selective.

Therefore, the scCO₂ copolymerization by Baradie and Shoichet [17], which was conducted at both higher temperature and pressure than the emulsion polymerization conducted by Murray et al. [19], should be more ideal (more random) than the emulsion polymerization. However, the opposite is found to be the case. The r_1r_2 for the scCO₂ polymerization is less than that for the emulsion system ($r_1r_2 = 0.01$ and 0.04 , respectively). This greater randomness of the emulsion polymerization is confirmed by examining the triad sequence of each series of

polymers [17, 19] which shows that the emulsion polymers have fewer alternating triads. Therefore, the effect of temperature and pressure appears to be reduced relative to the changes in the reactivity ratios associated with the change in polymerization medium from emulsion to scCO₂.

Using Equation (3.2) and the calculated literature values for r_{12} , r_{21} , r_{23} and r_{32} , the ratio of the reactivity ratios, $r_{13}:r_{31}$, for the CTFE-PDMSMA system were estimated to be 1:3300 and 1:3700 for the scCO₂ and emulsion polymerization systems, respectively. The three order of magnitude difference in reactivity ratios indicates that a CTFE-PDMSMA copolymer would not form as was seen experimentally for both polymerization media. By comparison, the value of $r_{13}:r_{31}$ for the TFE-PDMSMA system [11] was calculated at approximately 10000:1 demonstrating the greater reactivity of CTFE in this system.

3.4.4 Terpolymer Yield

Emulsion polymers had consistent yields of 27 – 31% whereas scCO₂ polymers had yields of 40 – 54% (Table 3.1). For a constant f_{POSSMA} (i.e., **scA** through **scC**), the yield of terpolymer increased with increasing f_{VAc} , over the range of f_{VAc} studied, for those polymers synthesized in scCO₂ whereas feed composition had minimal effect on the yield for the emulsion polymerization.

The effect of VAc on polymer yield for the scCO₂ based polymerizations can be explained as follows. For the compositions **scA** through **scC**, an increase in f_{VAc} leads to an increase in F_{VAc} . Therefore, the polymer will precipitate from solution at a lower molar mass as VAc is likely the least soluble of the three monomers in scCO₂ [16]. This leads to a greater volume fraction of the insoluble polymer phase

(ν_p) within the reactor. As seen in work by Liu et al. [43] an increase in ν_p , gives an increase in the rate of polymerization for the resulting polymers assuming that the locus of polymerization is at the polymer-solvent surface or the interior of the precipitated polymer particle. This assumption has some merit for the CTFE-VAc-PDMSMA system as VAc demonstrates chain growth within the polymer particle [43]. An increase in the rate of polymerization, R_p , will give an increase in yield as each polymer composition is taken to the same time point. This is not to imply that the rate of polymerization remains constant through the course of polymerization, but rather than at a given time point the four polymerizations, **emA** through **emD**, have differing rates of polymerization that are dependent of the amount of insoluble fraction in the reactor. The polymerization with the highest insoluble fraction (i.e., the highest R_p) will also have the highest yield as in this work yield is defined as the mass of polymer obtained divided by the mass of monomers added in the feed.

The almost constant yields obtained for the emulsion terpolymers suggest that yield depends not upon terpolymer composition but rather the characteristics of the emulsion. The constants between the emulsion reactions are the concentrations of the surfactant and initiator. According to Equation (3.5) [38], increasing the surfactant concentration will result in a greater number of micelles, N , and increase R_p (and subsequently yield). The number of micelles is also affected by the rate of initiation, shown in Equation (3.6) [38], which is determined by initiator concentration. An increase in initiator concentration will give higher conversion but at the expense of degree of polymerization.

$$R_p = \frac{N\bar{n}k_p[M]}{N_A} \quad (3.5)$$

$$N = k \left(\frac{R_i}{\mu} \right)^{2/5} (a_s S)^{3/5} \quad (3.6)$$

For Equations (3.5) and (3.6), R_p is the rate of polymerization, N is the concentration of micelles and particles, \bar{n} is the average number of radicals per micelle plus particle, k_p is the polymerization rate constant, $[M]$ is the monomer concentration, N_A is Avogadro's number, k is a constant between 0.37 and 0.53, R_i is the rate of initiation, μ is the rate of volume increase of the polymer particle, a_s is the interfacial area occupied by a surfactant molecule, and S is the total concentration of surfactant in the system.

3.4.5 Terpolymer Molar Mass

The GPC molar mass data, determined relative to polystyrene standards and summarized in Table 3.1, shows that molar mass increases as F_{VAC} increases or F_{PDMSMA} decreases for both polymerization media. This latter is likely due the pendant PDMS chain reducing the reactivity of the propagating radical as is seen for other bulky substituents on the ester functionality of methacrylates [44]. This appears contradictory as the reactivity ratios show that PDSMMA is the most reactive of the three monomers used. However, reactivity ratios greater than one signify that the radical prefers to homopolymerize. Since, the concentration of PDMSMA at the reactive site is likely reduced, due to the low amounts of PDMSMA in the feed, a propagating chain terminated by a PDMSMA radical is forced to cross-propagate. This reduces the reactivity of the propagating radical, particularly

since in the system studied the PDMSMA will only cross-propagate with the VAc and not the CTFE.

At PDMSMA levels below 1.0 mol%, as in compositions **emB**, **emC** and **emD**, the M_w and PDI increase suggesting a greater number of higher molar mass chains. Many authors [22-25, 45, 46] show that weight-average molar masses greater than 1000 kg/mol are required for significant long chain branching in PVAc; therefore, an increase in the branching of VAc within the terpolymers may be shifting the molar mass distribution to higher molar mass.

The emulsion terpolymers had higher molar masses than the scCO₂ terpolymers for all compositions, likely due to reduced termination reactions in the modified emulsion system. The use of an emulsion system, particularly with an organic soluble initiator, results in compartmentalization of the propagating radicals. Thus, the probability of a termination reaction occurring in the emulsion system is reduced when compared to the scCO₂ polymerization where the radicals may not be segregated, suggesting polymerization at the polymer-solvent interface for the scCO₂ reactions. Termination reactions within the polymer particle may be reduced even further since VAc polymerizations typically show significant aqueous termination [38]. A comparison of polymers **emA** and **scC** demonstrates that similar compositions can be achieved in both the emulsion and scCO₂, but the emulsion based polymer will have a higher molar mass.

3.4.6 Terpolymer Branching

Long chain branching¹ in the VAc containing polymers arises from incorporation of the VAc ester into the backbone through chain transfer to polymer or chain transfer to monomer [24-27, 46]. To make a direct comparison on the degree of long chain branching obtained in an emulsion polymerization to a polymerization in scCO₂, the VAc component of the polymers must fall either above or below the threshold molar mass (1000 kg/mol) demonstrated by Grcev et al. [23] for both medium. The molar mass of the VAc component for the polymers synthesized herein, based on M_w , falls between 328 and 2991 kg/mol, suggesting that a comparison as the effect of medium on branching may be confounded by molar mass. However, compositions **emA**, **emD** and **scC** have molar masses of the VAc component of 1107, 1231 and 1274 kg/mol, respectively, allowing a comparison of these three polymers.

Four methods were considered to examine the degree of branching in this work: hydrolysis of the VAc, ¹³C NMR, calculation of the branching ratio (g') from intrinsic viscosity measurements, and calculation of the branching density (ρ) from chain transfer to polymer. The first two methods were examined, but were not considered suitable for the polymers in this thesis for the reasons outlined below. The latter two methods suggest there is little to no difference in branching due to VAc between the emulsion-based and scCO₂-based polymers synthesized herein.

In hydrolyzing the VAc component of the terpolymer, the molar mass distribution of branched polymer is expected to shift to substantially lower molar

¹ A long chain branch is a polymeric branch.

masses on hydrolysis than a linear polymer due to cleavage of the VAc ester in the backbone. While this methodology is acceptable for the majority of VAc containing polymers, the terpolymers synthesized herein contain pendant siloxanes. Hydrolytic cleavage of siloxanes at the Si-O bond is well known [47]. This will result in terpolymers with a silanol pendant group and the potential for crosslinking since the hydrolytic cleavage of siloxanes is an equilibrium reaction. Subsequently, the loss of molar mass due to the cleavage of backbone VAc acetate groups may be confounded with an increase in molar mass from this crosslinking. Therefore, hydrolysis cannot be used to determine the extent of branching and alternative methods were explored.

Carbon-13 NMR can be considered the absolute technique for the determination of branching by examining the peak associated with the branch point. Britton et al. [48], show that the branch point due to chain transfer in VAc results in a ^{13}C peak of 61.0 ppm and calculate the degree of branching in the p(VAc) by Equation (3.7) where I_{60-62} is the integration of the aforementioned peak and I_{24-74} is the integration of the remaining main chain carbons.

$$\text{mol}\% \text{branches} = \frac{100 \times 0.81 I_{60-62}}{0.5 [I_{24-74} - (0.2 I_{60-62})]} \quad (3.7)$$

Similar to the hydrolysis methodology described above, the ^{13}C NMR technique is applicable to the majority of VAc containing polymers. However, due to the use of a methacryloxypropyl-terminated PDMS this technique cannot be used for the terpolymers in this thesis. The CH_2 group in the propyl link and adjacent to the ester functionality is equivalent to the CH_2 group used to distinguish the degree of branching for the VAc-containing polymers. Both structures are shown in Figure 3.5.

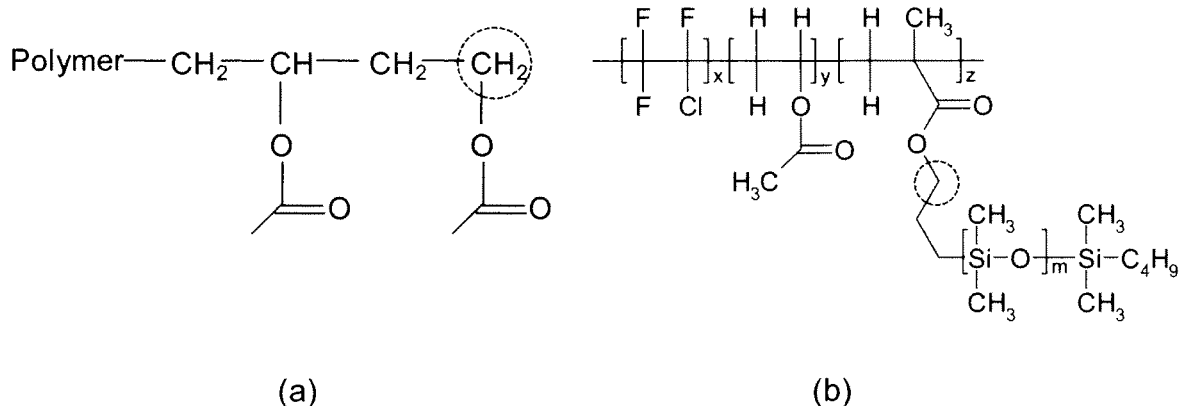


Figure 3.5: Equivalent CH_2 groups in (a) p(VAc) and (b) CTFE-VAc-PDMSMA terpolymer.

The branching ratio, g' , was calculated from the intrinsic viscosity of the polymers as determined by GPC using Equation (3.8) [49]:

$$g' = \left(\frac{[\eta]_B}{[\eta]_L} \right)_M, \quad (3.8)$$

where $[\eta]_B$ and $[\eta]_L$ are the intrinsic viscosities of the branched and linear polymer, respectively, at molar mass M . A more dense structure, corresponding to an increase in branching, will have a lower intrinsic viscosity for a given molar mass. Therefore, g' must be less than 1. For this to hold true, the intrinsic viscosity (see Table 3.4) of **scC** must be in the denominator of Equation (3.8) when comparing to **emA** and **emD**, [49] suggesting that **scC** has a lesser degree of branching than the polymers synthesized by emulsion. To quantify the absolute degree of branching, a linear analogue of the polymers with little to no branching is required, but unavailable at this time.

Obtaining the intrinsic viscosity of the polymers also allows for the calculation of the Mark-Houwink parameters for both the scCO_2 and emulsion-based terpolymers (Table 3.4 and plotted in Figure 3.6).

Table 3.4: Mark-Houwink parameters for CTFE-VAc-PDMSMA terpolymers as determined by GPC

Polymer Designation	Intrinsic Viscosity (dL/g)	log(K)	a
emA	0.0496	-4.07	0.4
emB	0.0652	-4.17	0.5
emC	0.0811	-4.00	0.4
emD	0.0376	-4.03	0.4
scA	0.0417	-5.04	0.6
scB	0.0466	-4.99	0.6
scC	0.0525	-4.78	0.6
scD	0.0306	-6.42	0.8

From Table 3.4 it can be seen that the a parameter of the emulsion polymers falls between 0.4 and 0.5 while the a parameter for the scCO₂ based polymers is greater, falling between 0.6 and 0.8. A lower a parameter can represent three scenarios: the emulsion based polymers 1) are less soluble in THF than the scCO₂ polymers, 2) adopt a hard sphere configuration rather than a more rod-like configuration in solution, or 3) have a greater degree of branching than the scCO₂ polymers. To determine if the emulsion based polymers are less soluble than the scCO₂ polymers compositions **emA** and **scC** were compared; polymer **emA** contains 42.5% CTFE, 55.4% VAc and 2.1% PDMSMA whereas polymer **scC** contains 36.8% CTFE, 60.6% VAc and 2.6% PDMSMA. Based on the typical error associated with the determination of polymer composition by quantitative NMR (10%), **emA** and **scC** can be considered to have the same composition. Therefore, the lower Mark-Houwink a parameter for **emA** relative to **scC** cannot be derived from a difference in

polymer solubility and this argument is extended to the other polymer compositions. This leads to the conclusion that the difference in a must arise from differences in polymer structure, i.e, Scenarios 2 or 3.

While the relative degree of branching is of the most interest, Scenario 3, there exist the possibility that the difference in the a parameter is simply due to Scenario 2. This means that the value of the a parameter alone cannot be used to conclusively determine the relative degree of branching between the polymers synthesized by emulsion or in $scCO_2$. There is no reason that a polymer with a rod-like structure and a greater a value cannot have a greater degree of branching than a spherical polymer with a similar composition. However, combined with the calculation of g' , the a parameter does suggest that the emulsion-based polymers may contain slightly more branches.

Since the difference in the a parameter is derived from structural changes and not a solvent effect, an examination of the Mark-Houwink plots provides insight into the effect of polymerization media on polymer structure. From Figure 3.6 it can be seen that the Mark-Houwink plots of **emA** and **scC** overlay one another with **emD** falling below both curves. The fact that the **emA** and **scC** curves are coincident suggests that the polymerization mechanism does not significantly affect the structure, or potentially the degree of branching. The above combined with the calculation of g' suggests that the structure of the $scCO_2$ based polymers is more rod-like with a similar to slightly lesser degree of branching than the comparable emulsion-based polymers.

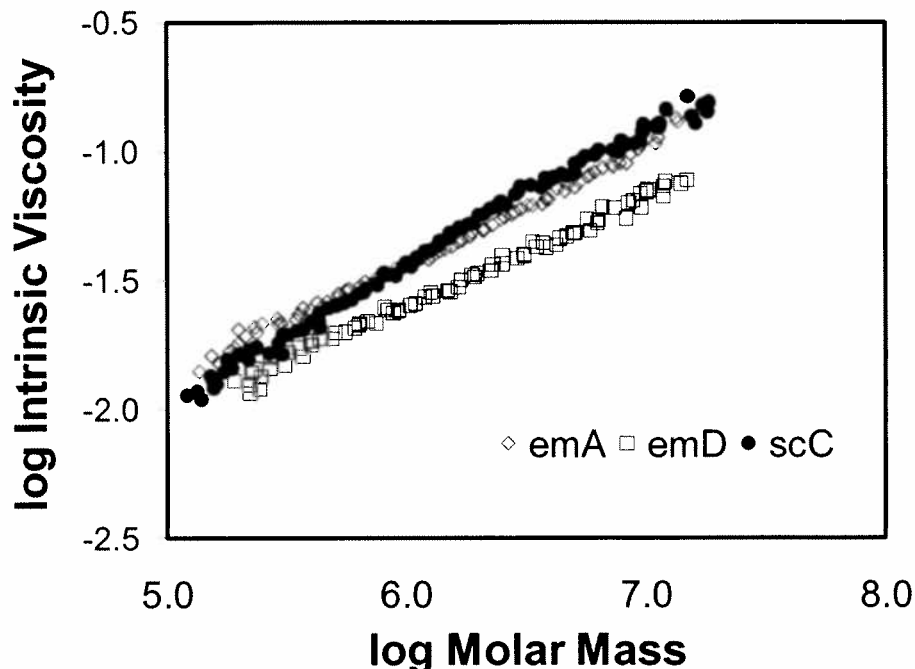


Figure 3.6: Mark-Houwink plot for CTFE-VAc-PDMSMA terpolymers

The third method used to examine the degree of branching confirms the similarity between the emulsion and scCO_2 based terpolymers. The degree of branching due to VAc through chain transfer to the polymer is used to calculate the branching density by Equation (3.9) [50]:

$$\rho = -C_p \left[1 + \left(\frac{1}{p} \right) \ln(1-p) \right], \quad (3.9)$$

where ρ is the branching density, which describes the number of branches per monomer molecule polymerized, C_p is the polymer transfer constant, and p is the extent of reaction. Since the degree of branching does not appear to depend on the polymerization method as established above, C_p is taken to be identical for both the scCO_2 and emulsion polymerizations. Therefore ρ depends on the extent of reaction and thus the degree of polymerization, thereby confirming the work of Grcev et al. [23]. Using the maximum C_p for VAc (4×10^{-4}) [26], and an extent of reaction of

between 40 and 65%, for the VAc component of the terpolymers synthesized herein, one calculates 1.6, 3.5 and 3.0 branches per terpolymer for the **emA**, **emD** and **scC**, respectively. Interestingly, the lower intrinsic viscosity of **emD** must be driven by an alternative mechanism. This is likely the effect of the long pendant group of the PDMSMA as discussed in Section 3.4.7 Terpolymer Viscosity.

The branches determined from Equation (3.9) are due to chain transfer to polymer by VAc. Chain transfer to monomer, which results in terminal double-bond polymerization, will also give long chain branching, yet various authors [24-27] have found that the number of branches due to terminal double-bond polymerization is equal to or less than that associated with chain transfer to polymer. The number of branches due to VAc is expected as Grcev et al. [23] shows that appreciable branching does not occur for VAc until molar masses on the order of 1000 kg/mol are achieved. The molar mass of the VAc component, which is responsible for the long chain branching, for **emA**, **emD** and **scC** are 1107, 1231 and 1274 kg/mol, respectively. In contrast, composition **scD** has a VAc component molar mass of 328 kg/mol and only 0.42 branches per terpolymer. The previously synthesized linear polymers [21] have a calculated VAc component molar mass between 26 and 118 kg/mol and 0.17 to 0.91 branches per terpolymers.

In conclusion, the effect of polymerization medium on branching appears to be minimal for this series of polymers. The linearity of polymers previously synthesized in scCO₂ [21] may not be solely related to a VAc driven mechanism (i.e., the reduction in hydrogen abstraction relative to propagation), but in part due to the lower molar masses associated with scCO₂ polymerization.

3.4.7 Terpolymer Viscosity

As the degree of branching due to VAc is similar between the emulsion and scCO₂ based polymers for a given molar mass, the difference in the intrinsic viscosity seen in the Mark-Houwink plots likely arises from either the CTFE or the PDMSMA. The PDMSMA monomer represents a long pendant group (the equivalent of a short chain branch²) in the polymer and the intrinsic viscosity of the terpolymers decreases as F_{PDMSMA} within the terpolymer increases (Figure 3.7). Therefore, the greater degree of branching, as seen by a lower intrinsic viscosity, in the scCO₂ based polymers arises from the greater incorporation of PDMSMA rather than VAc. Short-chain branching can modify the intrinsic viscosity of a polymer as work by Sun et al. [51] shows that as little as 5 mol% of 1-hexene in polyethylene-co-poly(1-hexene) copolymer results in a modification of the branching ratio. The branching ratio in the work by Sun is defined similarly to the branching ratio in this thesis. They are the ratio of the intrinsic viscosity of a linear to a branched analogue.

² A short chain branch is oligomeric. For conventional PDMS fluids, the properties do not become constant until a molar mass of approximately 6,000 g/mol is reached. The PDMSMA monomer has a molar mass of 900 g/mol and can be considered an oligomer.

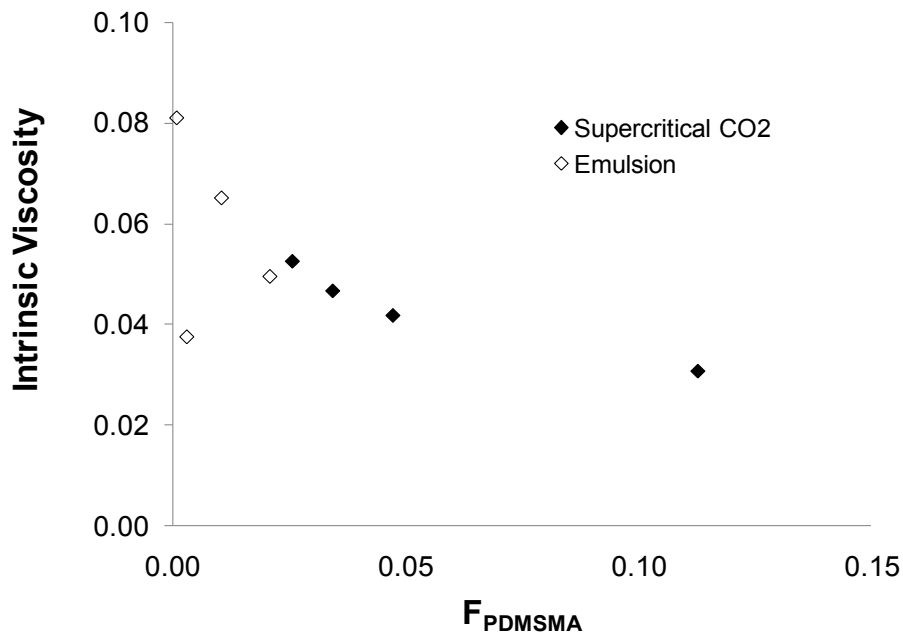


Figure 3.7: Effect of F_{PDMSMA} on intrinsic viscosity

From Figure 3.7, composition **emD** ($F_{PDMSMA} = 0.003$ and $[\eta] = 0.04$) appears to be an outlier. To determine if **emD** is an outlier, intrinsic viscosity as a function of $\log(F_{PDMSMA})$ was plotted as this empirical relationship appears valid for Figure 3.7 (shown in Figure 3.8 below). By excluding the data point associated with **emD**, the R^2 value for the linear fit improves from 0.49 to 0.95, suggesting a significantly better correlation. This leads to the following equation relating intrinsic viscosity and F_{PDMSMA} .

$$[\eta] = -0.0245 \times \log(F_{PDMSMA}) + 0.0105 \quad (3.10)$$

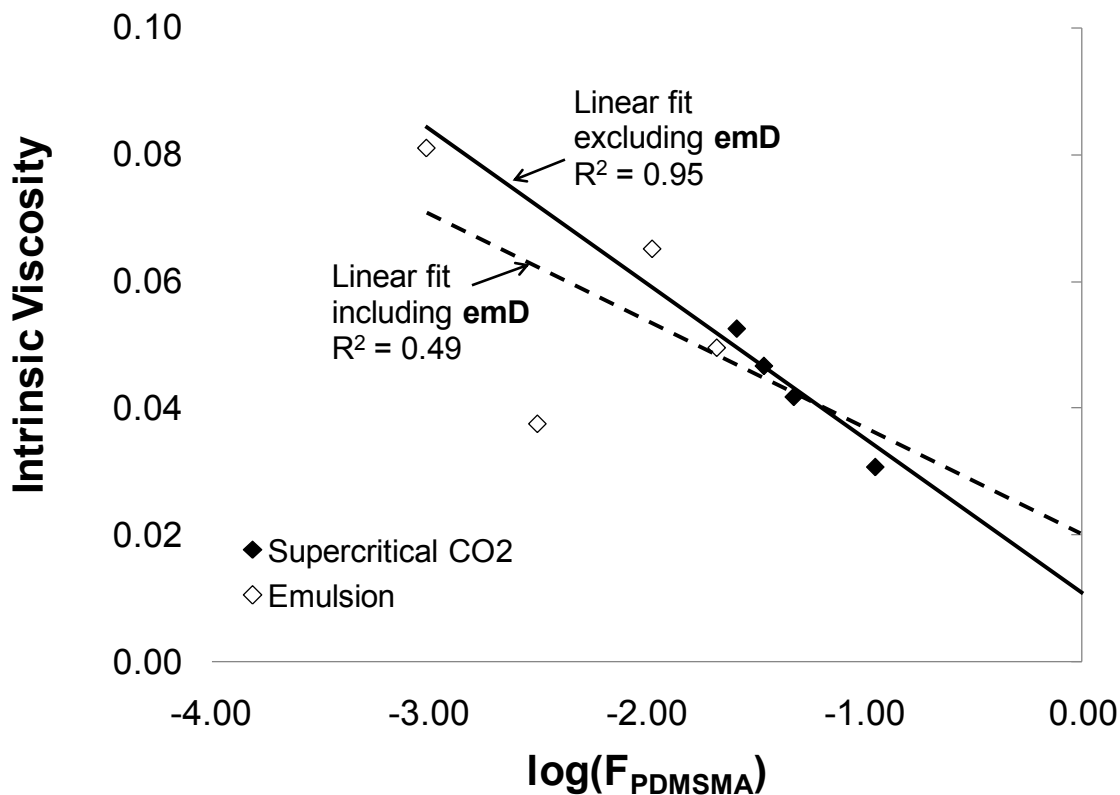


Figure 3.8: Effect of $\log(F_{PDMSMA})$ on intrinsic viscosity. The dashed line represents a linear fit of all data points. The solid line represents a linear fit of the data points excluding composition **emD.**

Using Equation (3.10), the predicted value of F_{PDMSMA} can be calculated from the intrinsic viscosity obtained by GPC. Using a statistical package (STATISTICA Kernel Release 5.5) the corrected F_{PDMSMA} for composition **emD** is 0.07 with a 95% upper confidence limit of 0.12 and a 95% lower confidence limit of 0.05; all of these values are well above the 0.003 calculated from quantitative NMR. Furthermore, comparing **scA** to **scD** shows an increase in F_{PDMSMA} from 0.047 to 0.115 (a factor of 2.5) when f_{PDMSMA} is doubled. The same comparison for **emA** and **emD** with the corrected F_{PDMSMA} for **emD** shows an increase in F_{PDMSMA} from 0.021 to 0.07 (a factor of 3.3) when f_{PDMSMA} is doubled rather than a decrease by a factor of 10. It

has been shown that the emulsion and scCO₂-based polymers are similar suggesting that the corrected F_{PDMSMA} for **emD** is the more appropriate value.

3.4.8 Thermal Analysis

Fluoropolymers are known for their thermal stability and PCTFE has a $T_{1\%}$ of 300 °C [52]. For the terpolymers synthesized herein, the decomposition temperature was measured by TGA for 1% and 50% mass loss when heating the samples at 5 °C/min in air (Table 3.5) with typical traces shown in Figure 3.9. For both polymerization media, there is an increase of at least 22 °C between composition D and the remaining compositions, A through C. This implies a shift in the initial decomposition mechanism from loss of the PDMSMA component with a $T_{1\%}$ of 226 °C [11] to decomposition by loss of acetic acid from the VAc group at 244 °C [11, 53], a difference of 18 °C. Yet composition **emD** has a lower PDMSMA content than **emA** and **emB**, implying potentially greater thermal stability. However, if the corrected F_{PDMSMA} calculated from the intrinsic viscosity of **emD** is used, $F_{\text{PDMSMA}} = 0.07$, the trend in thermal decomposition behaviour is as expected. This further confirms that the true value of F_{PDMSMA} for **emD** is on the order of 0.07 and that the quantitative NMR for **emD** may be returning a lower PDMSMA content in the polymer than expected, potentially due to differing solubility of the polymers in the CDCl₃. The further increase in the initial decomposition temperature above 244 °C reflects the presence of the CTFE, which enhances the thermal stability of the terpolymers. At $T_{50\%}$ no correlation in decomposition temperature and PDMSMA composition is observed.

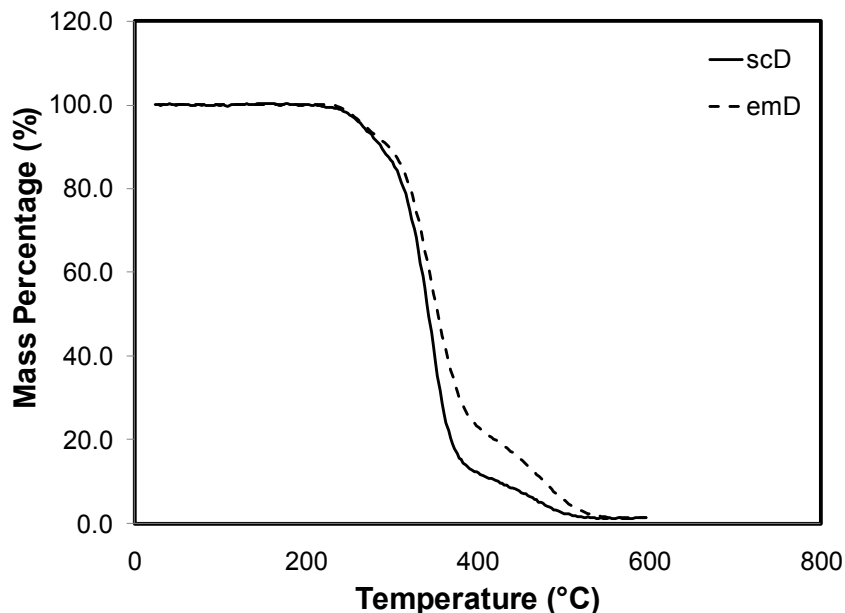


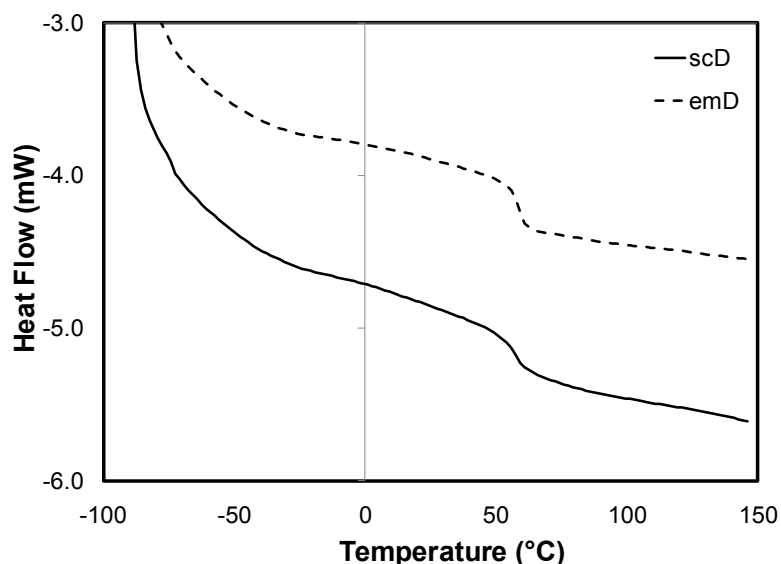
Figure 3.9: Typical TGA traces for scCO₂ and emulsion terpolymers

The terpolymers have T_g s of 48° to 56 °C, shown in Table 3.5 with typical traces shown in Figure 3.10. The known T_g s of the components are PCTFE = 52 °C and p(VAc) = 32 °C [16] and the T_g of p(PDMSMA) can be estimated by examining the T_g s of similar methacrylates. Other methacryloxypropyl-terminated silicon-containing polymers (Chapter 4) have T_g s that reflect the methacrylate component rather than the pendant siloxane and it is assumed that this will be true for PDMSMA. The pendant group of PDMSMA contains six CH₂ groups (a propyl group between the siloxane and the methacrylate functionality and a terminal *n*-butyl group on the siloxane), which when combined is the equivalent of heptyl methacrylate. Hexyl methacrylate has a T_g of -5 °C and octyl methacrylate has T_g of -20 °C [16] implying the T_g of the non-siloxane component of PDMSMA falls between these two values.

Table 3.5: Decomposition ($T_{1\%}$, $T_{50\%}$) and glass transition temperatures (T_g)

ID	Polymer Composition			$T_{1\%}$ (°C)	$T_{50\%}$ (°C)	T_g (°C)
	F_{CTFE}	F_{VAc}	F_{PDMSMA}			
emA	0.425	0.554	0.021	260	340	54
emB	0.405	0.584	0.011	268	347	54
emC	0.327	0.672	0.001	278	339	51
emD	0.458	0.539	0.003 (0.07)*	231	347	54
scA	0.442	0.511	0.047	259	356	56
scB	0.390	0.576	0.034	257	348	56
scC	0.368	0.606	0.026	259	344	50
scD	0.413	0.474	0.113	235	343	48

* The value in parentheses represents the corrected F_{PDMSMA}

**Figure 3.10: Typical DCS traces for $scCO_2$ and emulsion terpolymers**

The apparent single T_g associated with the terpolymers implies a homogenous phase structure. Assuming such a structure allows for the application of the Fox equation (Equation 2.5) to calculate the terpolymer T_g . To obtain T_g s for the terpolymers between 48° and 56 °C, the T_g for PDMSMA is calculated at 81 °C although this value appears elevated. The T_g of a methacrylate decreases as the length of the pendant group increases, Table 3.6. This is due to the increase in free

volume associated with the pendant group. The pendant group of PDMSMA consists of the aforementioned 6 CH₂ groups and a siloxane of 8 to 10 repeat units. Therefore, it is highly likely that the T_g for PDMSMA is lower than that of a hexyl methacrylate due to the increased length of the pendant group, particularly since the T_g for PDMS is -127 °C suggesting a significant free volume associated with this class of polymers. The T_g of 81 °C for PDMSMA is, therefore, at least 86 °C higher than expected based on a comparison with hexyl methacrylate. Furthermore, it appears that the PDMSMA has a minimal if any effect on the T_g of the terpolymers as this falls near the known T_gs of PCTFE and p(VAc) and subsequently, the CTFE-VAc-PDMSMA terpolymers are believed to be phase separated. This phase separation was seen previously in work on TFE-VAc-PDMSMA [11].

Table 3.6: Effect of pendant group on methacrylate glass transition temperature

Methacrylate	No. of CH ₂ groups	T _g (°C) [16]
Hexyl methacrylate	5	-5
Octyl methacrylate	7	-20
Dodecyl methacrylate	11	-65
Octadecyl methacrylate	17	-100

The T_gs between 48° and 56 °C for the terpolymers represent the CTFE-VAc component, yet these temperatures are elevated by 6° to 15 °C over the expected T_g as calculated by the Fox equation when the weight percentages of only CTFE and VAc are accounted for. This may be due to the alternating CTFE-VAc (BAB) sections of the terpolymers. An alternating structure can stiffen the polymer backbone relative to the component homopolymers, p(VAc) or PCTFE, resulting in a copolymer T_g that is higher than either component alone. A similar effect has been seen with ethylene-CTFE alternating copolymers where the T_g of polyethylene is

-30 °C [16], the T_g of PCTFE is 52 °C, and the T_g of the copolymer is 65 °C [54].

Table 3.1 shows that for the terpolymers synthesized herein 71 to 95% of the triads in the polymer backbone contain at least one CTFE or PDMSMA, suggesting a large degree of alternation.

3.5 Conclusions

A series of new CTFE-VAc-PDMSMA terpolymers were successfully synthesized in both $scCO_2$ without a surfactant and by a modified aqueous emulsion polymerization with an oil-soluble initiator and a fluorosurfactant. Vinyl acetate was required for the copolymerization of CTFE and PDMSMA, bridging the large reactivity difference between CTFE and PDMSMA. Those terpolymers synthesized in $scCO_2$ had higher yield, lower molar masses, and contained more PDMSMA than the equivalent emulsion analogue. This higher PDMSMA content led to slightly lower thermal stability but did not affect the glass transition temperature. One T_g was observed corresponding to the CTFE-VAc component of the terpolymers. Long chain branching due to VAc did not depend upon the polymerization medium for polymers of similar molar mass. Together the results demonstrate that the emulsion polymerization technique is a viable alternative to $scCO_2$, overcoming the high pressure required as similar polymers with respect to composition and structure can be achieved by both methods. The $scCO_2$ polymers, however, incorporate more PDMSMA, which may be important to low surface energy applications. These terpolymers may find application as coatings in electrophotography or other applications where the combination of high thermal stability and low surface energy is required.

3.6 References

1. Boutevin B and Pietrasanta Y. *Progress in Organic Coatings* 1985;13(5):297-331.
2. Zeigler JM and Fearon Gordon FW. *Silicon-Based Polymer Science: A Comprehensive Resource*. Washington, DC: American Chemical Society, 1990.
3. Thorpe AA, Peters V, Smith JR, Nevell TG, and Tsibouklis J. *Journal of Fluorine Chemistry* 2000;104(1):37-45.
4. Furukawa Y and Kotera M. *Journal of Polymer Science Part A-Polymer Chemistry* 2002;40(18):3120-3128.
5. Suzuki H, Takeishi M, and Narisawa I. *Journal of Applied Polymer Science* 2000;78(11):1955-1963.
6. Murase H, Nanishi K, Kogure H, Fujibayashi T, Tamura K, and Haruta N. *Journal of Applied Polymer Science* 1994;54(13):2051-2062.
7. Boutevin B, Guida-Pietrasanta F, and Ratsimihety A. *Journal of Polymer Science Part A-Polymer Chemistry* 2000;38(20):3722-3728.
8. Smith DW and Babb DA. *Macromolecules* 1996;29(3):852-860.
9. Shiho H and DeSimone JM. *Journal of Polymer Science Part A-Polymer Chemistry* 2000;38(17):3100-3105.
10. Shiho H and DeSimone JM. *Journal of Polymer Science Part A-Polymer Chemistry* 2000;38(7):1139-1145.
11. Baradie B and Shoichet MS. *Macromolecules* 2005;38:5560-5568.
12. Shimizu T. *Fluorinated Acrylic Ester Polymers*. In: Scheirs J, editor. *Modern Fluoropolymers*. Chichester, New York: Wiley, 1997. pp. 507-523.
13. Bajzer WX and Kim YK. *Poly(fluorosilicones)*. *Kirk-Othmer Encyclopedia of Chemical Technology*, vol. 11. pp. 722-729.
14. Davis SV, Chen J-H, Aslam M, and Wu F. *Canada Patent 2280308*, 1999
15. Kim DK, Lee SB, Doh KS, and Nam YW. *Journal of Applied Polymer Science* 1999;74(8):1917-1926.

16. Brandrup J, Immergut EH, and Grulke EA. Polymer Handbook, 4th ed. Toronto: John Wiley & Sons Inc., 1999.
17. Baradie B and Shoichet MS. *Macromolecules* 2002;35(9):3569-3575.
18. Jones CW. United States Patent 5723556, 1998
19. Murray DL, Harwood HJ, Shendy SMM, and Piirma I. *Polymer* 1995;36(20):3841-3848.
20. Sperling LH. *Introduction to Physical Polymer Science*, 2nd ed. Toronto: John Wiley & Sons, Inc., 1992.
21. Lousenberg RD and Shoichet MS. *Macromolecules* 2000;33(5):1682-1685.
22. Modena M, Borsini G, and Ragazzini M. *European Polymer Journal* 1967;3:5-12.
23. Grcev S, Schoenmakers P, and Iedema P. *Polymer* 2004;45(1):39-48.
24. Graessley WW and Mittelhauser HM. *Journal of Polymer Science Part A-2-Polymer Physics* 1967;5(3Pa2):431-454.
25. Friis N, Goosney D, Wright JD, and Hamielec AE. *Journal of Applied Polymer Science* 1974;18(4):1247-1259.
26. Tobita H. *Polymer* 1994;35(14):3032-3038.
27. Iedema PD, Grcev S, and Hoefsloot HCJ. *Macromolecules* 2003;36(2):458-476.
28. Yaws CL. *Handbook of Vapor Pressure*, 1994.
29. Polic AL, Duever TA, and Penlidis A. *Journal of Polymer Science Part A-Polymer Chemistry* 1998;36(5):813-822.
30. Alduncin JA, Forcada J, Barandiaran MJ, and Asua JM. *Journal of Polymer Science Part A-Polymer Chemistry* 1991;29(9):1265-1270.
31. Asua JM, Rodriguez VS, Sudol ED, and Elaasser MS. *Journal of Polymer Science Part A-Polymer Chemistry* 1989;27(11):3569-3587.
32. Luo YW and Schork FJ. *Journal of Polymer Science Part A-Polymer Chemistry* 2002;40(19):3200-3211.
33. Nomura M and Fujita K. *Makromolekulare Chemie-Rapid Communications* 1989;10(11):581-587.

34. Barton J and Karpatyova A. *Makromolekulare Chemie-Macromolecular Chemistry and Physics* 1987;188(4):693-702.
35. Nomura M and Suzuki K. *Industrial & Engineering Chemistry Research* 2005;44(8):2561-2567.
36. Dunn AS. Harkins, Smith-Ewart and Related Theories. In: Lovell PA and El-Aasser MS, editors. *Emulsion Polymerization and Emulsion Polymers*. Toronto: John Wiley and Sons Ltd., 1997. pp. 126-163.
37. Nomura M, Ikoma J, and Fujita K. Kinetics and Mechanisms of Particle Formation and Growth in the Emulsion Polymerization Initiated by the Oil-Soluble Initiator, 2,2'-Azobisisobutyronitrile. In: Daniels ES, Sudol ED, and El-Aasser MS, editors. *Polymer Latexes: Preparation, Characterization and Applications*, vol. 492. Atlanta: ACS Symposium Series, 1991. pp. 55-71.
38. Odian G. *Principles of Polymerization*, 4th ed. Hoboken, NJ: John Wiley & Sons, Inc., 2004.
39. Stagnari F, Chiarini M, and Pisante M. *Journal of Pesticide Science* 2007;32(1):16-23.
40. Baradie B, Shoichet MS, Shen ZH, McHugh MA, Hong L, Wang Y, Johnson JK, Beckman EJ, and Enick RM. *Macromolecules* 2004;37(20):7799-7807.
41. Watkins JJ and Mccarthy TJ. *Macromolecules* 1995;28(12):4067-4074.
42. Rossignoli PJ and Duever TA. *Polymer Reaction Engineering* 1995;3(4):361-395.
43. Liu T, DeSimone JM, and Roberts GW. *Chemical Engineering Science* 2006;61(10):3129-3139.
44. Penelle J, Verraver S, Raucq P, and Marchandbrynaert J. *Macromolecular Chemistry and Physics* 1995;196(3):857-867.
45. Matsumoto M and Ohyanagi Y. *Journal of Polymer Science* 1960;46(148):520-523.
46. Graessley WW, Hartung RD, and Uy CW. *Journal of Polymer Science Part A-2-Polymer Physics* 1969;7(11PA):1919-1935.
47. Brook MA. *Silicon in Organic, Organometallic, and Polymer Chemistry*. Toronto: John Wiley & Sons, Inc., 2000.

48. Britton D, Heatley F, and Lovell PA. *Macromolecules* 1998;31(9):2828-2837.
49. Striegel AM. Long-Chain Branching Macromolecules: Analysis by SEC. *Encyclopedia of Chromatography*: Taylor & Francis, 2005. pp. 1008-1012.
50. Flory PJ. *Journal of the American Chemical Society* 1947;69(11):2893-2899.
51. Sun T, Brant P, Chance RR, and Graessley WW. *Macromolecules* 2001;34(19):6812-6820.
52. Zulfiqar S, Rizvi M, Munir A, Ghaffar A, and McNeill IC. *Polymer Degradation and Stability* 1996;52(3):341-348.
53. Holland BJ and Hay JN. *Polymer* 2002;43(8):2207-2211.
54. Khanna YP, Sibilia JP, and Chandrasekaran S. *Macromolecules* 1986;19(9):2426-2431.

4 Synthesis and Decomposition of Fluorocarbon-Silsesquioxane Polymers

4.1 Abstract

A series of homo-, co-, and terpolymers of chlorotrifluoroethylene (CTFE), methacryloxypropyl-terminated silsesquioxane (POSSMA), and vinyl acetate (VAc) were synthesized in supercritical CO₂ (scCO₂) using AIBN initiation. Polymer composition was determined through reactivity ratios and NMR analysis. The CTFE-POSSMA copolymers have a blocky structure resulting from consecutive homopolymerization due to significantly different reactivity ratios whereas CTFE-VAc-POSSMA terpolymers have an alternating-like structure of CTFE and VAc with minimal (2 mol%) POSSMA inclusion. When cast as films from solution, both the co- and terpolymers show a surface enriched in POSSMA with the majority of the compositions synthesized having surfaces resembling that of homopolymeric p(POSSMA) in terms of hydrophobicity and silicon surface composition, demonstrating the surface activity of the POSSMA. The thermal stability of the polymers increases with CTFE content except for the copolymer containing 81 mol% CTFE. Decomposition of the polymers was examined in air and an inert N₂ atmosphere. In air, the copolymers give 40 to 47 wt% char due to oxidation of the silsesquioxane to SiO₂ while in N₂, no residue is seen. The opposite occurs for the terpolymers with a carbonaceous residue of approximately 20 wt% forming in N₂. The decomposition mechanism is elucidated. Flammability of the polymers was also examined where the terpolymer had lower flammability than a similar copolymer. Of the polymers synthesized, the p(CTFE-POSSMA-VAc) with the highest CTFE content is of particular interest as it displays flammability similar to p(CTFE) and

surface properties comparable to p(POSSMA) resulting in a low-flammability, hydrophobic polymer for potential applications as an additive to paint formulations.

4.2 Introduction

Fluorosilicones are known for excellent low temperature capabilities, since they retain their ductility to lower temperatures than other commercially available fluoroelastomers, as well as chemical and thermal stability [1]. However, in the presence of acid or base catalysts the thermal stability of fluorosilicones is reduced from a potential 350 °C to 150 °C [2]. The initial thermal decomposition of fluorosilicones is due to random chain scission of the siloxane backbone [3]. To prevent (or limit) this chain scission, fluorocarbons can be included in the polymer backbone, thereby blocking additional chain unzipping. Numerous authors [4-10], have synthesized these hybrid fluorosilicones. However, this class of fluorosilicone typically relies on multi-step condensation reactions which can lead to lower molar masses (M_n typically less than 20 kg/mol) [8-10]. Another way to synthesize fluorosilicone polymers has the siloxane as the pendant group and the fluorocarbon as the backbone, a structure that is the reverse of typical commercial fluorosilicones such as poly(3,3,3-trifluoropropyldimethylsiloxane) (PTFPMS). These reverse fluorosilicones have been synthesized by grafting polysiloxane macromers onto fluorocarbon backbones [11-13] through either the addition of an epoxide-terminated [11] or isocyanate-terminated siloxane to a fluoropolymer containing a pendant alcohol [12, 13] although low molar masses are still observed due to the low M_n (15.5 kg/mol) of the starting fluorocarbon [12]. To improve the molar mass, fluorocarbon-siloxane copolymers were synthesized by free radical polymerization

[14, 15]; however, both the fluorocarbon and siloxane moieties were pendant to the hydrocarbon main chain, likely limiting overall thermal stability as the siloxane component has a decomposition temperature of 226 °C [16] and the fluorocarbon component has a decomposition temperature on the order of 280 °C [17].

To achieve high thermal stability, Baradie and Shoichet pursued fluorosilicones with a fluorinated backbone, which were synthesized in a one-step radical polymerization using supercritical CO₂ (scCO₂) [16]. This approach takes advantage of the solubility of both fluorine- and siloxane-containing monomers in scCO₂, an environmentally benign solvent, and leads to the higher molar masses desired. Additionally, the polymers formed exhibit excellent thermal stability as well as promising surface characteristics for potential use in electrophotography [18-20]. However, these polymers are limited in that a purely hydrocarbon-based component, vinyl acetate (VAc), is required to ensure that both the fluorocarbon and the siloxane groups are in the final polymer due to the large difference in reactivity between the fluorocarbon and the siloxane-containing monomers [16]. The VAc was also hypothesized by Baradie and Shoichet [16] to be the point of initial thermal decomposition and its removal may lead to polymers of greater thermal stability. Furthermore, the VAc has the highest surface energy of the three components [21] suggesting it provides little value to the functionality of the terpolymer although it may have benefit in other unexamined areas such as mechanical properties.

This Chapter describes the synthesis of a fluorocarbon-silicon containing polymer, based on chlorotrifluoroethylene (CTFE) and heptaisobutyl monomethacryloxypropyl polyhedral oligomeric silsesquioxane (POSSMA), formed

by radical copolymerization in supercritical CO₂ without a hydrocarbon-based link. It was hypothesized that the reactivity ratios of POSSMA and CTFE would be close enough for copolymerization [22] rather than the 1000-fold difference in reactivity ratios seen between the fluorocarbon and siloxane component of the polymers previously synthesized by Baradie and Shoichet [16]. Supercritical CO₂ was chosen despite the work with emulsion polymerization in Chapter 3 for two reasons. First, the POSS moiety is synthesized through hydrolysis followed by condensation [2]. This is reversible and using an aqueous based system may cause reversion of the POSS moiety. Second, one of the design criteria for the polymers in this thesis is low surface energy and the work described in Chapter 3 showed that the incorporation of PDMSMA, the surface active component, was greater in scCO₂ than in emulsion.

To test the hypothesis, copolymers of CTFE and POSSMA were synthesized and subsequently characterized for reactivity ratios, thermal stability, decomposition, flammability and surface free energy. Additionally, the first synthesis of a polyhedral oligomeric silsesquioxane (POSS) containing homopolymer in scCO₂ is reported and for comparison, polymers wherein the hydrocarbon-based component, VAc, was maintained. The polymerization of CTFE is also safer than that of TFE, which has the potential to self-polymerize explosively. While CTFE is less thermally stable than TFE, this loss may be mitigated by the greater thermal stability of silsesquioxanes over siloxanes [2]. Additionally, silsesquioxanes have demonstrated low flammability [23-26], and chlorine is a significantly better flame retardant than fluorine [27] with CTFE exhibiting quite low flammability [28] making

copolymers of these components attractive as additives for paint formulations. This is particularly true with the potential for a low energy surface from the POSSMA component.

4.3 Experimental

4.3.1 Materials

All materials were used as received unless otherwise specified.

Chlorotrifluoroethylene, methyl ethyl ketone (MEK), and vinyl acetate were purchased from Sigma-Aldrich Co. (Ontario, Canada). Isopropanol and pentane were purchased from Caledon Laboratories Ltd. (Ontario, Canada).

Azobisisobutyronitrile (AIBN) was supplied by E.I. Du Pont de Nemours as Vazo® 64. Heptisobutyl monomethacryloxypropyl polyhedral oligomeric silsesquioxane (POSSMA) was purchased from Hybrid Plastics (Hattiesburg, MS).

4.3.2 Polymerization

All polymerizations were carried out under supercritical CO₂ in a high-pressure stainless steel reactor. Prior to addition to the reactor, the free radical initiator, AIBN (2 mol% based on monomer mass), was re-crystallized from methanol (0.3 M solution), and dried under vacuum for several hours at room temperature. Subsequently, solid POSSMA was added and the reactor evacuated and placed in a liquid nitrogen bath. Vinyl acetate was added by cannula, typically at 0 °C, and the reactor contents degassed. The CTFE was then added while ensuring that the reactor temperature did not rise above the boiling point (-28 °C) of liquid CTFE. The amount of CTFE added was determined by measuring the mass lost by the CTFE gas cylinder. The total mass of the all monomers was approximately 20 g.

Supercritical fluid purity CO₂ was added while the reactor was heated to 10 °C, such that the resulting pressure was approximately 55 bar. The reactor was then heated to the reaction temperature of 65 ± 1 °C, having an initial pressure of 330 to 350 bar. Typical polymerizations were stopped after 72 h by cooling the reactor to room temperature and slowly venting to atmosphere. The reaction length of 72 hours was chosen to increase the incorporation of CTFE into the resulting polymers. The resulting polymer was removed from the reactor by dissolving in methyl ethyl ketone (MEK) and precipitated into a 10-fold excess of isopropanol. The polymer was then filtered and dried under vacuum (10 mm Hg) at 80 °C for 5 h. The CTFE-POSSMA copolymers were synthesized as above minus the addition of vinyl acetate to the reactor. Additionally, the copolymers were removed from the reactor by dissolution in pentane rather than methyl ethyl ketone. The POSSMA homopolymer was also synthesized as above with only POSSMA added to the supercritical reactor. As with the copolymers, the homopolymer was removed from the reactor by dissolution in pentane.

4.3.3 Bulk Analysis

Polymer molar mass was measured by gel permeation chromatography (GPC, Viscotek VE2001 GPCmax) using a Viscotek TDA302 detector for refractive index and viscosity. The mobile phase was THF at a flow rate of 1 mL/min, and the polymer molar mass was calculated relative to polystyrene standards using two ViscoGEL columns (GMHHR-M and GMHHR-H) in series. For detailed curves, see Appendix D. ¹H and ¹⁹F NMR spectra (Varian Gemini 400 spectrometer) were obtained in CDCl₃ at 399.95 and 376.30 MHz. For detailed spectra, see Appendix

A. Quantitative ^1H NMR was obtained using a pulse delay of 35 s and a pulse angle of 90° with α,α,α -trifluorotoluene (TFT) (^1H $T_1 = 6.7$ s) at a v/v% of 0.14 added as a reference to the CDCl_3 . To obtain quantitative ^{19}F NMR, a pulse delay of 2.0 s and pulse angle of 75° was used with the same TFT (^{19}F $T_1 = 2.1$ s) as a reference. In both the quantitative ^1H and ^{19}F NMR, the pulse delay and/or pulse angle were selected to ensure that the delay was a minimum of five times the longest T_1 , i.e. the ^1H or ^{19}F had returned to equilibrium prior to the next pulse. Alternative pulse sequences and delays where the delay was less than five times the longest T_1 were also examined and resulted in errors in the compositional feed as great as 80% for the CTFE and 325% for the POSSMA. This highlights the importance of selecting the appropriate pulse and delay sequence. Decoupling of the H and F was not completed since both H and F are high field elements. Considerable modification of the spectrometer is required to decouple the signals and this was not justified in this thesis as the methine peak associated with the VAc provided sufficient detail of the polymer backbone structure.

Reactivity ratios were calculated using the software RREVM Version 2.3 [29], which solves the differential form of the instantaneous copolymer composition equation, shown in Equation (4.1), using the error-in-variables model (EVM) method.

$$F_1 = \frac{r_1 f_1^2 + f_1 f_2}{r_1 f_1^2 + 2f_1 f_2 + r_2 f_2^2}, \quad (4.1)$$

where F_1 is the mole fraction of monomer 1 in the copolymer, f_1 and f_2 are the mole fractions of monomers 1 and 2 in the feed, and r_1 and r_2 are the monomer reactivity ratios for monomers 1 and 2. To calculate the reactivity ratios, estimates for the error

in the feed and polymer compositions are required. The error for the feed composition was calculated using Equations (4.2) to (4.7). The %errorf was calculated for each of the feed compositions used in determining the reactivity ratios and averaged to obtain 1.4%.

$$n_{CTFE(Max)} = \frac{M_{CTFE} + 0.1}{MW_{CTFE}}, \quad (4.2)$$

$$n_{CTFE(Min)} = \frac{M_{CTFE} - 0.1}{MW_{CTFE}}, \quad (4.3)$$

$$n_{POSSMA} = \frac{M_{POSSMA}}{MW_{POSSMA}}, \quad (4.4)$$

$$f_{CTFE(Max)} = \frac{n_{CTFE(Max)}}{n_{CTFE(Max)} + n_{POSSMA}}, \quad (4.5)$$

$$f_{CTFE(Min)} = \frac{n_{CTFE(Min)}}{n_{CTFE(Min)} + n_{POSSMA}}, \quad (4.6)$$

$$\%errorf = \frac{f_{CTFE(Max)} - f_{CTFE(Min)}}{f_{CTFE(Min)}} \times 100\%, \quad (4.7)$$

where $n_{CTFE(Max)}$ is the maximum number of moles of CTFE in the feed due to measurement error; $n_{CTFE(Min)}$ is the minimum number of moles of CTFE in the feed due to measurement error; M_{CTFE} is the mass of CTFE added; MW_{CTFE} is the molar mass of CTFE, 0.1 is the accuracy of the scale used to measure the mass of CTFE; n_{POSSMA} is the number of moles of POSSMA in the feed; M_{POSSMA} is the mass of POSSMA added; MW_{POSSMA} is the molar mass of POSSMA; $f_{CTFE(Max)}$ is the maximum mole fraction of CTFE in the feed due to measurement error; $f_{CTFE(Min)}$ is the minimum mole fraction of CTFE in the feed due to measurement error; and %errorf is the feed composition error for a given feed composition. A similar calculation can be done on the POSSMA component of the feed; however, the scale

used to determine the POSSMA mass (as well as VAc for the terpolymers) had significantly greater accuracy (± 0.001 g) and any error due to changes in POSSMA feed was negligible relative to the amount introduced by CTFE.

There were two sources of error considered in determining the polymer composition error. The first is the volume of TFT added as a standard and the second is the phase correction of the resulting NMR spectra. The volume of TFT added will determine the strength of the standard signal in the quantitative NMR against which the polymer signal is compared. Therefore, changes in the volume will change the polymer composition. To determine the error associated with the volume of TFT a similar methodology to that used for calculating the feed composition error of CTFE was used, Equations (4.8) to (4.13). The error in TFT measurement ($\%errorTFT$) was calculated at 4.4%.

$$n_{TFT} = \frac{V_{TFT} \rho_{TFT}}{MW_{TFT}} , \quad (4.8)$$

$$n_{CTFE} = \frac{I_{CTFE}}{I_{TFT}} n_{TFT} , \quad (4.9)$$

$$m_{CTFE} = n_{CTFE} MW_{CTFE} , \quad (4.10)$$

$$w_{CTFE} = \frac{m_{CTFE}}{m_{polymer}} , \quad (4.11)$$

$$F_{CTFE} = \frac{\frac{w_{CTFE}}{MW_{CTFE}}}{\left(1 - w_{CTFE}\right) \frac{w_{CTFE}}{MW_{POSSMA}} + \frac{w_{CTFE}}{MW_{CTFE}}} , \quad (4.12)$$

$$\%errorTFT = \frac{F_{CTFE(Max)} - F_{CTFE(Min)}}{F_{CTFE(Min)}} , \quad (4.13)$$

where n_{TFT} is the number of moles of TFT used as a standard for NMR analysis; V_{TFT} is the volume of TFT standard added; ρ_{TFT} is the density of TFT; MW_{TFT} is the molar mass of TFT; I_{TFT} is the area of integration for the TFT NMR signal; I_{CTFE} is the area of integration for the CTFE NMR signal; n_{CTFE} is the number of moles of CTFE in the polymer; m_{CTFE} is the mass of CTFE in the polymer aliquot used for NMR analysis; MW_{CTFE} is the molar mass of CTFE; $m_{polymer}$ is the mass of the polymer aliquot; w_{CTFE} is the weight fraction of CTFE in the polymer; MW_{POSSMA} is the molar mass of POSSMA; F_{CTFE} is the mole fraction of CTFE in the polymer; $F_{CTFE(Max)}$ is the maximum mole fraction of CTFE in the polymer based on a volume of TFT standard (V_{TFT}) that is 0.1 μL greater than the amount added (1.0 μL); $F_{CTFE(Min)}$ is the minimum mole fraction of CTFE in the polymer based on a volume of TFT standard (V_{TFT}) that is 0.1 μL less than the amount added (1.0 μL); and $\%error_{TFT}$ is the error in polymer composition due to measurement error in the volume of TFT standard.

Phase correction of NMR spectra is required due to variations in the starting point of the sine wave associated with the time domain signal. For example, a sine wave that starts at 0° , when Fourier transformed, will give a purely absorptive positive peak. However, a sine wave that is out of phase will result in a peak that is not purely positive, i.e. above the baseline of the spectra. The degree to which a resulting transformed peak will be out of phase typically varies as a linear function of chemical shift. This is corrected by setting a phase correction equal the intercept and slope of this linear function. The selection of the intercept and slope for a particular spectrum may vary each time it is determined as the selection is typically

done in a graphical manner. This will lead to slightly different peak shapes, and subsequently, slightly different integrations each time the phase of a spectrum is corrected.

Since the polymer composition is determined by the integration of the quantitative NMR spectra, there will be an error in the compositions associated with the above phase correction. To calculate the error associated with phase correction of the NMR spectra, the spectrum for each polymer composition was phased three times. The average mole fraction of CTFE and the percent error due to phasing for each composition was calculated according to Equations (4.14) to (4.16).

$$\%errorphase(i) = \frac{F_{CTFE(i)} - F_{CTFE(Avg)}}{F_{CTFE(Avg)}}, \quad (4.14)$$

$$\%errorphase(comp) = \frac{\sum \%errorphase(i)}{3}, \quad (4.15)$$

$$\%errorphase(overall) = \frac{\sum \%errorphase(comp)}{N}, \quad (4.16)$$

where $F_{CTFE(i)}$ is the mole fraction of CTFE for a given phasing of the NMR spectrum; $F_{CTFE(Avg)}$ is the average of the $F_{CTFE(i)}$ for a given polymer composition; $\%errorphase(i)$ is the percent error associated with one of the three phasings completed on the NMR spectrum; $\%errorphase(comp)$ is the average of the percent errors calculated for the three phasings of the NMR spectrum, i.e., the percent error due to phasing for a given polymer composition; $\%errorphase(overall)$ is the average of the percent error due to phasing; N is the total number of phasings completed and is equal to 36. The $\%errorphase(overall)$ equals 7.0%. As the mole fraction of POSSMA is greater than that of CTFE for all of the copolymer compositions, the percent error due to phasing of the mole fraction of CTFE must be greater than that

of POSSMA. The overall error of the polymer composition due to analysis of NMR is the sum of the error due to TFT and phasing and equals 11.4%.

4.3.4 Surface Analysis

Surface analysis was completed by measuring the dynamic water contact (advancing and receding) angles and the surface composition by X-ray photoelectron spectroscopy (XPS) of solvent-cast films on glass microscope cover slips. The terpolymers of p(CTFE-VAc-POSSMA) were dissolved in MEK whereas the copolymers of p(CTFE-POSSMA) and the homopolymers of p(POSSMA) were dissolved in pentane at a concentration of 0.1 g/L. The advancing and receding water contact angles were measured using a VCA Optima Surface Analysis System (AST Products Inc.). Six measurements at 3 locations (i.e., 18 measurements) on 3 separately prepared films for each polymer composition were taken for each of the advancing and receding contact angles. The XPS was conducted on a Leybold LHMax 200 using an Al $K\alpha$ X-ray source at 15 kV and 25 mA emission current at two take-off angles, 20° and 90°, to characterize the first 40 Å and 100 Å, respectively. Care was taken to expose the films to the X-ray for less than 5 minutes, using 192 eV for the survey scan, thereby limiting X-ray damage/decomposition of the polymer films. For detail spectra, see Appendix G.

4.3.5 Thermal Analysis

Glass transition temperatures (T_g) were measured using a TA Instruments Q1000 differential scanning calorimeter (DSC), under an inert nitrogen atmosphere, with a heating rate 10 °C/min and scanning range of -90° to 150 °C. The T_g was

determined from the second run of the polymer sample to remove residual processing effects. For detailed curves, see Appendix E. Thermogravimetric analysis (TGA) was performed using a TA Instruments Q50 Thermogravimetric Analyzer. Samples were subjected to a heating rate of 10 °C/min from 25° to 600 °C under a compressed air atmosphere or under an inert N₂ atmosphere from 25° to 800 °C. For detailed spectra, see Appendix F.

4.3.6 Decomposition Product Analysis

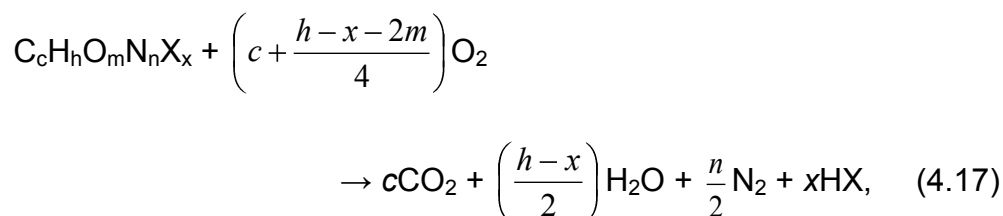
Mass spectra of the polymers were obtained from an HP5890 II gas chromatograph coupled with a VG Trio 100 mass spectrometer. Electron ionization was used at an energy level of 70 eV. An aliquot of polymer was placed into a small glass capillary tube, heated from 100° to 450 °C at 0.5 °C/s and the gaseous decomposition products analyzed. For detailed spectra, see Appendix C.

For XPS analysis, the solid decomposition residue was obtained by heating the polymer sample to the desired temperature using the Q50 Analyzer in either an inert or air atmosphere. For ¹³C solid state NMR analysis, a polymer sample was placed on a copper (Alloy 110, 99.9%) foil boat which was subsequently placed in a quartz reaction vessel and inserted into an Thermolyne 21100 Tube Furnace that was connected to a vacuum line. The quartz vessel was evacuated and purged with N₂ for a total of three cycles. The sample was then heated to the desired temperature at a nominal 10 °C/min heating rate under vacuum. To remove the sample, the quartz reaction vessel was placed under N₂ while cooling to room temperature and the sample removed. ¹³C CP-MAS NMR spectra (5 KHz spin rate, 5 s recycle delay, 2 ms contact time, π/2 pulse width of 4 μs, 10000 scans) were

acquired on a Bruker DSX 200 MHz (for ^1H) spectrometer (Bruker BioSpin, Germany) using a Bruker 4 mm solid state NMR probe. All spectra were referenced externally to adamantane (38.56 ppm & 29.50 ppm).

4.3.7 Flammability Analysis

The heat of combustion, h_c^0 , and the heat release capacity, η_c , characteristics which relate to the flammability of the polymer were determined by pyrolysis combustion flow calorimetry (PCFC) analysis [30]. In a typical experiment, approximately 1.0 to 5.0 mg of polymer sample is placed within a pyrolysis chamber and heated to 800 °C under N_2 at 10 °C/min. The gaseous products are sent to the combustion chamber where they are completely combusted under an O_2 atmosphere and the stoichiometric amount of O_2 is recorded. The h_c^0 and η_c are calculated by Equations (4.17) to (4.20).



$$C = h_{c,v}^0 / r_0 = 13.1 \pm 0.7 \text{ kJ/g-O}_2, \quad (4.18)$$

$$h_c^0 = h_{c,v}^0 (1 - \mu), \quad (4.19)$$

$$\eta_c = \frac{h_c^0 E_a}{eRT_p^2}, \quad (4.20)$$

where $h_{c,v}^0$ is the heat of complete combustion of the fuel gases; r_0 is the stoichiometric oxygen / fuel mass ratio; h_c^0 is the calculated total heat released for combustion; μ is the char yield; η_c is the heat release capacity; E_a is the global

activation energy for pyrolysis; $e = 2.718$; R is the gas constant; and T_p (K) is the temperature of the maximum mass loss rate. Equation (4.17) represents the base equation for the majority of polymers and contains nitrogen despite the lack of nitrogen in the polymers synthesized in this thesis.

4.4 Results and Discussion

4.4.1 Polymer Structure

A homopolymer of POSSMA, copolymers of CTFE and POSSMA, and terpolymers of CTFE, VAc, and POSSMA were separately synthesized in supercritical CO₂. For the purposes of this thesis, they have been designated as follows: C denotes CTFE; V denotes VAc; S denotes POSSMA. For example, a polymer designated **CVS(40-50-10)** is a terpolymer containing 40 mol% CTFE, 50 mol% VAc, and 10 mol% POSSMA. A polymer labelled **CS(40-60)** is a copolymer with 40 mol% CTFE and 60 mol% POSSMA. The homopolymers of CTFE, VAc, and POSSMA are C(100), V(100), and S(100), respectively. Finally, as a group the terpolymers will be referred to as CVS polymers and the copolymers as CS polymers.

The CVS polymers are similar to a series of terpolymers previously synthesized by Baradie and Shoichet [16] and by the author, discussed in Chapter 3, where the silicon-containing component was a methacryloxypropyl-terminated polydimethylsiloxane (PDMSMA). Attempts to synthesize fluorocarbon-PDMSMA copolymers proved unsuccessful. However, attaching the bulkier POSS, as compared with PDMS, substituent to the methacrylate group reduces the reactivity of the monomer [22] and copolymers of fluorocarbon-POSSMA are

possible. Comparing **CS(20-80)** to **CVS(46-52-02)** shows that the addition of VAc in the feed leads to significantly greater incorporation of CTFE into the polymer at the same nominal feed ratio. The feed compositions and resulting polymer compositions are given in Figure 4.1 with the molar mass and yield given in Table 4.1.

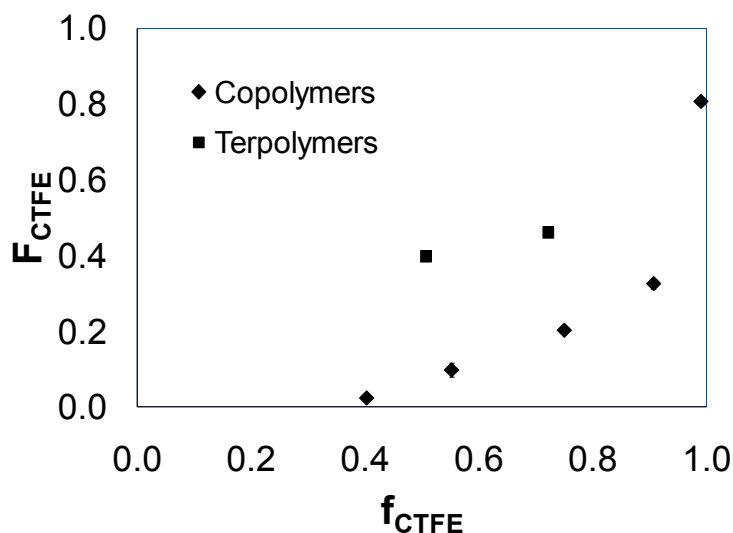


Figure 4.1: Effect of feed composition (f_i) on polymer composition (F_i). Polymer A resulted from $f_{VAc} = 0.47$ and $f_{POSSMA} = 0.03$ with $F_{VAc} = 0.59$ and $F_{POSSMA} = 0.01$. Polymer B resulted from $f_{VAc} = 0.25$ and $f_{POSSMA} = 0.03$ with $F_{VAc} = 0.52$ and $F_{POSSMA} = 0.02$.

Table 4.1: Molar mass and yield of polymers

Polymer	M_n (kg/mol)	M_w (kg/mol)	PDI	Yield (%)
S(100)	40	115	2.9	66
CS(02-98)	51	469	9.2	42
CS(10-90)	35	303	8.7	18 and 26
CS(20-80)	24	210	8.8	32
CS(33-67)	32	272	8.5	24
CS(81-19)	12	21	1.8	6
CVS(40-59-01)	32	107	3.3	24
CVS(46-52-02)	25	46	1.8	20

Increasing CTFE content in the feed resulted in a decreasing polymer yield, as shown in Table 4.1, although the yield achieved for CS(10-90) does not appear to follow this trend. However, a second experiment using the same nominal feed ratio resulted in yield of 26%. This highlights the variation in yields for these polymers. Thus, an increase in CTFE content in the feed results in a decreasing polymer yield although there may be some variability for a given feed composition. Interestingly, for the CS polymers, the molar conversion of CTFE and POSSMA is relatively constant across the feed ratios studied, at approximately 1.9% and 43%, respectively. The molar conversion of CTFE and POSSMA are calculated by dividing Equation (4.21) by Equation (4.22). Increased f_{CTFE} also resulted in lower molar mass on average.

$$\frac{m_i}{MW_i} = n_i \quad (4.21)$$

$$\frac{W_i Y}{MW_i} = N_i \quad (4.22)$$

where i represents CTFE or POSSMA, m_i is the mass of monomer added to the reactor, MW_i is the molar mass of the monomer, n_i is the number of moles of monomer in the feed, W_i is the weight fraction of monomer in the polymer as determined by quantitative NMR, Y is the mass yield of the polymer, and N_i is the number of moles of the monomer repeat in the polymer.

The polydispersity indices (PDIs) for these polymers are high relative to the theoretical values of 1.5 and 2 for a radical polymerization that terminates by combination or disproportionation, respectively. This likely arises from a combination of different reactive sites in the polymerization. For example, the radical may be

entrapped within a growing particle as in a dispersion polymerization versus a radical that is growing at the particle surface as in a precipitation polymerization. Additionally, in dispersion polymerization with a segregated radical there is the potential for the gel effect due to an increase in the local concentration of the monomer. This would increase the PDI.

Compositional drift was determined by comparing the polymers obtained from a feed ratio of CTFE to POSSMA of 1:1 over various times. As the length of the polymerization increases from 0 to 72 hours, F_{CTFE} increases, yet the yield is not a function of time as seen in Table 4.2. This may be due, in part, to variability in the loss of polymer during evacuation of the scCO₂ post-polymerization. The experimental time was taken from the moment the reactor reached the polymerization temperature of 65 °C, i.e. the 0 hour reaction was simply heated to temperature and cooled immediately. To gain further insight, reactivity ratios for the copolymers were calculated using the Error-in-Variables Method (EVM) [29] using a feed composition error of 1.4% and a polymer composition error of 11.4%. The reactivity ratios obtained are $r_{CTFE} = 0.15 \pm 0.12$ and $r_{POSSMA} = 19.3 \pm 4.3$. The large difference in reactivity ratios suggests a tendency to form a block-like copolymer [31] where POSSMA is incorporated into the polymer first with minimal CTFE followed by greater CTFE incorporation as the POSSMA feed decreases.

Table 4.2: Compositional drift of CS polymers: Impact of reaction time on polymer composition

Reaction Time (h)*	Polymer Composition (mol%)		Molar Mass (kg/mol)		Yield (%)
	CTFE	POSSMA	M _n	M _w	
0	4.3	95.7	23	103	35
3	4.7	95.3	55	408	46
8	4.3	95.7	73	702	38
24	7.0	93.0	53	304	26
72	9.8	90.2	35	303	18

* The reaction time is taken from the moment the reactor reaches temperature, i.e. 65 °C. In the case of 0 h, the reactor was heated to temperature and shut down immediately.

4.4.2 Surface Properties

The surface properties of the series of newly synthesized polymers were characterized by XPS and dynamic water contact angle measurements, the results of which are summarized in Table 4.4. The contact angle of a fluid to a polymer surface is representative of the surface energy and can be converted through Equation (4.23).

$$\gamma_{sv} = \gamma_{sl} + \gamma_{lv} \cos\theta, \quad (4.23)$$

where γ is the surface tensions; *sv*, *sl*, and *lv* represent the solid-vapour, solid-liquid, and liquid-vapour interfaces, respectively; and θ is the equilibrium contact angle for a chemically homogeneous, rigid, atomically smooth ideal surface.

The advancing water contact angles of all CS and CVS polymers are similar to that of the homopolymeric p(POSSMA), indicating that the POSSMA is present at the surface and that even low amounts of POSSMA in the bulk polymer composition

can result in a high advancing contact angle. This was confirmed by XPS analysis, which shows greater POSSMA at the surface than in the bulk composition.

The mol% of POSSMA at the film surface was calculated from all of the peaks obtained by XPS (C, Cl, F, O, and Si). This allows for an estimate of the error associated with the technique. The atomic percentage obtained for Cl was set to 1.0, which is equivalent to a polymer containing one CTFE unit. The number of POSSMA units was then determined by calculating the ratio of the expected oxygen, silicon and carbon (8, 14 and 35, respectively) to the values obtained from XPS. In the case of carbon, the two carbon atoms associated with CTFE are subtracted. An example of the calculation for **CS(33-67)** is shown in Table 4.3. A similar calculation using fluorine as a basis was also completed and the overall mean \pm standard deviation is reported in Table 4.4.

Table 4.3: Calculation of mol% POSSMA at polymer film surface for CS(33-67)

Atom	Atomic Percentage (%)	No. of atoms based on Cl (one CTFE unit)	No. of POSSMA units based on a given atom	Mol% POSSMA at surface
C	58.72	234.9	6.7	86.9
O	22.84	91.36	6.5	86.7
Si	16.98	67.92	8.5	89.5
F	1.21	4.84		
Cl	0.25	1.00		
Average				87.7
Standard Deviation				1.2

Table 4.4: Surface properties of CS and CVS polymers. Values are reported as mean \pm std. dev (n = 6 for the mol% POSSMA at the film surface; n = 3 for the water contact angles)

Polymer	Mol% POSSMA at film surface by XPS	Water Contact Angles	
		Advancing	Receding
S(100)	100.0	113 \pm 2	100 \pm 2
CS(02-98)	98.6 \pm 1.2	112 \pm 3	105 \pm 5
CS(10-90)	94.0 \pm 2.3	110 \pm 1	96 \pm 2
CS(20-80)	92.7 \pm 0.1	113 \pm 1	96 \pm 4
CS(33-67)	84.7 \pm 4.3	111 \pm 1	96 \pm 4
CVS(46-52-02)	78.8 \pm 7.1	110 \pm 2	89 \pm 2
CVS(40-59-01)	57.1 \pm 4.2	110 \pm 2	78 \pm 1 [†]
C(100)	0.0	91 \pm 2 [*]	67 \pm 3 [†]

* Significantly different from other advancing contact angles at $p < 0.01$.

† Significantly different from other receding contact angles at $p < 0.01$.

The minimal change in advancing contact angle is expected as Dettre and Johnson [32] state that the advancing contact angle does not vary greatly with increased surface coverage by the high-contact angle (low surface energy) component once a coverage of approximately 40% is achieved. All of the CS and CVS polymers have the requisite 40% coverage by POSSMA, the high-contact angle component. In contrast, the receding contact angle will increase as the coverage of the low surface energy component increases from 80 to 100%. Again, the minimum coverage value of 80% is consistent with the CS and CVS polymer systems as only **CVS(40-59-01)** has a contact angle that is statistically different from the homopolymer of POSSMA and the surface coverage of POSSMA is below 80%.

The advancing contact angle reflects the hydrophobic component of a copolymer (or blend) which is the siloxane component in this system. The receding contact angle reflects the less hydrophobic component of the copolymer, which for

the CTFE-POSSMA system is CTFE with the homopolymer having a receding contact angle of 67° versus p(POSSMA) with a receding contact angle of 100° . With increasing CTFE in the CS copolymers, the receding water contact angle decreases, resulting in greater hysteresis between advancing and receding contact angles. For the CVS terpolymers, the receding contact angle decreased further with increased VAc content while the advancing contact angle was largely unchanged, notwithstanding the low F_{POSSMA} .

Contact angle hysteresis is derived from surface heterogeneity, both physical and/or chemical. Chemical heterogeneity includes differences in chemical composition, and local adsorption, swelling or dissolution of the solid by the liquid whereas variation in the surface roughness is the most common physical cause. [33]. The contribution to contact angle hysteresis due to surface roughness can be estimated by examining **S(100)** and **C(100)** since these represent homogeneous surfaces. Therefore, the only cause of contact angle hysteresis for **S(100)** and **C(100)** is surface roughness. The difference in advancing and receding contact angles are $13^\circ \pm 3^\circ$ and $24^\circ \pm 4^\circ$, respectively. Only **CVS(40-59-01)** has a contact angle hysteresis that is greater than these values ($32^\circ \pm 2^\circ$) suggesting further contribution to the hysteresis from chemical heterogeneity. Neumann and Good [34] show that chemically heterogeneous surfaces domain sizes of $0.1 \mu\text{m}$ result in contact angle hysteresis of 10° . Therefore, for **CVS(40-59-01)** at 57% surface coverage of POSSMA, it appears that CTFE-VAc domains on the order of $0.1 \mu\text{m}$ are present and contribute to the contact angle hysteresis.

4.4.3 Thermal Properties

The glass transition temperatures of the polymers were determined by DSC. Both CS and CVS polymers had a single T_g , indicating that the polymers were not phase-separated. The T_g s of the CS polymers ranged from 41° to 48 °C, which are similar to that of isotactic PMMA [35], reflecting the methacrylate backbone of POSSMA. In contrast, the T_g s of the CVS polymers were between 55° and 56 °C. The T_g of the various constituents are 52 °C for p(CTFE) [21], 32 °C for p(VAc) [21], and 42 °C for p(POSSMA). The T_g of the terpolymers was calculated based on the Fox equation and resulted in T_g s of 42 °C for **CVS(46-52-02)** and 41 °C for **CVS(40-59-01)**, which are 13 and 15 °C lower than the experimental values, respectively. This higher experimental temperature may be due to an alternating structure in the terpolymer that can stiffen the polymer backbone relative to the component homopolymers, p(VAc) or PCTFE, resulting in a copolymer T_g that is higher than either component alone. This effect has been seen with ethylene-CTFE alternating copolymers where the T_g of polyethylene is -30 °C [21], the T_g of PCTFE is 52 °C, and the T_g of the copolymer is 65 °C. To determine if the CVS polymers have an alternating structure, the repeat unit pattern was elucidated by examining the triad sequences of the terpolymers using ^1H NMR [36], Table 4.5, which shows that the CVS polymers have an alternating structure with one CTFE in over 90% of the triad sequences.

Table 4.5: Triad composition of CVS polymers

Polymer	Percentage of Given Triad Sequence (A = VAc; B = CTFE)		
	BAB	BAA + AAB	AAA
CVS(40-59-01)	40.2	50.5	9.3
CVS(46-52-02)	73.4	25.2	1.4

The decomposition of the CS and CVS polymers was examined in air and under an inert N₂ atmosphere by TGA. The initial decomposition temperature under N₂ as a function of CTFE content is shown in Figure 4.2. It can be seen that the initial decomposition temperature, $T_{0.5\%}$, increases with greater incorporation of CTFE in the polymer.

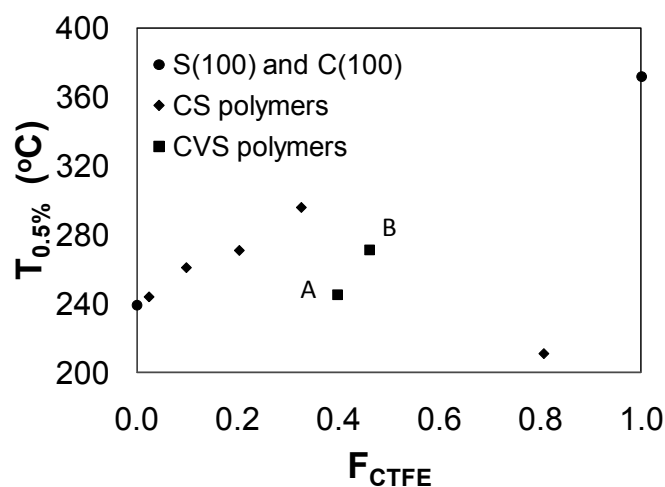


Figure 4.2: Effect of F_{CTFE} on initial decomposition temperature. Note: Polymer A contains $F_{VAc} = 0.59$ and $F_{POSSMA} = 0.01$. Polymer B contains $F_{VAc} = 0.52$ and $F_{POSSMA} = 0.02$.

In TGA, the initial mass loss will be recorded once the vapour pressure of the gaseous products formed through decomposition is greater than the ambient partial pressure. At this point, the gaseous products will diffuse from the sample [37]. Poly(chlorotrifluoroethylene) has extremely low gaseous permeability [21]; therefore, the incorporation of CTFE will inhibit the diffusion of the gaseous products, shifting

the initial decomposition, as recorded by TGA, to higher temperatures. Decreasing permeability of the polymers as a function of increasing F_{CTFE} is corroborated by comparing the TGA results with the preparation of samples for ^{13}C analysis. The TGA of the polymer samples occurred under an inert nitrogen atmosphere. To obtain a similar mass loss for the polymer under vacuum, a lower temperature was required. For example to obtain a 3% mass loss in N_2 required heating the sample to $300\text{ }^\circ\text{C}$ whereas the same mass loss was achieved under vacuum at less than $250\text{ }^\circ\text{C}$.

The polymer decomposition was also examined by DSC. Figure 4.3 shows a slight endotherm prior to the exothermic decomposition for both the CS and CVS polymers. Further examination of Figure 4.3 shows that only **CS(81-19)** has purely exothermic decomposition indicating that the initial decomposition mechanism must differ from the other CS polymer compositions which display an initial endothermic peak. This potentially explains the lower thermal stability of **CS(81-19)** relative to the other CS polymers despite a higher CTFE content. The prominence of CTFE in this polymer suggests that it behaves similar to p(CTFE) where decomposition to monomer and other small molecule halogens is seen [38].

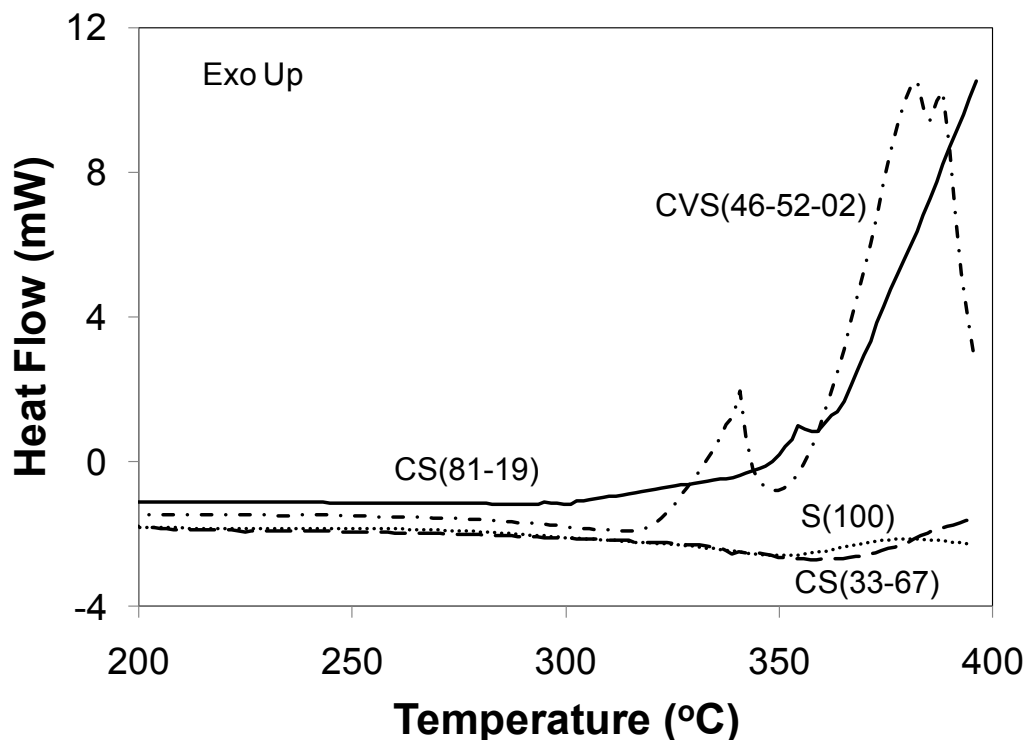


Figure 4.3: Decomposition of polymers by DSC (N_2 , $10\text{ }^\circ\text{C}/\text{min}$ heat rate, hermetic Al pan)

4.4.4 Polymer Decomposition

The full TGA traces for typical polymers are shown in Figure 4.4 for CS, CVS, p(POSSMA) [S(100)], p(VAc) [V(100)] and PCTFE [C(100)] in both air and N_2 . A comparison of Figure 4.4a and b shows that the CS polymers decompose fully under an inert atmosphere yet result in a residue of 40 to 47 wt% when heated under air. This is likely due to the oxidation of the silsesquioxane cage to SiO_2 . The expected amount of SiO_2 for each polymer was calculated, assuming complete conversion of the Si to SiO_2 , resulting in 48 to 51 wt%. Fina et al. [39] have shown that a POSS cage with isobutyl groups will begin to evaporate at $200\text{ }^\circ\text{C}$, which may explain the lower experimental values observed as some of the POSSMA may be lost through a sublimation process.

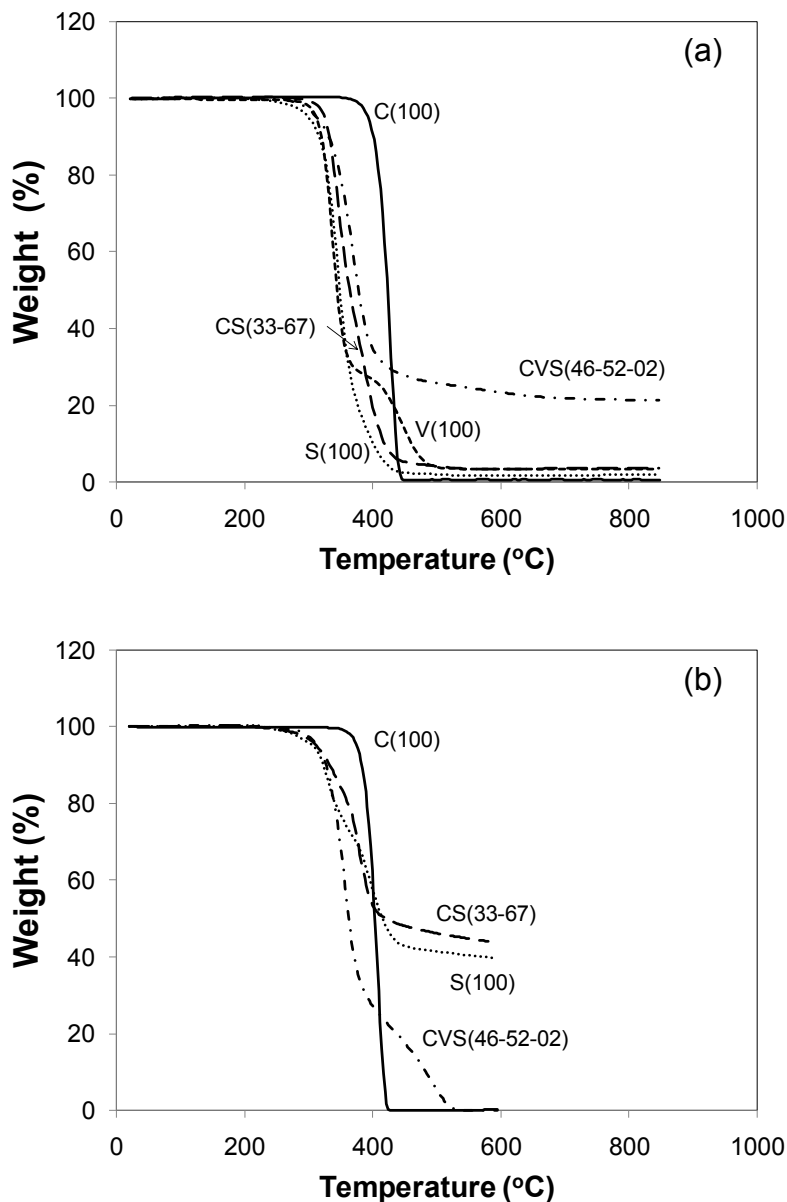


Figure 4.4: TGA traces of a select group of polymers under (a) N_2 , and (b) air

Poly(chlorotrifluoroethylene) decomposes predominantly to monomer and C_3F_5Cl through a radical mechanism at 350 °C [38]. Amir et al. [40] have shown that a copolymer of methyl methacrylate and POSSMA decomposes through loss of the methyl methacrylate and the methacryloxypropyl group followed by the formation of a carbonaceous residue from the remaining R-groups on the POSS cage.

Additionally, they observed some sublimation of the intact POSSMA at lower

temperatures, a phenomenon also seen by Fina et al. [39]. To determine the mechanism for the initial decomposition in the CS polymers, they were heated at 0.5 °C/min from 100° to 450 °C, and the gaseous products analyzed by mass spectrometry. The spectra showed predominately POSSMA monomer and both the intact POSS cage and the POSS cage without the isobutyl group. Thus it is likely that the initial decomposition consisted of depolymerization and sublimation of the POSSMA followed by separation of the methacrylate and POSS components, similar to the mechanism shown by Amir et al. [40]. In an inert atmosphere, this process continues unabated whereas in air the Si is oxidized to SiO₂. There appeared to be minimal loss of the CTFE component as evidenced by the lack of associated decomposition products in the mass spectra.

The solid decomposition products (char residue) of the CS polymers were examined by XPS. The number of techniques available for the study of char residue is limited due to the black, amorphous, insoluble nature of the char, and while XPS is a surface analytical technique, it overcomes these characteristics of char [41]. To reduce the surface aspect of the XPS analysis, two to three scans of the polymer in powder form were run in the same location, etching into the char residue and providing a bulk composition. A representative polymer, **CS(33-67)**, was heated to 300°, 380°, and 460 °C resulting in a char residue of 98.5%, 80%, and 46% of the original mass, respectively. The decomposition pathway was determined using the following equation:

$$Err = \sum (A_i^{XPS} - A_i^{CALC})^2 + \sum (R_{ij}^{XPS} - R_{ij}^{CALC})^2, \quad (4.24)$$

where i and j represents any atom found in the polymer excluding H, A_i^{XPS} is the atom% from XPS, A_i^{CALC} is the calculated atom% after the loss of the decomposition products, R_{ij}^{XPS} is the ratio of the atom percentages of any two atoms within the polymer (e.g., C and F) from XPS, and R_{ij}^{CALC} is the ratio of the calculated atom percentages of the same two atoms (e.g., C and F) within the polymer after the loss of the decomposition products. The value of Err in Equation (4.24) was minimized similar to the manner in which residuals are minimized to obtain the least squares fit of a data set. This minimization was constrained in that the mass loss obtained in determining the calculated atom percentages and ratios must match that recorded by the TGA in the formation of the XPS samples, which determines A_i^{XPS} and R_{ij}^{XPS} . Furthermore, only those decomposition products previously determined in the literature for the constituent monomers were removed from the polymer. That is, only CTFE and C_3F_5Cl were removed for CTFE rather than another combination of the three elements. By examining the expected decomposition products from literature [38-40, 42] and the temperatures at which they likely form, for example, the initial decomposition product for VAc is the loss of the acetate group at 244 °C, as well as minimizing Equation (4.24), the decomposition pathways for **CS(33-67)** and **CVS(46-52-02)** were determined. The results are shown in Tables 4.6 and 4.7 and are based on a theoretical polymer containing 100 monomer units.

Table 4.6: Calculation of decomposition products for CS(33-67).

	No Heat		T = 300 °C		T = 380 °C		T = 460 °C	
	XPS	CALC	XPS	CALC	XPS	CALC	XPS	CALC
A _C	60.29	60.02	56.5	60.26	58.95	58.47	18.15	18.11
A _F	1.94	2.46	1.91	2.51	1.52	1.72	2.48	2.47
A _O	21.72	23.35	25.38	23.43	22.92	24.35	50.58	50.53
A _{Si}	15.03	13.34	15.81	13.39	16.42	15.27	28.79	28.88
A _{Cl}	0.80	0.82	0.40	0.41	0.19	0.19	0.00	0.00
R _{C/F}	31.08	24.35	29.58	24.00	38.78	33.96	7.32	7.32
R _{C/O}	2.78	2.57	2.23	2.57	2.57	2.40	0.36	0.36
R _{C/Si}	4.01	4.50	3.57	4.50	3.59	3.83	0.63	0.63
R _{C/Cl}	75.36	73.06	141.25	148.50	310.26	311.33	N/A	N/A
R _{F/O}	0.09	0.11	0.08	0.11	0.07	0.07	0.05	0.05
R _{F/Si}	0.13	0.18	0.12	0.19	0.09	0.11	0.09	0.09
R _{F/Cl}	2.43	3.00	4.78	6.19	8.00	9.17	N/A	N/A
R _{O/Si}	1.45	1.75	1.61	1.75	1.40	1.59	1.76	1.75
R _{O/Cl}	27.15	28.42	63.45	57.75	120.63	129.67	N/A	N/A
R _{Si/Cl}	18.79	16.24	39.53	33.00	86.42	81.33	N/A	N/A
Wt % Remaining	100	100	97.6	98.5	80	80	45	46
<i>Err</i>	65.17		185.00		137.01		0.01	
Decomposition Products Lost								
C ₃ F ₅ Cl					7		7	
C ₂ F ₃ Cl					3		9	
PMA*					38		54	
POSSMA			1		6		13	
<i>i</i> -Bu					10		317	
Cl			17		17		17	
O added							108	

* Propylmethacrylate

Table 4.7: Calculation of decomposition products of CVS(46-52-02).

	No Heat		T = 300 °C		T = 375 °C		T = 450 °C	
	XPS	CALC	XPS	CALC	XPS	CALC	XPS	CALC
A _C	54.47	54.53	56.61	54.85	58.74	58.81	65.45	64.98
A _F	16.25	15.23	9.58	15.38	11.48	12.77	5.67	6.14
A _O	18.71	19.87	19.86	19.84	17.74	20.36	18.8	17.33
A _{Si}	5.27	5.30	11.03	5.35	10.33	6.08	9.88	11.55
A _{Cl}	5.29	5.08	2.87	4.57	1.72	1.98	0.19	0.00
R _{C/F}	3.35	3.58	5.91	3.57	5.12	4.61	11.54	10.59
R _{C/O}	2.91	2.74	2.85	2.76	3.31	2.89	3.48	3.75
R _{C/Si}	10.34	10.29	5.13	10.25	5.69	9.68	6.62	5.63
R _{C/Cl}	10.30	10.74	19.72	12.00	34.15	29.77	N/A	N/A
R _{F/O}	0.87	0.77	0.48	0.78	0.65	0.63	0.30	0.35
R _{F/Si}	3.08	2.88	0.87	2.88	1.11	2.10	0.57	0.53
R _{F/Cl}	3.07	3.00	3.34	3.37	6.67	6.46	N/A	N/A
R _{O/Si}	3.55	3.75	1.80	3.71	1.72	3.35	1.90	1.50
R _{O/Cl}	3.54	3.91	6.92	4.34	10.31	10.31	N/A	N/A
R _{Si/Cl}	1.00	1.04	3.84	1.17	6.01	3.08	N/A	N/A
Wt % Remaining	100	100	98.5	98.4	74	73	28	29
Err	2.95		184.84		74.50		7.59	
Decomposition Products Lost								
C ₃ F ₅ Cl					3		14	
C ₂ F ₃ Cl					13		17	
PMA*					1		4	
POSSMA					1		2	
<i>i</i> -Bu							11	
Acetate			1		15		48	
Cl			5		17		17	

* Propylmethacrylate

The initial decomposition products for **CS(33-67)** at 300 °C were likely POSSMA and HCl as seen in Table 4.6. The loss of POSSMA is consistent with the results of Amir et al. [40] and Fina et al. [39] who saw sublimation of the POSS

component at temperatures below 300 °C. The loss of HCl due to thermal decomposition has been observed in other chlorinated polymers [27]. At 380 °C, the polymer decomposition includes the loss of intact POSSMA, which in turn decomposes to methacryloxypropyl and isobutyl groups, and loss of CTFE and C_3F_5Cl [38]. This decomposition continues at 460 °C where 88% of the remaining Si has oxidized to SiO_2 and approximately 1 in 5 POSSMA molecules subliming intact. The oxidation of POSSMA to SiO_2 likely occurs through peroxidation of the isobutyl group to obtain a hydrogen-substituted POSS [43], which undergoes intermolecular rearrangement, exchanging Si-O and Si-H bonds, to form the SiO_2 network [44].

The loss of between 10 to 20% of the POSSMA molecules to sublimation is found for all of the CS polymer compositions. The percentage of POSSMA that sublimates is calculated by determining the weight percent of CS polymer that remains when all of the constituents other than silicon and oxygen (i.e., C, H, F, and Cl) have been released as decomposition products and all of the silicon was converted to SiO_2 by incorporating additional oxygen from the atmosphere. For p(POSSMA), 51 wt% remains if there is complete conversion to SiO_2 ; this would be the char yield as determined by TGA. The 51 wt% is greater than the 41 wt% char yield determined experimentally for p(POSSMA) [S(100)] as shown in Figure 4.5b. To obtain a 41 wt% char yield, 80% of the silicon was converted to SiO_2 , and therefore, 20% of the silicon was lost due to sublimation of POSSMA. The data for the remaining p(POSSMA) and the remaining CS polymers is shown in Table 4.8.

Table 4.8: Percentage of POSSMA lost due to sublimation.

Polymer	Char Yield for Full Conversion to SiO ₂ (%)	Experimental Char Yield (%)	Si Converted to SiO ₂ (%)	POSSMA sublimed (%)
S(100)	51	41	80	20
CS(02-98)	51	46	90	10
CS(10-90)	50	44	85	15
CS(20-80)	48	47	90	10
CS(33-67)	45	44	82	18

The decomposition of CVS polymers was similarly assessed, with the addition of ¹³C NMR analysis of the char residue, using **CVS (46-52-02)** as the representative sample. At 300 °C, the first product lost is the acetic acid from VAc, which continues as temperature increases. By 375 °C, all of terpolymer components have begun to decompose: POSSMA (and the methacryloxypropyl group itself) are lost through sublimation; and CTFE and C₃F₅Cl are formed. At 450 °C, all of the VAc pendant acetate groups are lost, more of the POSSMA methacryloxypropyl and isobutyl groups are lost, and the CTFE component of the polymer has decomposed primarily to monomer. Finally, by this stage the first loss of isobutyl groups from the POSSMA is seen.

In contrast to the CS polymers where no residue was observed when decomposed in an inert atmosphere and 40 to 47 wt% residue was observed in air, decomposition of the CVS polymers results in a residue of 21 wt% under an inert atmosphere with minimal residue in an air environment. By comparison, p(VAc) gives 4 wt% char in an inert atmosphere. Poly(vinyl acetate) decomposes through elimination of the acetic acid. This forms a polyene structure which decomposes further to give the carbonaceous residue [42]. Figure 4.4a shows a similar initial

drop in weight percent for both the CVS polymers and p(VAc), and based on XPS, a similar loss of the acetate groups occurs for the CVS polymers. However, the resulting structure formed by the CVS polymers, shown in Figure 4.5, does not decompose upon further heating as is the case with p(VAc).

Char formation proceeds through the following steps: cross-linking, aromatization, fusion of aromatics, turbostratic char formation, and graphitization [41]. One of these steps must be increased relative to p(VAc) for the CVS polymers through the incorporation of either CTFE or POSSMA. Due to the minimal incorporation of POSSMA (maximum 2 mol%), it is likely that CTFE is affecting the decomposition mechanism. In the CVS polymers, the CTFE interferes with the formation of the polyene structure observed after p(VAc) decomposition, which requires a string of VAc repeats adjacent to one another. From Table 4.5, it can be seen that both **CVS(40-59-01)** and **CVS(46-52-02)** have at least one CTFE in 91% and 99% of the triad sequences, respectively.

In addition to limiting the formation of the polyene structure, CTFE enhances the crosslinking of CVS polymers. The loss of the acetate group in the BAB triad will result in an alkene whereas the loss of the acetate group in the BAA or AAB triad will result in a diene flanked by a CF_2 or CFCl group. This presence of an alkene and a diene in close proximity allows for Diels-Alder cycloaddition. While the Diels-Alder reaction can occur in p(VAc), the presence of electron withdrawing group (CF_2 or CFCl) on the alkene increases the reactivity [45] and subsequently, the crosslinking reaction. The above mechanisms and resulting structure are shown below in Figure 4.5. As can be seen, the combination of CTFE and VAc results in a significantly

different structure that does not undergo a secondary decomposition as seen with the polyenic structure of p(VAc). For Figure 4.5b, the number that follows the polymer designation gives the percentage of the polymer backbone that has that structure. For example, CVS(40-59-01) contains 40% of the structure which results in an alkene upon decomposition and 50% of the structure which results in a diene.

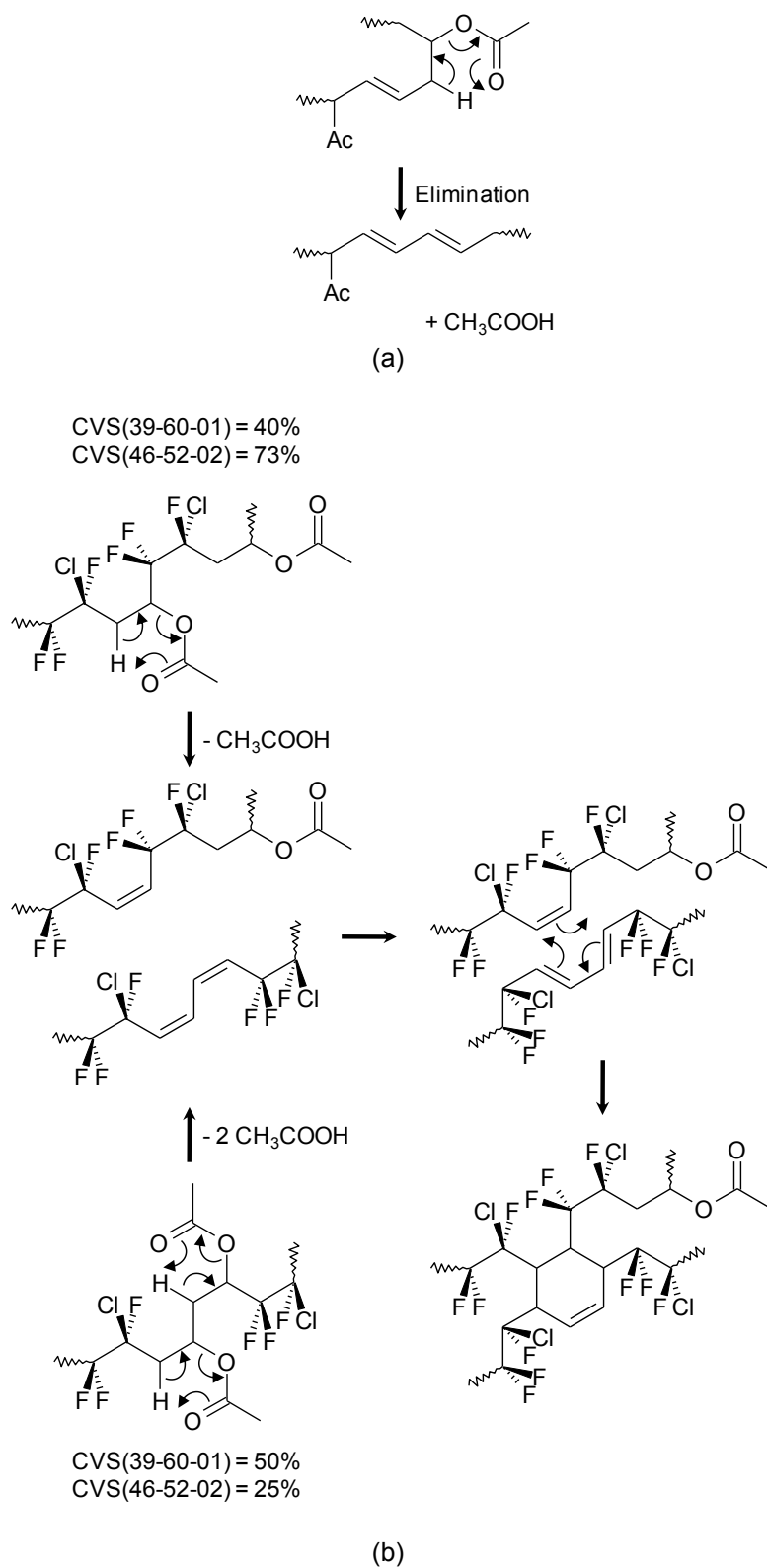


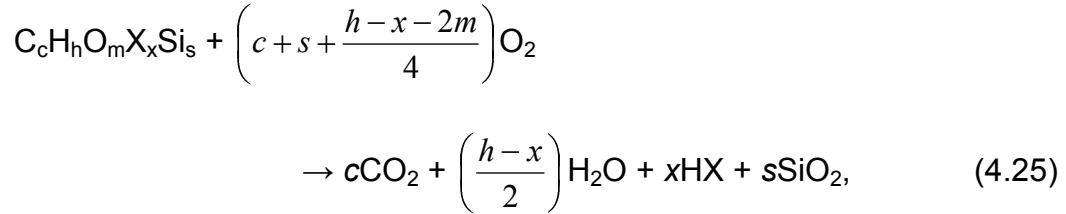
Figure 4.5: Decomposition mechanisms for: (a) V(100) – adapted from [42] and (b) CVS polymers

4.4.5 Flammability

The flammability of the polymers was determined through pyrolysis combustion flow calorimetry (PCFC) giving the heat release capacity, η_c , and the total heat released, h_c^0 . For both of these metrics, a lower value corresponds to decreased flammability. The results are shown in Table 4.9 below. The flammability of both p(POSSMA) and the **CS(33-67)** was significantly higher than that of p(CTFE). Additionally, the **CVS(46-52-02)** had a flammability on the order of p(CTFE) despite the incorporation of the more flammable VAc component. This is likely due to the decomposition pathway of **CVS(46-52-02)** where acetic acid is released rather than the entire VAc molecule as discussed in the following pages. The h_c^0 can be calculated a priori through Equations (4.18), (4.19), and (4.25) [30] and the values obtained for the various polymers are seen in Table 4.10. Equation (4.25) has been modified to include oxidation of the Si component and exclude the impact of nitrogen as there is no nitrogen in the polymers synthesized herein. As can be seen, the value for the **CS(33-67)** matches well whereas the h_c^0 of the **CVS(46-52-02)** is higher than experimental results.

Table 4.9: Flammability of CS and CVS polymers as determined by PCFC analysis

Polymer	η_c (J/g-K)	h_c^0 (kJ/g-fuel)	
		Experimental	Calculated
S(100)	462	24.3	24.2
CS(33-67)	349	22.8	22.1
CVS(46-52-02)	107	5.3	11.2
C(100)	106	3.5	3.6



$$C = h_{c,v}^0 / r_0 = 13.1 \pm 0.7 \text{ kJ/g-O}_2, \quad (4.18)$$

$$h_c^0 = h_{c,v}^0 (1 - \mu), \quad (4.19)$$

$$\eta_c = \frac{h_c^0 E_a}{eRT_p^2}, \quad (4.20)$$

where $h_{c,v}^0$ is the heat of complete combustion of the fuel gases; r_0 is the stoichiometric oxygen / fuel mass ratio; h_c^0 is the calculated total heat released for combustion; and μ is the char yield, η_c is the heat release capacity; E_a is the global activation energy for pyrolysis; $e = 2.718$; R is the gas constant; and T_p (K) is the temperature of the maximum mass loss rate

Pyrolysis-combustion flow calorimetry determines the h_c^0 based on the gaseous products that enter the oxidation chamber. The calculated h_c^0 implies that the all of the decomposition products of **CS(33-67)** enter the gaseous phase and subsequently, pass to the oxidation chamber. This confirms the decomposition mechanism where both CTFE and POSSMA components produce volatile products. Equation (4.19) shows how the h_c^0 is mitigated by the formation of char. However, the char yield in PCFC is calculated based on the mass remaining in the nitrogen chamber, and does not include any char formed in the oxidation chamber. As seen from the TGA results, CS polymers form 40 to 47 wt% char upon heating in air, yet this is not factored into the calculation of h_c^0 . Due to this, the h_c^0 obtained for

CS(33-67) through PCFC analysis may be artificially high. In contrast, other authors [24-26] have seen reduced flammability through the incorporation of POSS moieties using cone calorimetry. If the oxidative char yield is taken into account, the h^0_c of p(POSSMA), for example, would reduce from 24.2 kJ/g-fuel to 14.5 kJ/g-fuel. The decrease in h^0_c due to oxidative char is significant as it will result in a decrease in the heat release capacity from 462 to 275 J/g-K. This represents a change in the UL-94 rating of the polymer from HB or horizontal burning to potentially V-0, which is a self extinguishing polymer.

For **CVS(46-52-02)**, the postulated decomposition mechanism is loss of the acetate group, cross-linking through Diels-Alder cycloaddition, and continued decomposition and aromatization. If we modify the calculated h^0_c value from Equations (4.18) and (4.19) such that only acetic acid rather than the entire VAc repeat unit is incorporated and use the ratios determined by the polymer composition, the h^0_c value reduces from 11.2 to 6.4 kJ/g-fuel. This can be compared to the experimental value of 5.3 kJ/g-fuel. The difference of 1.1 kJ/g-fuel between the experimental and calculated values falls well within that seen for other polymers as shown in Table 4.10.

Table 4.10: Comparison of experimental (DOT/FAA/AR-01/31) [46] and calculated h^0_c values for various polymers

Polymer	h^0_c (kJ/g-fuel)		Difference
	Experimental	Calculated	
Polytetrafluoroethylene	3.7	4.2	0.5
Polyvinyl chloride	11.3	14.2	2.9
Polymethyl methacrylate	24.3	25.1	0.8
Polyvinyl acetate	19.2	21.6	2.4
Acrylonitrile-Butadiene-Styrene	36.6	40.9	4.3

4.5 Conclusions

A series of homo-, co- and terpolymers containing CTFE, VAc, and POSSMA have been synthesized in scCO₂ using AIBN initiation. These represent the first POSS containing polymers synthesized in scCO₂ taking advantage of the environmentally benign nature of scCO₂ as well as the reduced purification required. The copolymers are the first reverse fluorosilicones synthesized by a radical polymerization method without the necessity of incorporating a third hydrocarbon-based monomer. The surface of these co- and terpolymers are enriched with POSSMA leading to surface properties equivalent to that of p(POSSMA) although contact angle hysteresis increases with greater CTFE content reflecting increasing heterogeneity of the surface. The mechanism of thermal decomposition for both the CS and CVS polymers has been elucidated and explains the flammability results seen. These flammability results suggest the importance of determining the effect of oxidative char on the total heat released as determined by pyrolysis combustion flow calorimetry, particularly for silicon containing polymers. Of particular note is the terpolymer **CVS(46-52-02)**, which displays flammability on the order of p(CTFE), but a surface that is not statistically different from p(POSSMA) while incorporating the lower cost monomer VAc providing a potential additive to paint formulations that would enhance their flame resistance and hydrophobicity.

4.6 References

1. Scheirs J. *Modern Fluoropolymers: High Performance Polymers for Diverse Applications*. Toronto: John Wiley & Sons, 1997.
2. Brook MA. *Silicon in Organic, Organometallic, and Polymer Chemistry*. Toronto: John Wiley & Sons, Inc., 2000.
3. Dvornic PR and Lenz RW. *High Temperature Siloxane Elastomers*. New York: Huthig & Wepf Verlag Basel, 1990.
4. Guida-Pietrasanta F and Boutevin B. *Advanced Polymer Science* 2005;179:1-27.
5. Boutevin B, GuidaPietrasanta F, Ratsimihety A, and Caporiccio G. *Main Group Metal Chemistry* 1997;20(2):133-136.
6. Ameduri B, Boutevin B, Guida-Pietrasanta F, Manseri A, Ratsimihety A, and Caporiccio G. *Journal of Polymer Science Part A-Polymer Chemistry* 1996;34(15):3077-3090.
7. Boutevin B, Caporiccio G, Guida-Pietrasanta F, and Ratsimihety A. *Macromolecular Chemistry and Physics* 1998;199(1):61-70.
8. Smith DW and Babb DA. *Macromolecules* 1996;29(3):852-860.
9. Rizzo J and Harris FW. *Polymer* 2000;41(13):5125-5136.
10. Conrad MPC and Shoichet MS. *Polymer* 2007;48(18):5233-5240.
11. Suzuki H, Takeishi M, and Narisawa I. *Journal of Applied Polymer Science* 2000;78(11):1955-1963.
12. Suzuki H, Kobayashi T, and Takeishi M. *Polymer Journal* 2000;32(5):447-451.
13. Baradie B, Lai PHM, and Shoichet MS. *Canadian Journal of Chemistry- Revue Canadienne De Chimie* 2005;83(6):553-558.
14. Shiho H and DeSimone JM. *Journal of Polymer Science Part A-Polymer Chemistry* 2000;38(17):3100-3105.
15. Shiho H and DeSimone JM. *Journal of Polymer Science Part A-Polymer Chemistry* 2000;38(7):1139-1145.
16. Baradie B and Shoichet MS. *Macromolecules* 2005;38:5560-5568.

17. Shimizu T. Fluorinated Acrylic Ester Polymers. In: Scheirs J, editor. Modern Fluoropolymers: Wiley, 1997. pp. 507-523.
18. Bajzer WX and Kim YK. Poly(fluorosilicones). Kirk-Othmer Encyclopedia of Chemical Technology, vol. 11. pp. 722-729.
19. Davis SV, Chen J-H, Aslam M, and Wu F. Canada Patent 2280308, 1999
20. Kim DK, Lee SB, Doh KS, and Nam YW. Journal of Applied Polymer Science 1999;74(8):1917-1926.
21. Brandrup J, Immergut EH, and Grulke EA. Polymer Handbook, 4th ed. Toronto: John Wiley & Sons Inc., 1999.
22. Penelle J, Verraver S, Raucq P, and Marchandbrynaert J. Macromolecular Chemistry and Physics 1995;196(3):857-867.
23. Schwab JJ and Lichtenhan JD. Applied Organometallic Chemistry 1998;12(10-11):707-713.
24. Bourbigot S, Duquesne S, and Jama C. Macromolecular Symposia 2006;233:180-190.
25. Devaux E, Rochery M, and Bourbigot S. Fire and Materials 2002;26(4-5):149-154.
26. Liu L, Hu Y, Song L, Nazare S, He SQ, and Hull R. Journal of Materials Science 2007;42(12):4325-4333.
27. Grand AF and Wilkie CA. Fire Retardency of Polymeric Materials. New York: Marcel Dekker, Inc., 2000.
28. Lyon RE and Janssens ML. Polymer Flammability. In: Administration USDoTFA, editor., vol. DOT/FAA/AR-05/14, 2005. pp. 82.
29. Polic AL, Duever TA, and Penlidis A. Journal of Polymer Science Part A- Polymer Chemistry 1998;36(5):813-822.
30. Lyon RE and Walters RN. Journal of Analytical and Applied Pyrolysis 2004;71(1):27-46.
31. Odian G. Principles of Polymerization, 4th ed. Hoboken, NJ: John Wiley & Sons, Inc., 2004.
32. Dettre RH and Johnson J, R.E. The Journal of Physical Chemistry 1965;69(5):1507-1515.

33. Shanahan MER. Effects of Surface Flaws on the Wettability of Solids. In: Mittal KL, editor. Contact Angle, Wettability and Adhesion. Utrecht, The Netherlands: VSP, 1993. pp. 159-171.
34. Neumann AW and Good RJ. Journal of Colloid and Interface Science 1972;38(2):341-358.
35. Lichtenhan JD, Otonari YA, and Carr MJ. Macromolecules 1995;28(24):8435-8437.
36. Murray DL, Harwood HJ, Shendy SMM, and Piirma I. Polymer 1995;36(20):3841-3848.
37. Hatakeyama T and Quinn FX. Thermal Analysis: Fundamentals and Applications to Polymer Science, 2nd ed. Toronto: John Wiley & Sons, 1999.
38. Rizvi M, Munir A, Zulfiqar S, and Zulfiqar M. Journal of Thermal Analysis 1995;45:1597-1604.
39. Fina A, Tabuani D, Carniato F, Frache A, Boccaleri E, and Camino G. Thermochemica Acta 2006;440(1):36-42.
40. Amir N, Levina A, and Silverstein MS. Journal of Polymer Science Part A-Polymer Chemistry 2007;45(18):4264-4275.
41. Levchik S and Wilkie CA. Char Formation. In: Grand AF and Wilkie CA, editors. Fire Retardancy of Polymeric Materials. New York: Marcel Dekker, Inc., 2000. pp. 171-217.
42. Holland BJ and Hay JN. Polymer 2002;43(8):2207-2211.
43. Fina A, Tabuani D, Frache A, Boccaleri E, and Camino G. Octaisobutyl POSS Thermal Degradation. In: Le Bras M, Wilkie CA, Bourbigot S, Duquesne S, and Jama C, editors. Fire Retardancy of Polymers: New Applications of Mineral Fillers. Tyne and Wear: Royal Society of Chemistry, 2005. pp. 202-220.
44. Siew YK, Sarkar G, Hu X, Hui J, See A, and Chua CT. Journal of the Electrochemical Society 2000;147(1):335-339.
45. McMurry J. Organic Chemistry, 2nd ed. Toronto: Brooks/Cole Publishing Company, 1996.

46. Walters R and Lyon RE. Calculating Polymer Flammability from Molar Group Contributions. In: United States Department of Transportation FAA, editor., 2001. pp. 24.

5 Conclusions and Recommendations

5.1 Thermal Stability

This thesis examined improving the thermal stability of traditional fluorosilicones by modifying the polymer structure with respect to the location of the siloxane and fluorinated components. In traditional fluorosilicones the backbone consists of a siloxane with a pendant fluorinated group, which leads to thermal decomposition at approximately 150 °C, particularly in the presence of acidic or basic catalysts. Two alternatives were synthesized and studied: hybrid fluorosilicones where the fluorine and siloxane are both in the polymer backbone, and reverse fluorosilicones where the siloxane is the pendant group of a fluorinated backbone. Three methods of synthesis were examined: condensation polymerization for the hybrid fluorosilicone; emulsion polymerization and polymerization in supercritical CO₂ (scCO₂) to obtain the reverse fluorosilicones. This Chapter discusses the resolution of each of the hypotheses stated in Chapter 1 as well as the results of the studies on additional properties associated with each series of polymers such as branching and flammability.

The general hypothesis of this thesis was that the hybrid and reverse fluorosilicones synthesized herein will have higher thermal stability, as measured by the initial thermo-oxidative decomposition temperature, than traditional fluorosilicones. The initial thermo-oxidative decomposition temperature of the polymers is given in Figure 5.1. These temperatures were obtained through thermogravimetric analysis (TGA) with a heating rate of 5 °C/min in an air environment. For comparison the initial thermo-oxidative decomposition

temperatures of homopolymers of the co- and terpolymer constituents are also given as well as a poly(3,3,3-trifluoropropylmethylsiloxane) (PTFPMS) with a molar mass of 14 kg/mol. The initial thermal decomposition temperatures (inert atmosphere) were not recorded for all polymer compositions. This approach was taken as the majority of applications will likely be in an oxidative environment. Three of the reverse fluorosilicone polymers have thermo-oxidative stabilities greater than the commercially available fluorosilicone, PTFPMS, suggesting this class of polymers provides some improvement in thermal stability depending on the polymer composition.

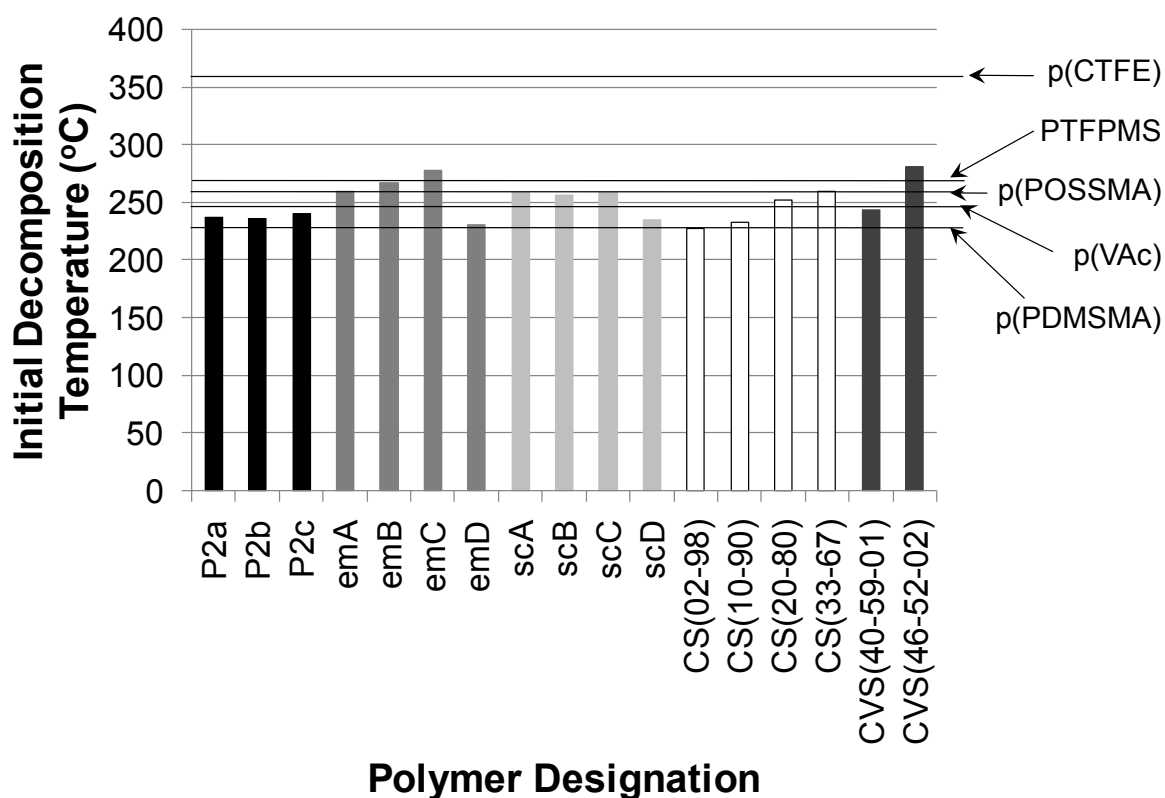


Figure 5.1: Initial thermo-oxidative decomposition temperature for all synthesized polymers

The polymers also exhibit thermo-oxidative stabilities in the range of 228° to 281 °C. As a reminder, the desired operating temperatures for the fuser roller system, which is a potential application of these polymers, discussed in Chapter 1 required operating temperatures between 200° to 260 °C. With decomposition temperatures above the lower operating threshold, this suggests that the polymers meet this design criterion and may have potential in this area. Since all of the polymers synthesized herein meet the design criterion (i.e, any one of the polymers would be acceptable for this application), the need to replicate any individual polymer is reduced relative to the case where only one of the polymers meets the design criterion. However, the synthesis of two polymers with the same feed composition ($f_{\text{CTFE}} = 0.593$ and $f_{\text{POSSMA}} = 0.407$) albeit at different concentrations, resulted in polymer compositions of $F_{\text{CTFE}} = 0.051$ and 0.043 , respectively. The error associated with the polymer composition as determined by quantitative NMR is 11.4%. Based on this error, these values can be considered equivalent and demonstrate the repeatability of the polymer synthesis.

5.1.1 Hybrid Fluorosilicones

To prevent the intrachain rearrangement, hybrid fluorosilicones are composed of a fluorinated component interspersed between the siloxane. The hybrids synthesized in this work follow this structure and based on the decomposition mechanism elucidated in Chapter 2 are successful at preventing the intrachain rearrangement. The decomposition mechanism has shifted to the cleavage of the Si-Ar bond. Interestingly, this occurs even in polymer **P2c** where the siloxane length is greater than that required (4 siloxane repeat units) for intrachain rearrangement.

This may, in part, be due to the bulkiness of the fluorinated block, which consists of a diaromatic-substituted perfluorocyclobutane and prevents the proper spatial arrangement of the siloxane for intrachain rearrangement to occur as shown in Figure 1.3. This confirms the work by Rizzo and Harris [1] where hybrids containing a siloxane-based link with more than four siloxane repeat units and a bulky fluoroaromatic unit also demonstrated elevated decomposition temperatures. Therefore, incorporating a sufficiently large fluorocarbon unit in a hybrid fluorosilicone will allow for low glass transition temperatures since longer siloxane links similar to PDMS can be used; the T_g of PDMS is $-127\text{ }^\circ\text{C}$ [2]. This will result in a polymer that retains ductility to lower temperature increasing the operating range.

5.1.2 Reverse Fluorosilicones

By changing to a fluorinated backbone in the case of the reverse fluorosilicones, intrachain rearrangement is no longer the predominant decomposition pathway. Furthermore, if this pathway is still active only pendant groups will be lost with the majority of the polymer structure intact. This suggests that only those properties related to the pendant siloxane will be adversely affected in the initial heating stages.

The change in decomposition pathway results in thermo-oxidative stabilities between 231° to $278\text{ }^\circ\text{C}$ for the CTFE-VAc-PDMSMA terpolymers and 244° to $281\text{ }^\circ\text{C}$ for the CTFE-VAc-POSSMA terpolymers. These values can be compared to the TFE-VAc-PDMSMA terpolymers synthesized by Baradie and Shoichet [3] where the thermo-oxidative decomposition temperatures ranged from 238° to $244\text{ }^\circ\text{C}$.

More specifically, the compositions in Table 5.1 show the effect of the polymer constituents on thermo-oxidative decomposition.

Table 5.1: Comparison of the thermo-oxidative stability of reverse fluorosilicones with same nominal feed composition and molar mass

Polymer	Mole Percent (%)			Molar Mass (kg/mol)*		T _{1%} (°C)
	TFE or CTFE	VAc	PDMSMA or POSSMA	M _w	M _n	
Baradie and Shoichet	40.4	57.4	2.2	170	53	238 (260) [†]
emA	42.5	55.4	2.1	154	61	260
scC	36.8	60.6	2.6	170	47	259
CVS(46-52-02)	46.1	52.2	1.7	46	25	281

* Relative to polystyrene standards

[†] 260 °C represents a cross-linked version of this polymer

Comparing the TFE-VAc-PDMSMA terpolymer [3] to **emA** and **scC** demonstrates the effect of changing the fluoromonomer from TFE to CTFE. The use of CTFE results in un-crosslinked terpolymers that have equivalent thermo-oxidative decomposition temperatures to the cross-linked TFE-based terpolymer. This is likely due to a modification of the reactivity ratios in the CTFE system as was suggested in Chapter 1: Section 1.4.3 and Chapter 3: Sections 3.2 and 3.4.3. The CTFE results in a more alternating structure based on previous work [4]; there is a decrease in the number of AAA triads (where A represents VAc) in the polymer backbone with the percentage of AAA triads shown in Figure 5.2. As demonstrated in Chapter 4: Figure 4.6 this will lead to a shift in decomposition mechanism from the formation of a polyene to the formation of ring structures through enhancement of a Diels-Alder mechanism. Due to the thermodynamic stability of ring structures relative to alkenes, the CTFE increases the thermal stability of the

CTFE-VAc-PDMSMA polymers over a TFE-VAc-PDMSMA of the same nominal composition and molar mass. Therefore, incorporating the fluorocarbon with the highest thermal stability does not necessarily translate into a terpolymer with the highest thermal stability for this system, but instead it is dependent on the decomposition mechanism.

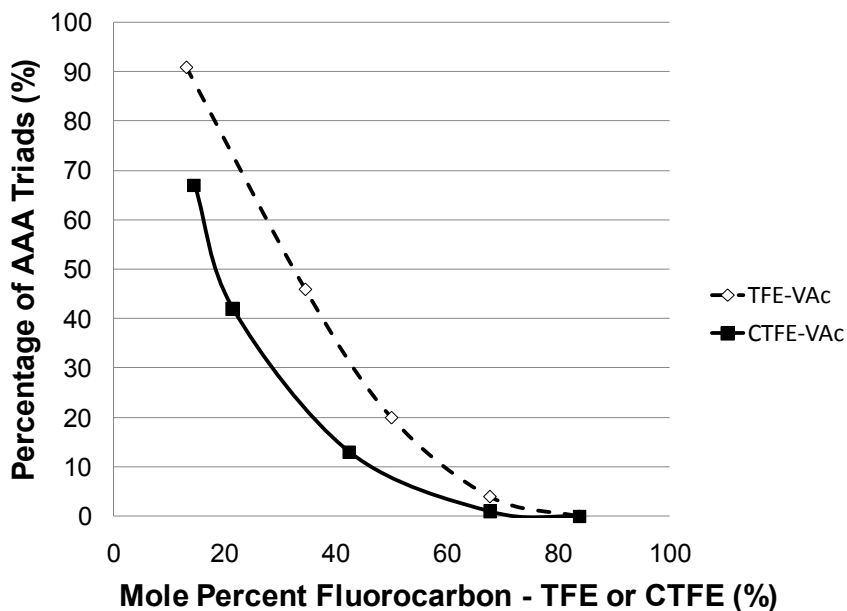


Figure 5.2: Effect of fluorocarbon on percentage of AAA triads (data from [4])

The replacement of PDMSMA with POSSMA increases the thermal stability another 20 °C. Again, it appears that the POSSMA further enhances the Diels-Alder mechanism over the formation of a polyene. The percentage of AAA triads reduces from 14 (**emA**) and 20 (**scC**) to 1.4 for **CVS(46-52-02)**. This, combined with the effect of replacing TFE with CTFE, highlights the importance of the decomposition mechanism on thermal stability. In designing a thermally stable co- or terpolymer, it is not sufficient to simply incorporate the monomers that result in the most thermally stable homopolymers.

This conclusion that the decomposition mechanism is the most important factor in determining thermal stability is confirmed by comparing the decomposition of the CTFE-POSSMA copolymers to the CTFE-VAc-POSSMA terpolymers. Of the three monomers, p(VAc) has the lowest thermo-oxidative decomposition temperature at 244 °C [3], followed by p(POSSMA) at 256 °C and PCTFE at 359 °C. Therefore, a copolymer of CTFE-POSSMA, based on homopolymer decomposition temperatures alone, should have a higher thermo-oxidative stability. In fact, the maximum decomposition temperature achieved by the copolymers synthesized herein is 260 °C versus the 281 °C for the terpolymer. The removal of VAc results in a decomposition mechanism in the copolymers that occurs at a lower temperature.

5.1.3 Comparison of Hybrid and Reverse Fluorosilicones

A comparison of the postulated decomposition mechanisms for both the hybrid fluorosilicones and the POSSMA copolymers synthesized herein suggests that the hybrid fluorosilicones may have higher thermal stability. The literature also gives a similar relationship as hybrid fluorosilicones typically have $T_{50\%}$ decomposition temperatures typically between 400° and 500 °C [1, 5-10] versus 360° to 400 °C [3] for reverse fluorosilicones. The Si-C bond, which is the initial decomposition point for the hybrid fluorosilicones synthesized herein, has a mean bond enthalpy of 318 kJ/mol although specific bond enthalpies as high as 374 kJ/mol [11] are seen. By comparison, the C-Cl bond or C-C bond, the initial point of decomposition for the POSSMA copolymers, have mean bond enthalpies of 338 and 348 kJ/mol [12], respectively. An examination of Figure 5.1 reveals that the hybrid fluorosilicones have higher thermo-oxidative stabilities than four of the reverse

fluorosilicones: **emD**, **scD**, **CS(02-98)** and **CS(10-90)**. This contradicts the expected order of decomposition based on mean bond enthalpies since 338 and 348 kJ/mol are greater than 318 kJ/mol. However, mean bond enthalpies are averages of the bond enthalpies for a particular pair of atoms and subject to variation depending on the specific locations of the bond in question as seen above for the Si-C bond. In the case of the PDMSMA containing polymers, **emA** through **emD** and **scA** through **scD**, there appears to be a shift in decomposition mechanism from PDMSMA driven decomposition to VAc driven as discussed in Chapter 3. Therefore, it is hypothesized that the Si-C bond enthalpy of the hybrid fluorosilicones synthesized herein falls between the energy associated with these two decomposition mechanisms.

For **CS(02-98)** and **CS(10-90)**, these polymers contain the lowest weight percentage of CTFE. Thus, the initial decomposition temperatures of the remaining CTFE-POSSMA polymers may be artificially elevated due to the measurement technique relative to the hybrid fluorosilicones. That is, the true initial decomposition temperature of the CTFE-POSSMA polymers is lower than that recorded by TGA. Poly(chlorotrifluoroethylene) has extremely low gaseous permeability [2]; therefore, the incorporation of CTFE will inhibit the diffusion of the gaseous products, shifting the initial decomposition, as recorded by TGA, to higher temperatures.

Interestingly, the thermo-oxidative stability of the CTFE-POSSMA copolymer is lower than that of the POSSMA homopolymer. Bolln et al. [13] examined the thermo-oxidative decomposition of a series of octaalkyl-POSS polymers and found in all cases the mass of the POSS increased prior to decomposition. They attributed

this to crosslinking of the POSS molecules through oxidation. A similar oxidation of POSS was seen in this work and was discussed in Chapter 4. This increase in mass will move the initial decomposition point (as measured by mass loss relative to the initial mass) to higher temperatures. Therefore, chemical reactions are occurring in the POSSMA polymer, yet decomposition (again as measured by mass loss) does not appear to be occurring.

5.2 Hypotheses Tested

The general hypothesis of this thesis was that:

1. the hybrid and reverse fluorosilicones synthesized herein will have a higher thermal stability, as measured by the initial thermo-oxidative decomposition temperature, than traditional fluorosilicones.

This hypothesis has been confirmed. The work also demonstrated that an understanding of the potential decomposition mechanism should drive the selection of future monomers for the synthesis of reverse fluorosilicones and in general, thermally stable polymers, rather than simply selecting those monomers whose homopolymers have the highest thermal stability.

While the general hypothesis was confirmed, within each series of polymers synthesized herein – hybrid (one series) and reverse fluorosilicones (four series) – more specific hypotheses were made which represent important advances for each class of fluorosilicone.

For the hybrid fluorosilicones, it was hypothesized that:

2. removal of the ether oxygen (i.e., directly linking the fluorinated and aromatic component) would increase the thermal stability, as measured by the initial thermo-oxidative decomposition temperature, of the resulting hybrid.

A series of hybrid fluorosilicones with increasing weight percentage of the siloxane component were synthesized through a condensation polymerization method to confirm this hypothesis. Specifically, the fluorinated component consists of a diaromatic-substituted perfluorocyclobutane without a linking oxygen. Unexpectedly, the removal of the ether oxygen in these polymers leads to lower thermal stabilities than comparable polymers, disproving the hypothesis, as well as lower glass transition temperatures. The lower glass transition temperatures arise due to the removal of the stabilizing anomeric effect and enhancing the strength of the silicon-aromatic bond.

Importantly, this series of hybrid fluorosilicones also confirmed that a sufficiently bulky fluorinated component will allow for siloxane linkers of greater than four silicon atoms without reintroducing the chain scission seen for traditional fluorosilicones. This provides an alternative approach to the hybrid fluoroether-siloxane polymers in achieving polymers with large operating temperature ranges, i.e. low glass transition temperatures and high decomposition temperatures. Furthermore, the importance of electronic effects on the glass transition temperature of polymers was seen.

For the reverse fluorosilicones, the following two hypotheses were postulated:

3. moving from a supercritical CO₂ polymerization medium to an aqueous-based medium will modify the reactivity ratios between the fluorocarbon and siloxane-containing monomers such that a copolymer can be synthesized
4. changing the fluoromonomer from TFE to CTFE and the silicon-containing monomer from PDMSMA to POSSMA will modify the reactivity ratios such that a copolymer of CTFE and POSSMA can be synthesized using supercritical CO₂.

To confirm these hypotheses, four series for reverse fluorosilicones were synthesized through two polymerization techniques, emulsion and in supercritical CO₂. This represents the first synthesis of reverse fluorosilicones by an emulsion method. Neither the use of CTFE nor an emulsion polymerization medium was successful in eliminating VAc from the polymers containing PDMSMA as the silicon component. However, changing the PDMSMA to POSSMA allowed the elimination of VAc from the polymers when supercritical CO₂ was used as a polymerization medium, confirming hypothesis 4. This represents the first reverse fluorosilicone synthesized in supercritical CO₂ that does not contain a purely hydrocarbon-based component.

The work on the PDMSMA-containing reverse fluorosilicones also demonstrated that the long-chain branching between polymers synthesized by emulsion and supercritical CO₂ is equivalent given the same molar mass. This is important as it suggests that these CTFE-VAc-PDMSMA terpolymers can be synthesized through an industrially available polymerization method. The

CTFE-VAc-PDMSMA terpolymers represent potential high temperature lubricants; specifically, for the fuser roller system in electrophotographic printing.

The work on the POSSMA-containing reverse fluorosilicones showed that the homopolymerization of POSSMA in supercritical CO₂ is a viable polymerization method and that a terpolymer with flammability on the order of CTFE and the surface properties of POSSMA is achievable. The first result is significant as polymerization in scCO₂ represents an environmentally benign alternative to solvent based methods [14]. Supercritical CO₂ also offers increased simplicity in the purification of the polymers as the solvent is vented to atmosphere. The flammability of the CTFE-VAc-POSSMA terpolymers while interesting is more important for the results of the pyrolysis combustion flow calorimetry technique used to determine the flammability. The work by Walters and Lyon [15] using molar group contributions to calculate the heat release capacity cites only one polymer as the source of the value for silicon. Furthermore, the technique used to calculate the flammability should be examined with respect to polymers that form significant oxidative char as this is not taken into account in the calculation of the heat release capacity. As the technique can be used to screen small quantities of polymer for potential flame resistance, polymers that form oxidative char may be discounted prematurely. This is particularly important when the field of flame retardants is moving away from halogenated compounds due to toxicity and POSS-containing compounds appear to represent a viable alternative.

5.3 Recommendations

For the hybrid fluorosilicones, optimization of the synthetic technique to improve the molar mass should be undertaken. This will allow a more direct comparison with the aromatic polyethers synthesized in other groups [1, 5, 16-18]. Alternative silicon-based linkers such as a POSS molecule or siloxanes with functionality greater than two may also be examined in an effort to expand the repertoire of hybrid fluorosilicones.

For all of the terpolymers synthesized herein, alternative fluorocarbon monomers and silicon-containing monomers could be examined. For example vinylidene fluoride (VDF) may be used to reduce the glass transition temperature thereby increasing the operating range of the polymers; the T_g of VDF is $-43\text{ }^\circ\text{C}$ [2] versus $52\text{ }^\circ\text{C}$ for CTFE. However, the use of VDF will likely decrease the alternating character of the polymer as shown by Baradie and Shoichet [4] potentially reducing the thermal stability. Rather a fluorocarbon monomer that increases the alternating character of the terpolymers is desired to enhance the cross-linking reactions that lead to char formation and lower flammability. To obtain an alternating copolymer $r_1 = r_2 = 0$ and $r_1r_2 = 0$. Hexafluoropropylene (HFP) may be a suitable fluorocarbon since the estimated ratio of r_{HFP} to r_{VAc} is 0.6. This estimate is based on the same methodology used in Chapter 3, Equation (3.2) to determine the ratio of r_{CTFE} and r_{PDMSMA} and using the HFP/VDF reactivity ratios [19] and the VDF/VAc reactivity ratios [2]. However, the alternating character cannot be guaranteed as this ratio may arise from $r_{HFP} = 0.8$ and $r_{VAc} = 1.3$ with $r_1r_2 = 1.1$, which gives an ideal or random copolymerization. The shift in the field of flame retardants to non-halogenated forms

due to concerns over toxic off-gases suggests that reduction and/or elimination of the fluorocarbon component may also be beneficial.

For the PDMSMA containing terpolymers synthesized by emulsion, a siloxane with greater water solubility should be examined, for example a PDMSMA with fewer siloxane repeat units, as this may allow for an increase in the siloxane content of the resulting polymers. The availability of mono-functional PDMS monomers limits the selection of other polymerizable moieties. However, the judicious use of a difunctional PDMS, such as α,ω -vinyl- or α,ω -methacryloxypropyl-terminated PDMS, may enhance the thermal stability through crosslinking and potentially lead to improved mechanical properties as seen in Chapter 1, Section 1.2.3.1 Thermal Stability for traditional fluorosilicones.

The flammability of the POSSMA polymers and other polymers that exhibit significant oxidative char should be further studied to refine the pyrolysis combustion flow calorimetry technique. Alternative methacryloxy-based POSS molecules with greater thermal stability should also be examined such as those containing ring structures (cyclohexyl or phenyl) attached to the silicon rather than the isobutyl-containing POSS used in this thesis. It is likely this will not shift the decomposition mechanism from that seen in Chapter 4 Figure 4.5b, but the initial decomposition temperature may increase.

POSS-acrylates may also have potential as comonomers allowing for greater incorporation of the CTFE or other fluoromonomers as acrylates are less reactive than comparable methacrylates to polymerization [2, 20] and may have similar solubility in supercritical CO₂ [21]. Only one POSS-acrylate (an aliphatic

heptaisobutyl monomer comparable to the POSSMA used herein) is commercially available at present and it is likely that POSS molecules containing ring structures will have greater thermal stability.

5.4 References

1. Rizzo J and Harris FW. *Polymer* 2000;41(13):5125-5136.
2. Brandrup J, Immergut EH, and Grulke EA. *Polymer Handbook*, 4th ed. Toronto: John Wiley & Sons Inc., 1999.
3. Baradie B and Shoichet MS. *Macromolecules* 2005;38:5560-5568.
4. Baradie B and Shoichet MS. *Macromolecules* 2002;35(9):3569-3575.
5. Smith DW and Babb DA. *Macromolecules* 1996;29(3):852-860.
6. Pierce OR and Kim YK. *Rubber Chemistry and Technology* 1971;44(5):1350-1362.
7. Ameduri B, Boutevin B, Guida-Pietrasanta F, Manseri A, Ratsimihety A, and Caporiccio G. *Journal of Polymer Science Part A-Polymer Chemistry* 1996;34(15):3077-3090.
8. Boutevin B, Caporiccio G, Guida-Pietrasanta F, and Ratsimihety A. *Macromolecular Chemistry and Physics* 1998;199(1):61-70.
9. Boutevin B, Guida-Pietrasanta F, Ratsimihety A, and Caporiccio G. *Main Group Metal Chemistry* 1997;20(2):133-136.
10. Riley MO, Kim YK, and Pierce OR. *Journal of Fluorine Chemistry* 1977;10(2):85-110.
11. Walsh R. *Accounts of Chemical Research* 1981;14(8):246-252.
12. Atkins PW. *Physical Chemistry*, 5th ed. New York: W.H. Freeman and Company, 1994.
13. Bolln C, Tsuchida A, Frey H, and Mlhaupt R. *Chemistry of Materials* 1997;9(6):1475-1479.
14. Lichtenhan JD, Otonari YA, and Carr MJ. *Macromolecules* 1995;28(24):8435-8437.

15. Walters R and Lyon RE. Calculating Polymer Flammability from Molar Group Contributions. In: United States Department of Transportation FAA, 2001. pp. 24.
16. Smith DW, Babb DA, Shah HV, Hoeglund A, Traiphol R, Perahia D, Boone HW, Langhoff C, and Radler M. *Journal of Fluorine Chemistry* 2000;104(1):109-117.
17. Smith DW, Ji J, Narayan-Sarathy S, Neilson RH, and Babb DA. Fluorosilicones containing the perfluorocyclobutane aromatic ether linkage. In: Clarson SJ, editor. *Silicones and Silicone-Modified Materials*, vol. 729. Washington, D.C.: American Chemical Society, 2000. pp. 308-321.
18. Smith DW, Narayan-Sarathy S, Ji JM, Neilson RH, Traiphol R, and Perahia D. *Abstracts of Papers of the American Chemical Society* 2001;221:86-87.
19. Ahmed TS, DeSimone JM, and Roberts GW. *Macromolecules* 2006;39(1):15-18.
20. Odian G. *Principles of Polymerization*, 4th ed. Hoboken, NJ: John Wiley & Sons, Inc., 2004.
21. DeSimone JM. US Patent 5496901, 1996.

Appendix A: Nuclear Magnetic Resonance (NMR) Spectra

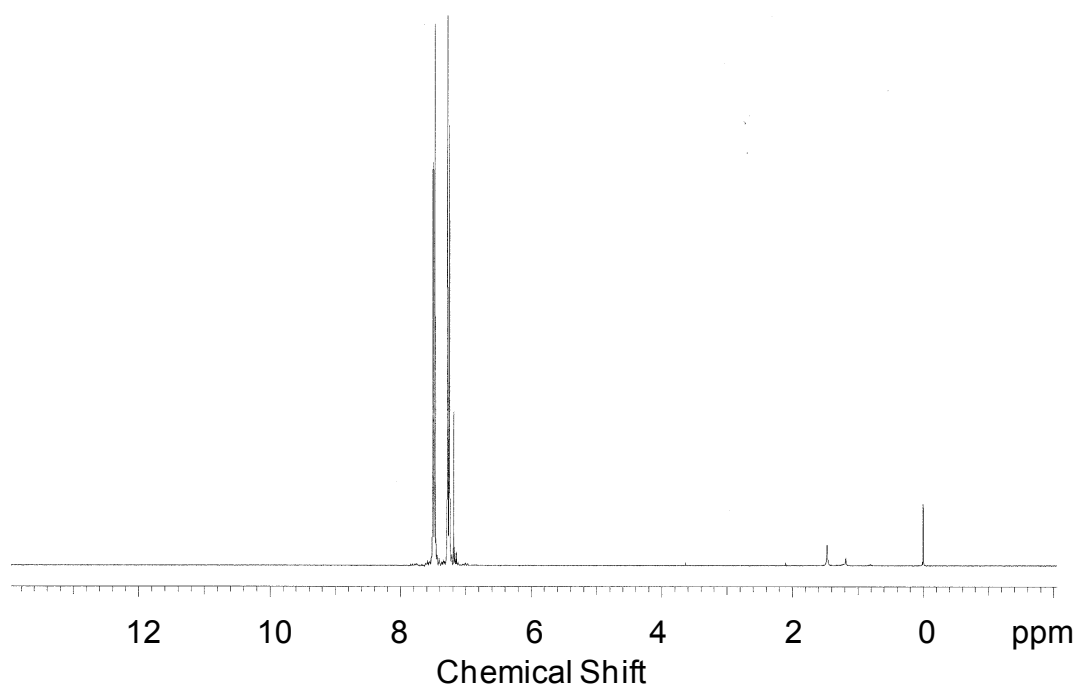


Figure A.1: ^1H NMR of I2

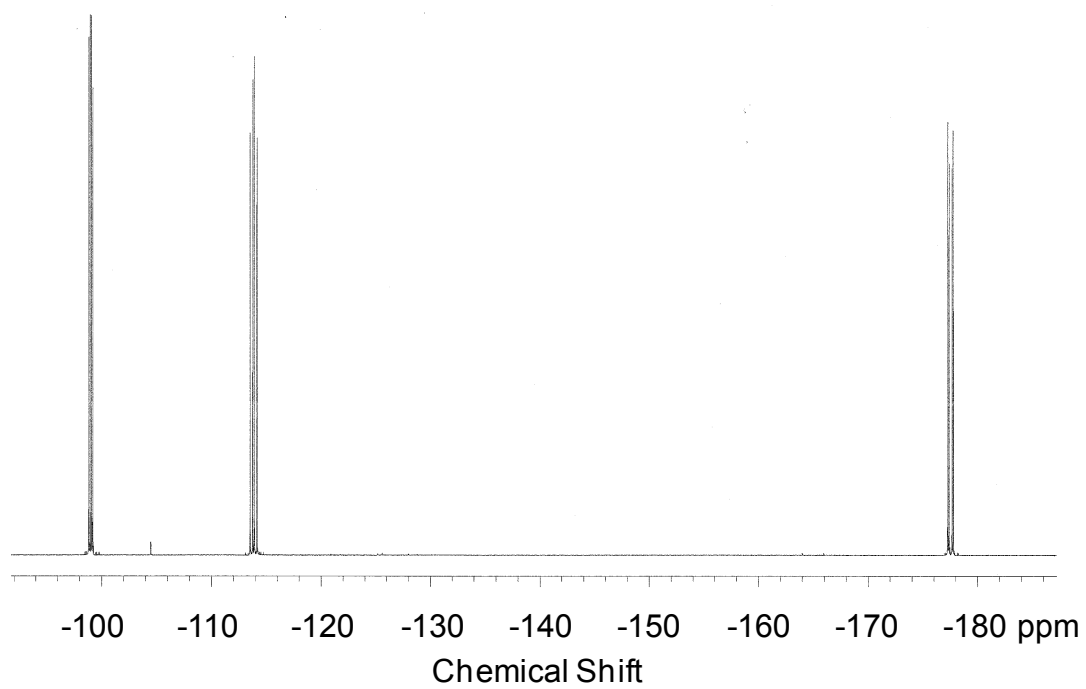


Figure A.2: ^{19}F NMR of I2

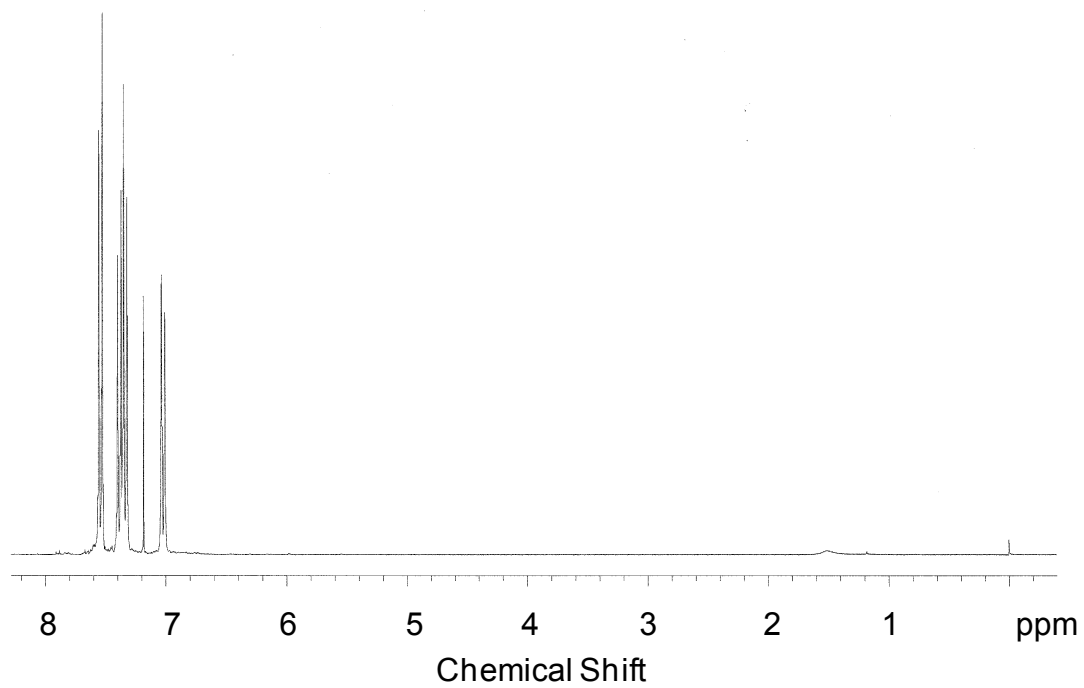


Figure A.3: ^1H NMR of M2

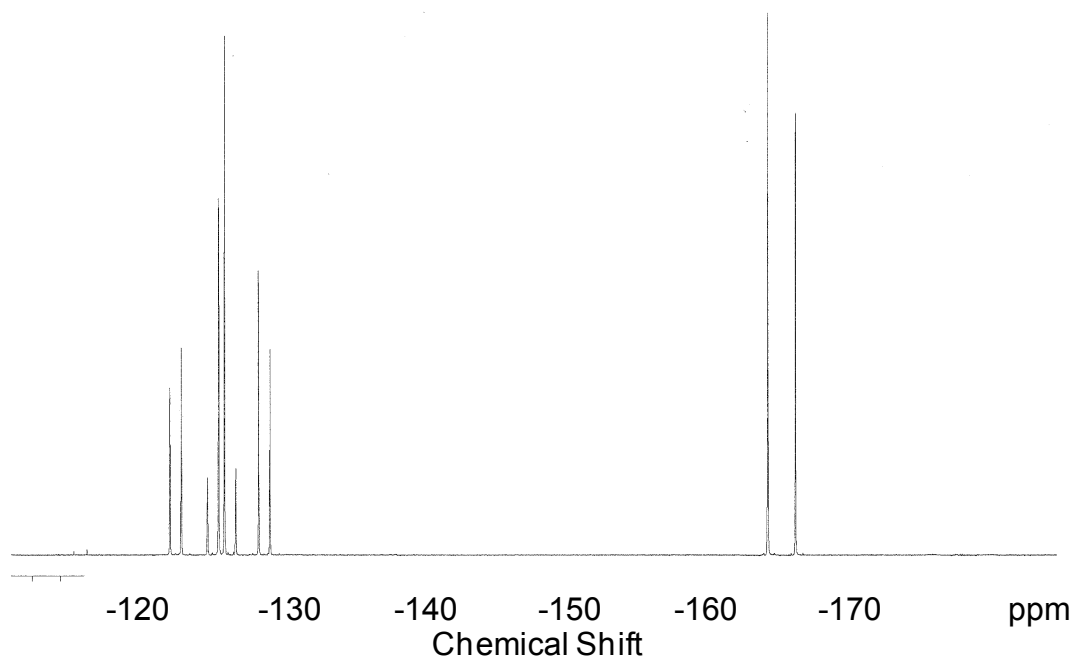


Figure A.4: ^{19}F NMR of M2

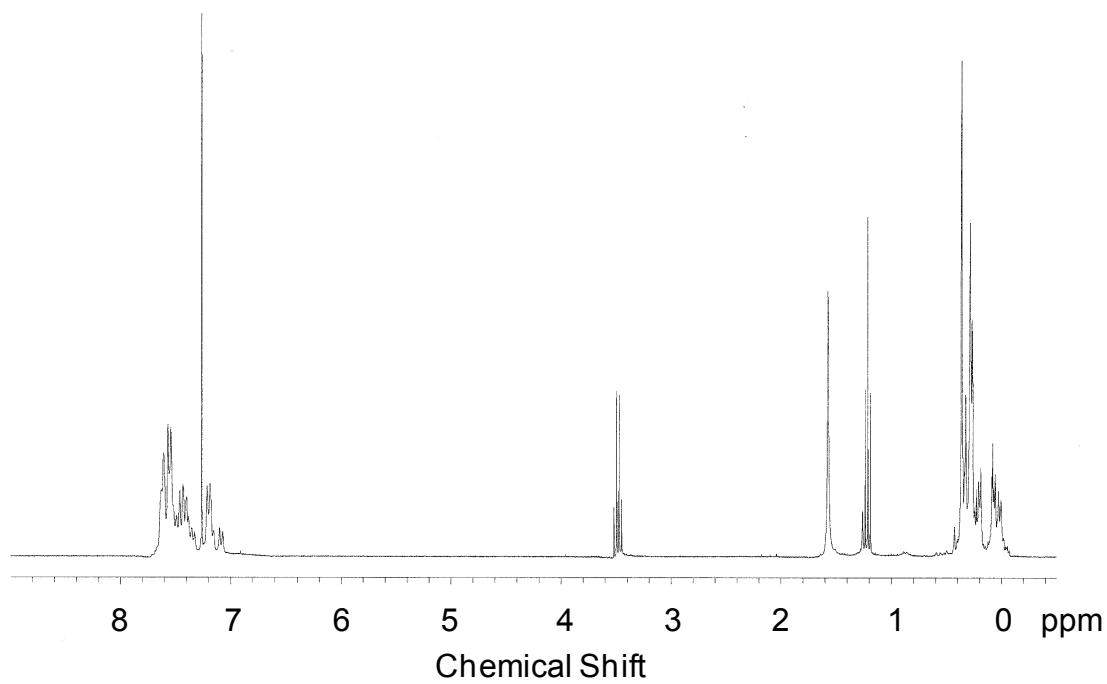


Figure A.5: ^1H NMR of P2a

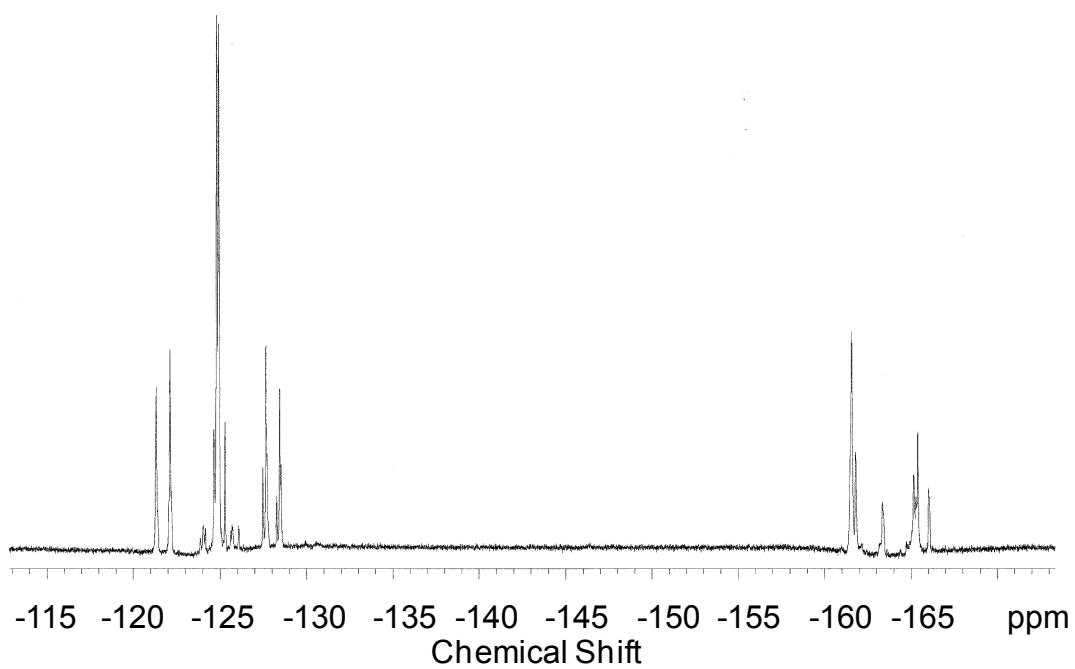


Figure A.6: ^{19}F NMR of P2a

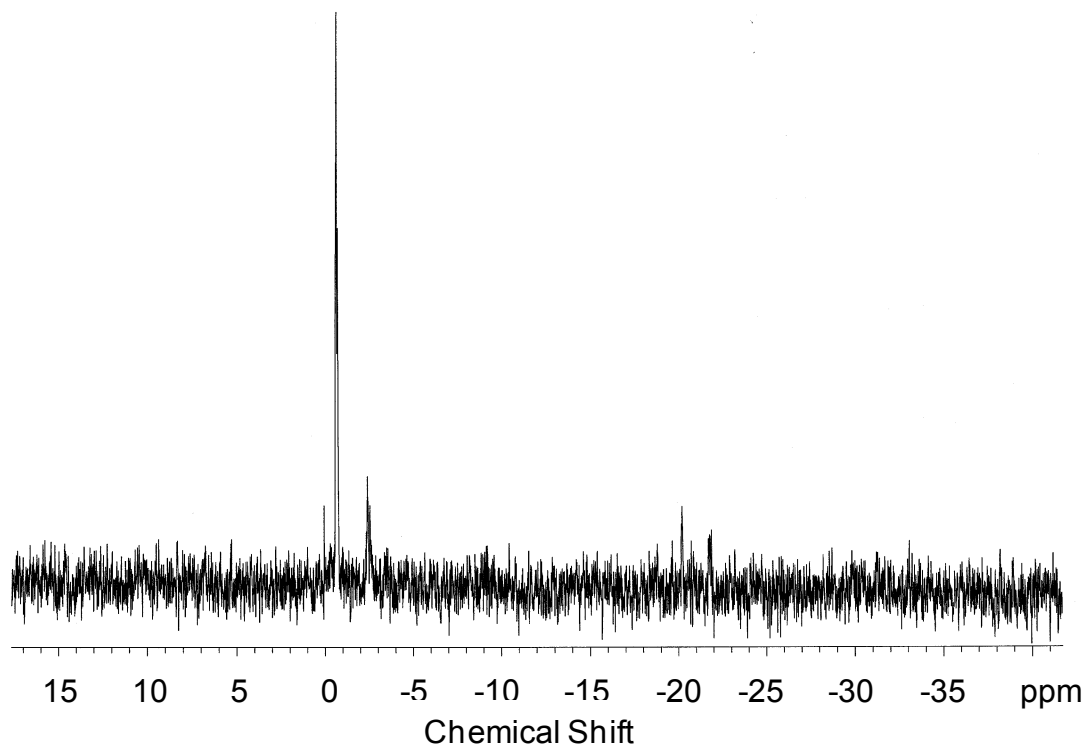


Figure A.7: ^{29}Si NMR of P2a

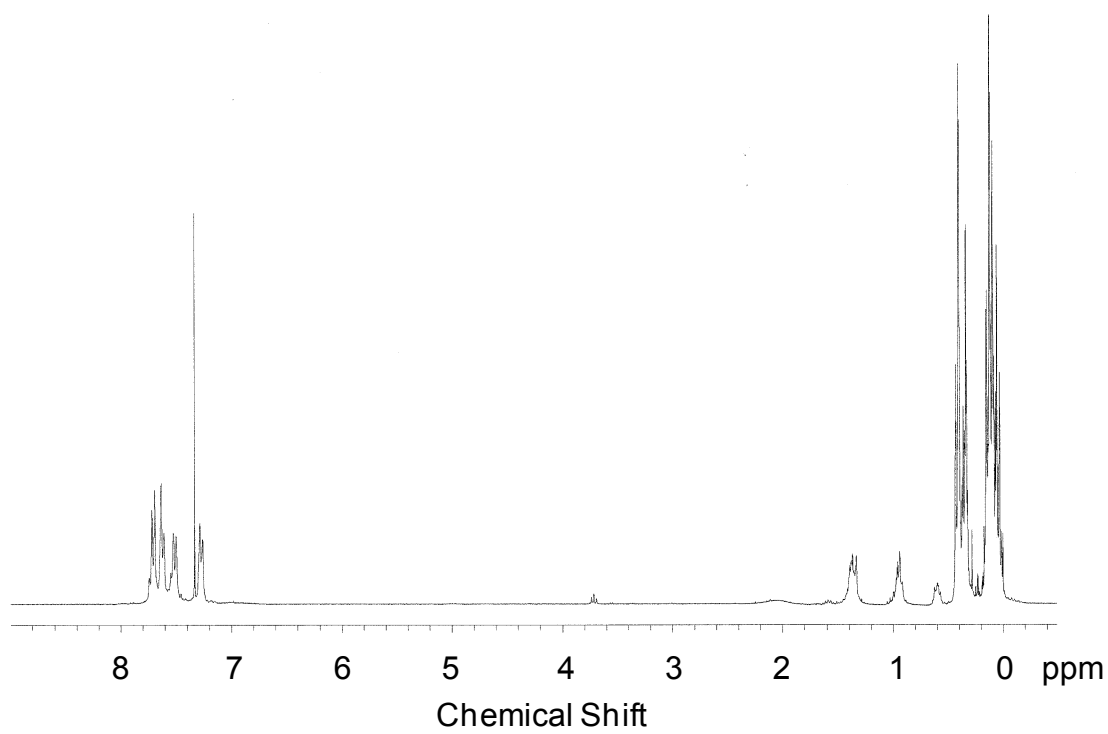


Figure A.8: ^1H NMR of P2b

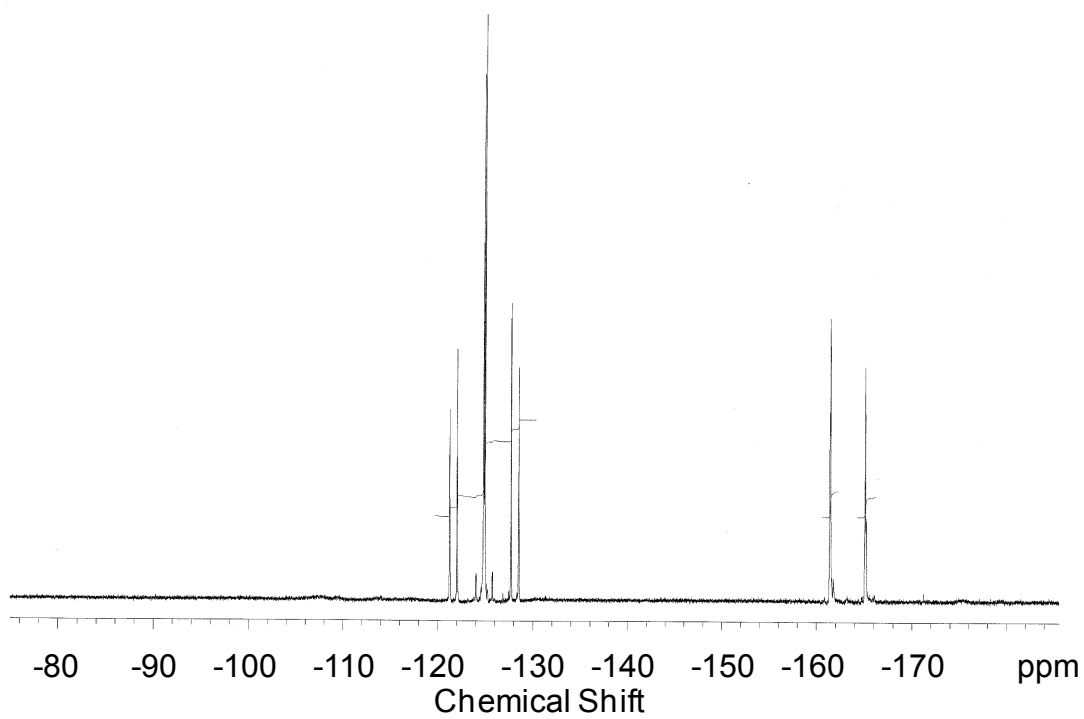


Figure A.9: ^{19}F NMR of P2b

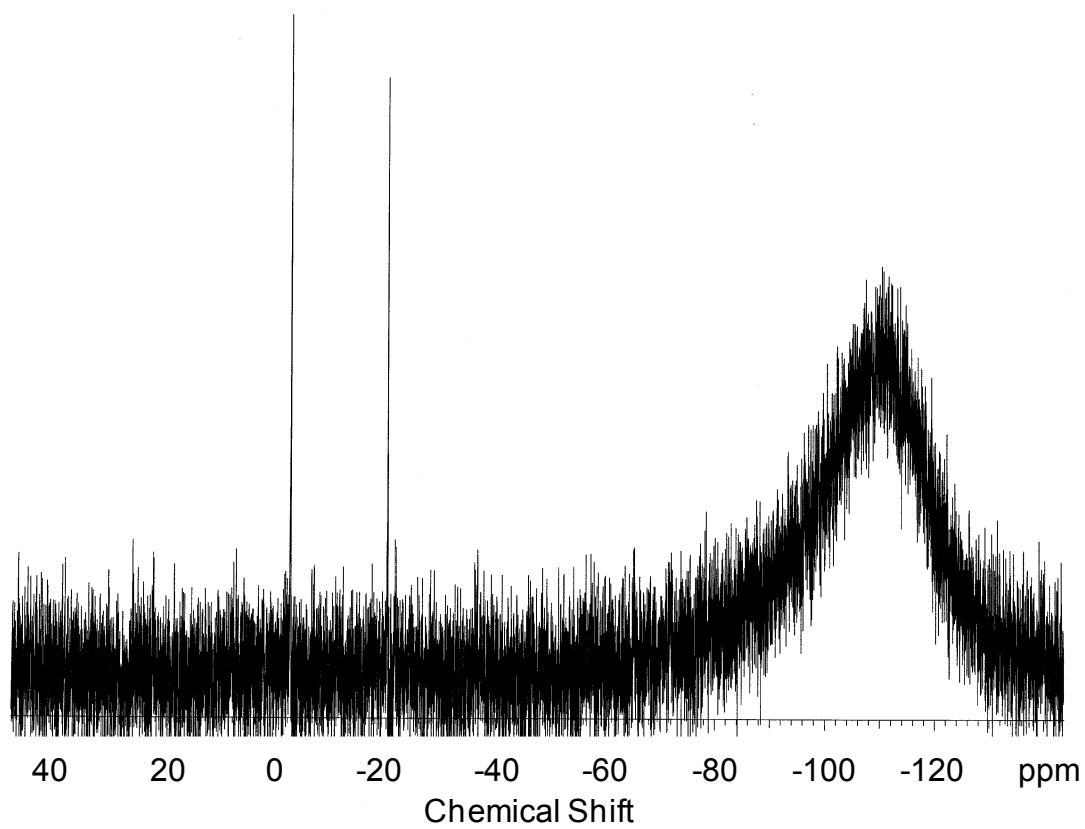
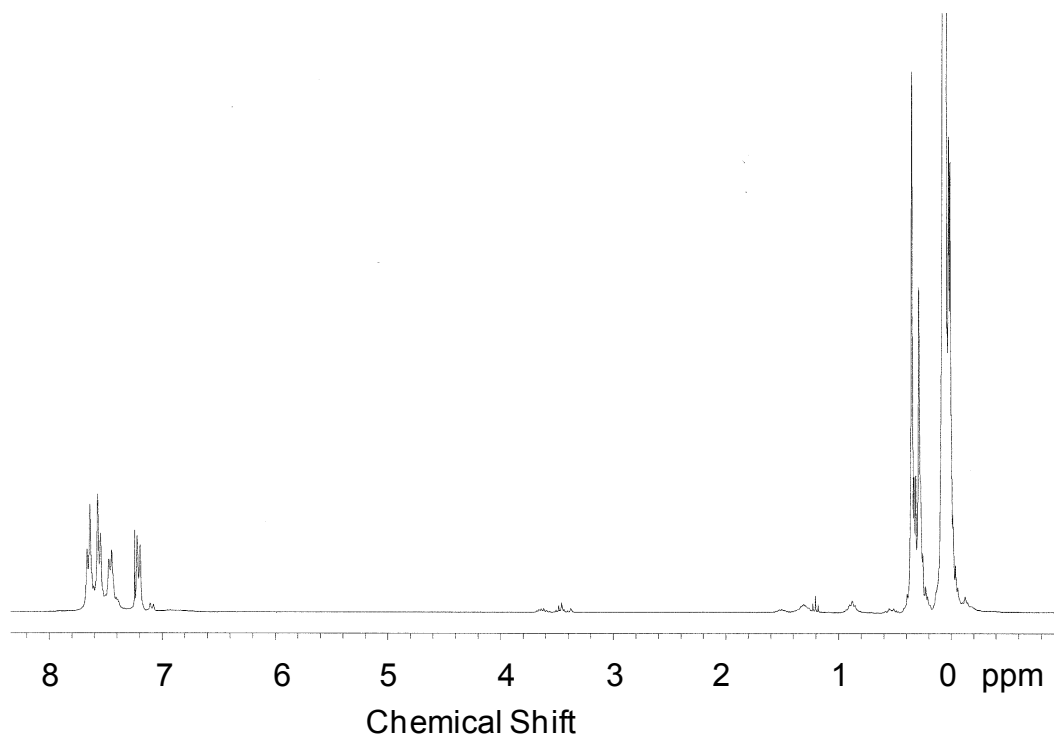
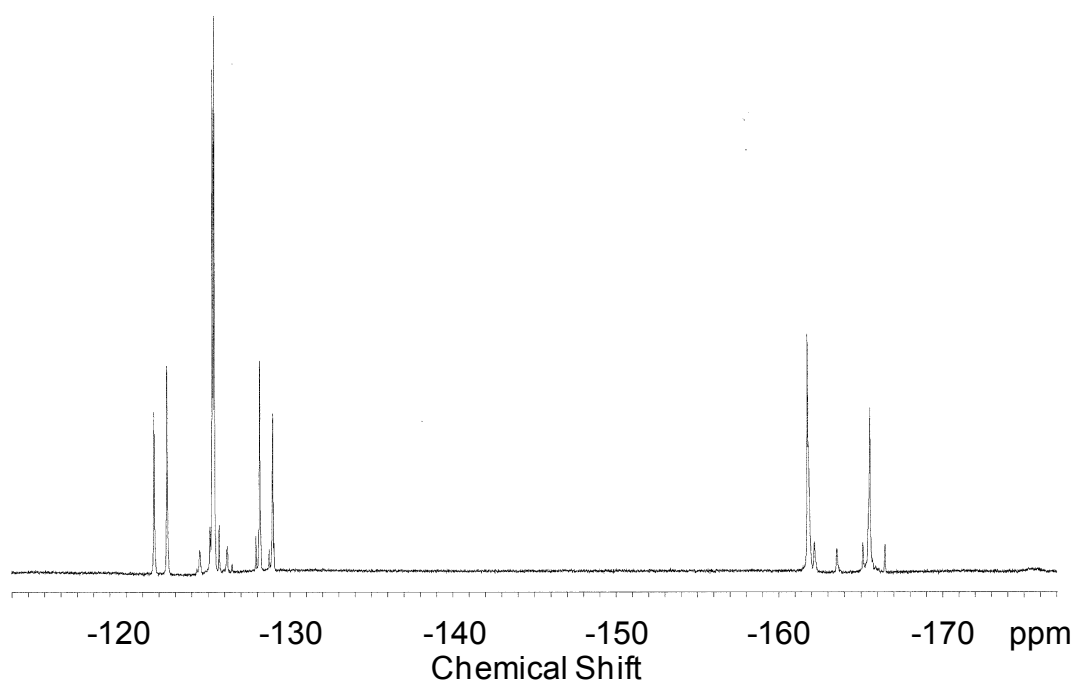


Figure A.10: ^{29}Si NMR of P2b

Figure A.11: ^1H NMR of P2cFigure A.12: ^{19}F NMR of P2c

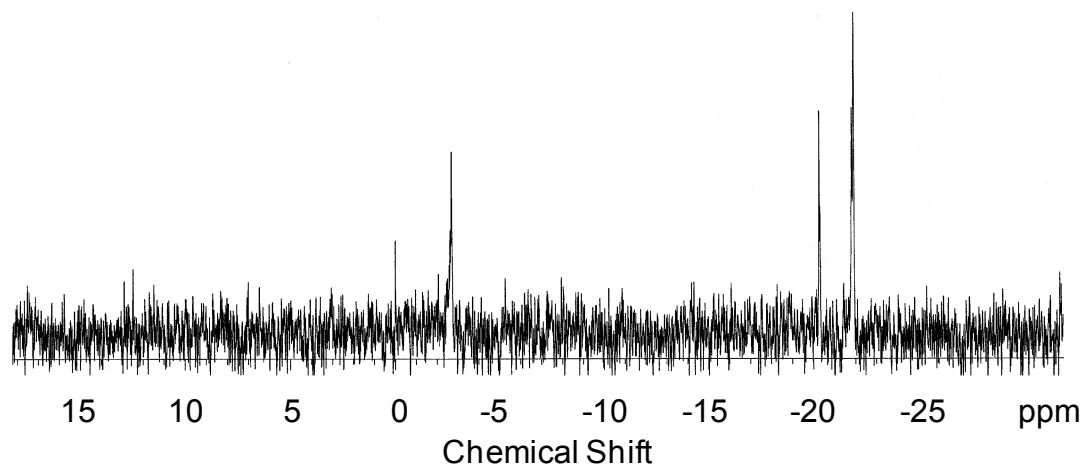


Figure A.13: ^{29}Si NMR of P2c

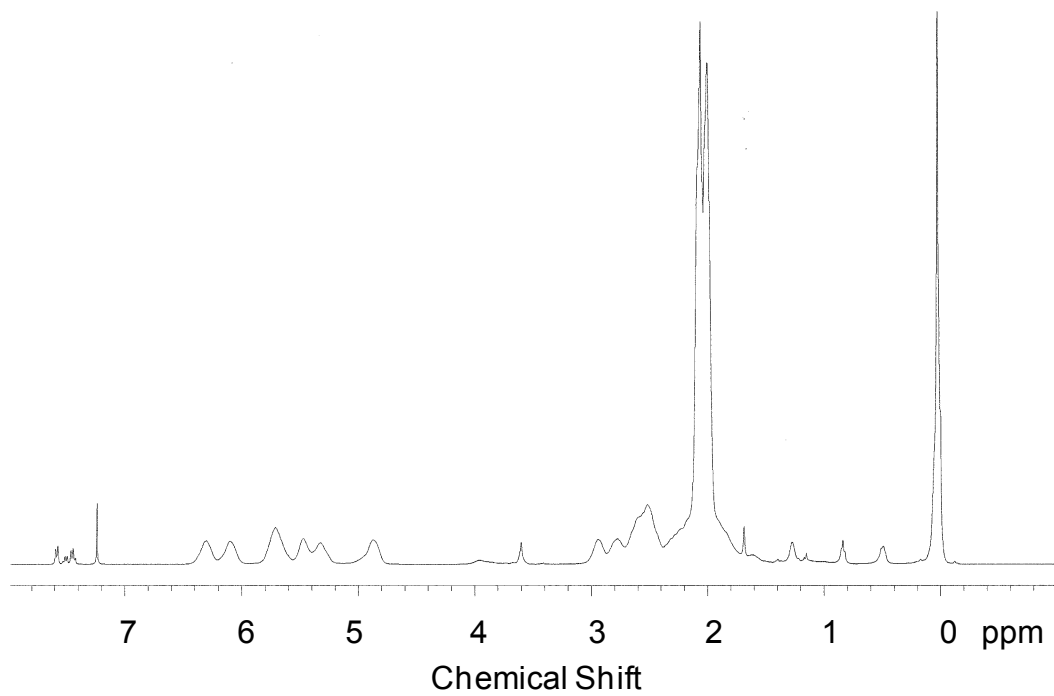


Figure A.16: ^1H NMR of emB

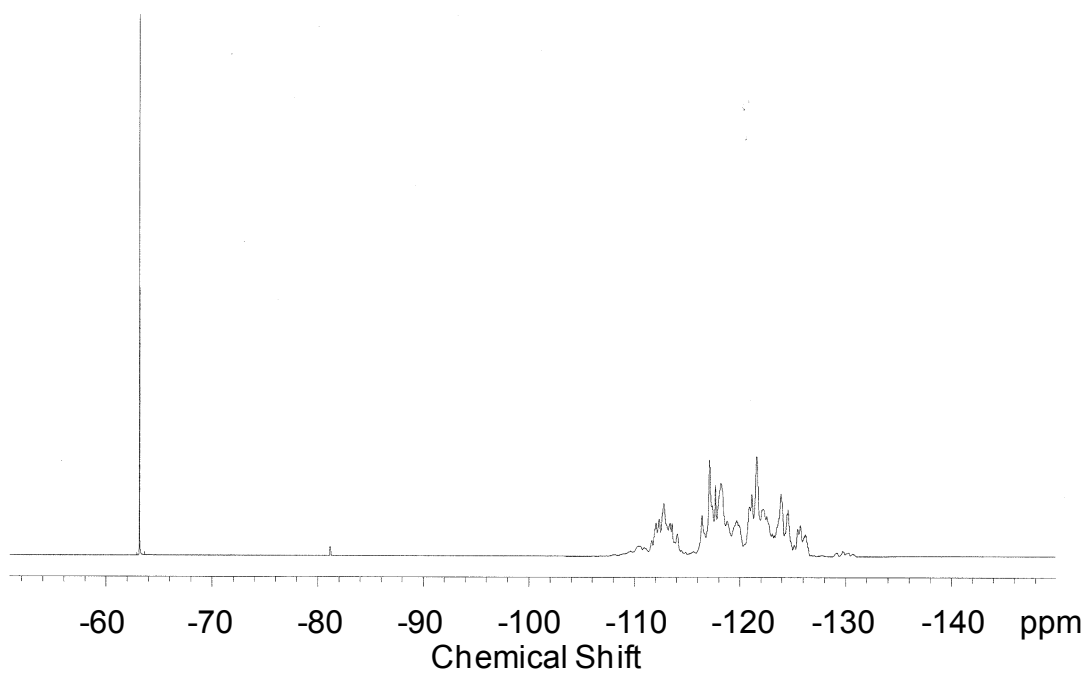


Figure A.17: ^{19}F NMR of emB

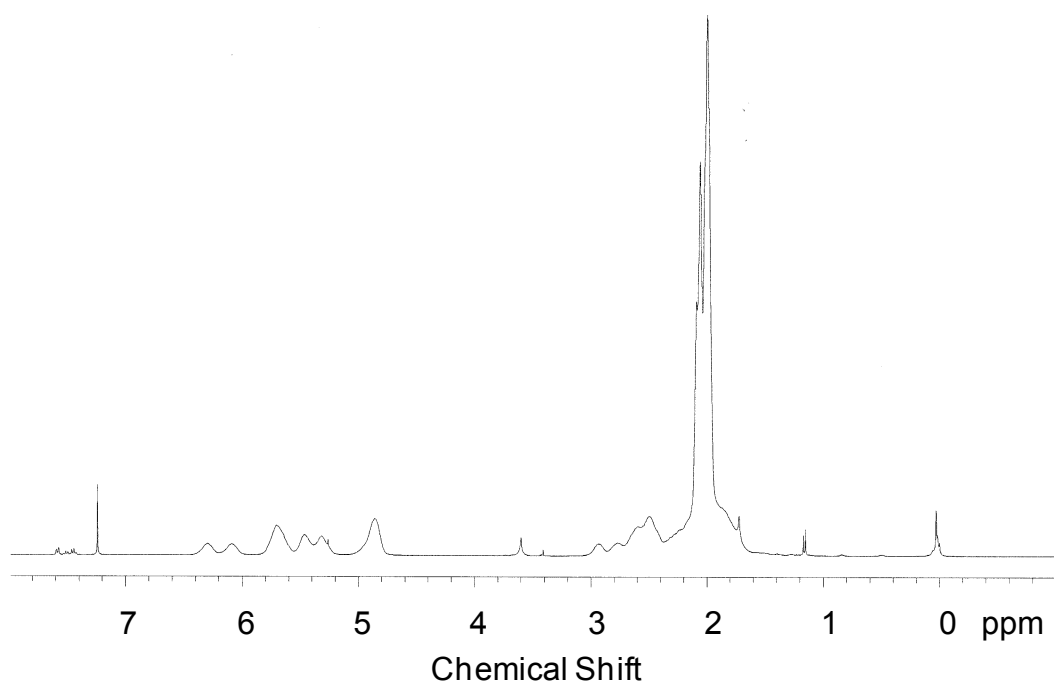


Figure A.18: ^1H NMR of emC

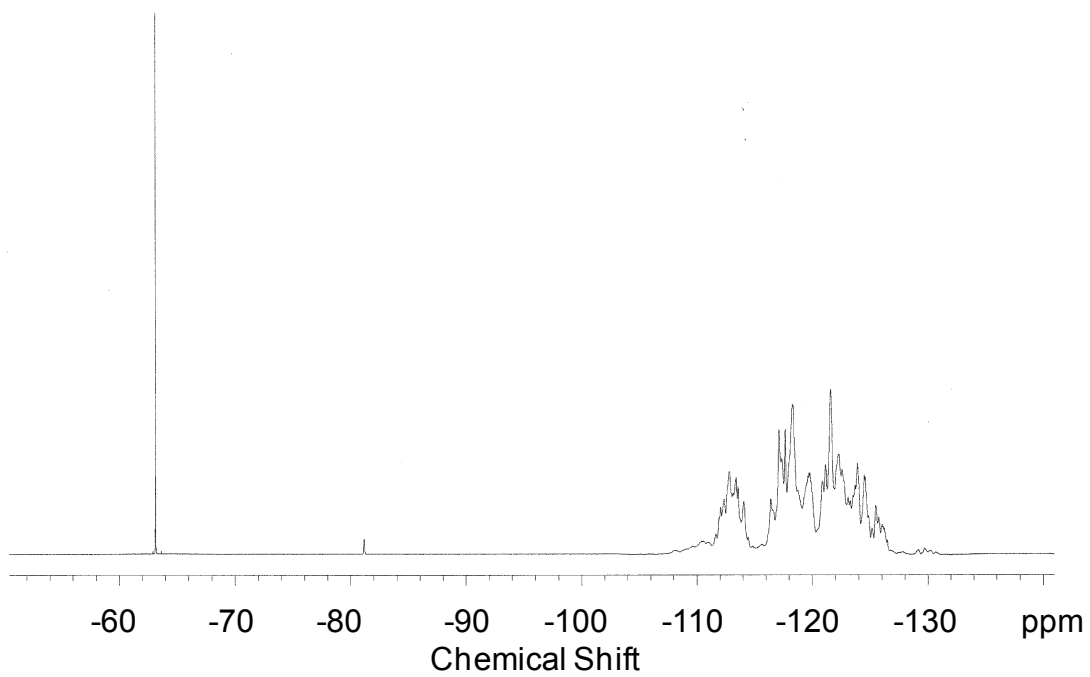


Figure A.19: ^{19}F NMR of emC

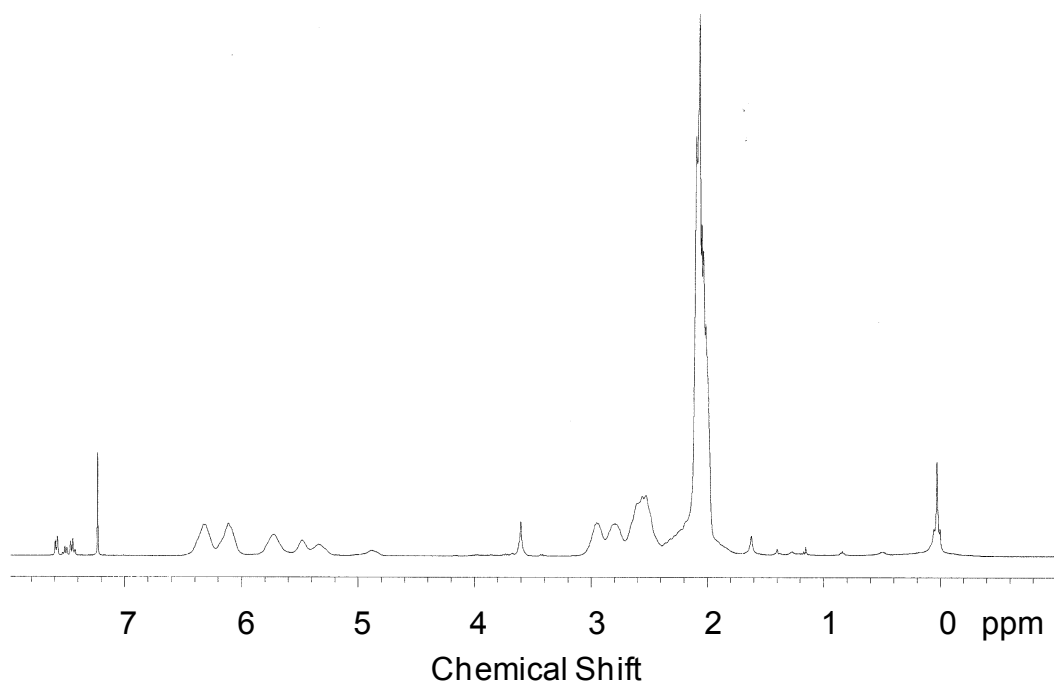


Figure A.20: ^1H NMR of emD

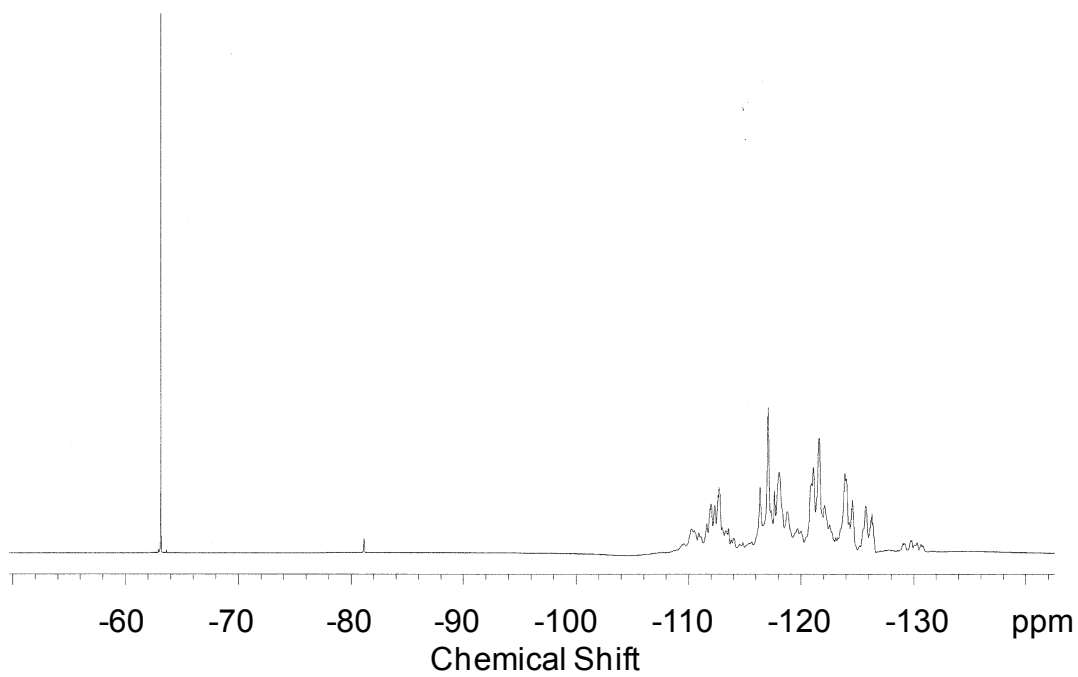


Figure A.21: ^{19}F NMR of emD

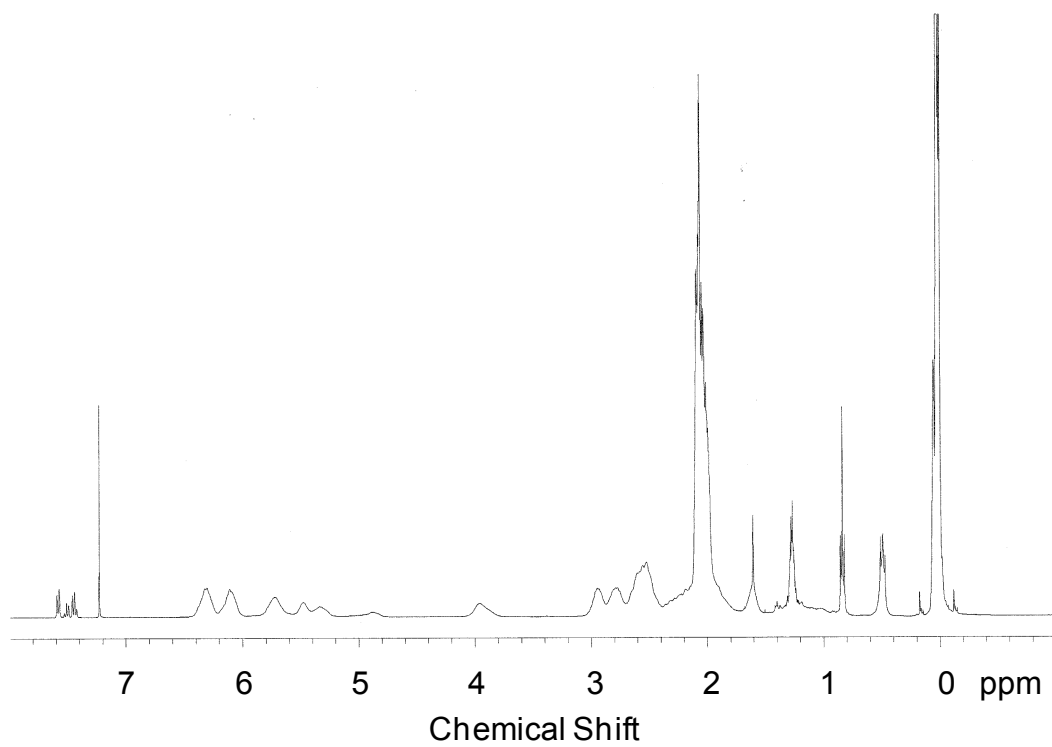


Figure A.22: ^1H NMR of scA

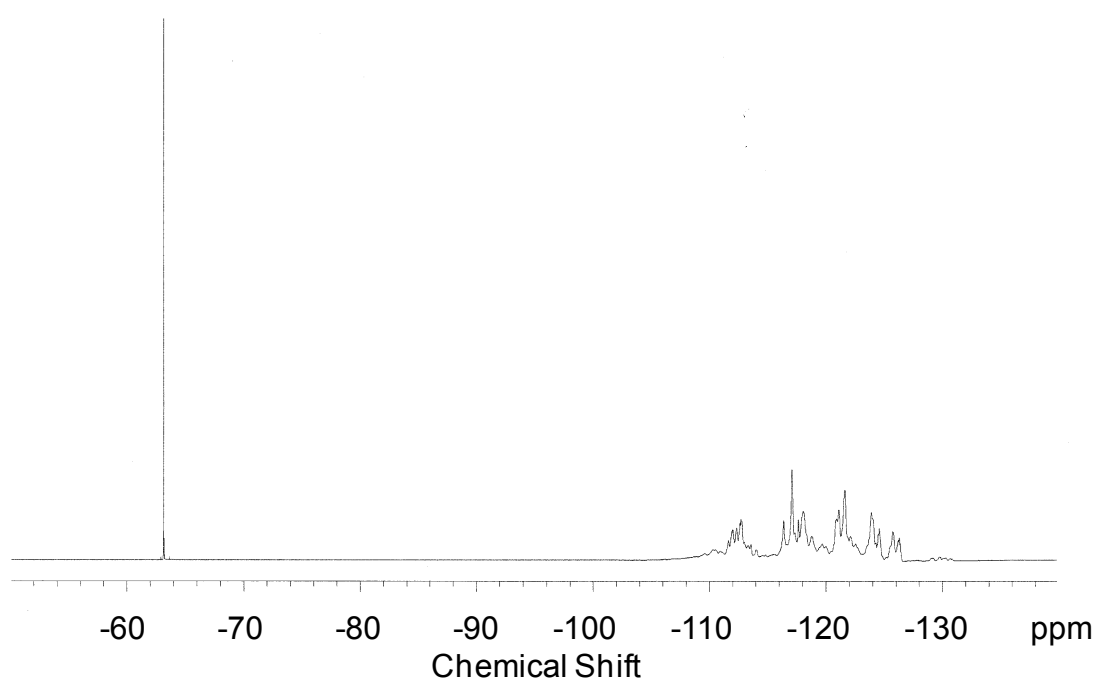


Figure A.23: ^{19}F NMR of scA

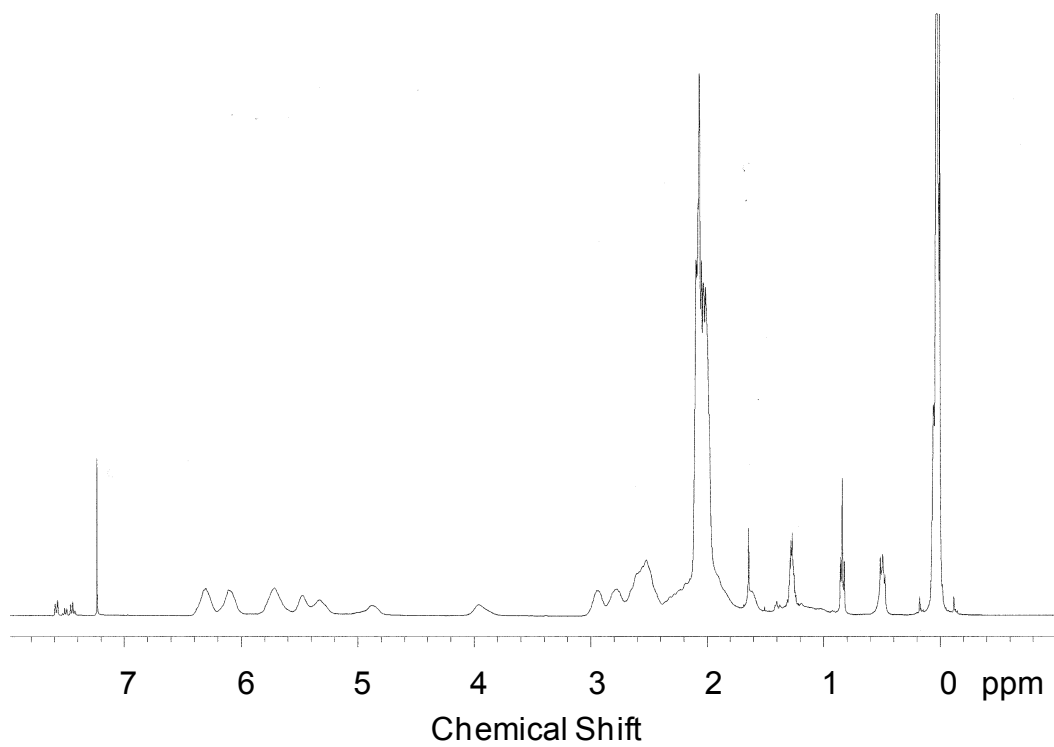


Figure A.24: ^1H NMR of scB

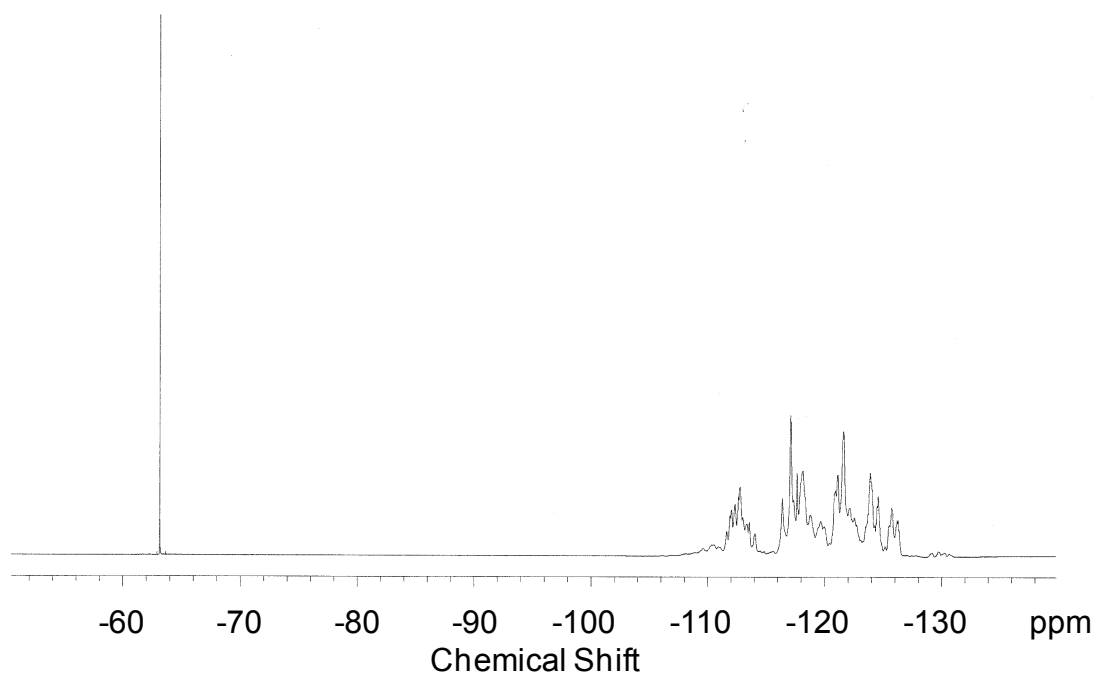


Figure A.25: ^{19}F NMR of scB

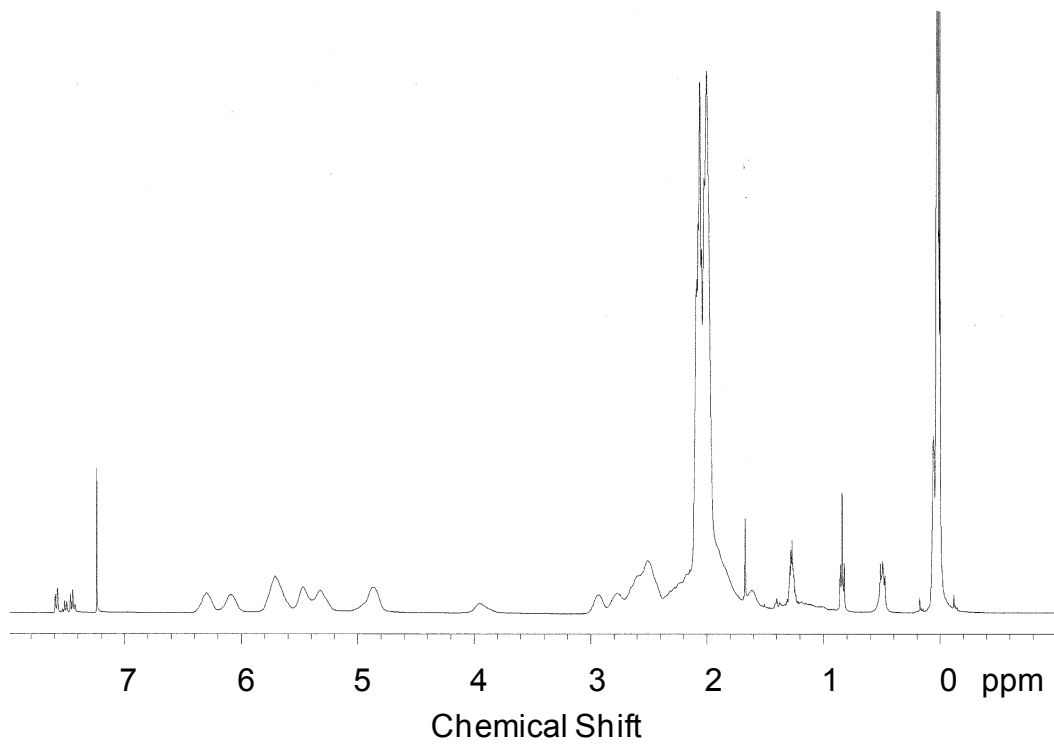


Figure A.26: ^1H NMR of scC

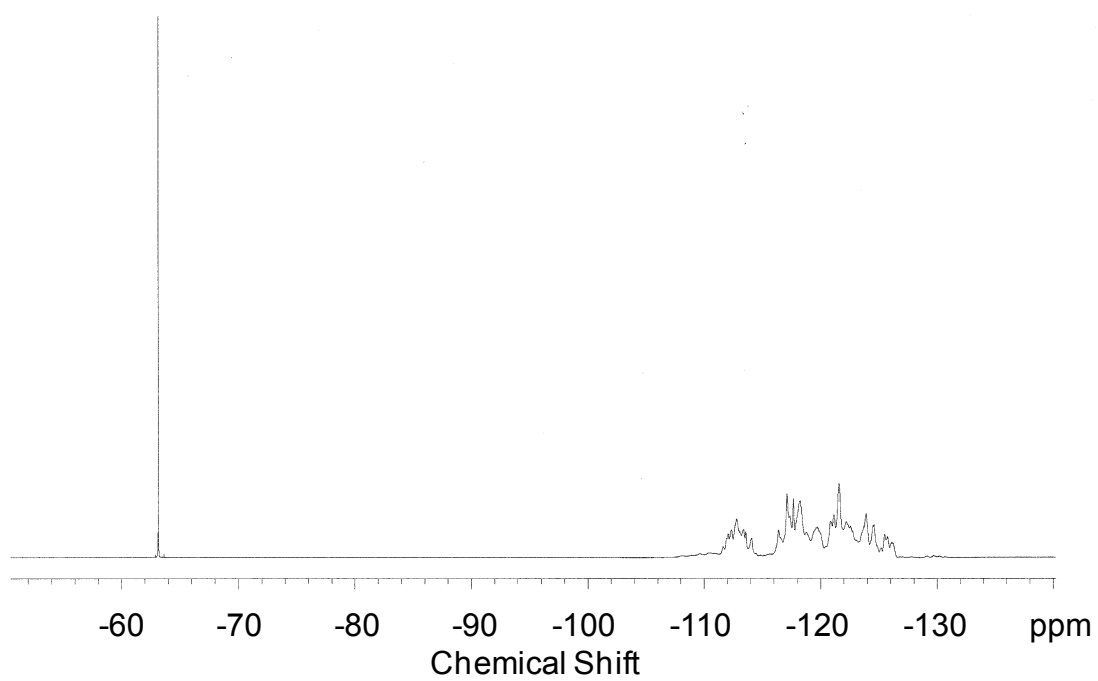


Figure A.27: ^{19}F NMR of scC

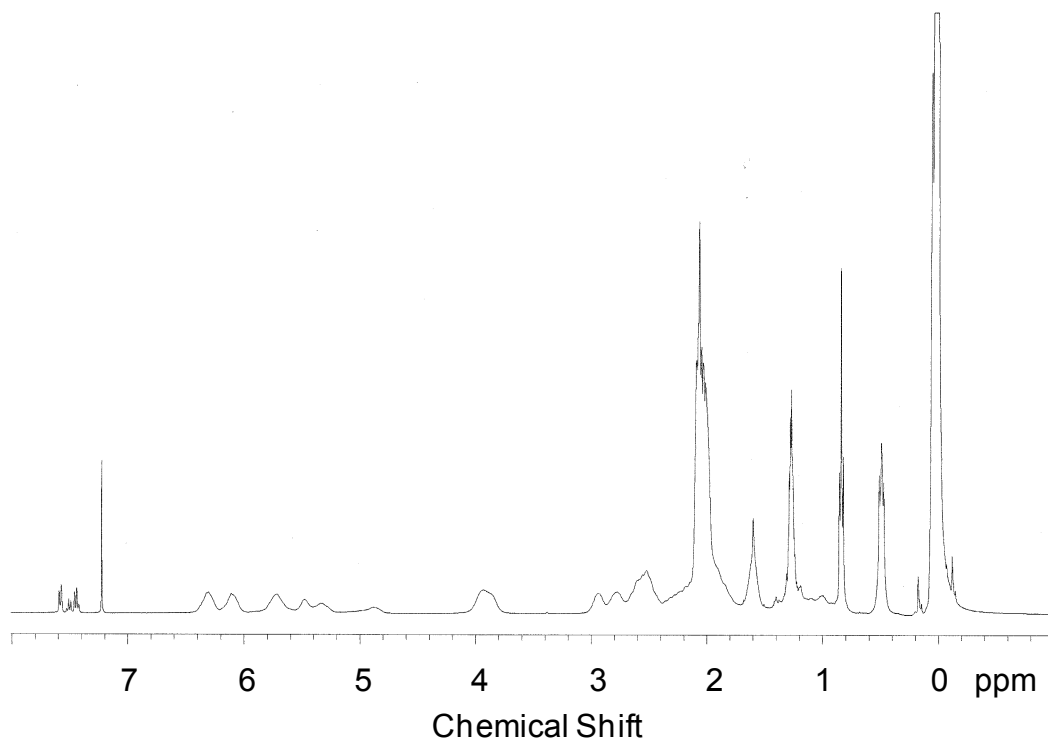


Figure A.28: ^1H NMR of scD

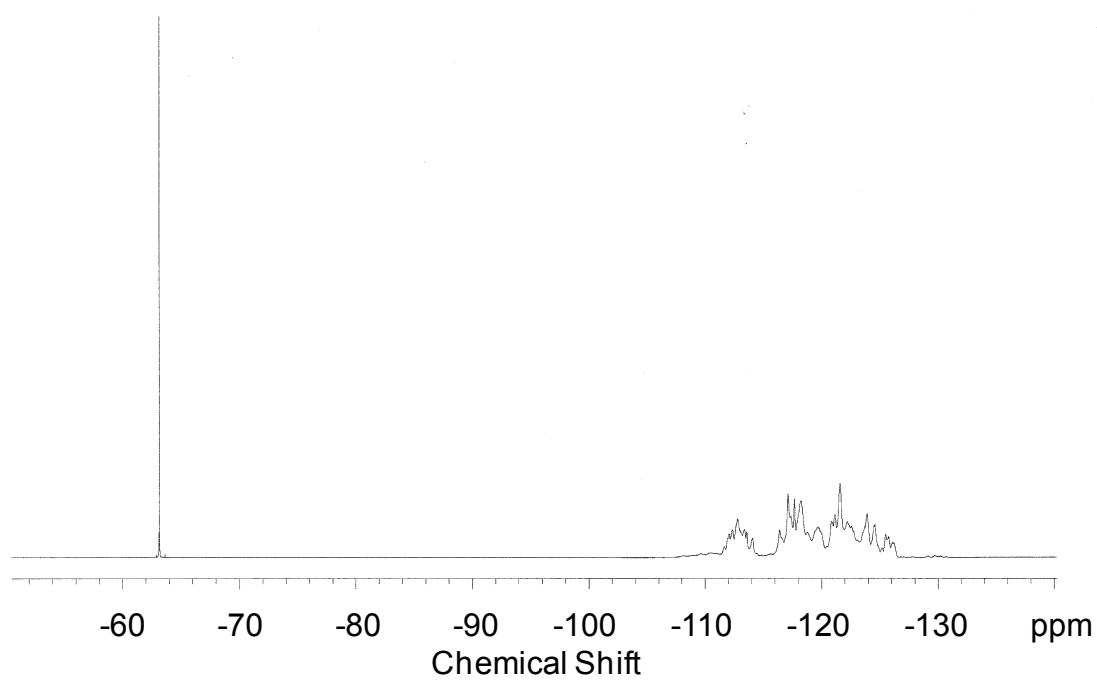


Figure A.29: ^{19}F NMR of scD

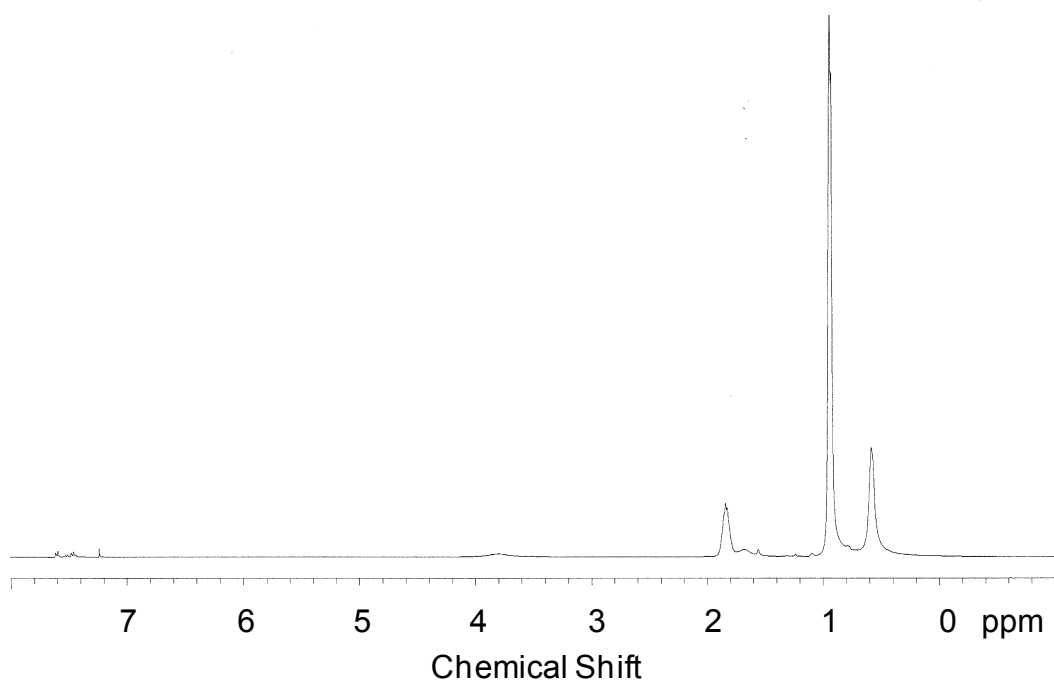


Figure A.30: ^1H NMR of S(100)

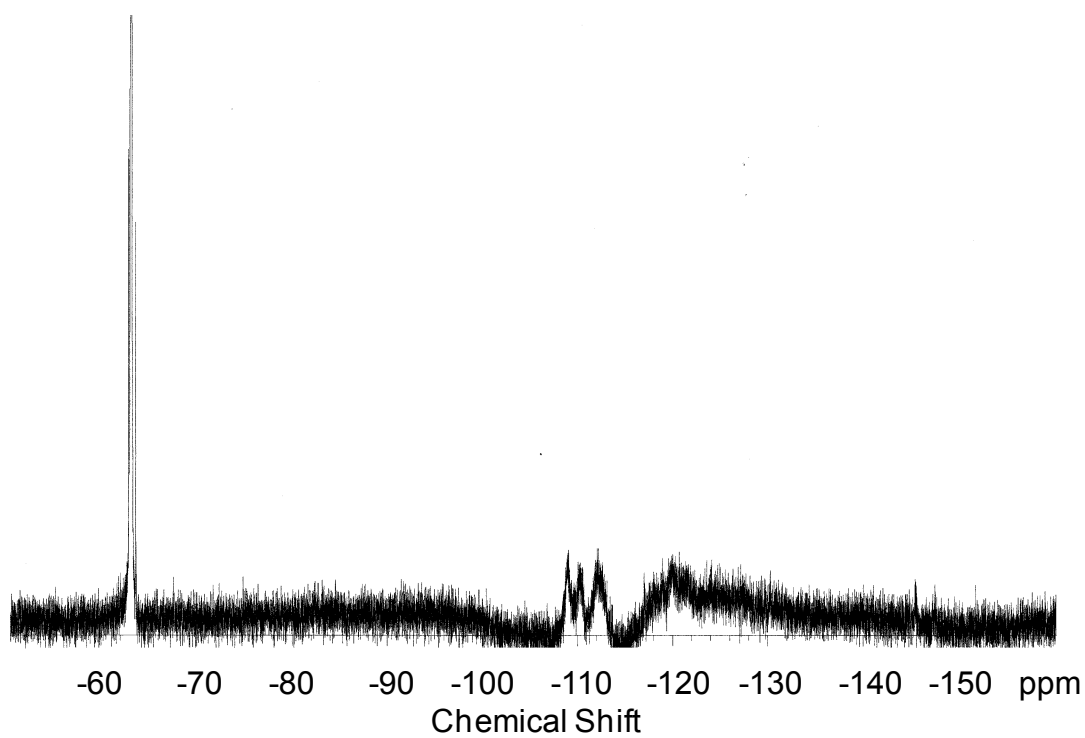


Figure A.31: ^{19}F NMR of CS(02-98)

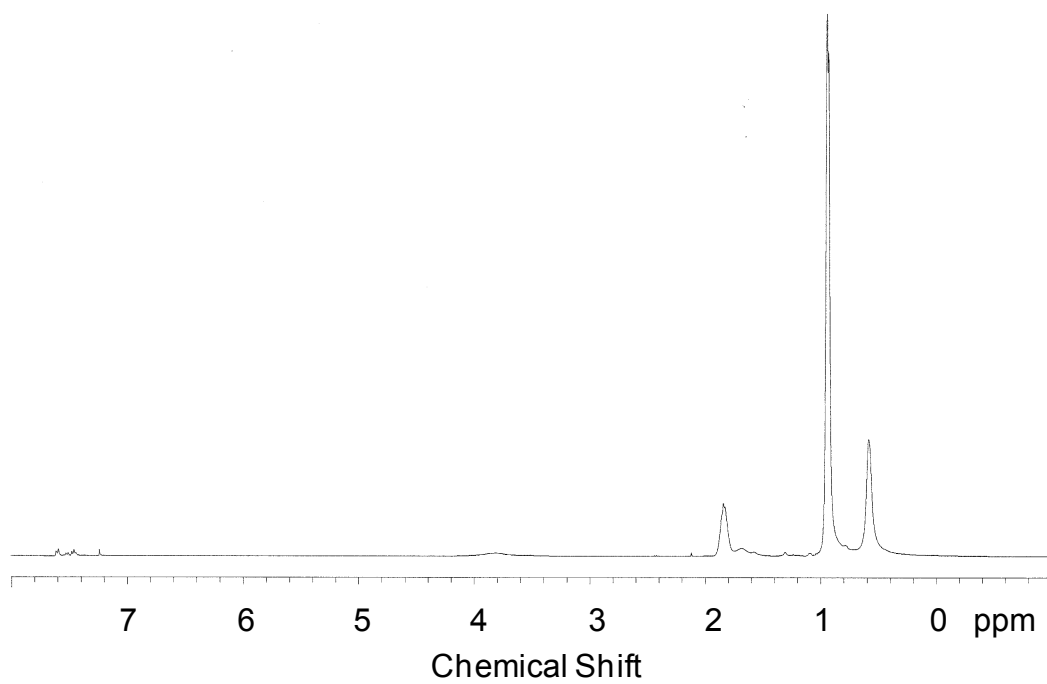


Figure A.32: ^1H NMR of CS(10-90)

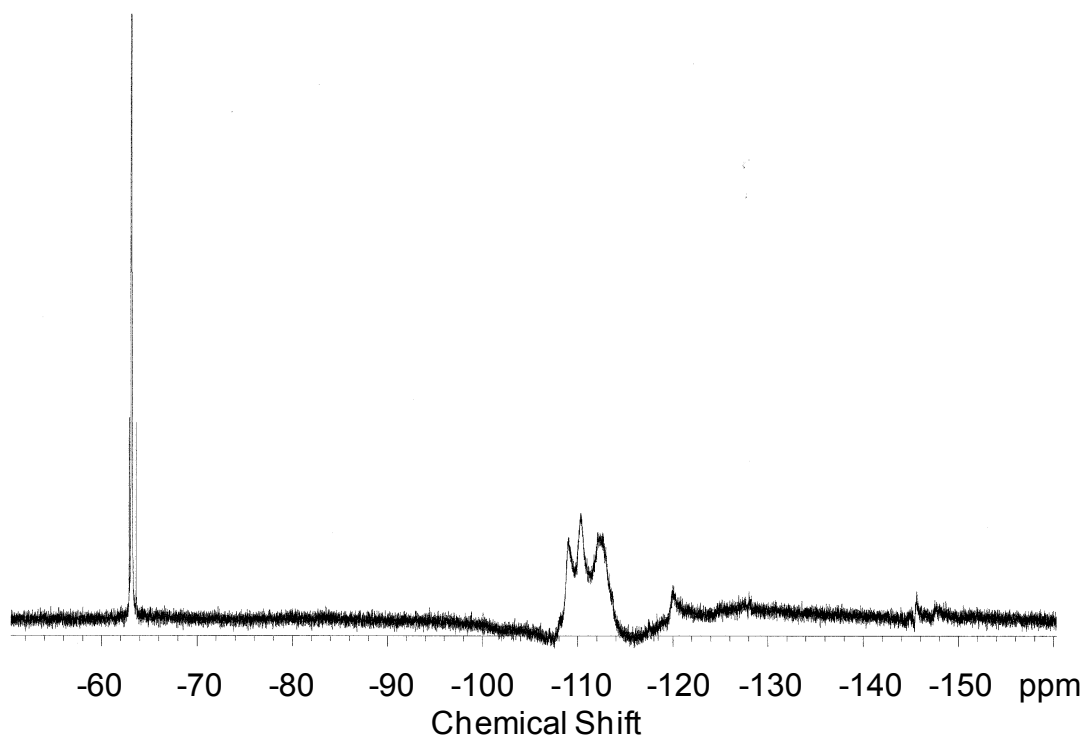


Figure A.33: ^{19}F NMR of CS(10-90)

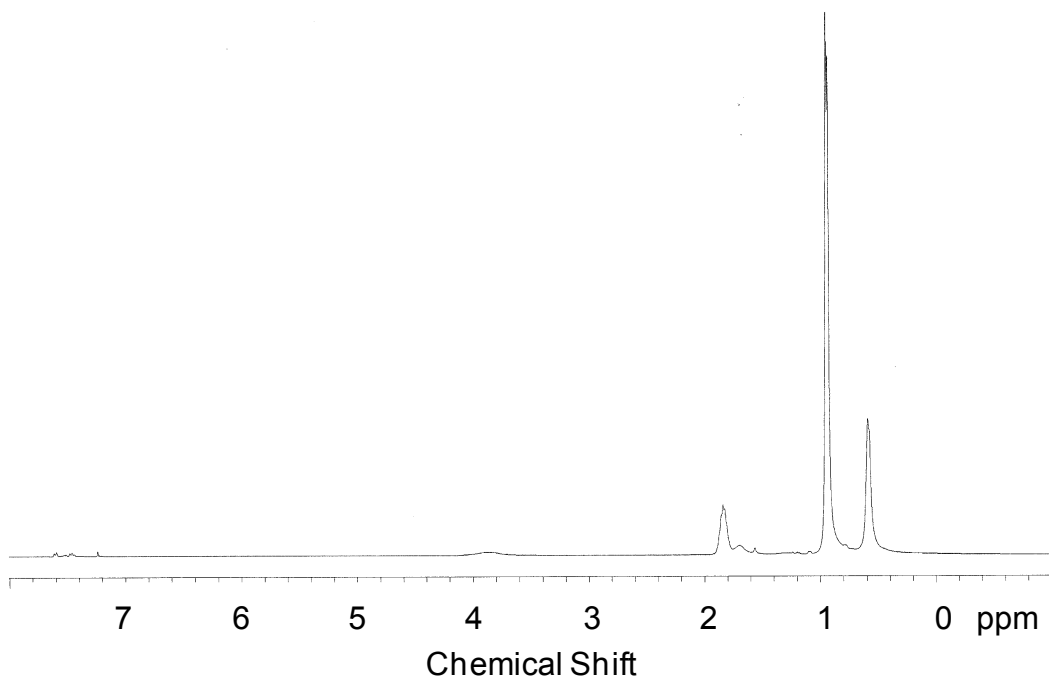


Figure A.34: ^1H NMR of CS(20-80)

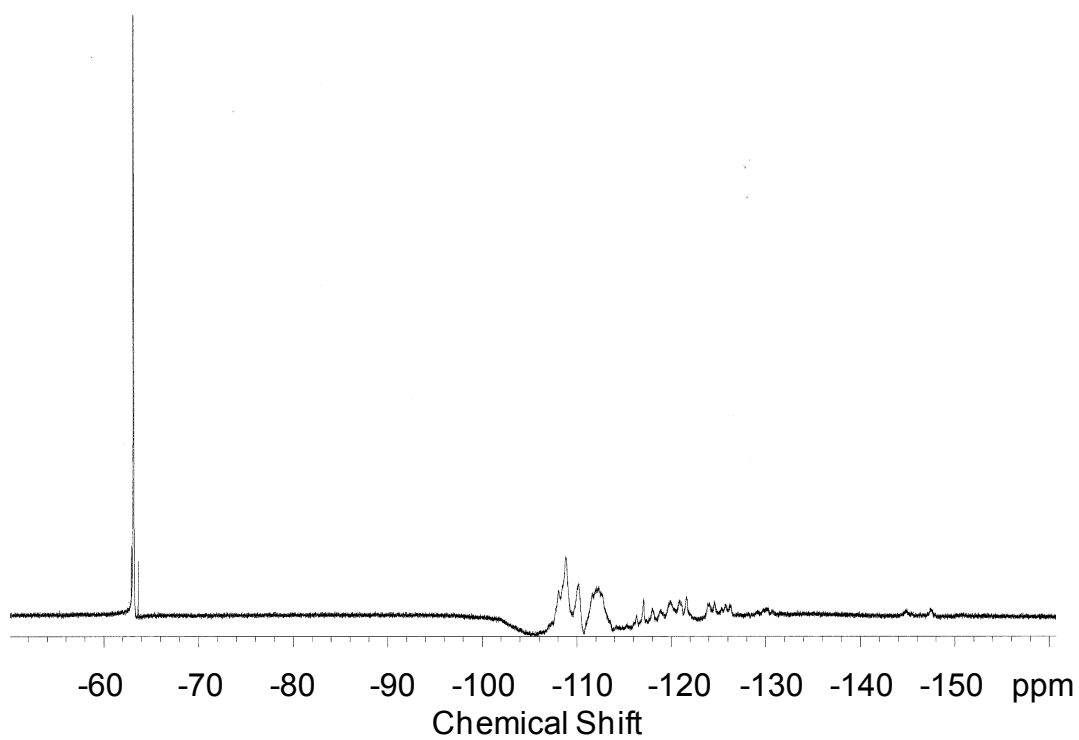


Figure A.35: ^{19}F NMR of CS(20-80)

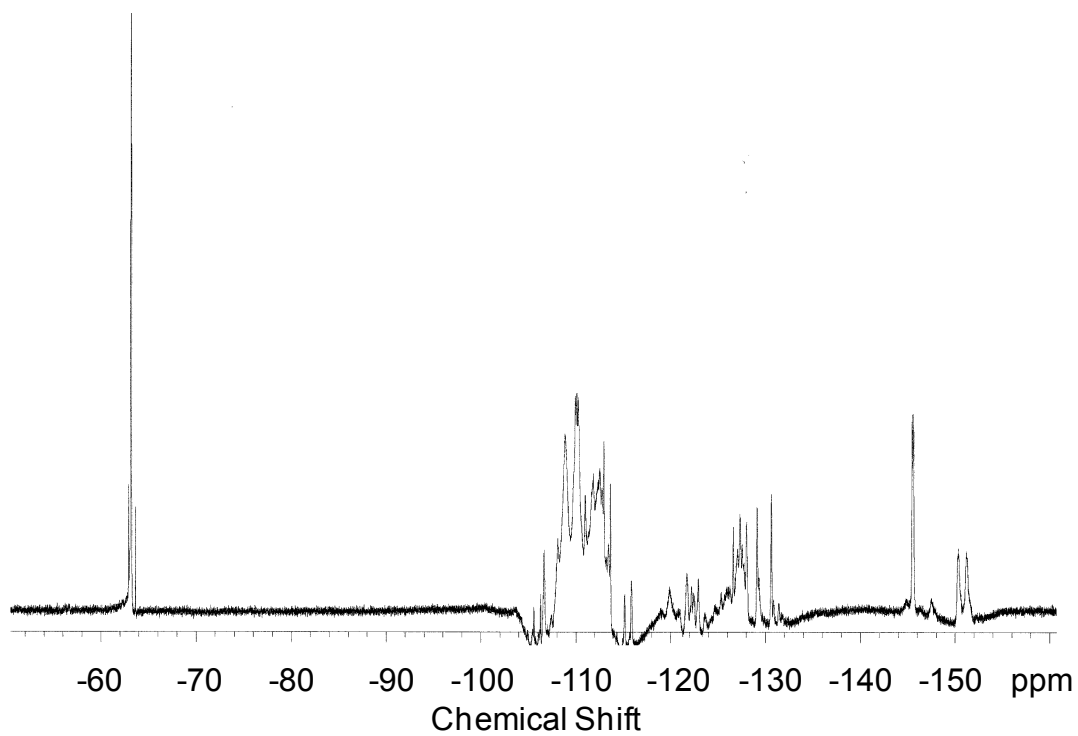


Figure A.36: ^{19}F NMR of CS(33-67)

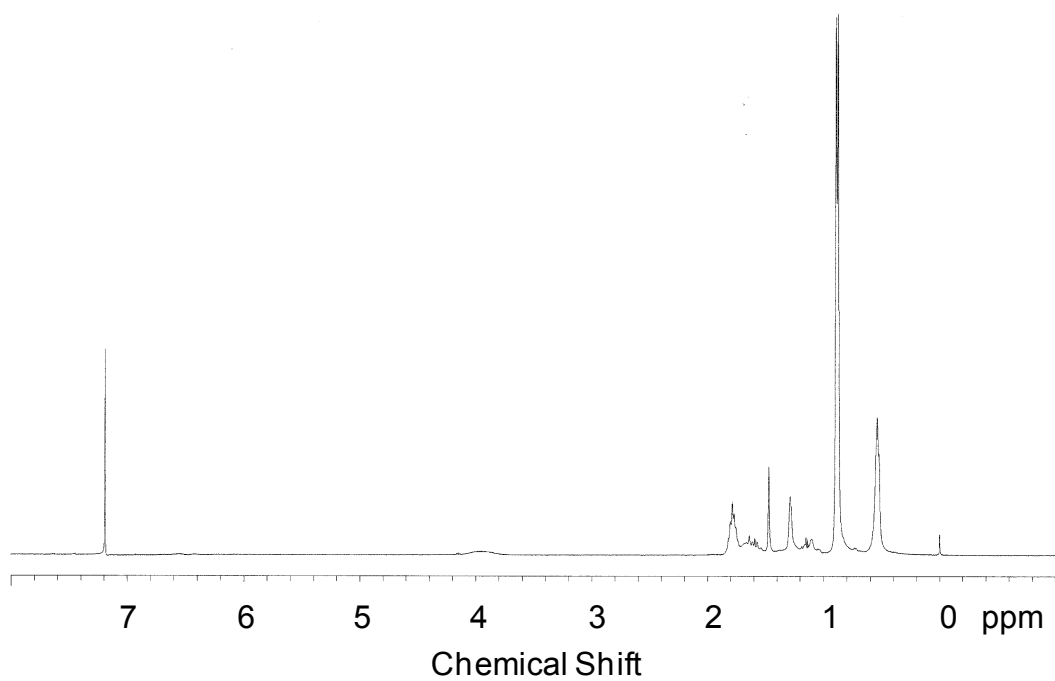


Figure A.37: ^1H NMR of CS(81-19)

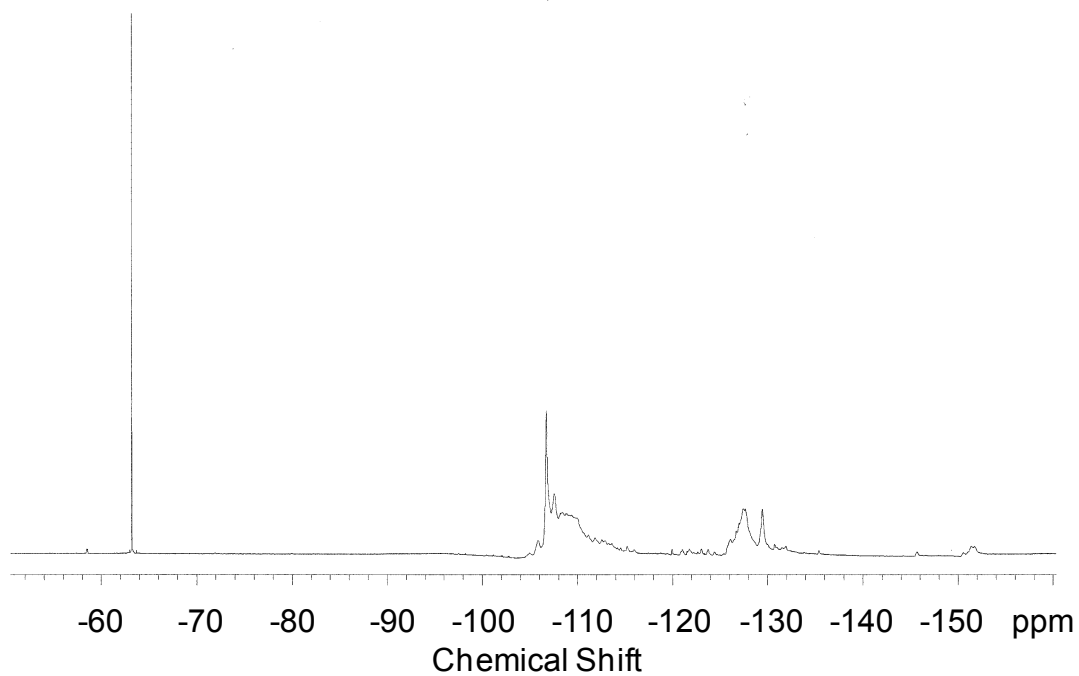


Figure A.38: ^{19}F NMR of CS(81-19)

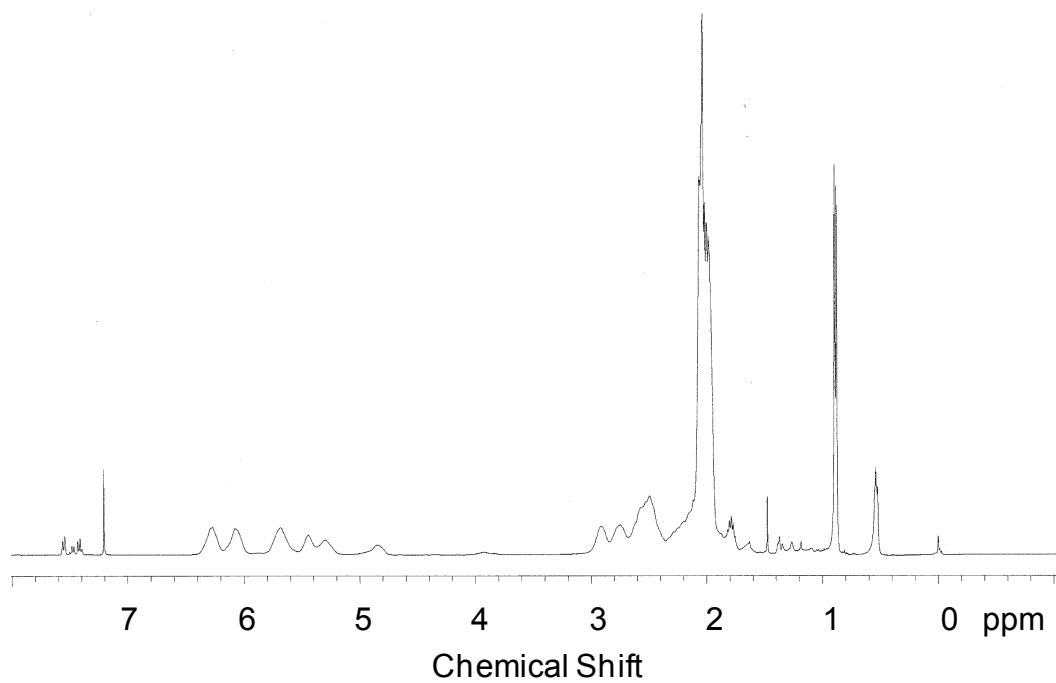


Figure A.39: ^1H NMR of CVS(40-59-01)

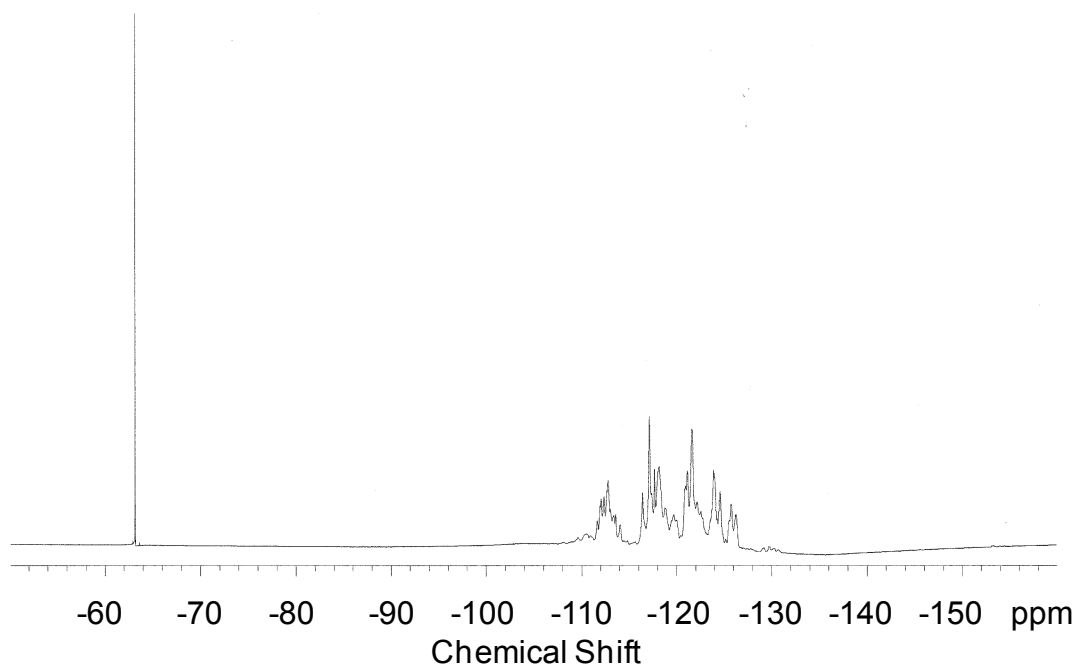


Figure A.40: ^{19}F NMR of CVS(40-59-01)

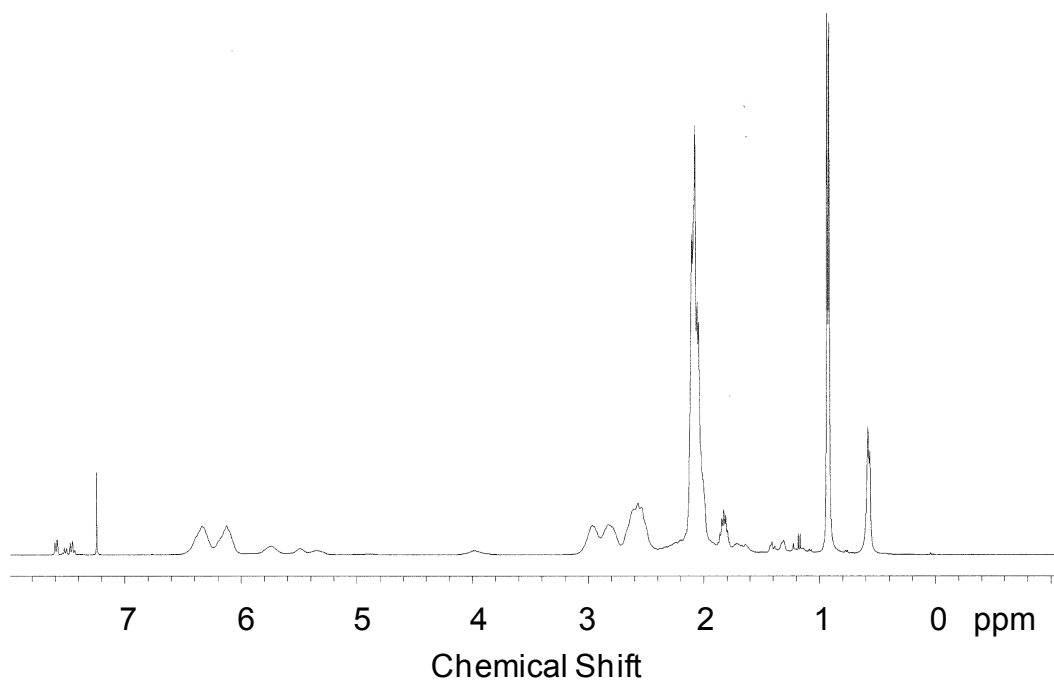


Figure A.41: ^1H NMR of CVS(46-52-02)

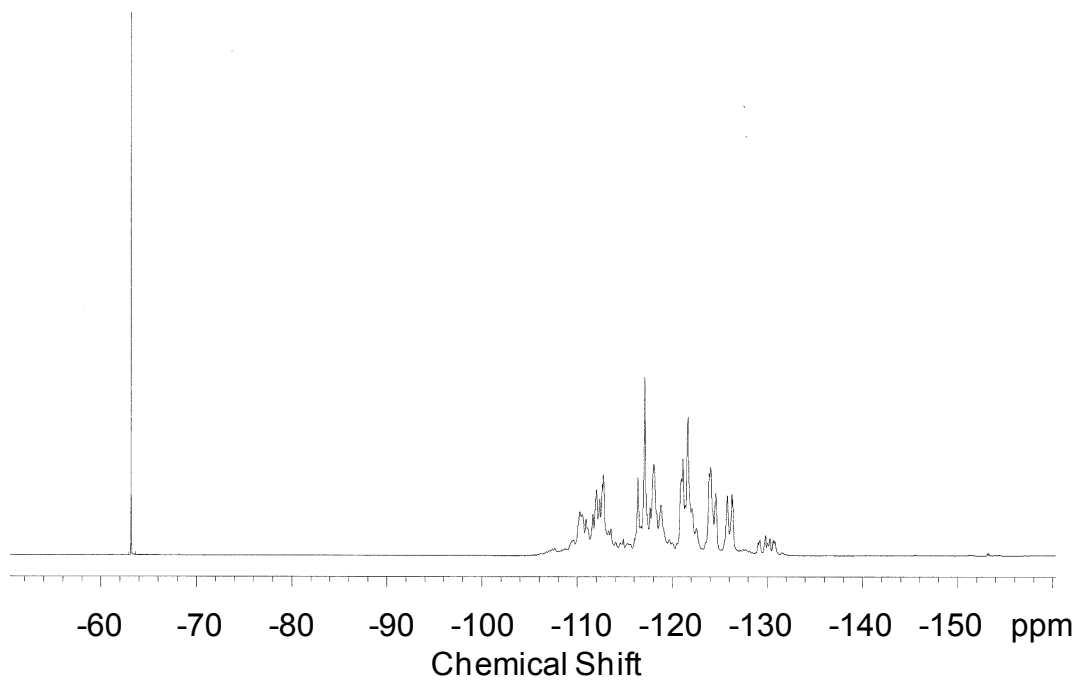


Figure A.42: ^{19}F NMR of CVS(46-52-02)

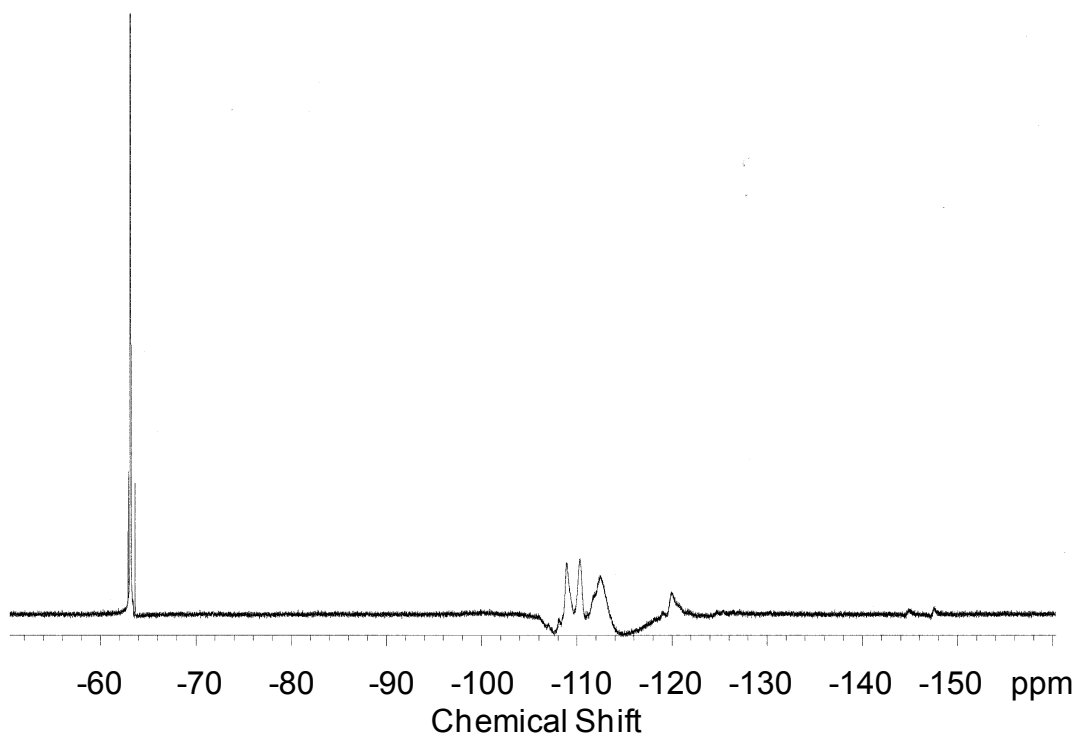


Figure A.43: ^{19}F NMR of CS(50-50), Reaction Time = 0 h

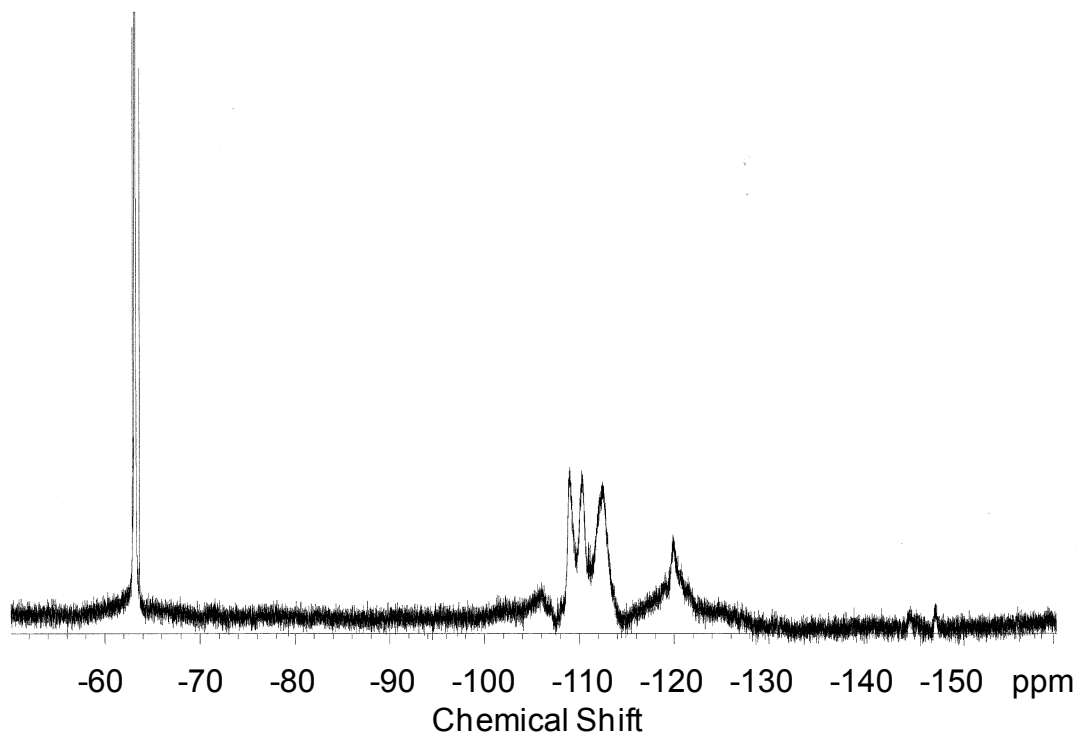


Figure A.44: ^{19}F NMR of CS(50-50), Reaction Time = 3 h

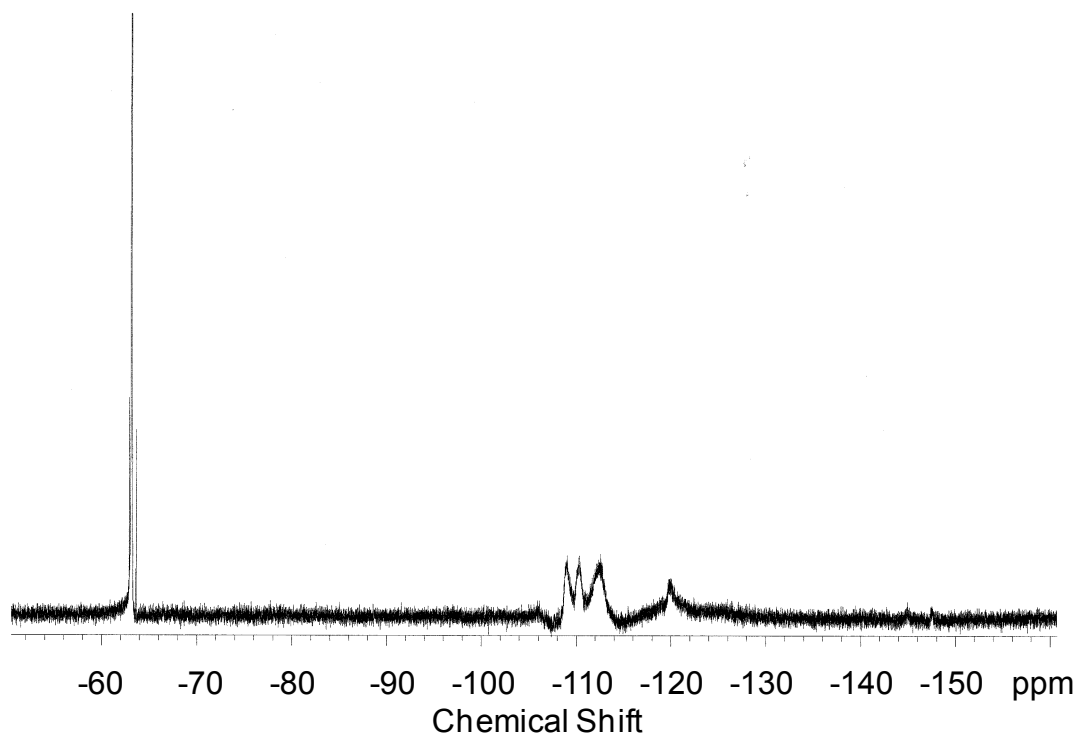


Figure A.45: ^{19}F NMR of CS(50-50), Reaction Time = 8 h

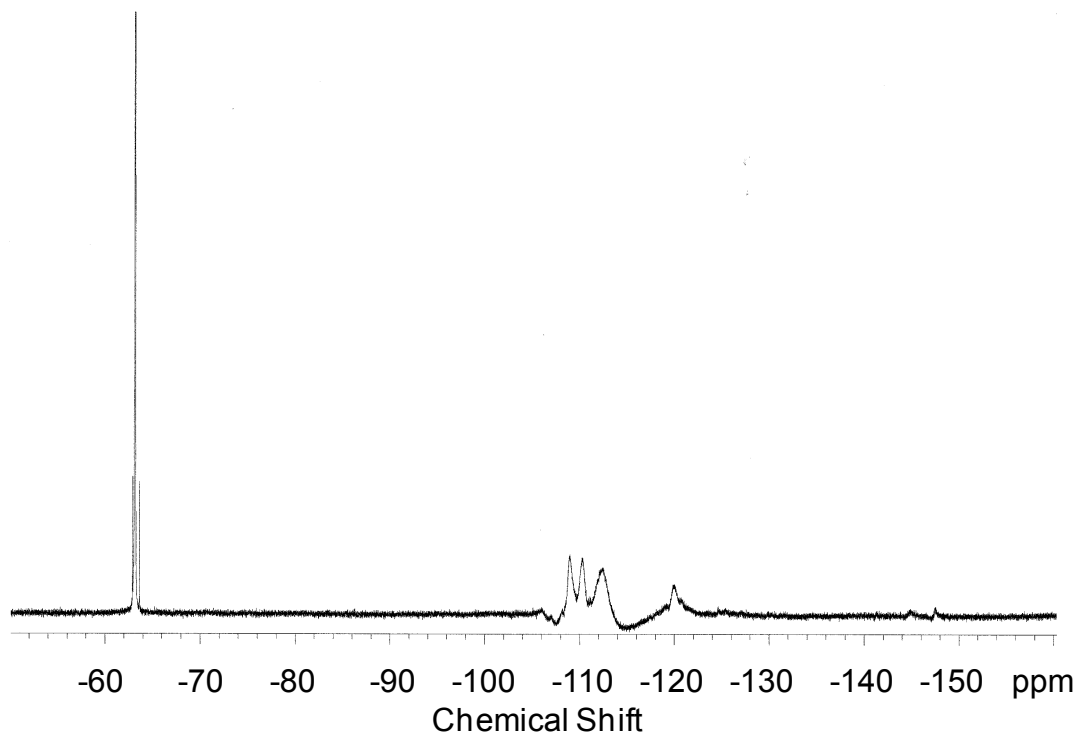


Figure A.46: ^{19}F NMR of CS(50-50), Reaction Time = 24 h

Appendix B: Fourier-Transform Infrared (FT-IR) Spectra

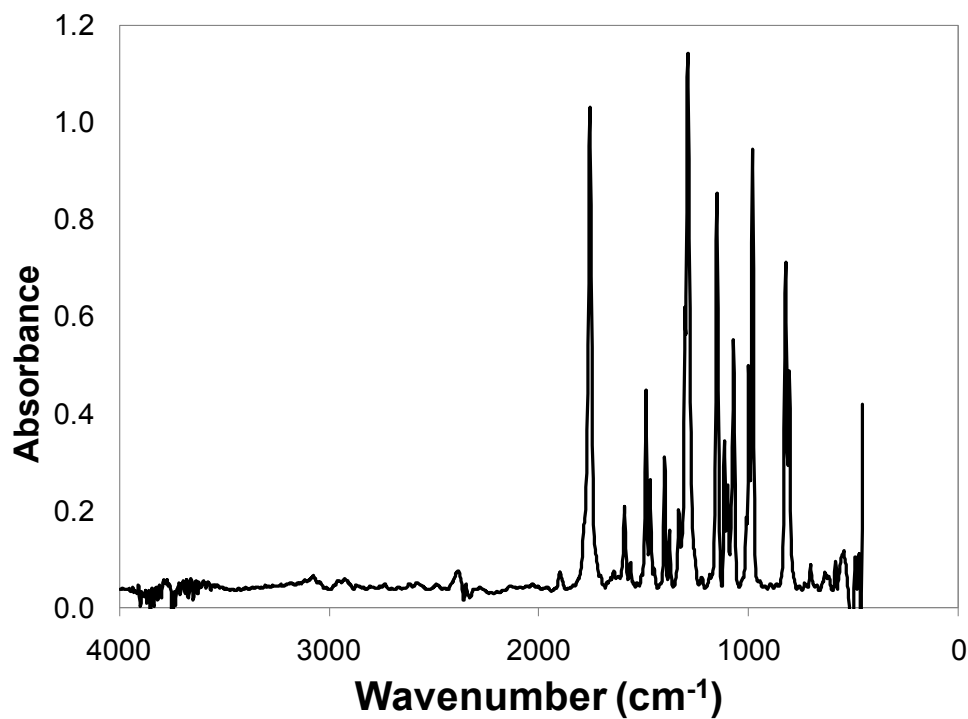


Figure B.1: FT-IR of I2

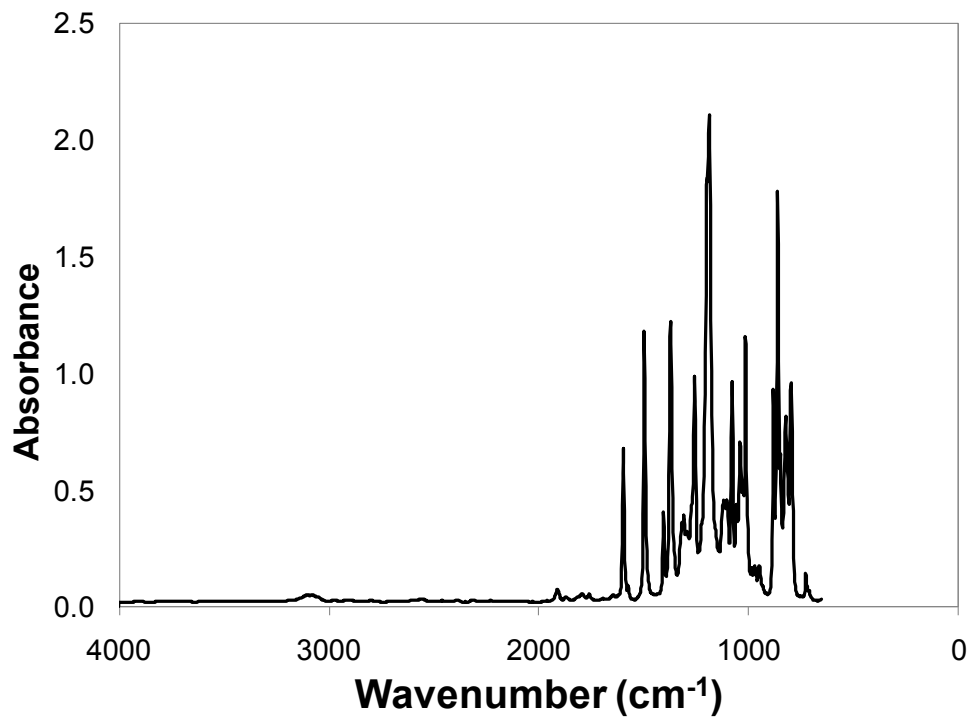


Figure B.2: FT-IR of M2

Appendix C: Gas Chromatography (GC) and Mass Spectroscopy (MS) Spectra

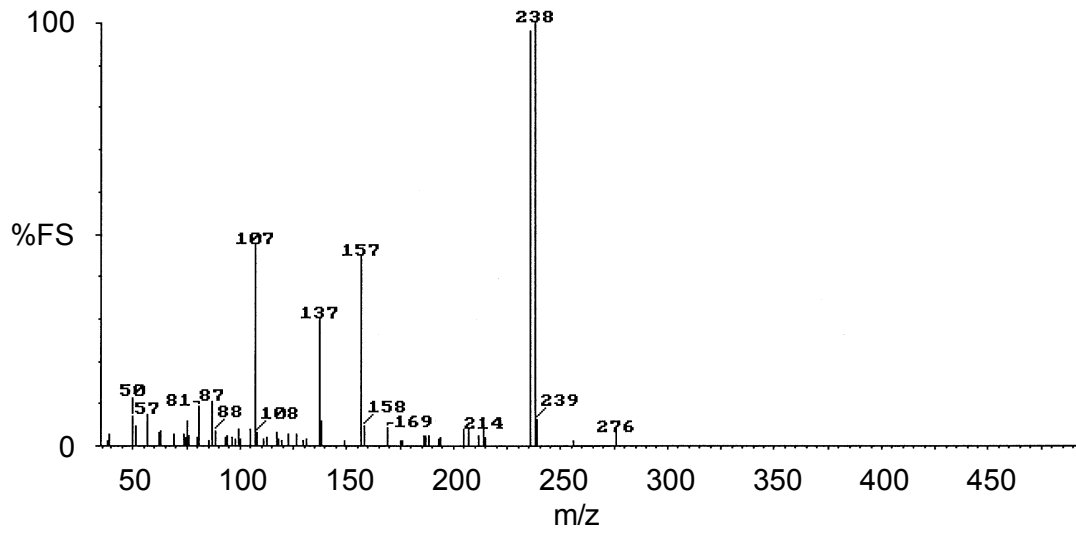


Figure C.1: MS of M2

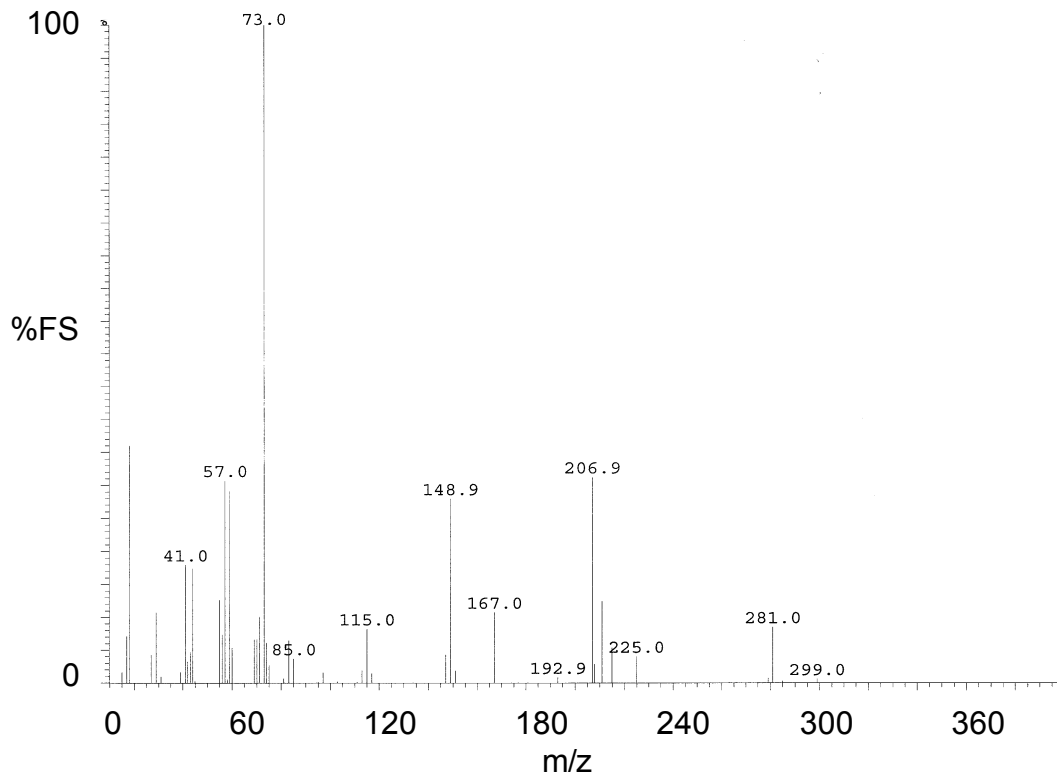


Figure C.2: MS of P2b at T = 238 °C

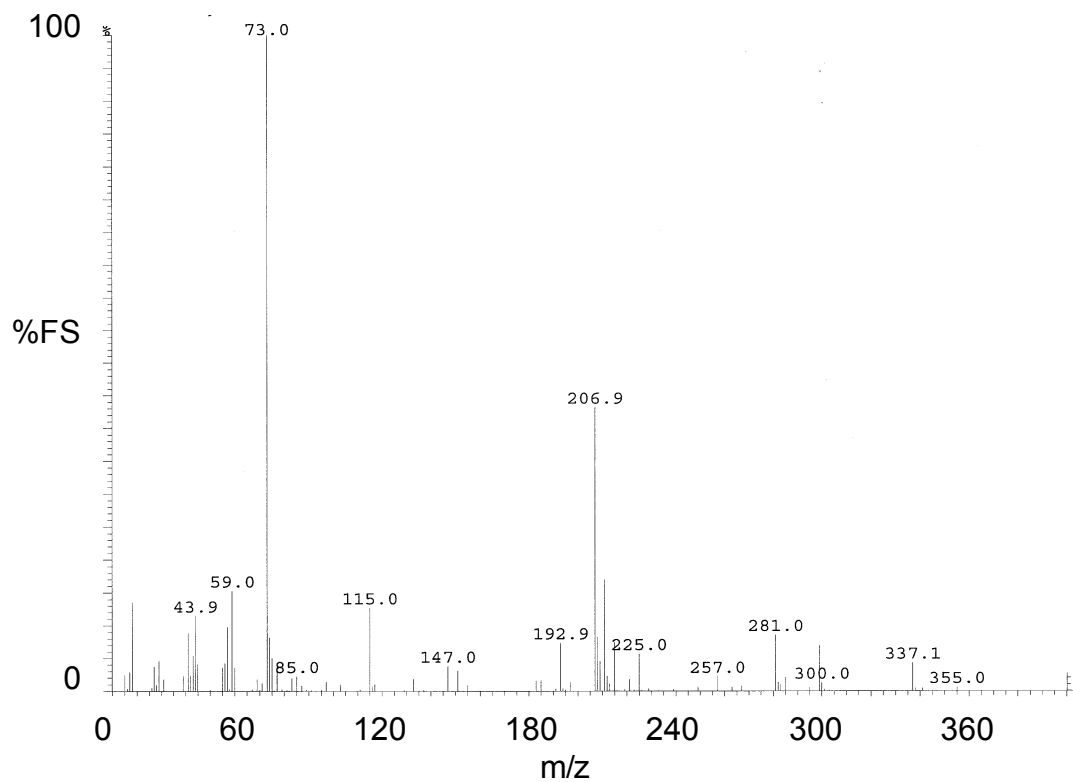


Figure C.3: MS of P2b at T = 308 °C

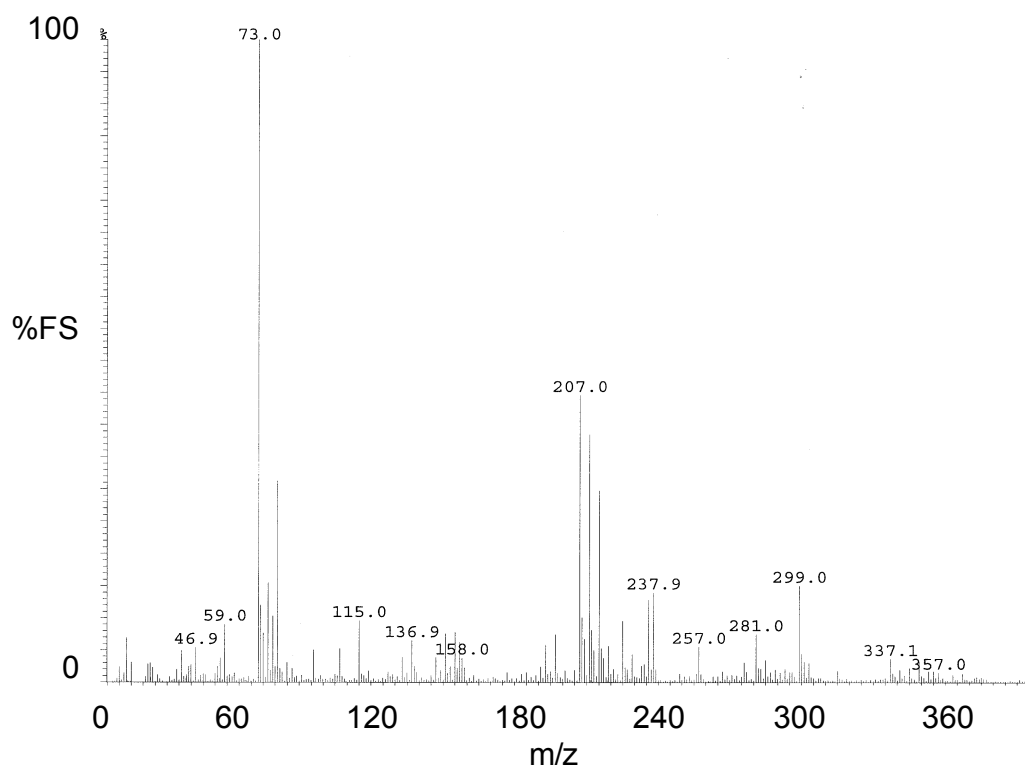


Figure C.4: MS of P2b at T = 450 °C

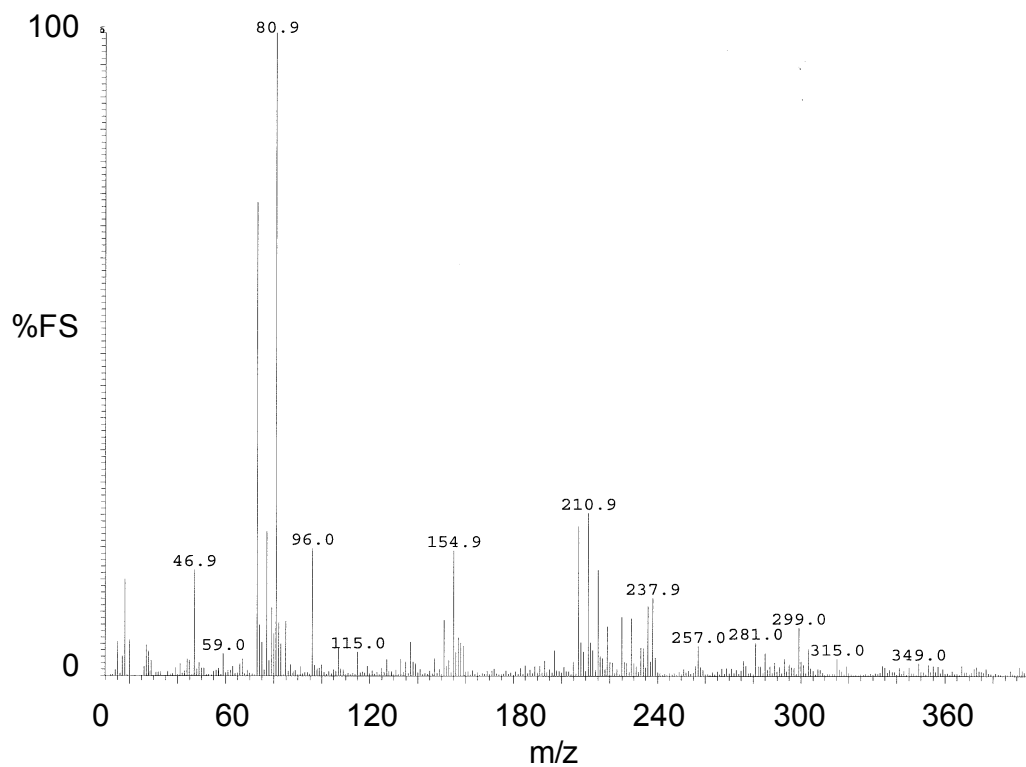


Figure C.5: MS of P2b at T = 450 °C

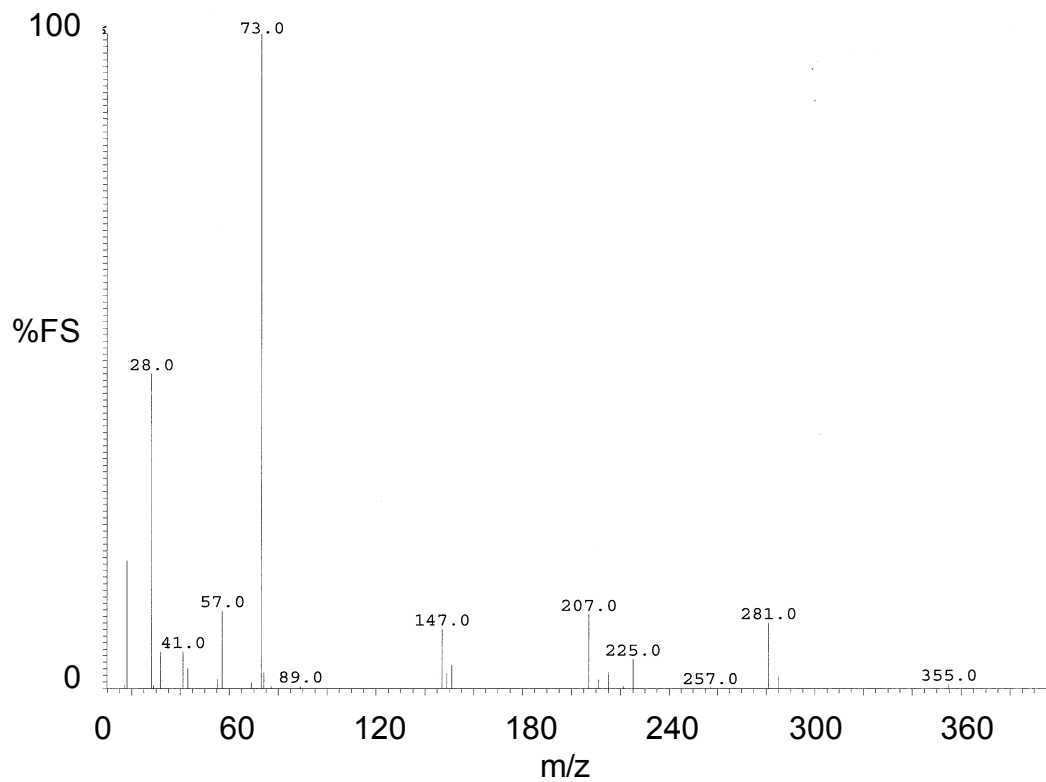


Figure C.6: MS of P2c at T = 194 °C

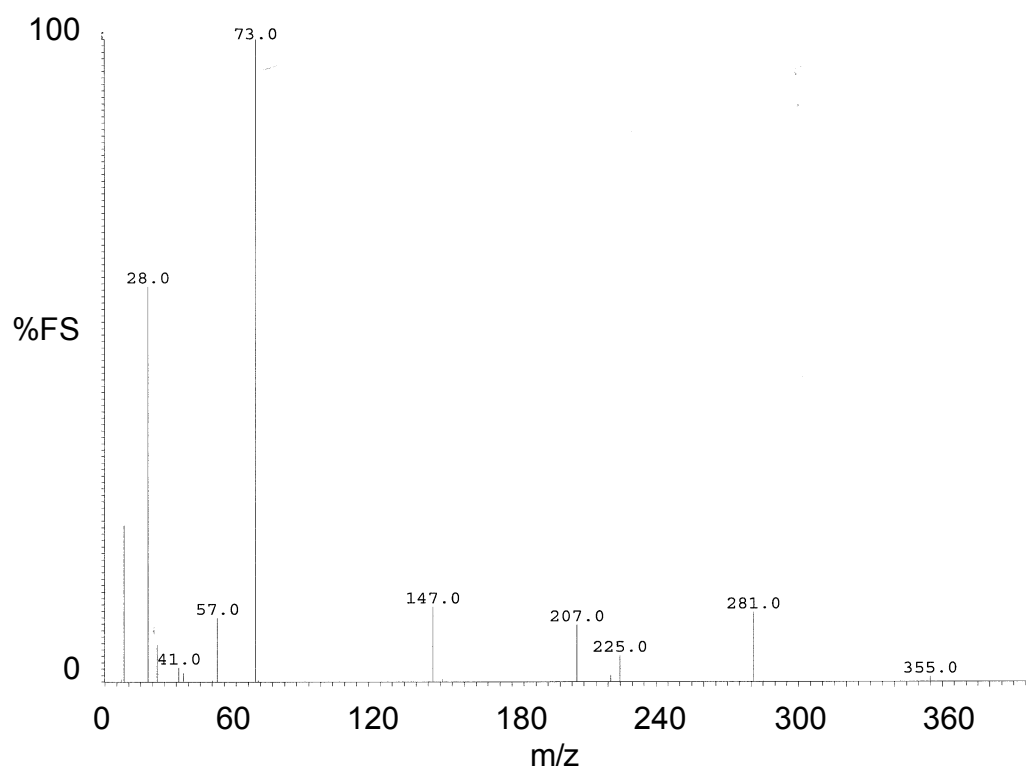


Figure C.7: MS of P2c at T = 239 °C

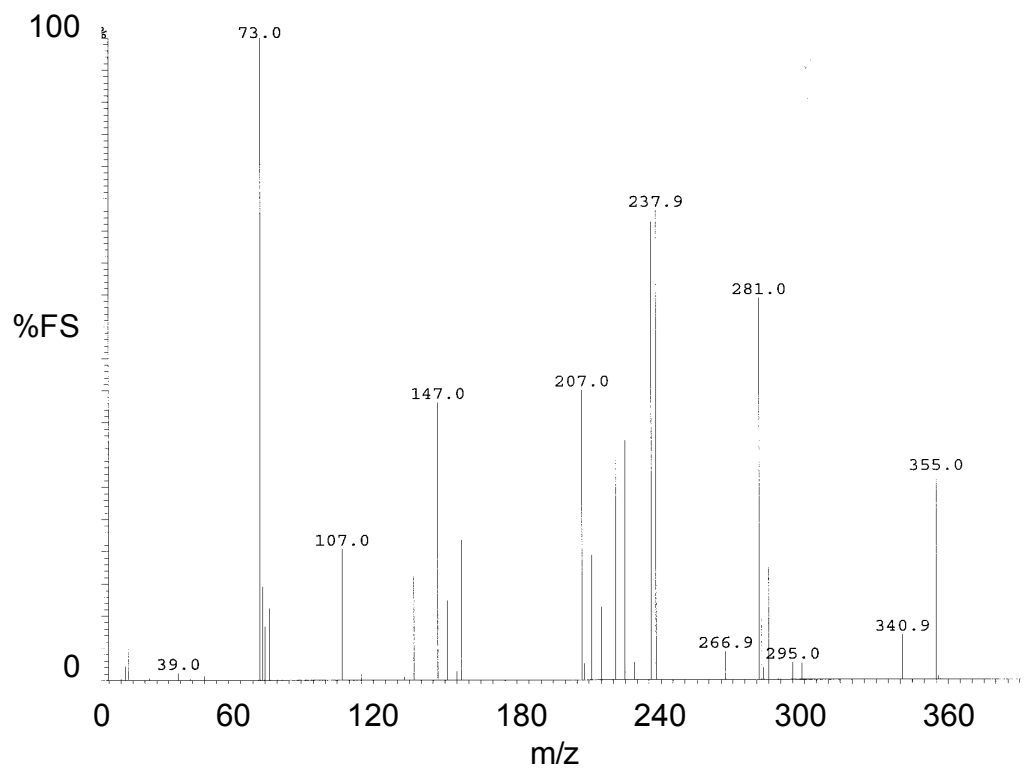


Figure C.8: MS of P2c at T = 334 °C

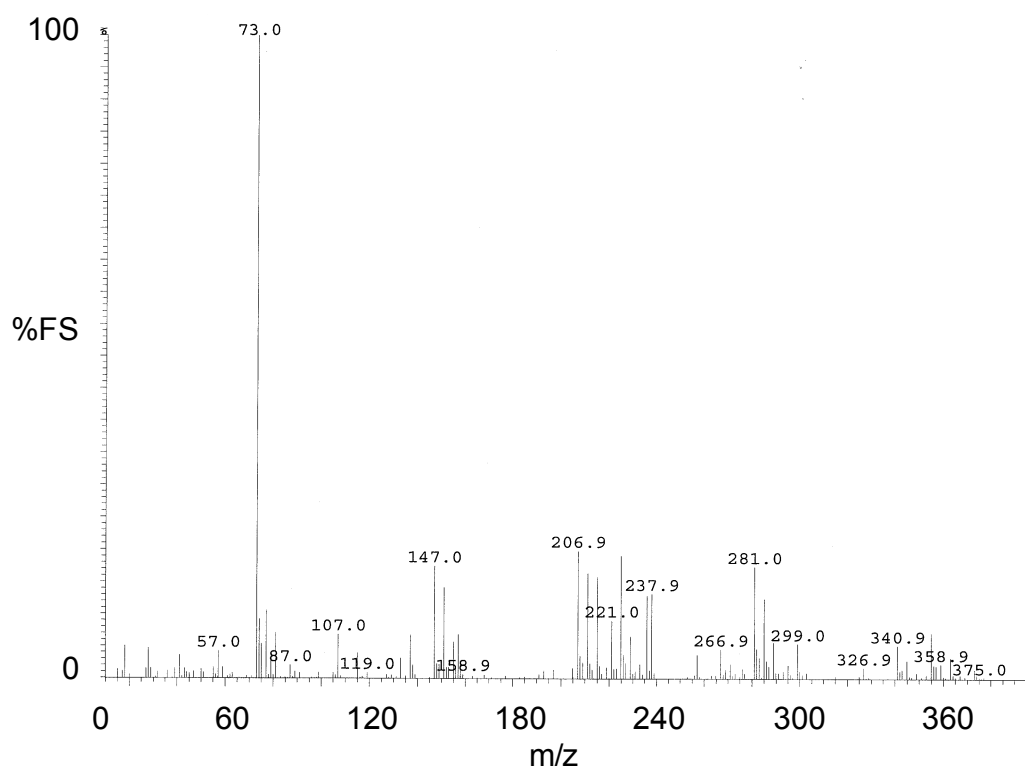


Figure C.9: MS of P2c at T = 450 °C

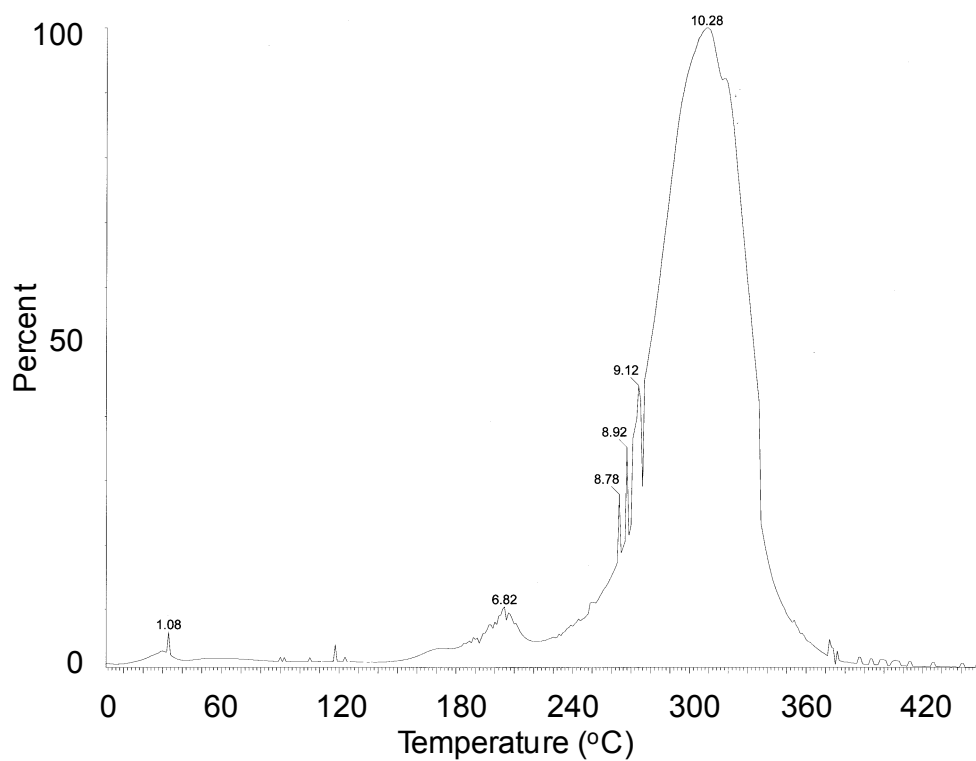


Figure C.10: GC of CS(02-98)

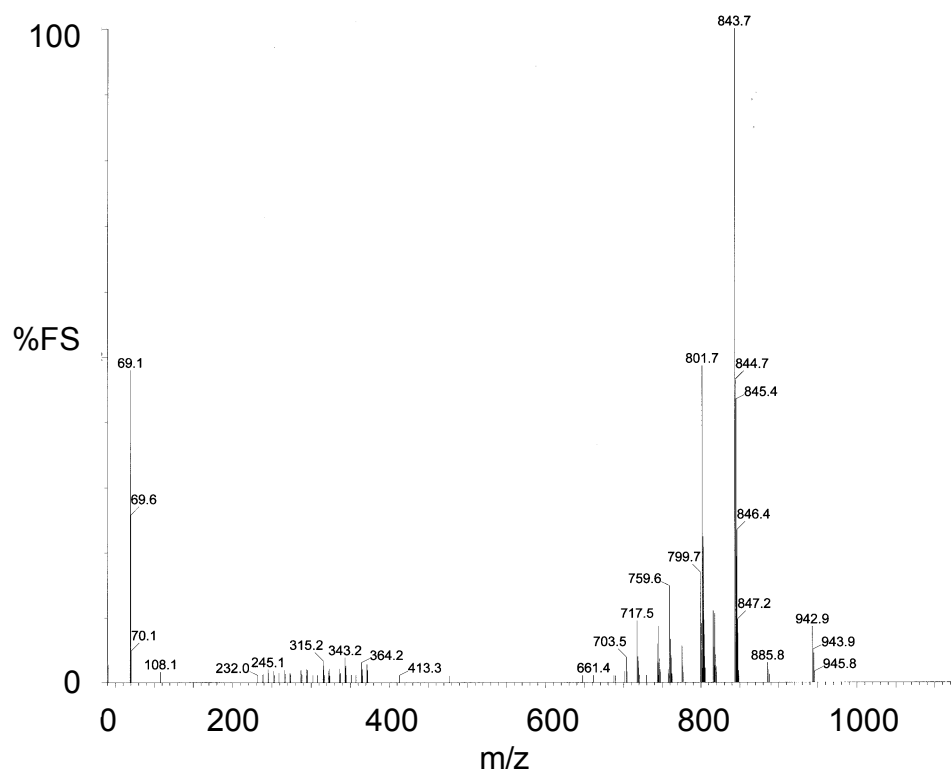


Figure C.11: MS of CS(02-98) at T = 310 °C

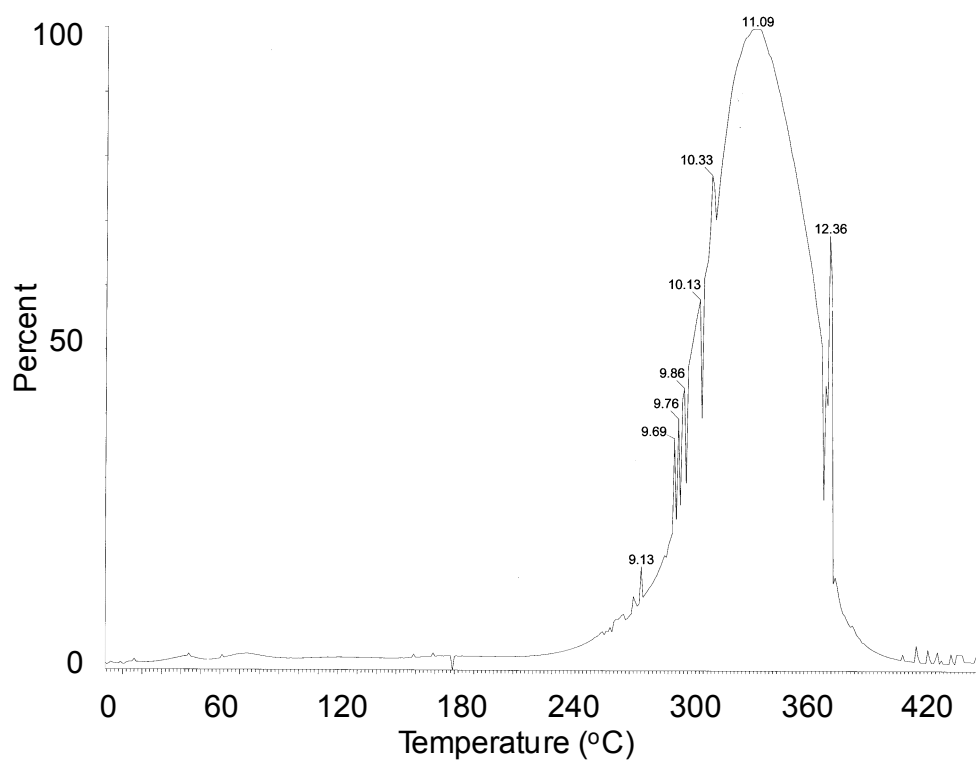


Figure C.12: GC of CS(10-90)

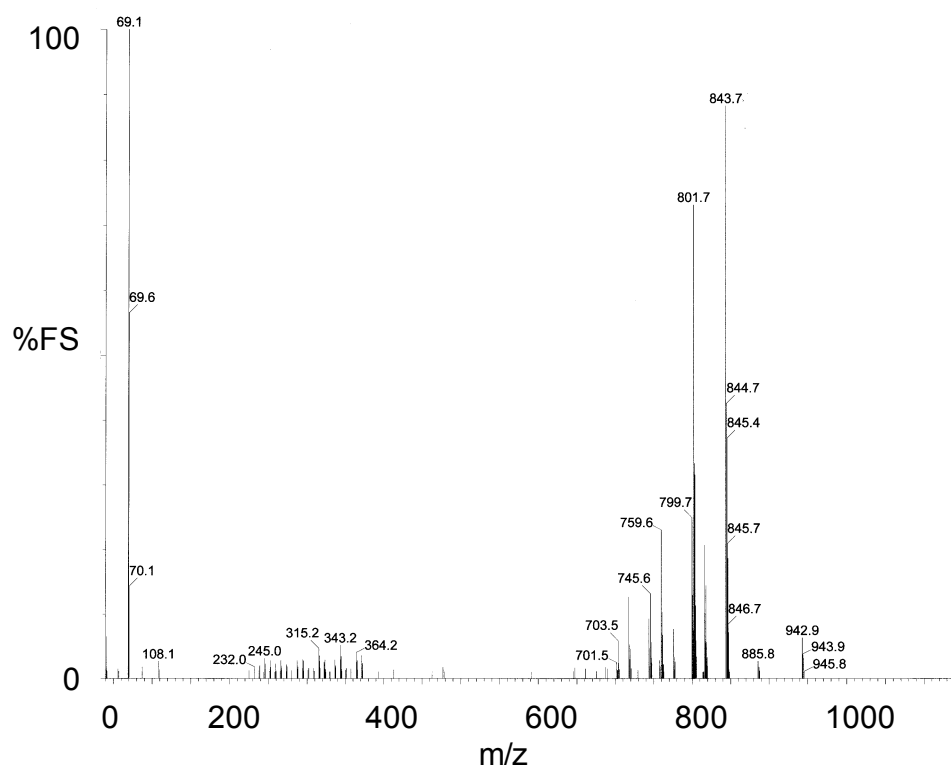


Figure C.13: MS of CS(10-90) at T = 337 °C

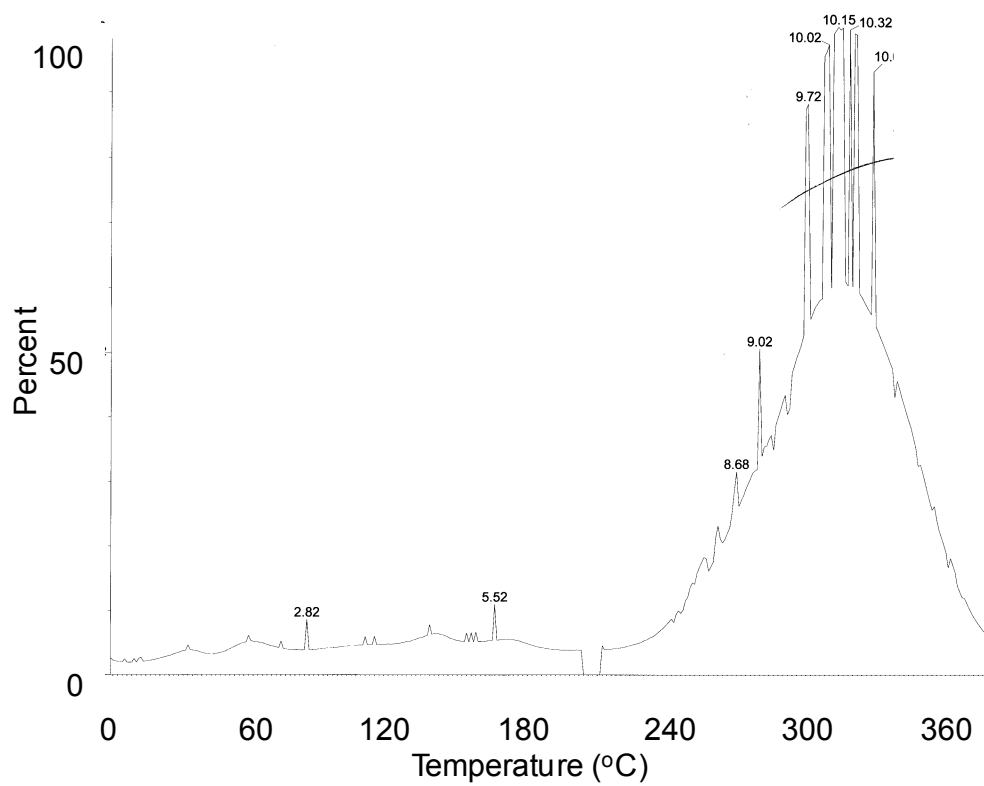


Figure C.14: GC of CS(20-80)

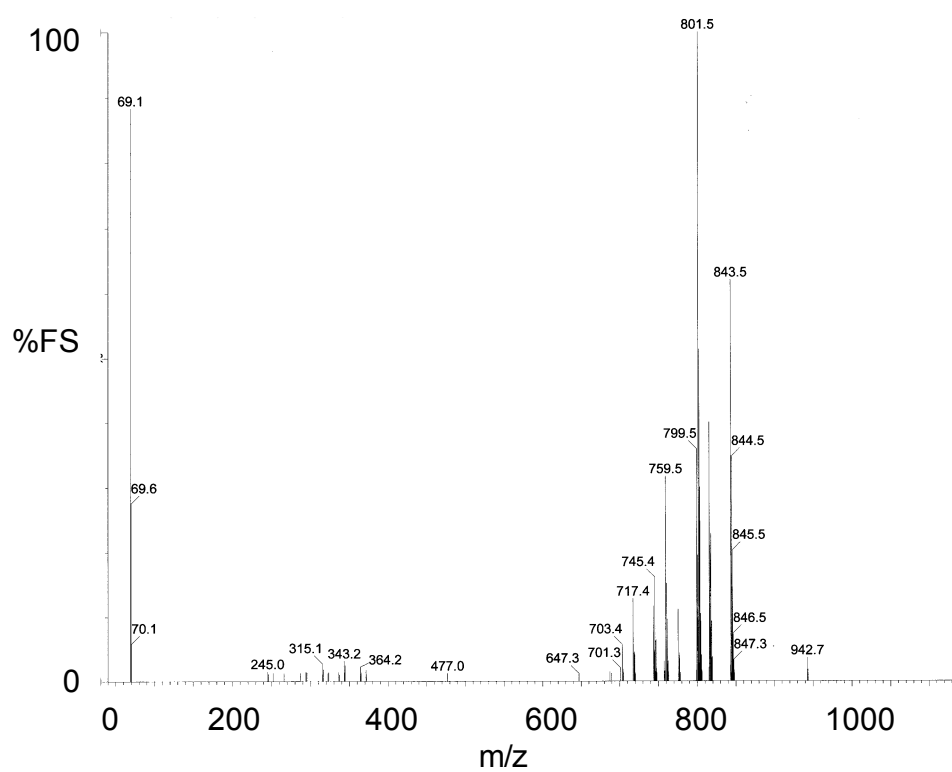


Figure C.15: MS of CS(20-80) at T = 349 °C

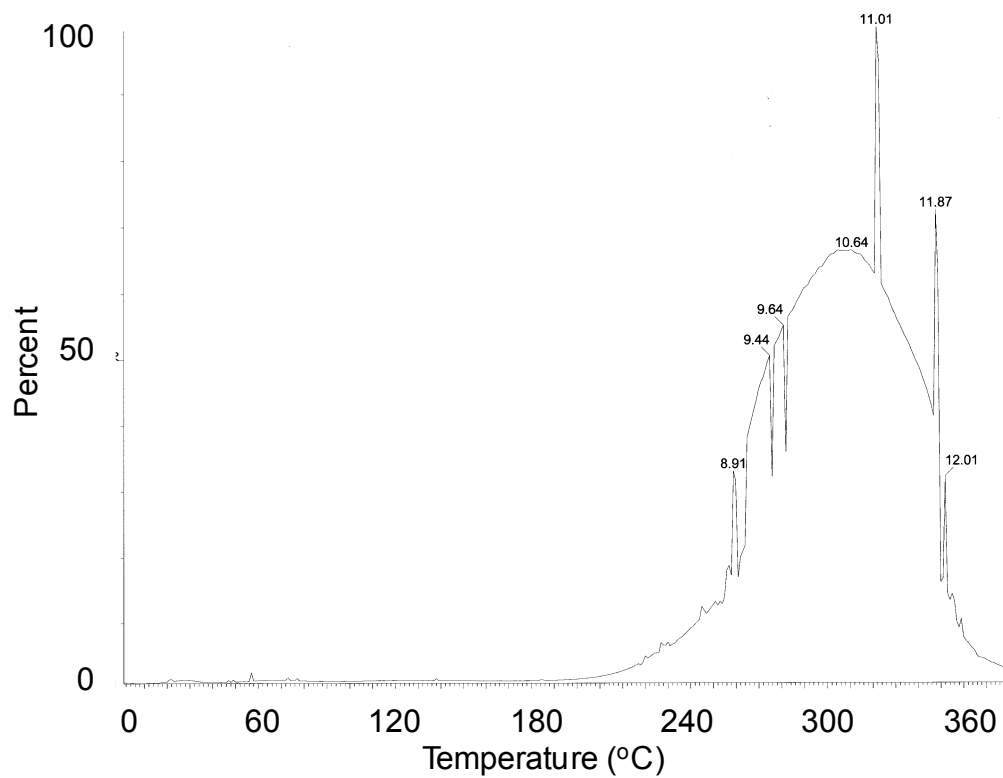


Figure C.16: GC of CS(33-67)

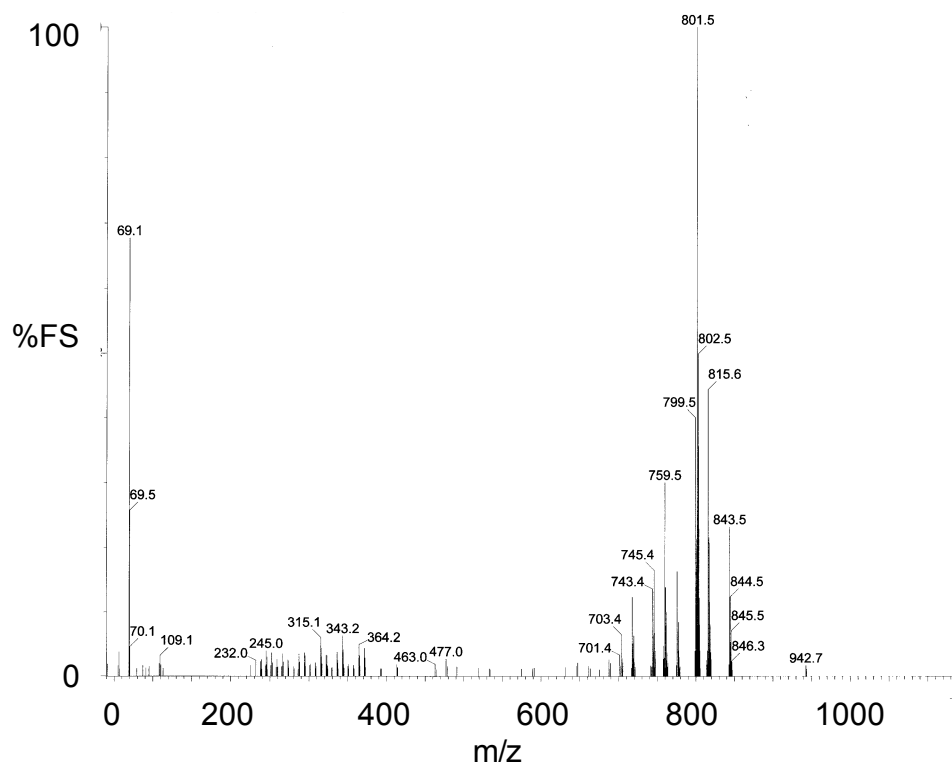


Figure C.17: MS of CS(33-67) at T = 367 °C

Appendix D: Gel Permeation Chromatography (GPC) Curves

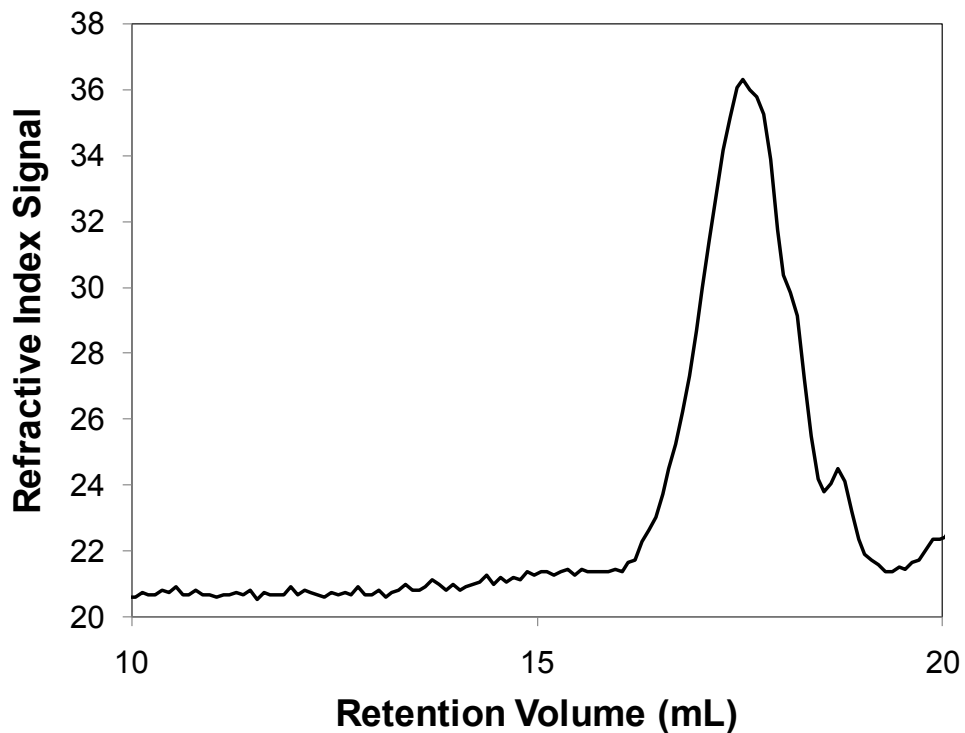


Figure D.1: P2a

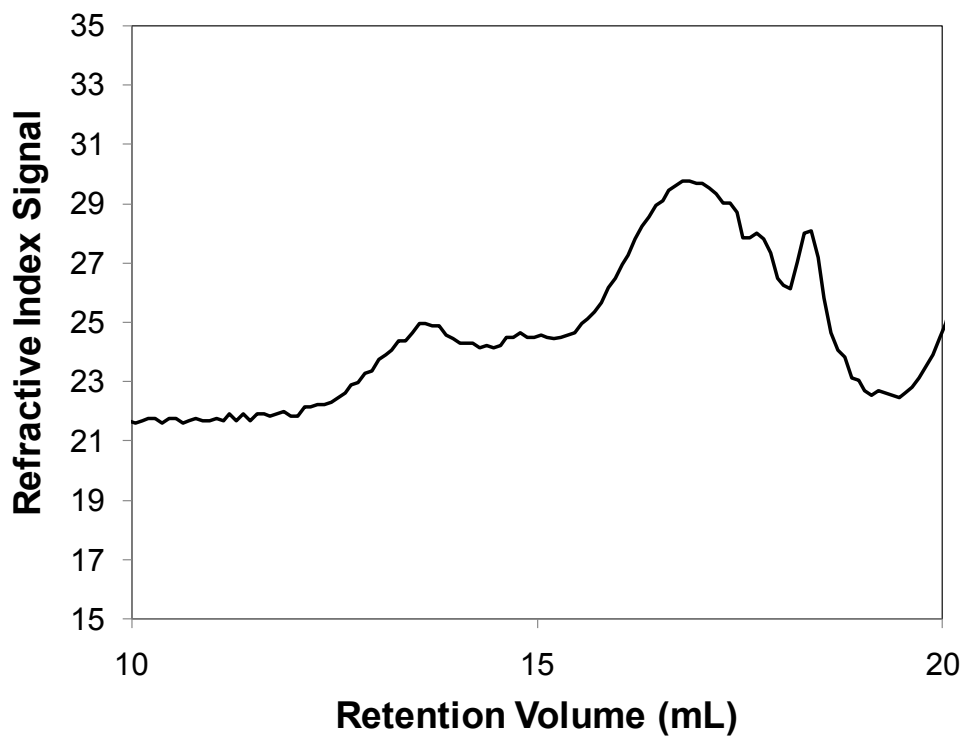


Figure D.2: P2b

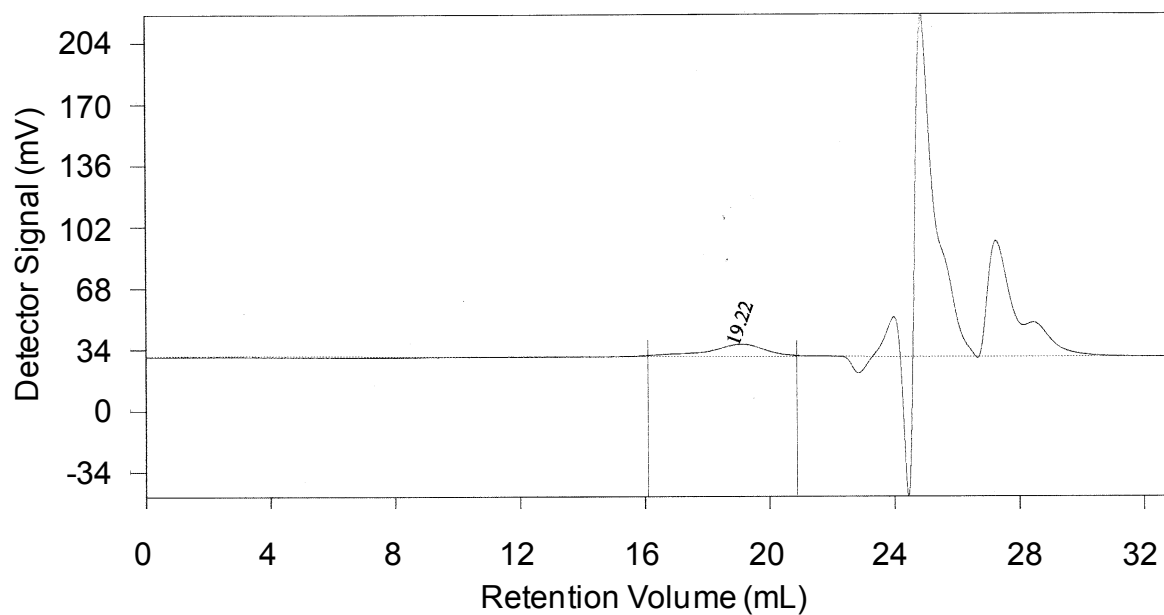


Figure D.3: P2c

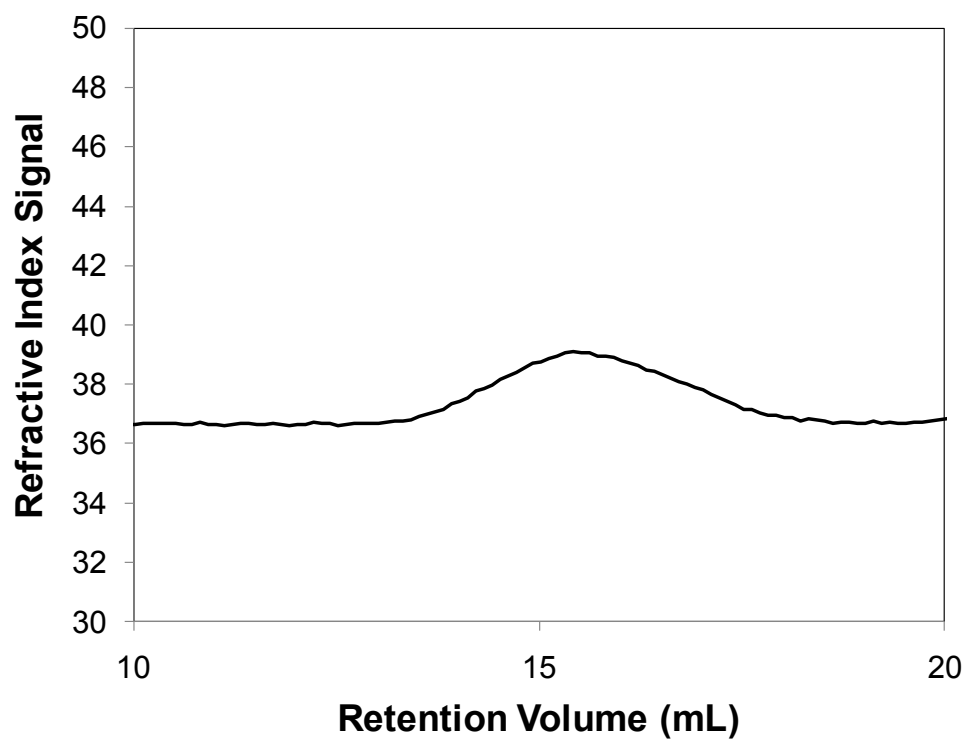


Figure D.4: emA

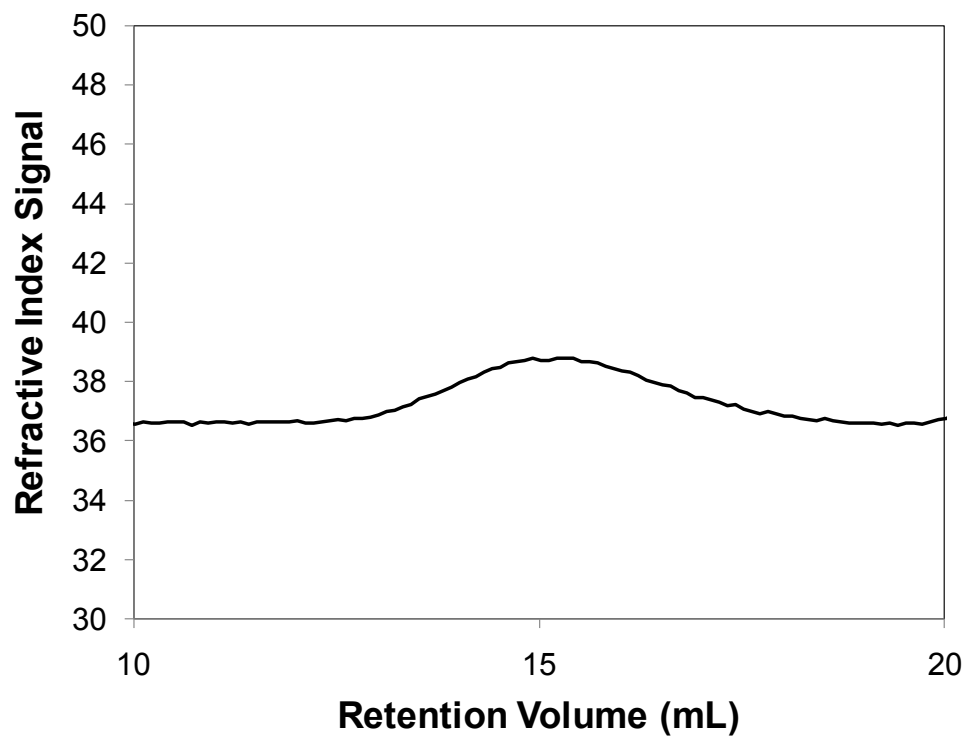


Figure D.5: emB

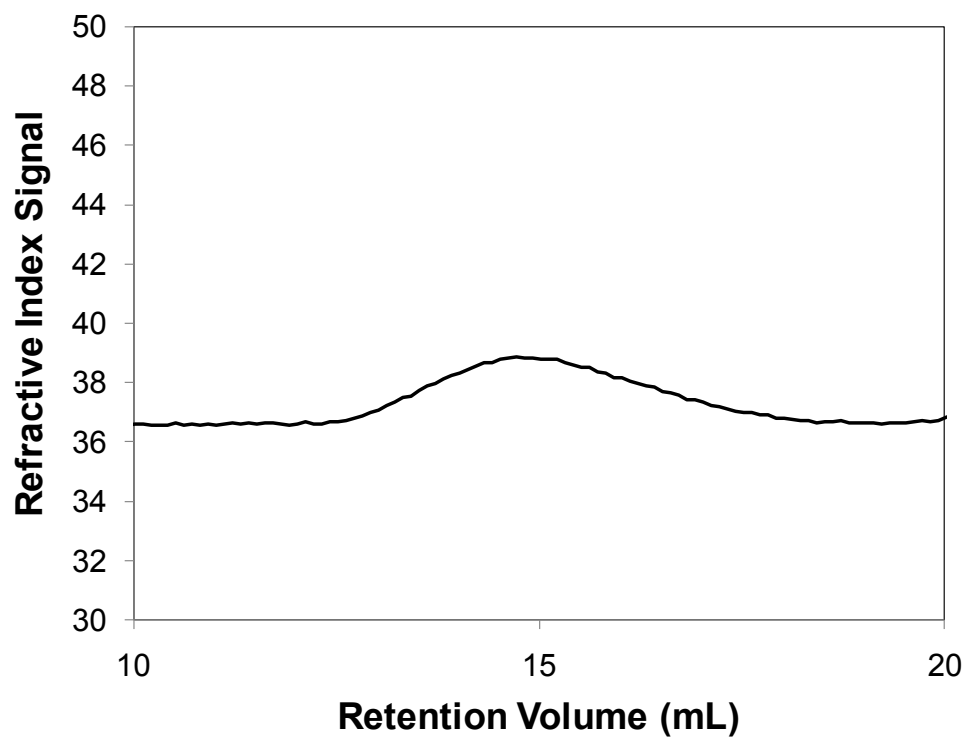


Figure D.6: emC

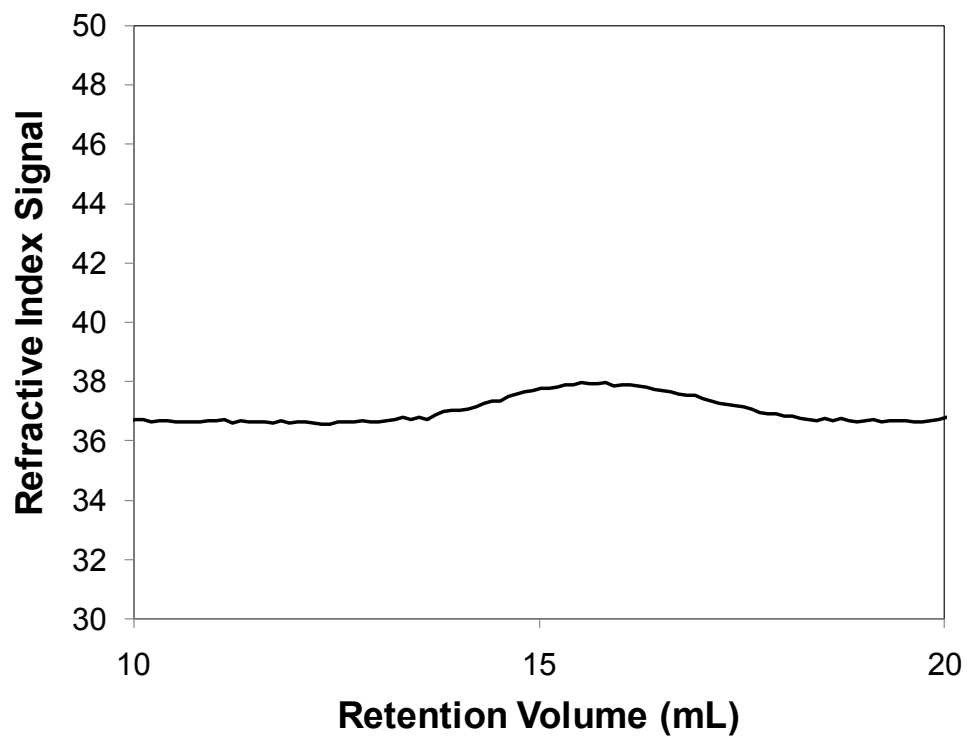


Figure D.7: emD

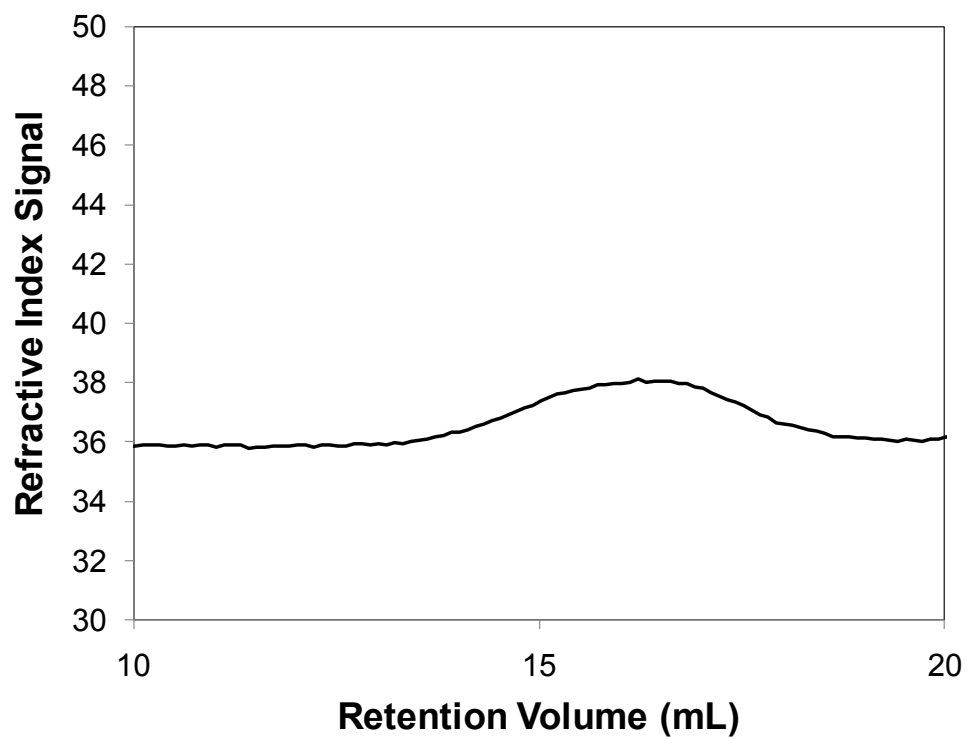


Figure D.8: scA

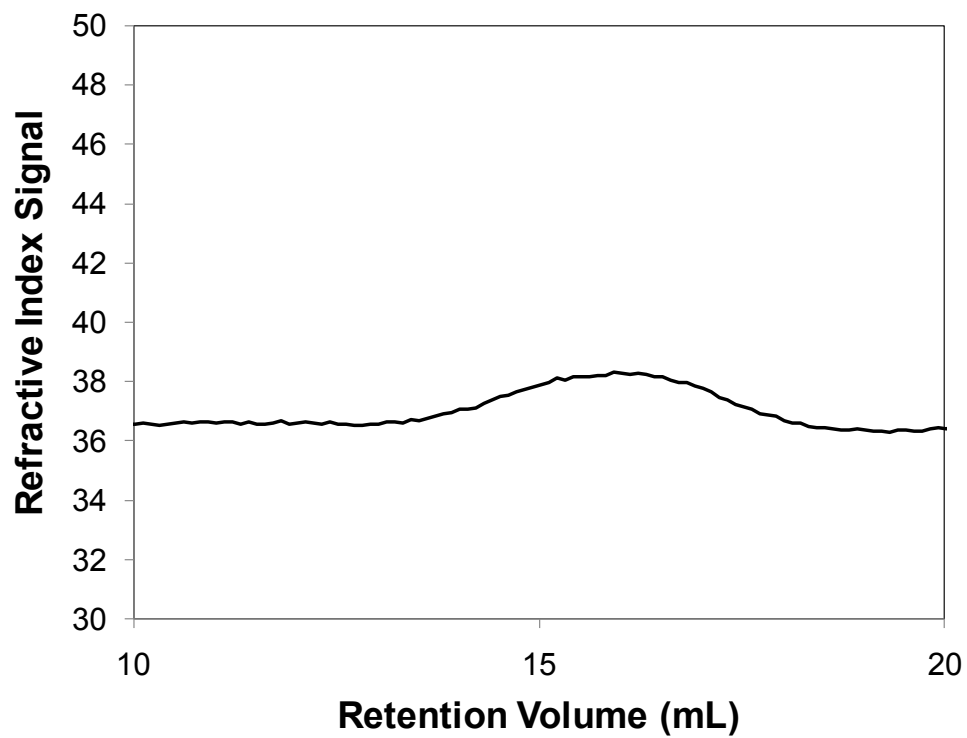


Figure D.9: scB

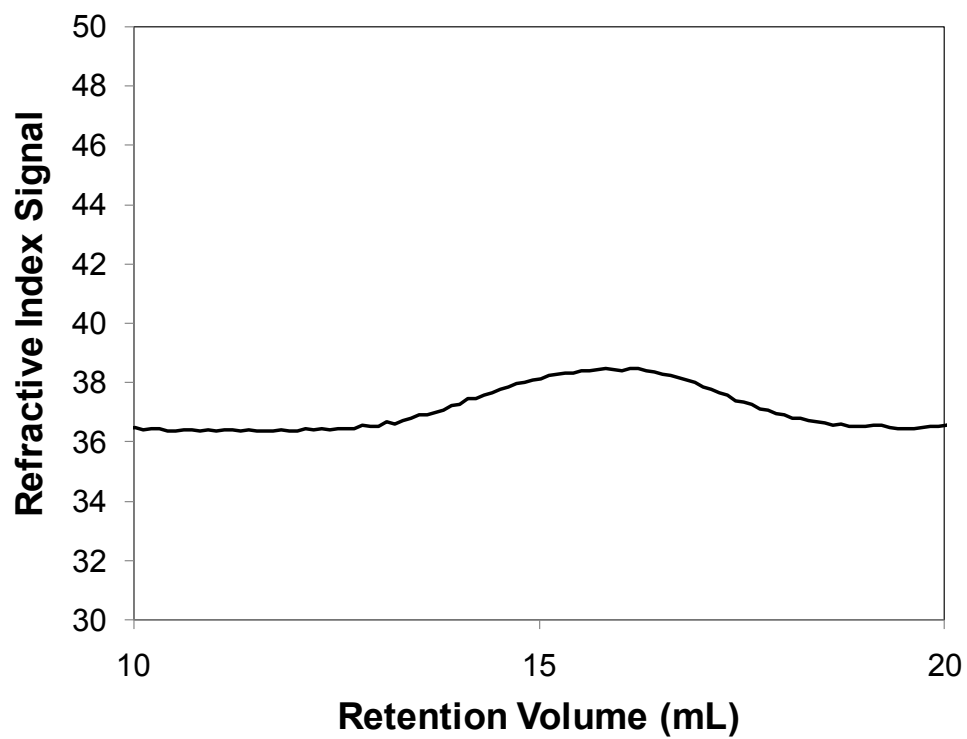


Figure D.10: scC

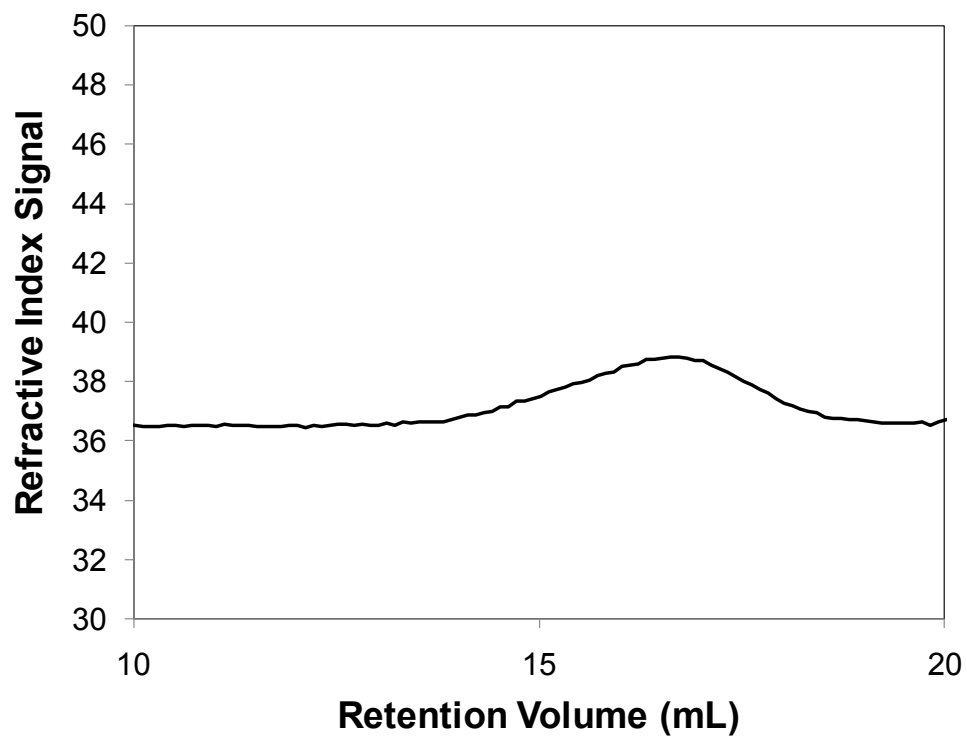


Figure D.11: scD

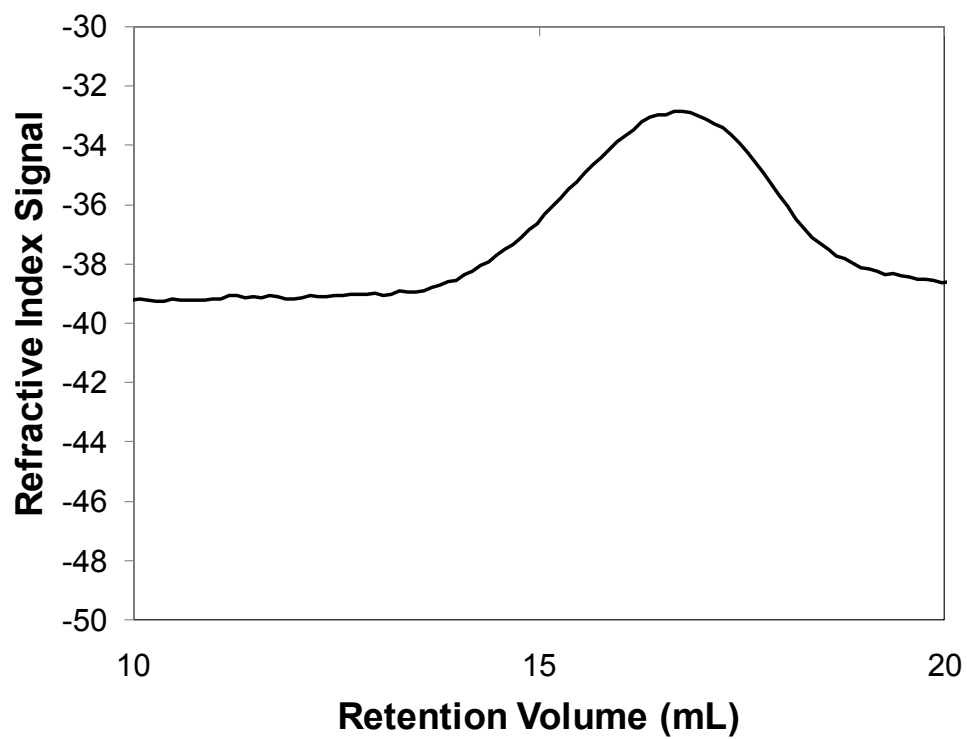


Figure D.12: S(100)

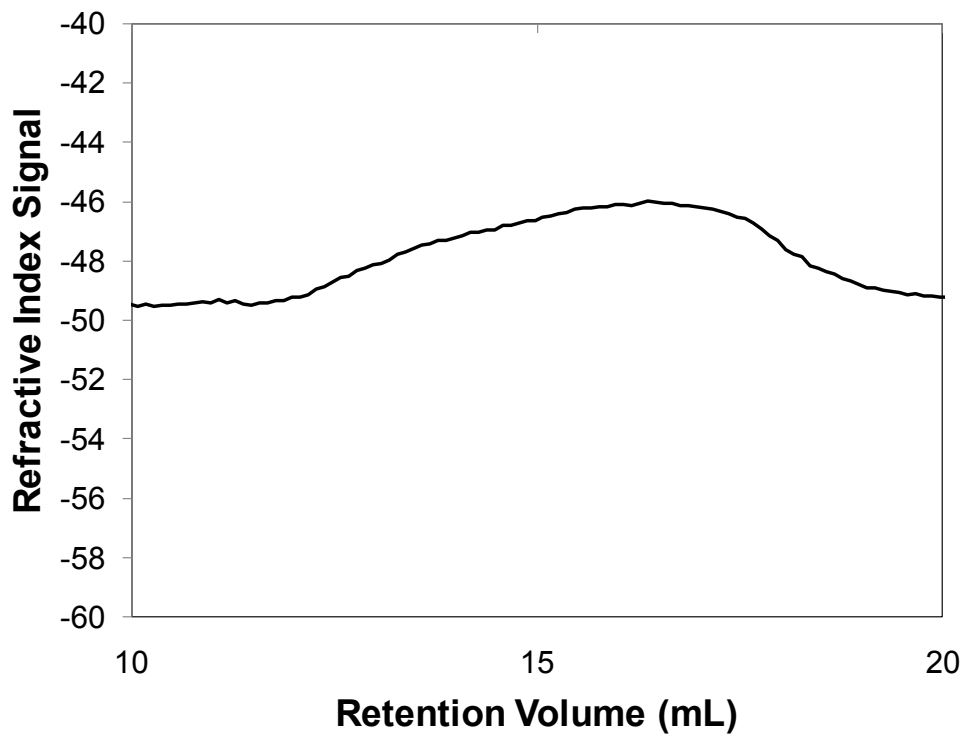


Figure D.13: CS(02-98)

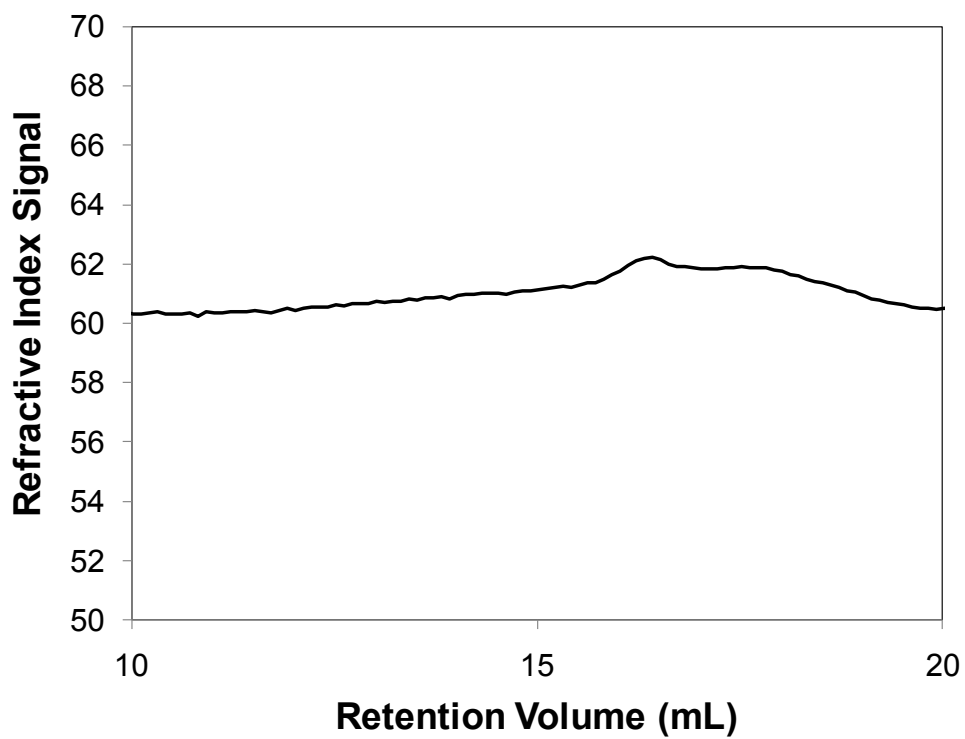


Figure D.14: CS(10-90)

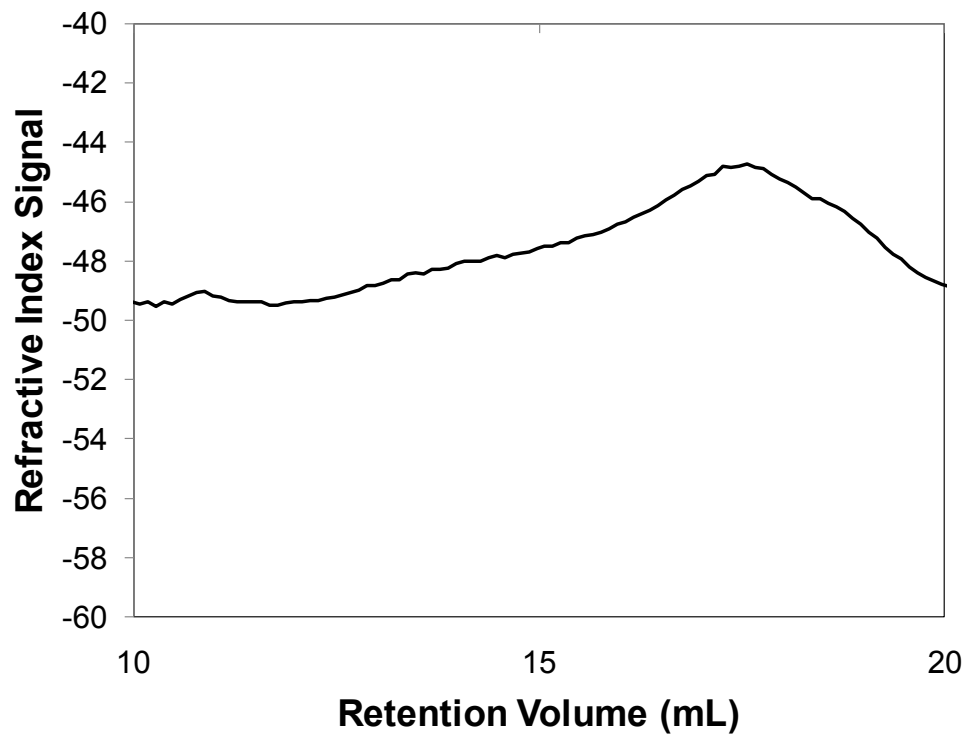


Figure D.15: CS(20-80)

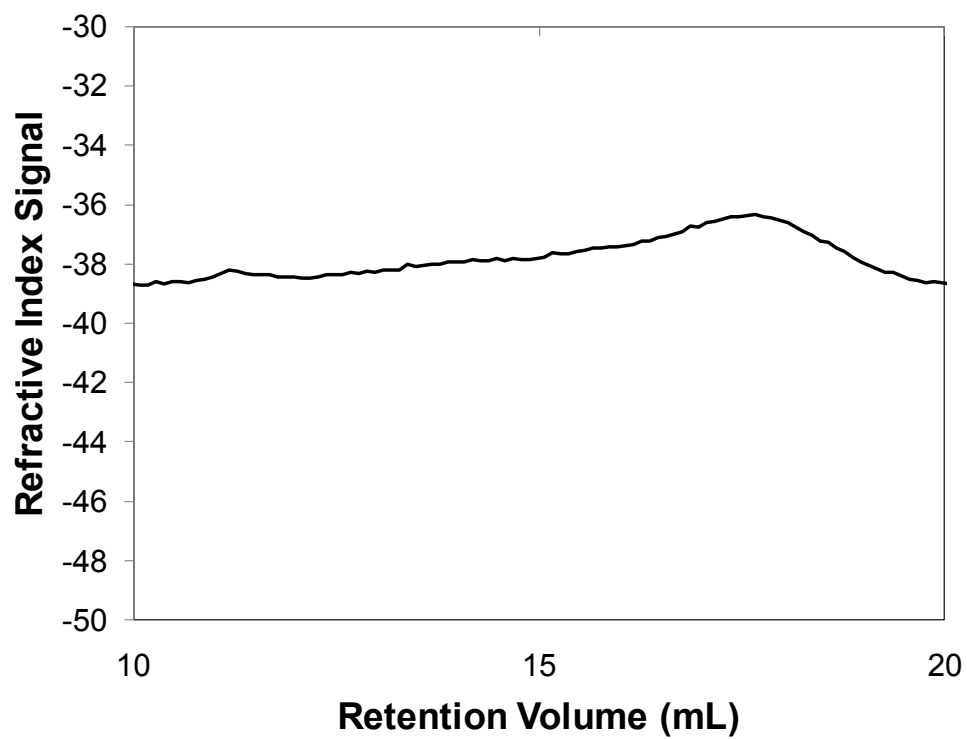


Figure D.16: CS(33-67)

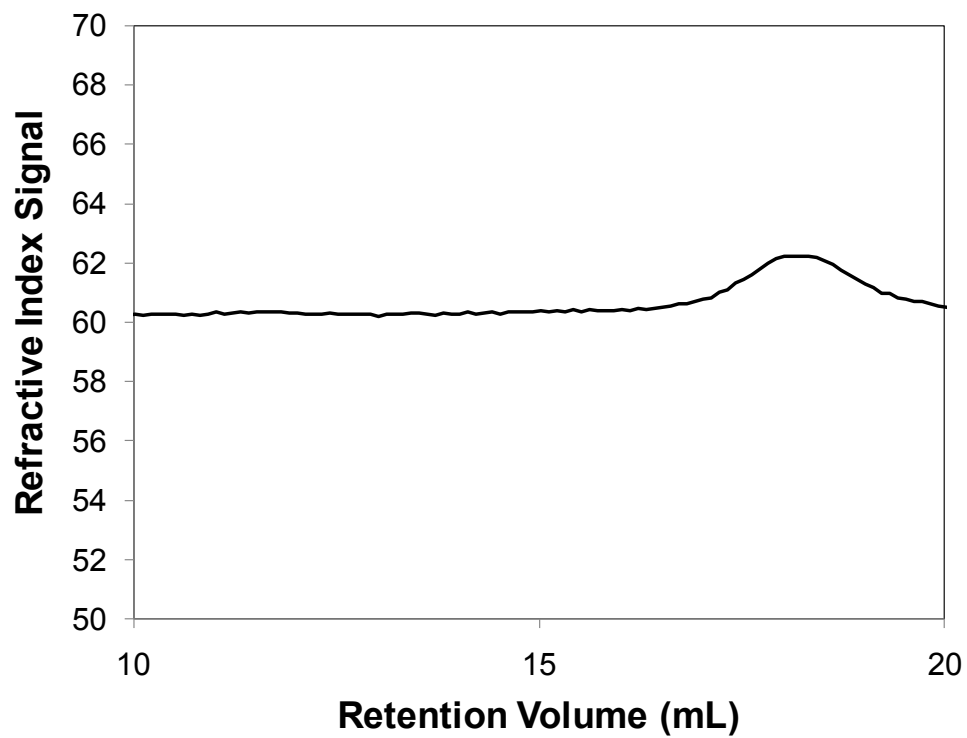


Figure D.17: CS(81-19)

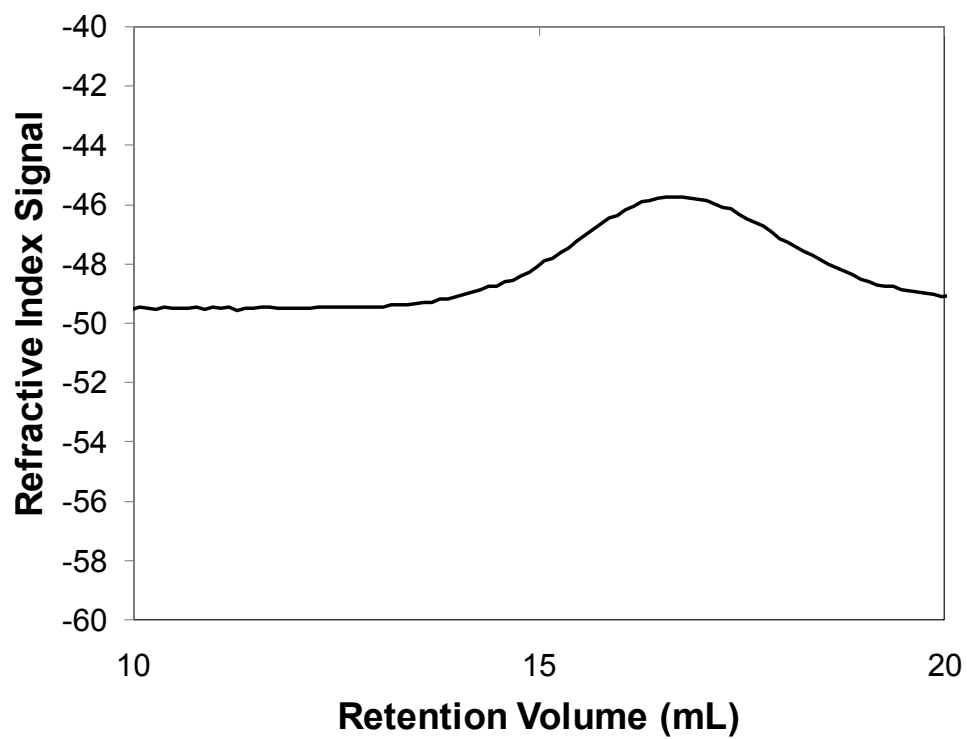


Figure D.18: CVS(40-59-01)

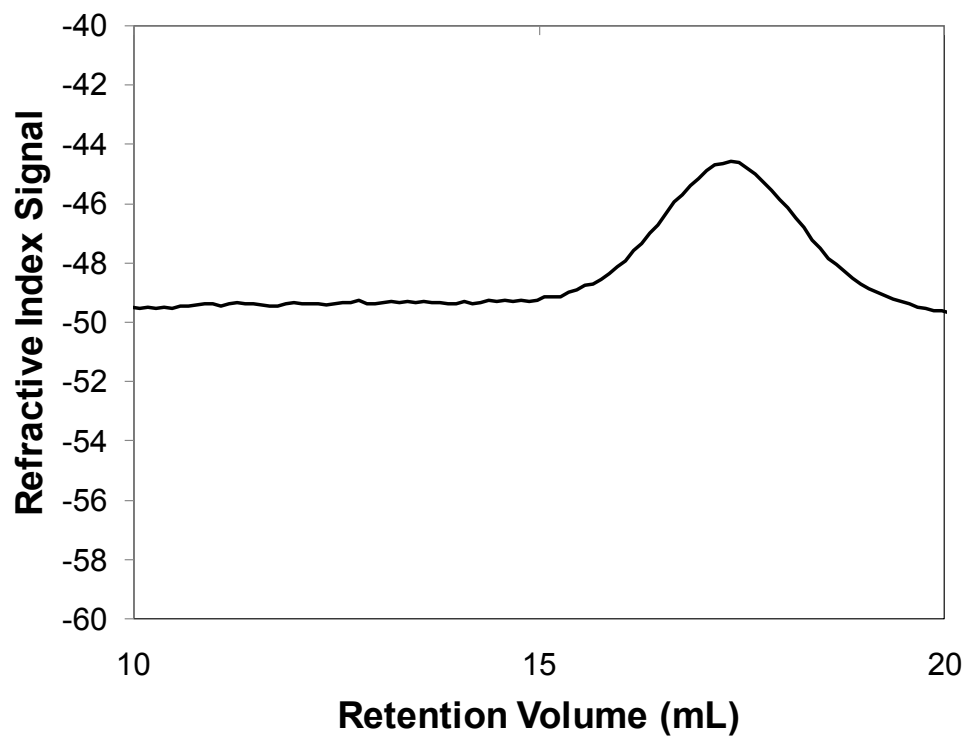


Figure D.19: CVS(46-52-02)

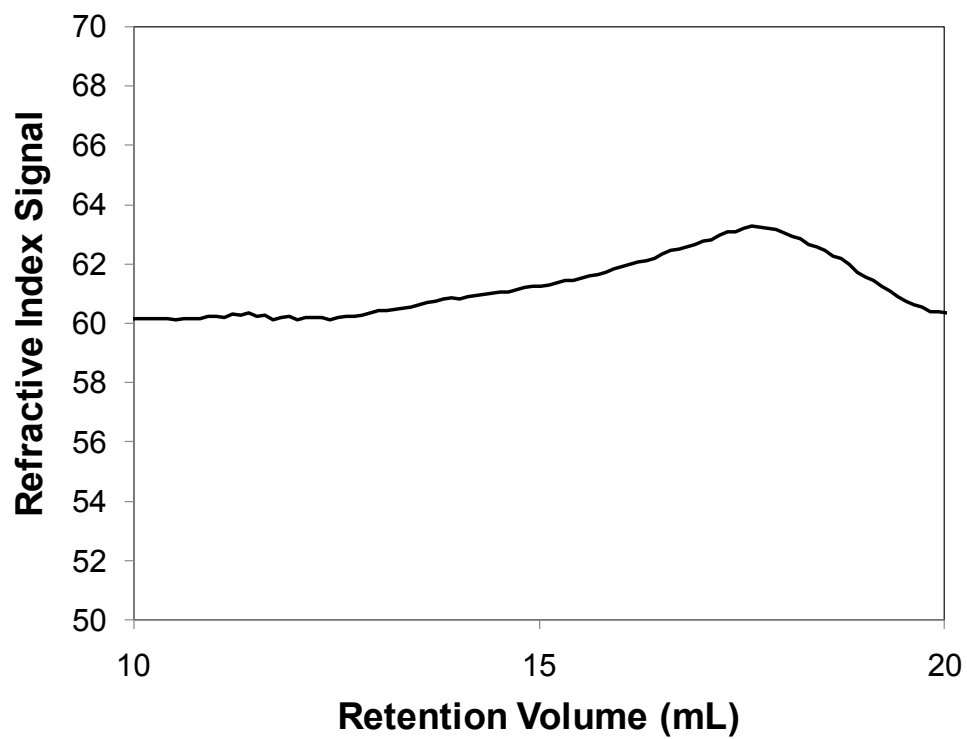


Figure D.20: CS(50-50), Reaction Time = 0 h

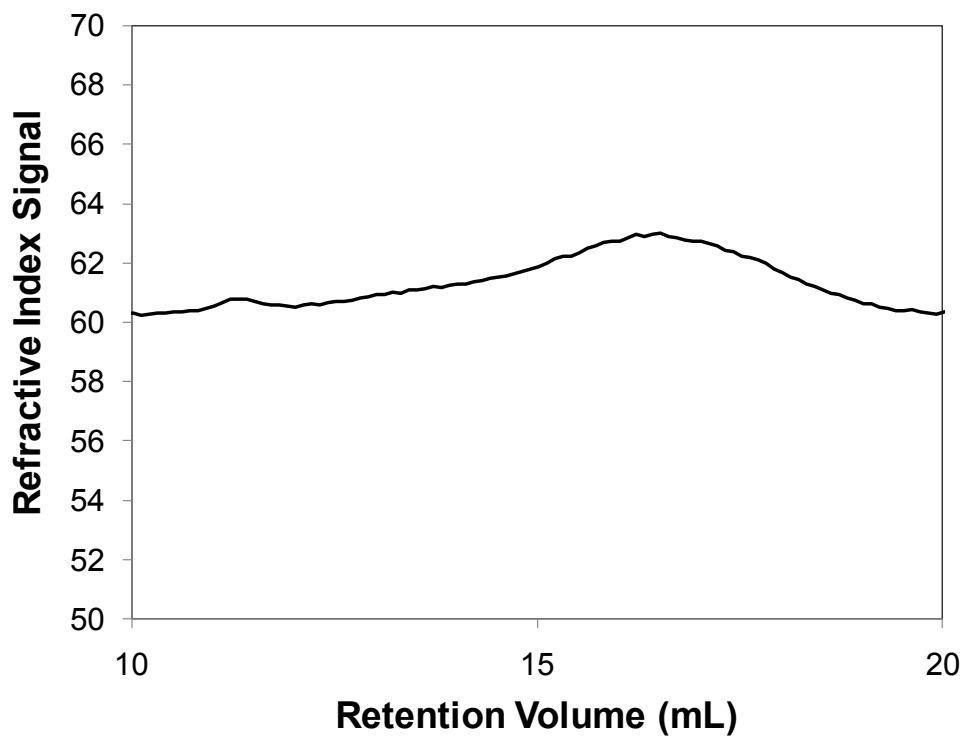


Figure D.21: CS(50-50), Reaction Time = 3 h

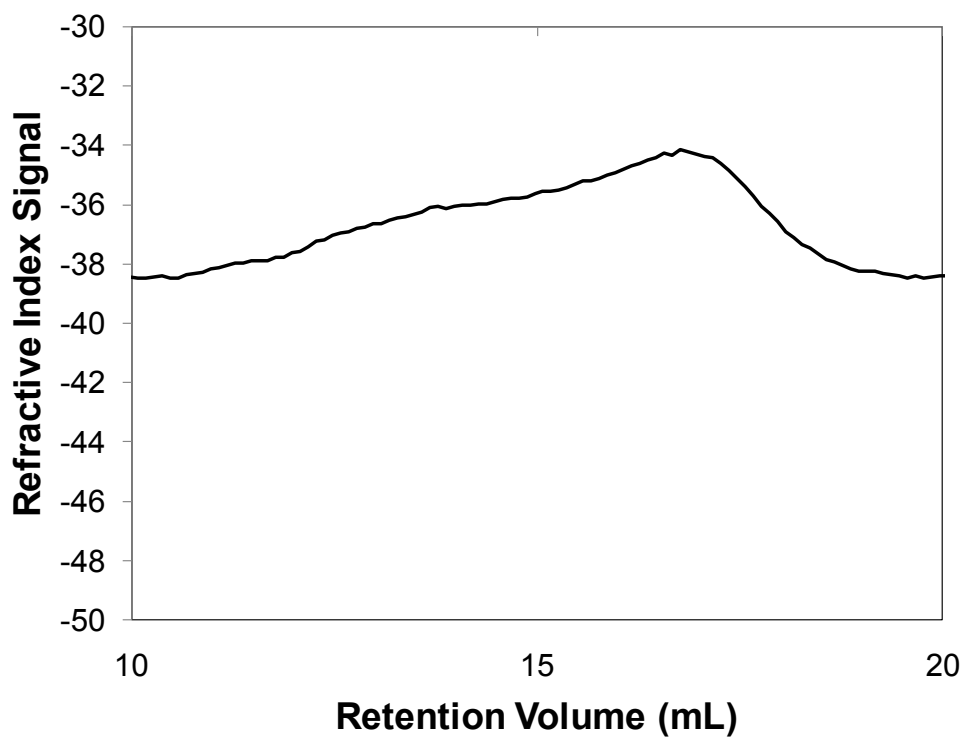


Figure D.22: CS(50-50), Reaction Time = 8 h

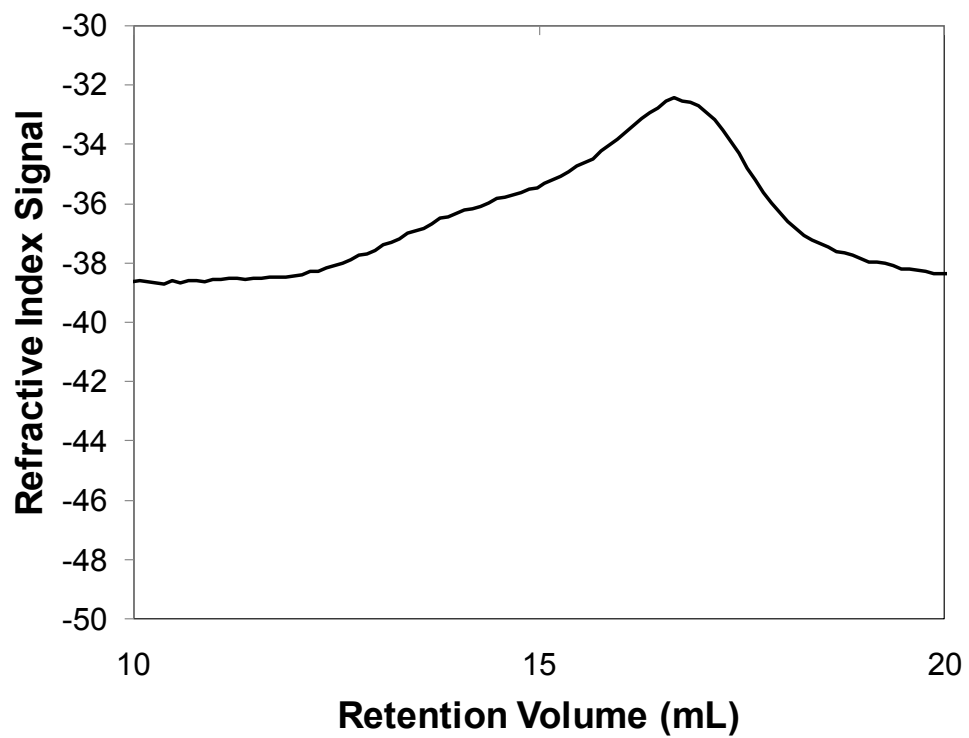


Figure D.23: CS(50-50), Reaction Time = 24 h

Appendix E: Differential Scanning Calorimetry (DSC) Traces

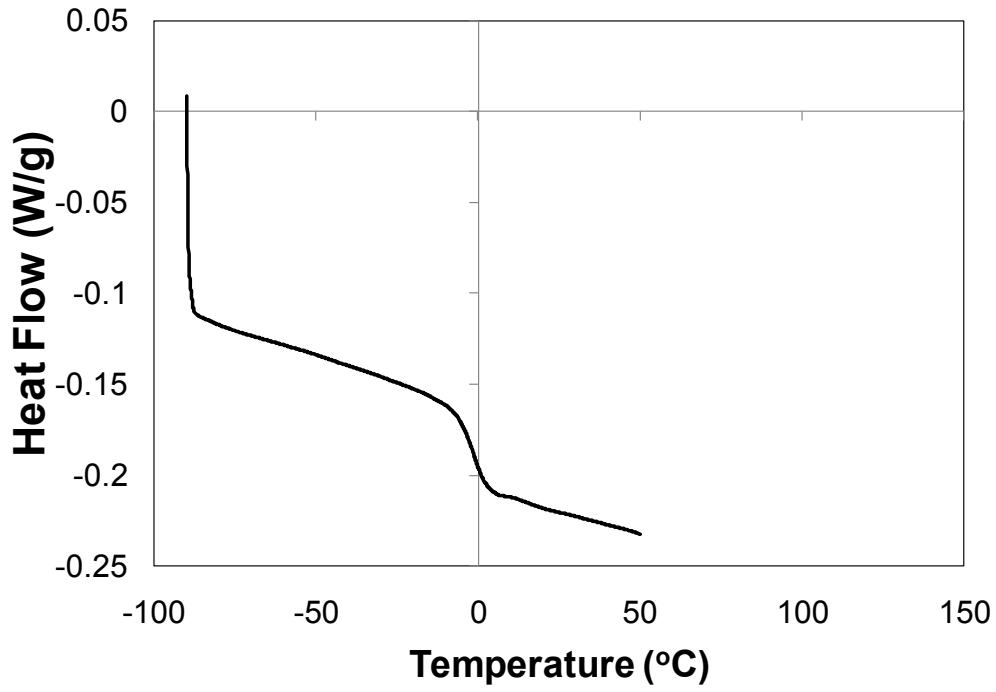


Figure E.1: P2a

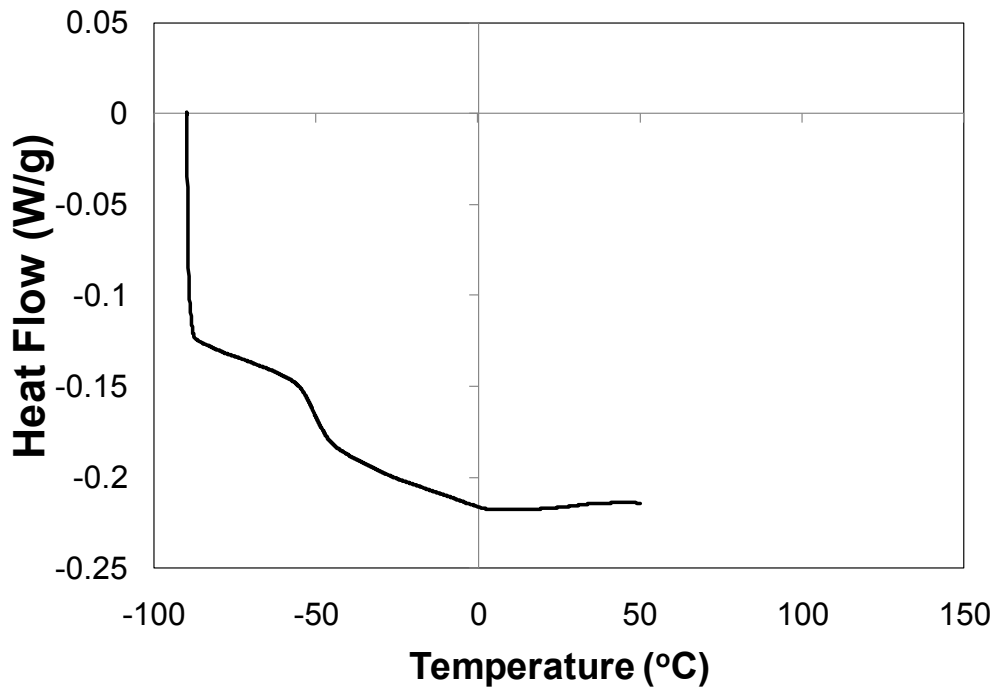


Figure E.2: P2b

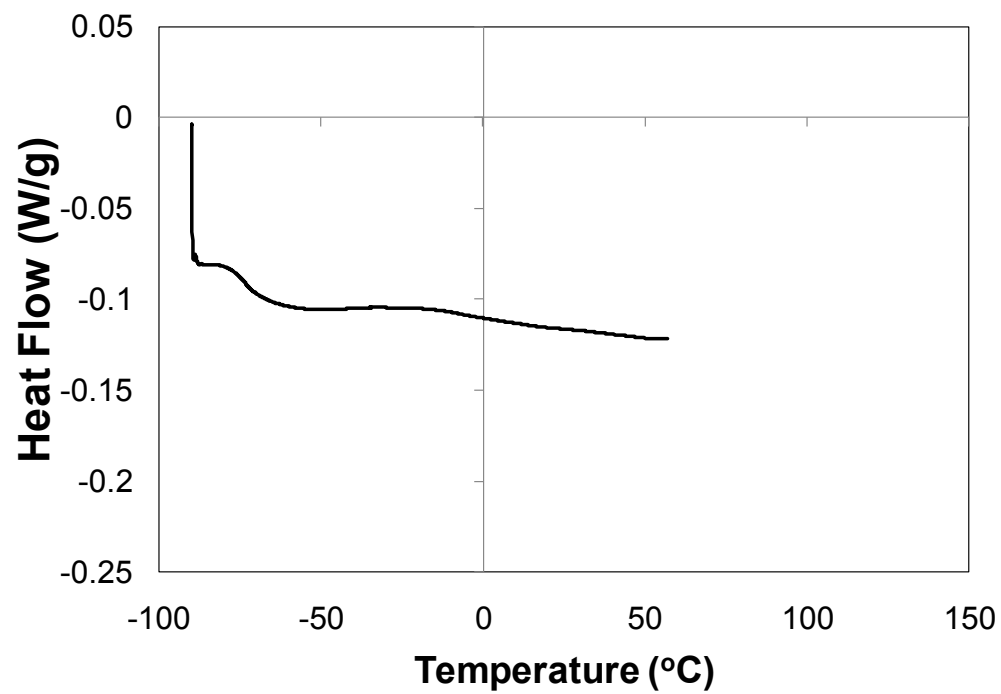


Figure E.3: P2c

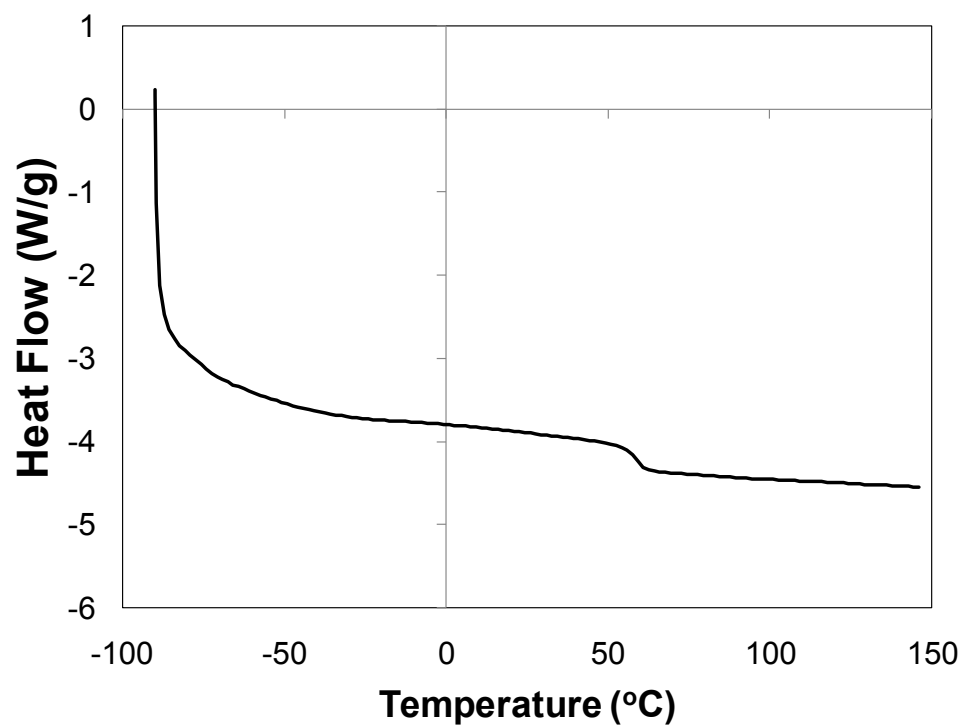


Figure E.4: emD

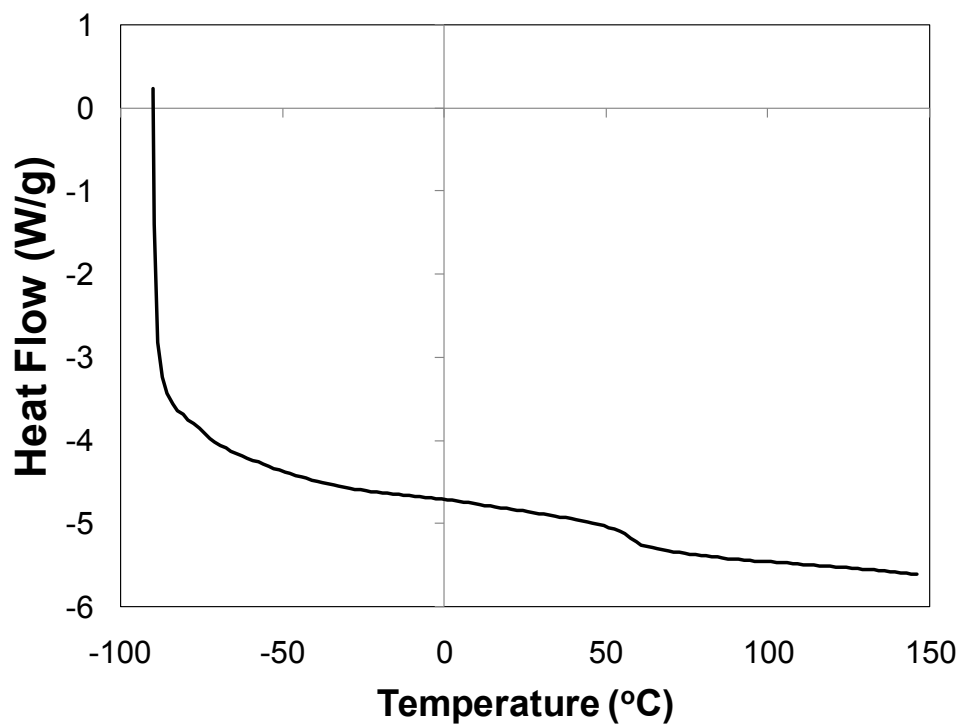


Figure E.5: scD

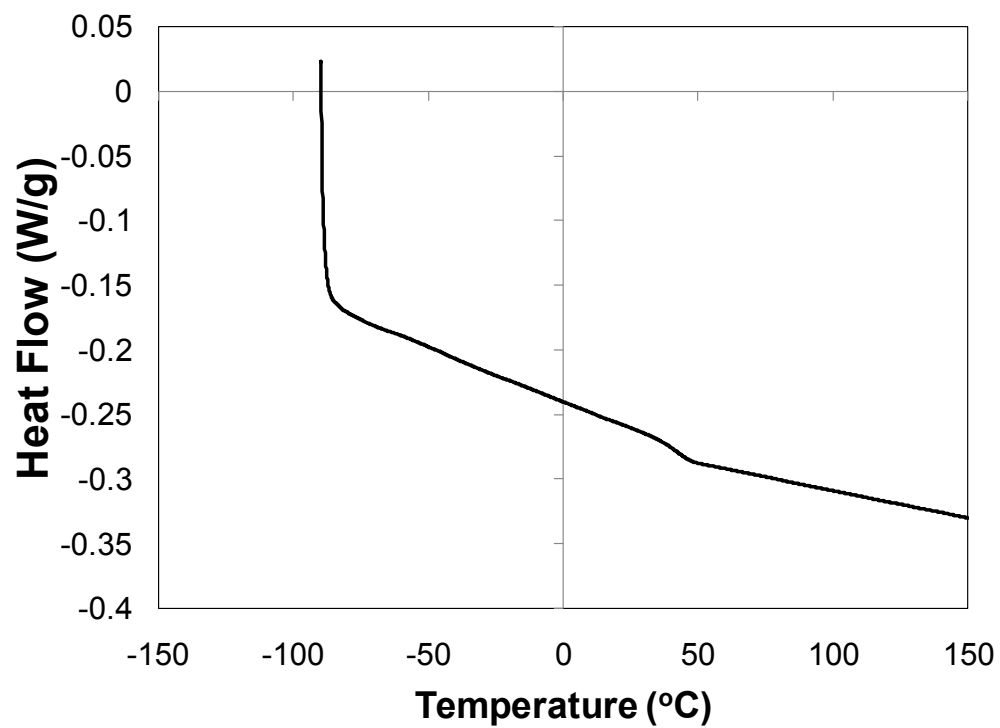


Figure E.6: S(100)

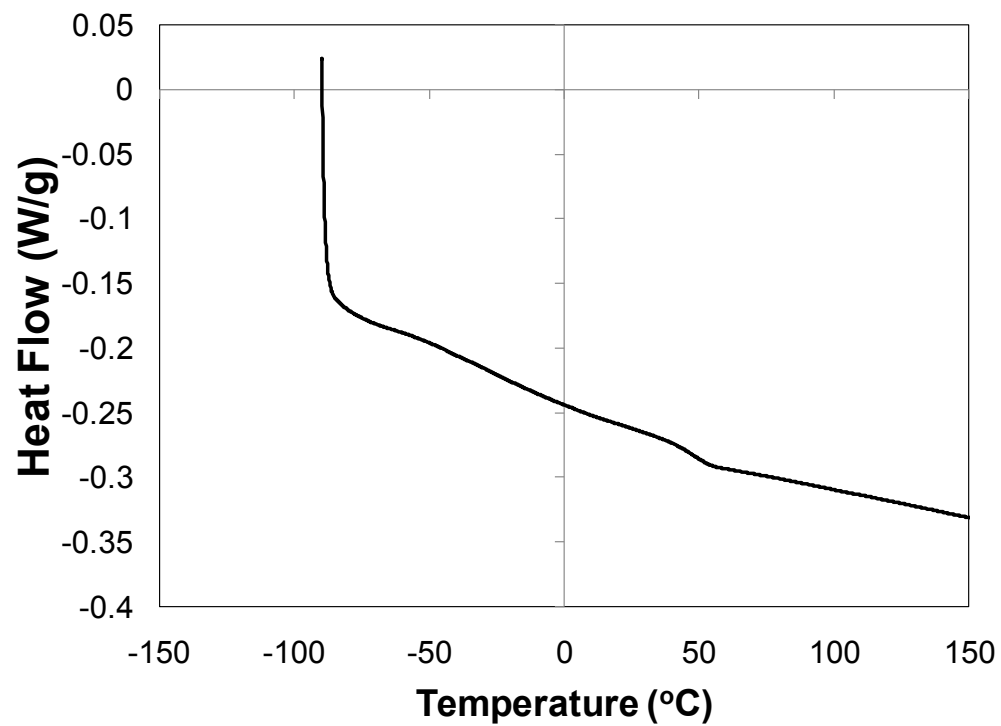


Figure E.7: CS(02-98)

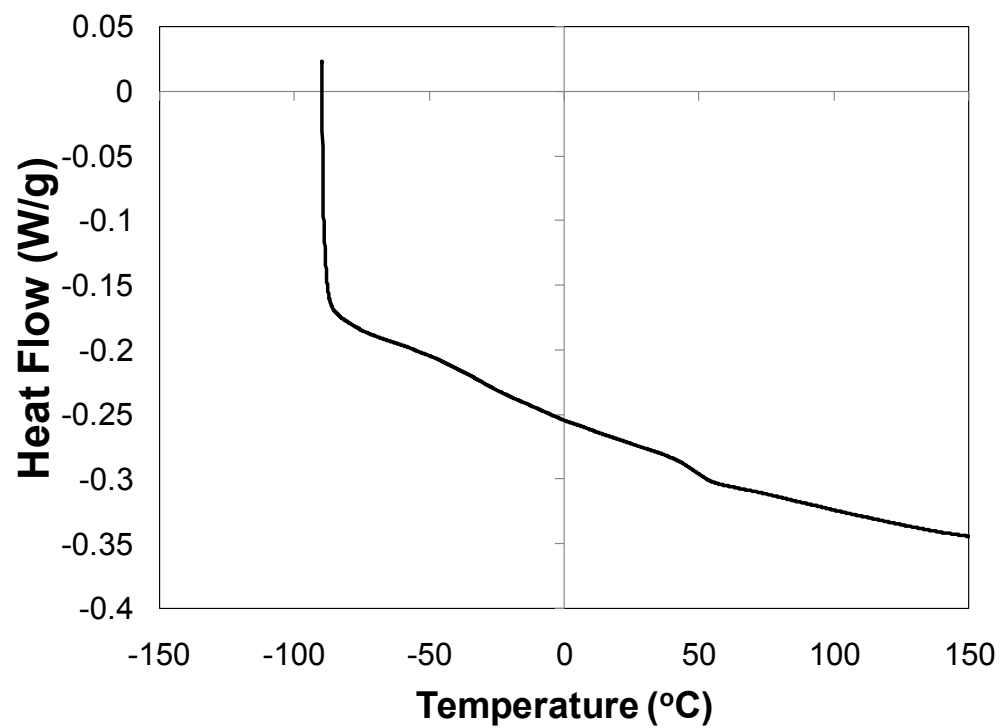


Figure E.8: CS(10-90)

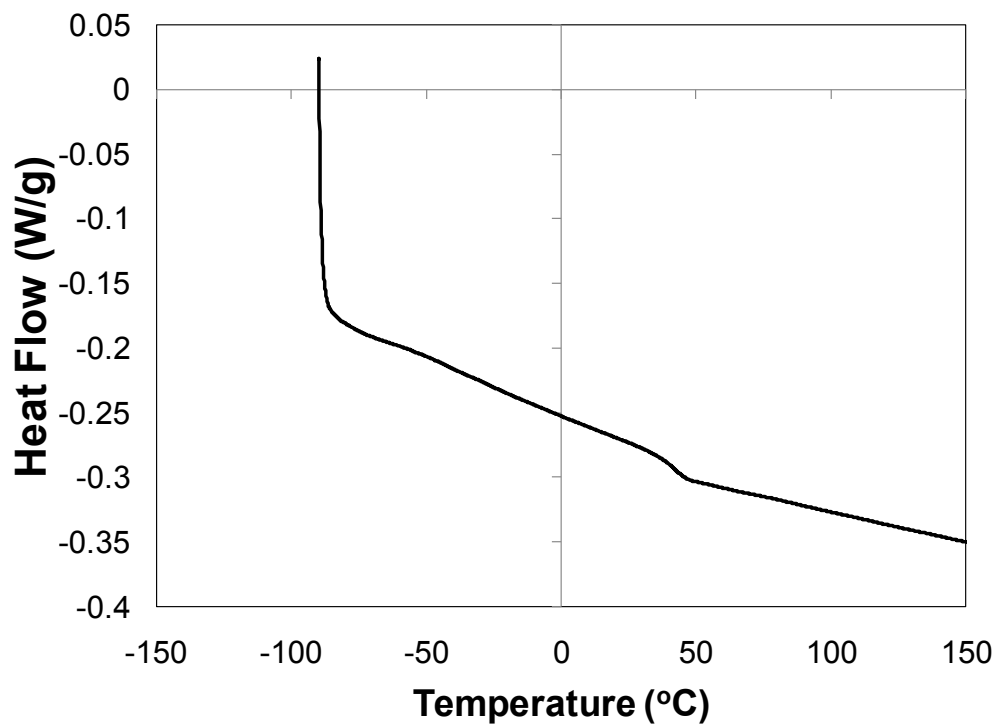


Figure E.9: CS(20-80)

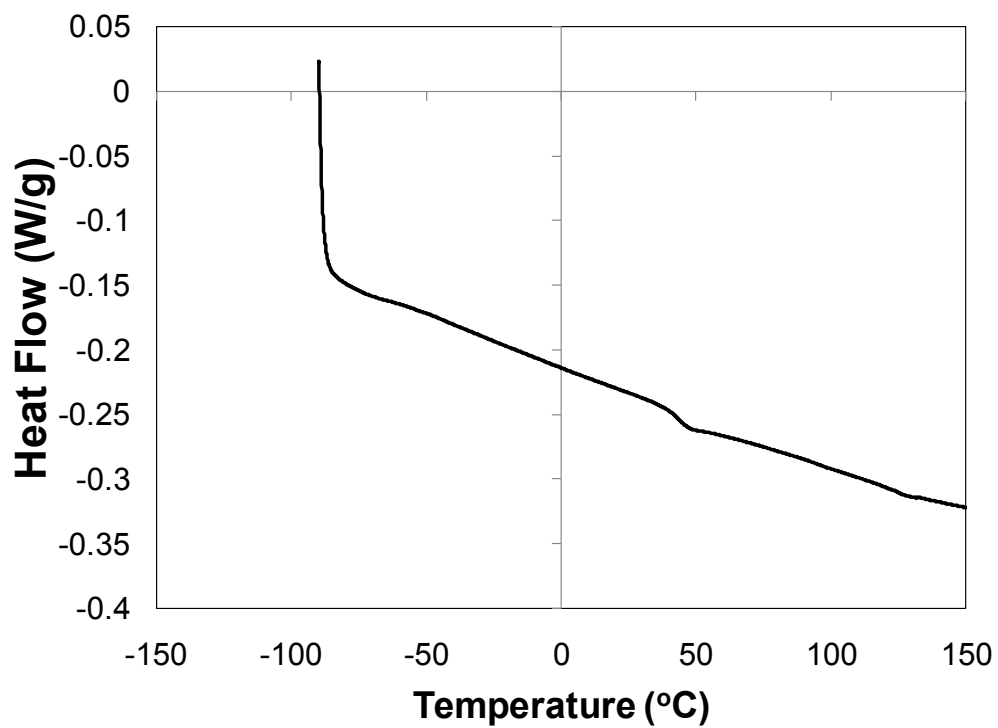


Figure E.10: CS(33-67)

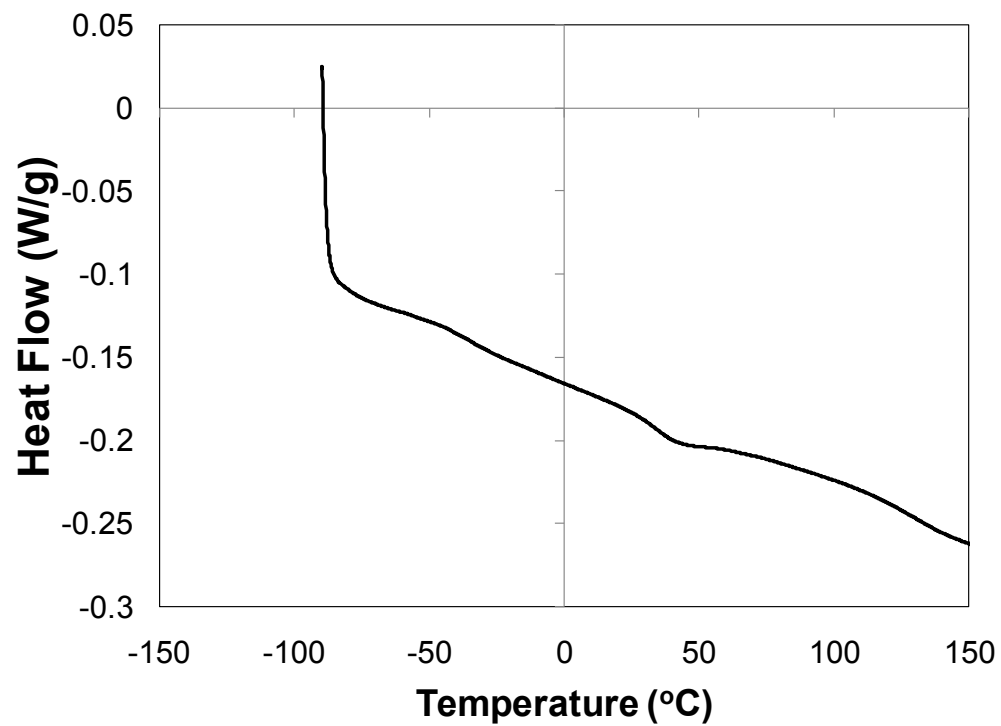


Figure E.11: CS(81-19)

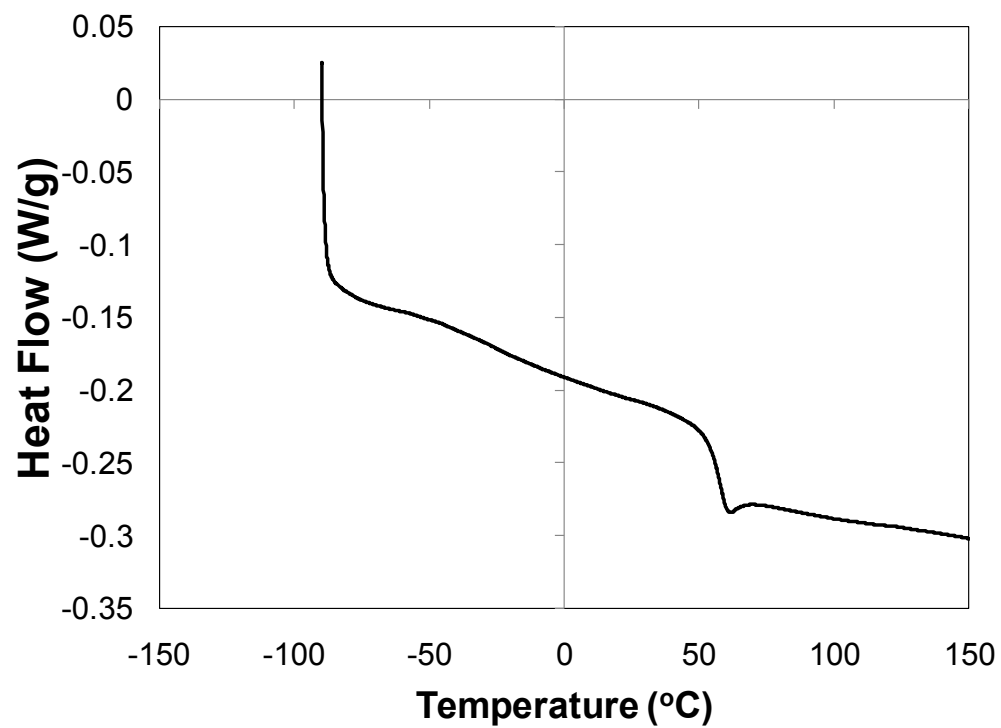


Figure E.12: CVS(40-59-01)

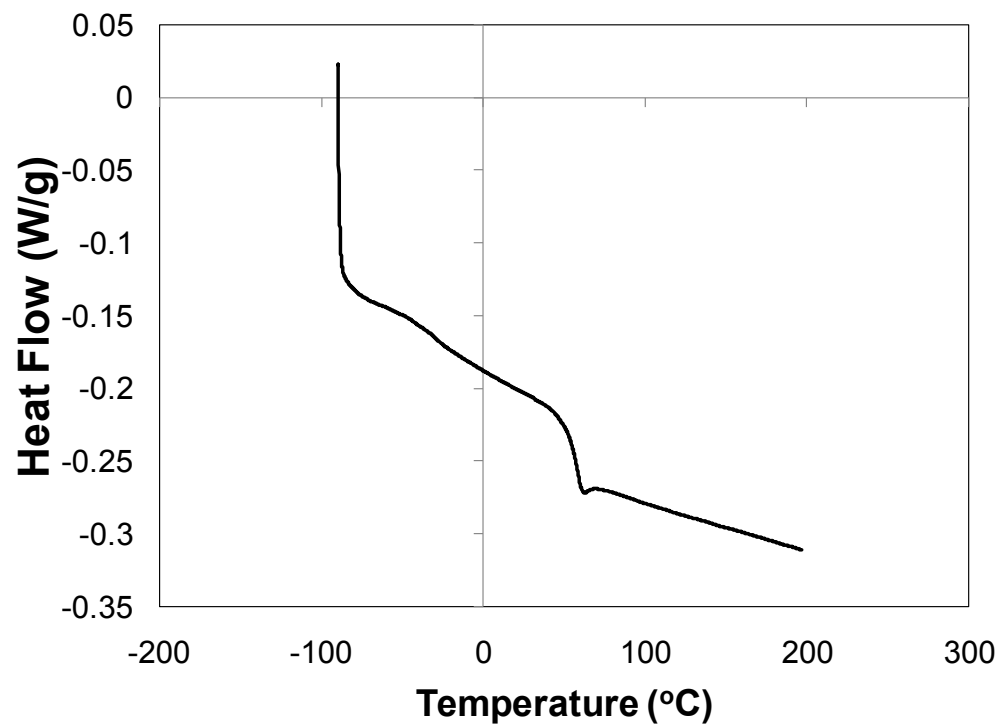


Figure E.13: CVS(46-52-02)

Appendix F: Thermal Gravimetric Analysis (TGA) Traces

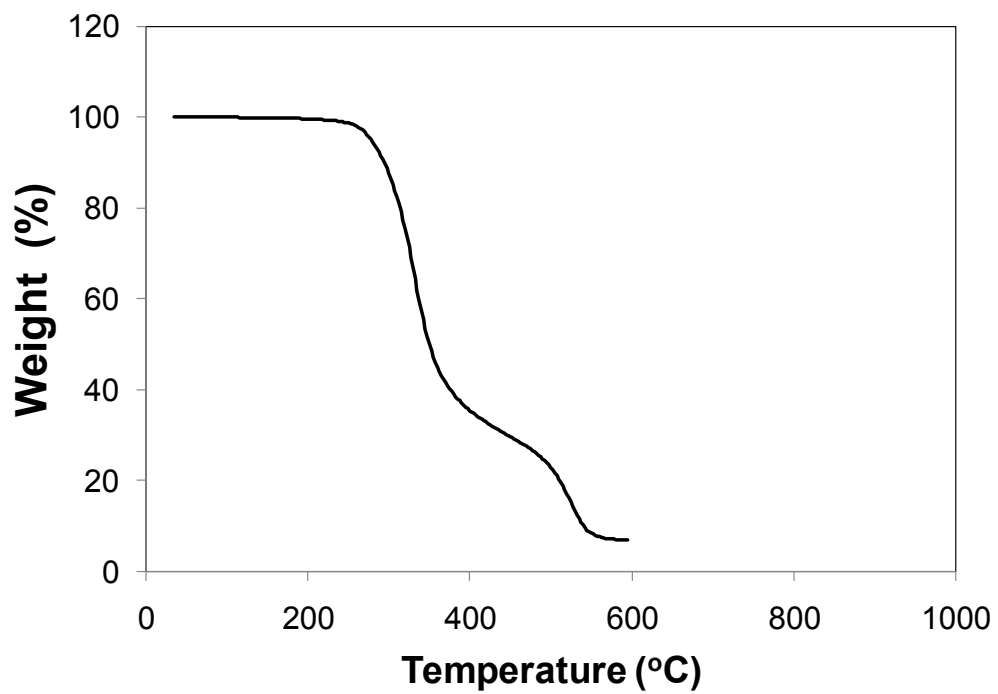


Figure F.1: P2a in air

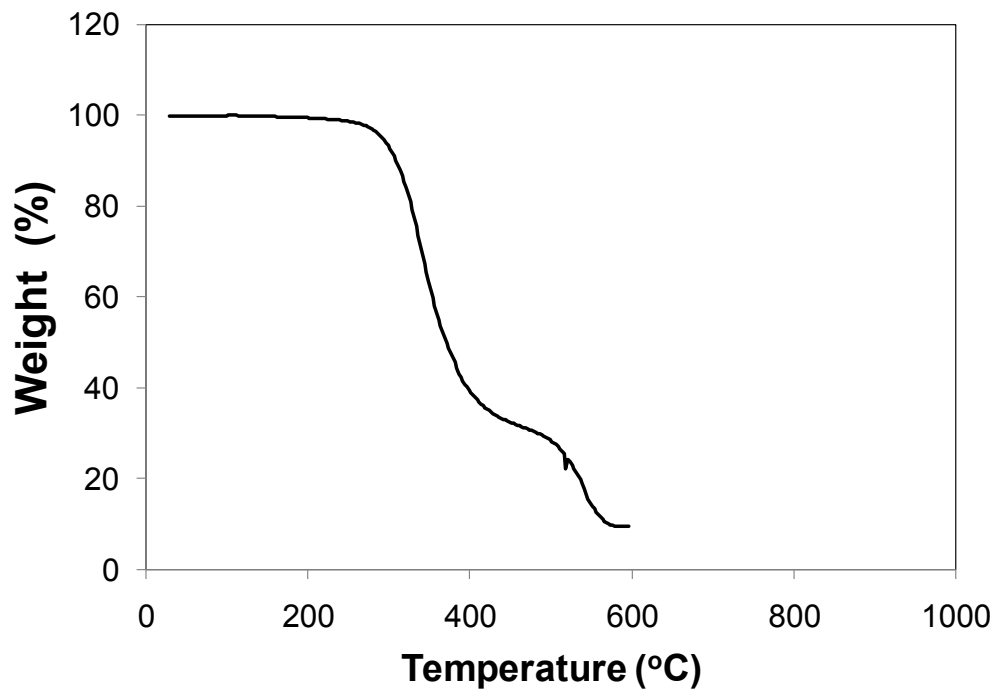


Figure F.2: P2b in air

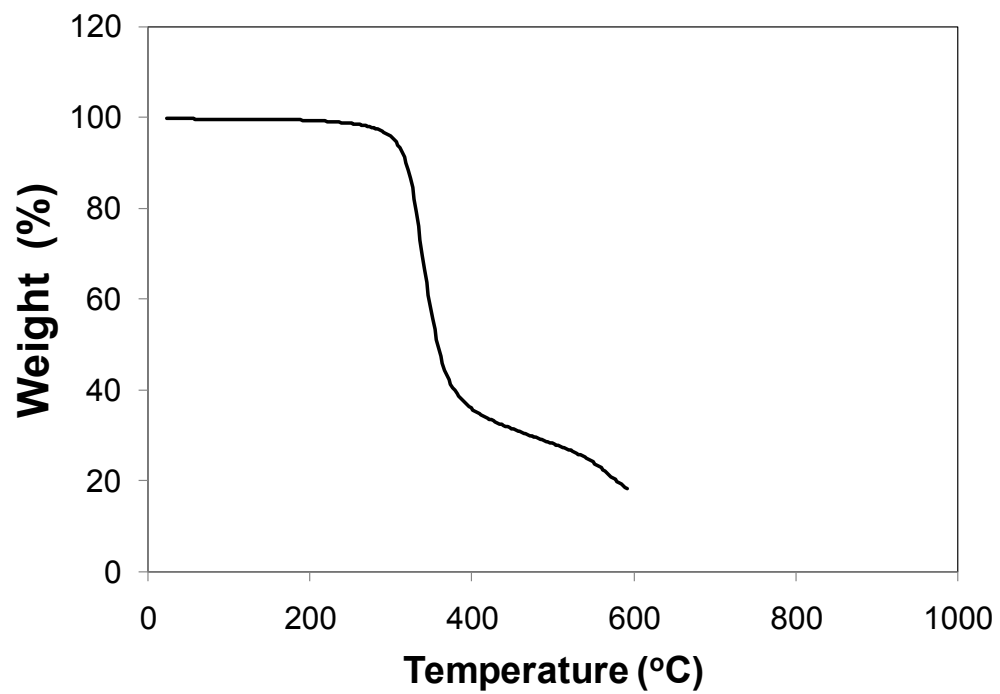


Figure F.3: P2c in air

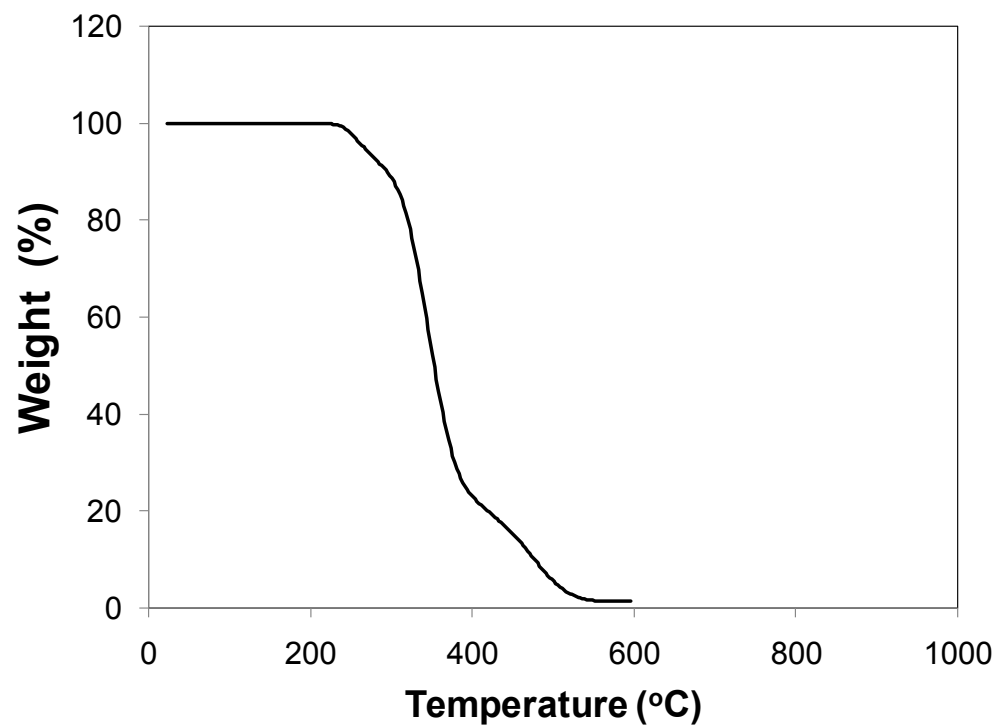


Figure F.4: emD in air

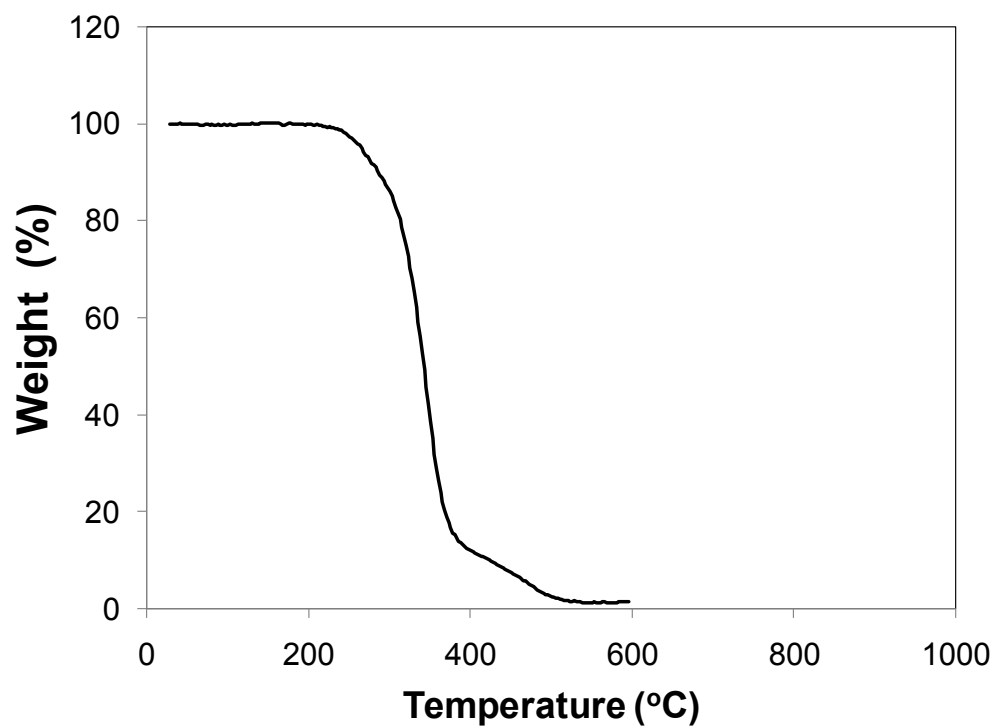


Figure F.5: scD in air

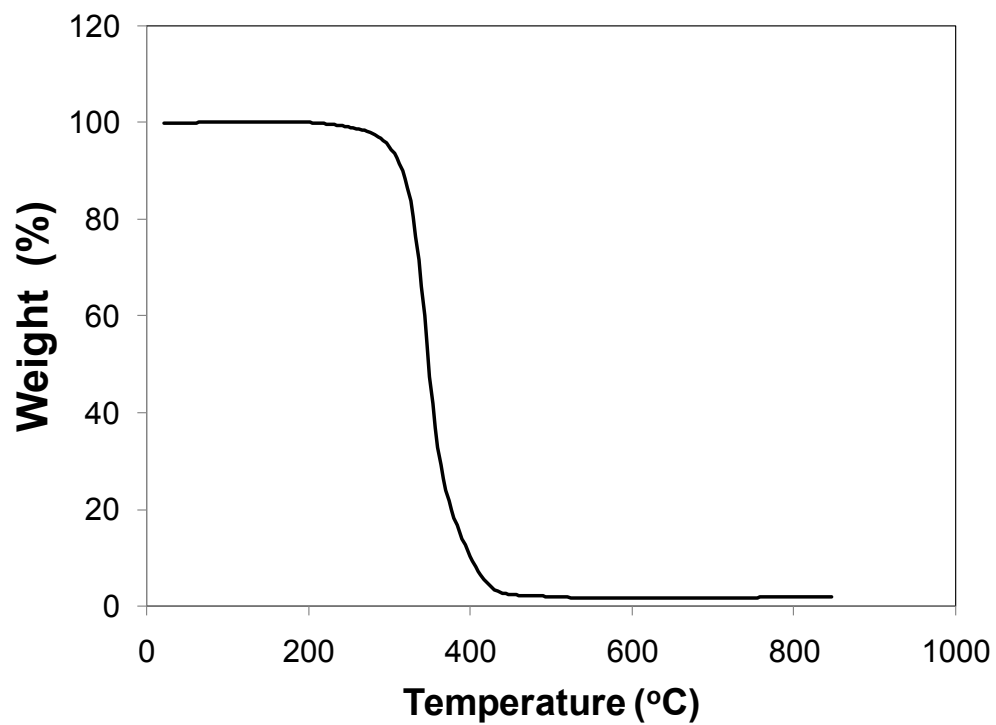
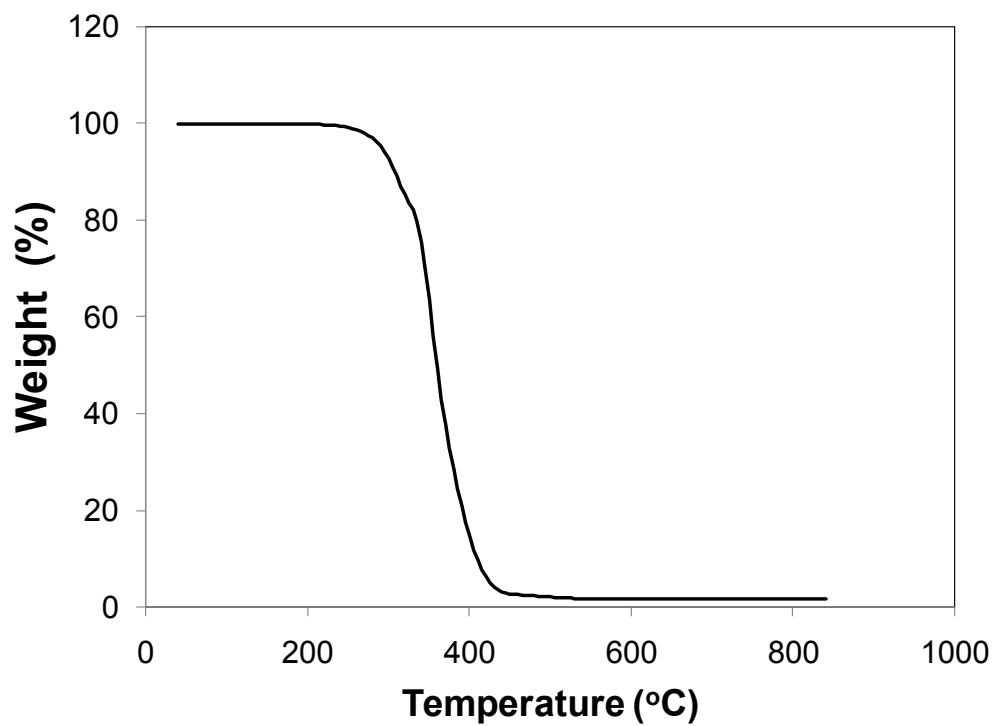
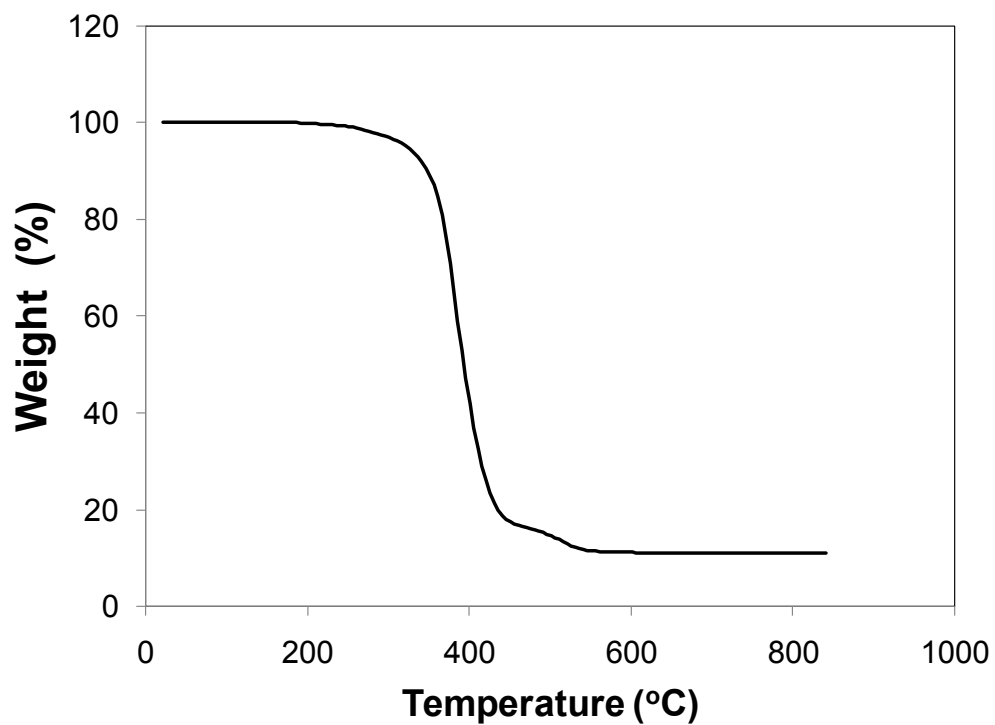
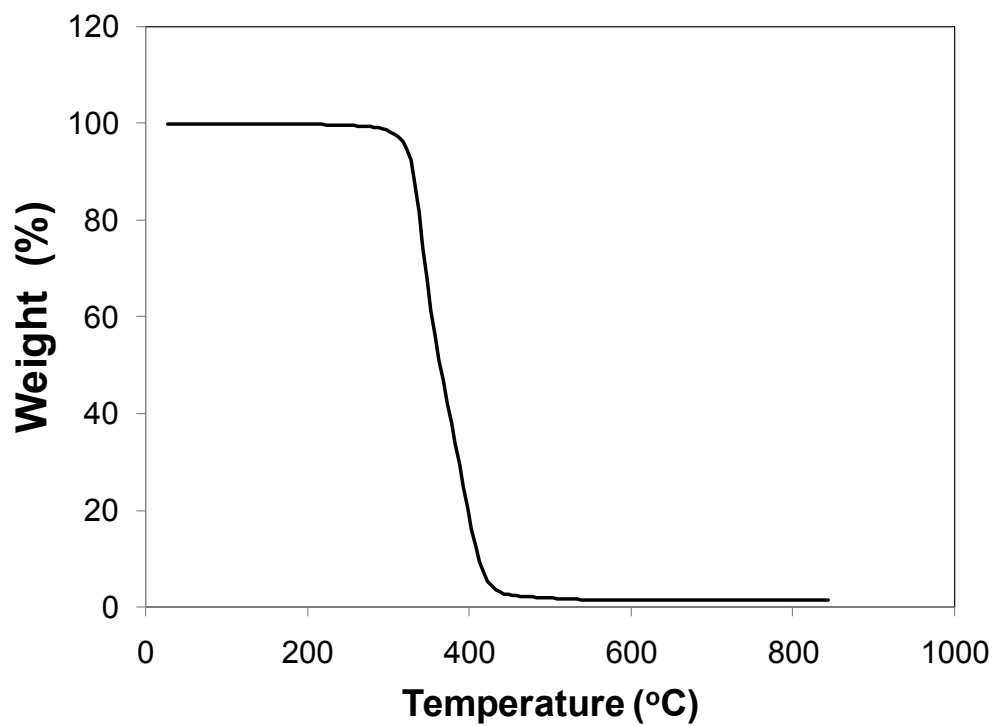
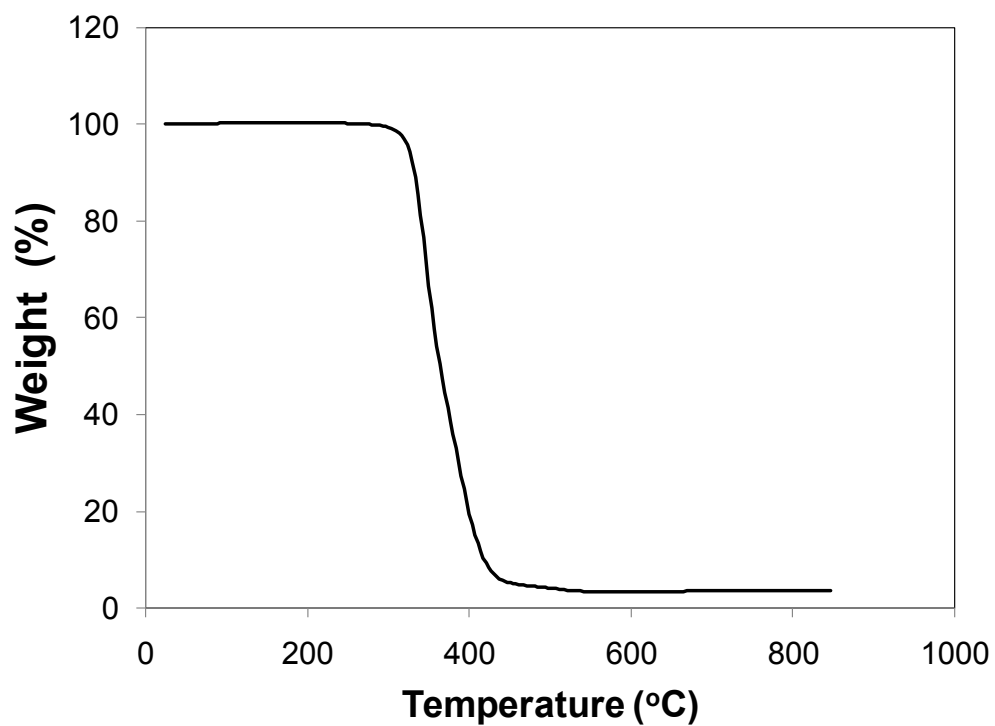
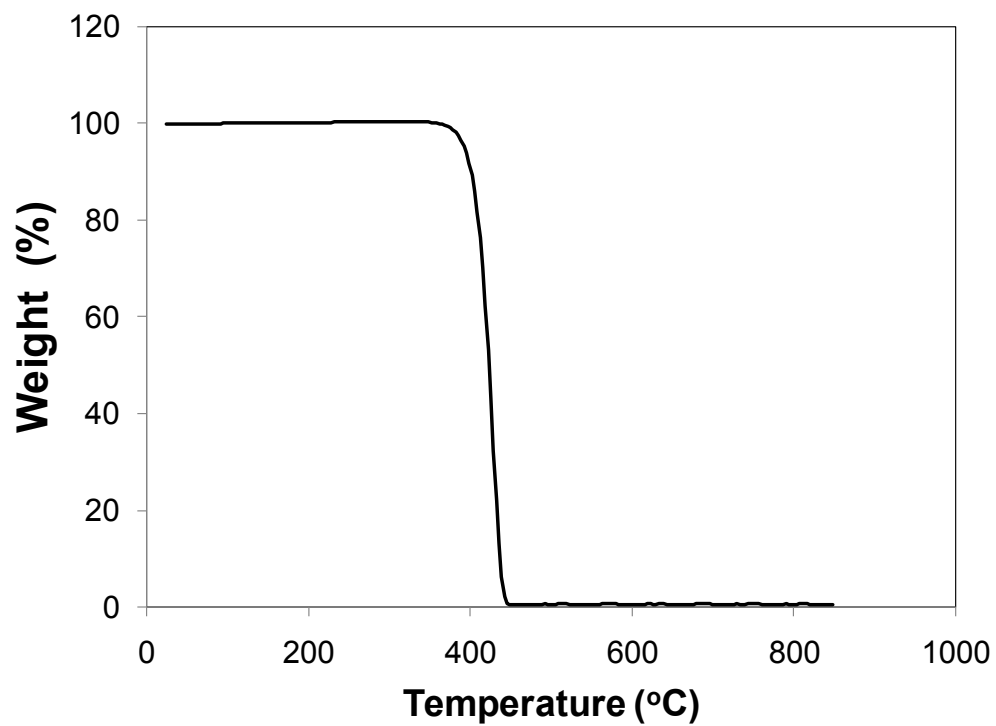
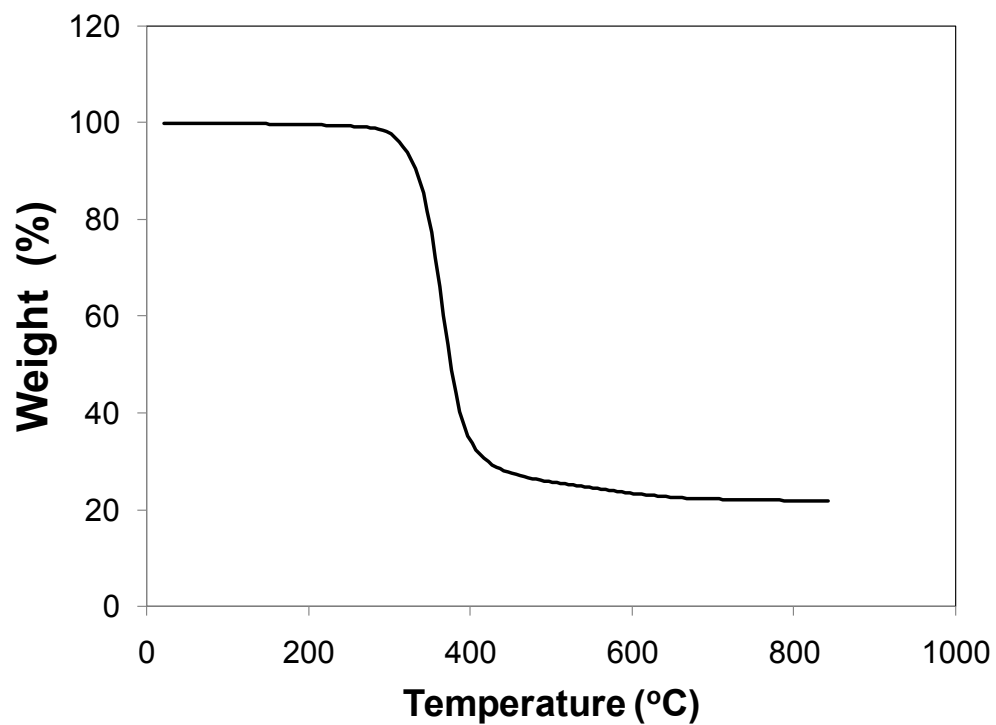
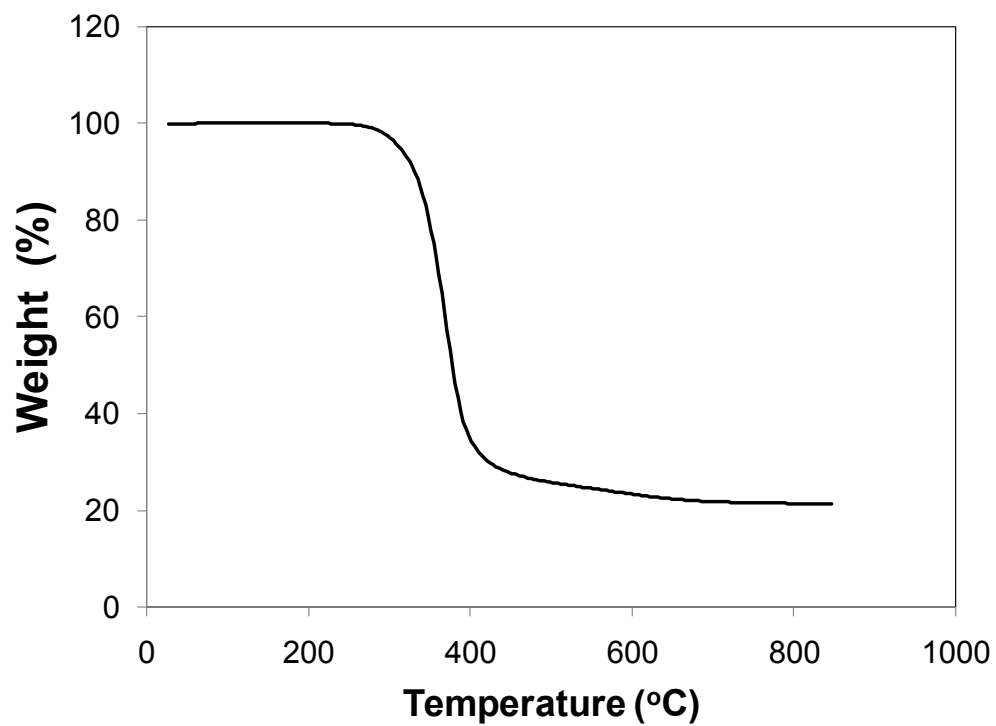
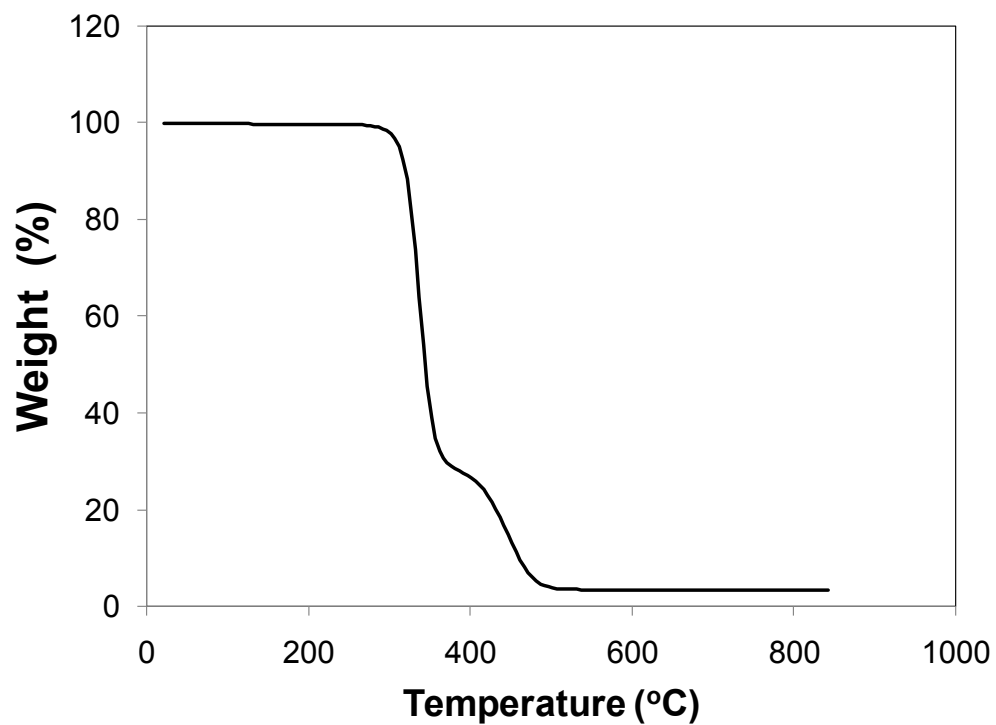


Figure F.6: S(100) in N₂

Figure F.7: CS(02-98) in N₂Figure F.8: CS(10-90) in N₂

Figure F.9: CS(20-80) in N₂Figure F.10: CS(33-67) in N₂

Figure F.11: C(100) in N₂Figure F.12: CVS(40-59-01) in N₂

Figure F.13: CVS(46-52-02) in N₂Figure F.14: V(100) in N₂

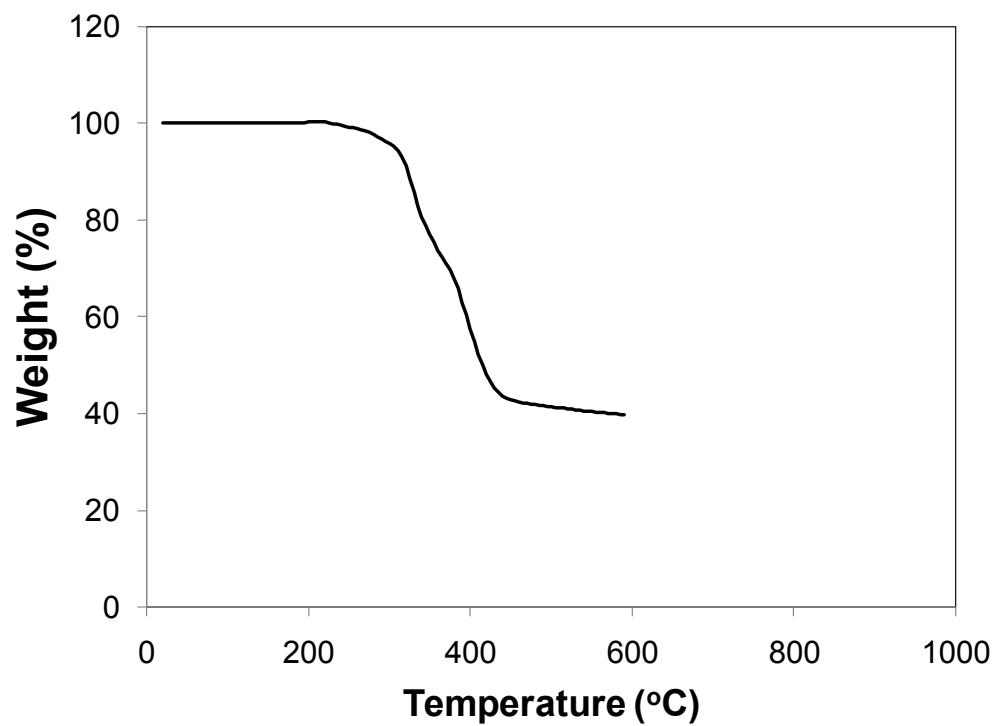


Figure F.15: S(100) in air

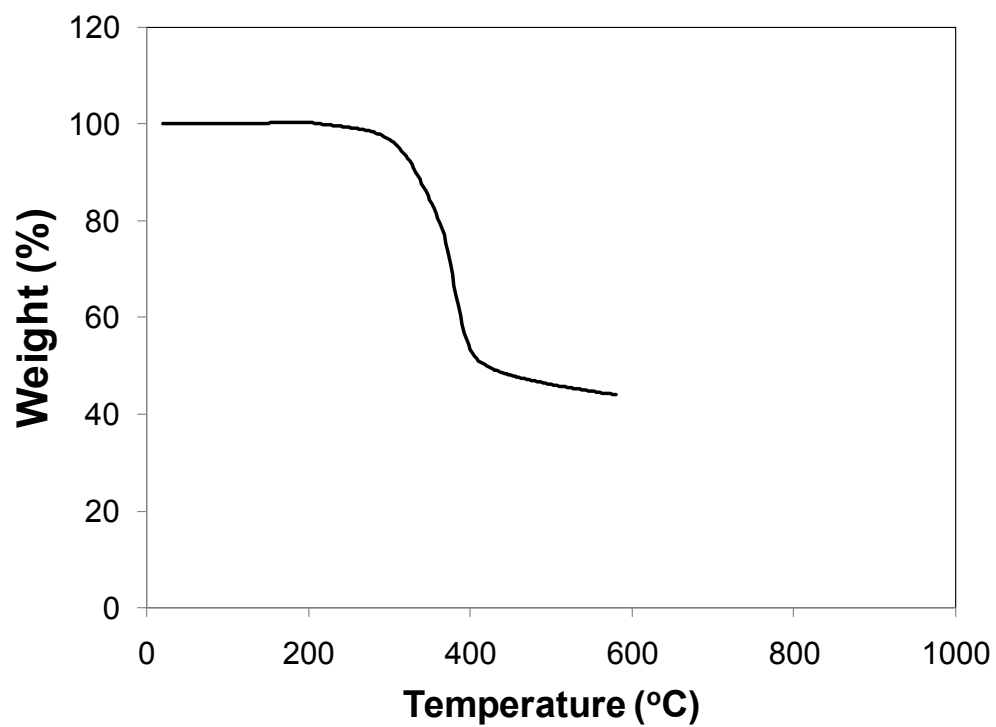


Figure F.16: CS(33-67) in air

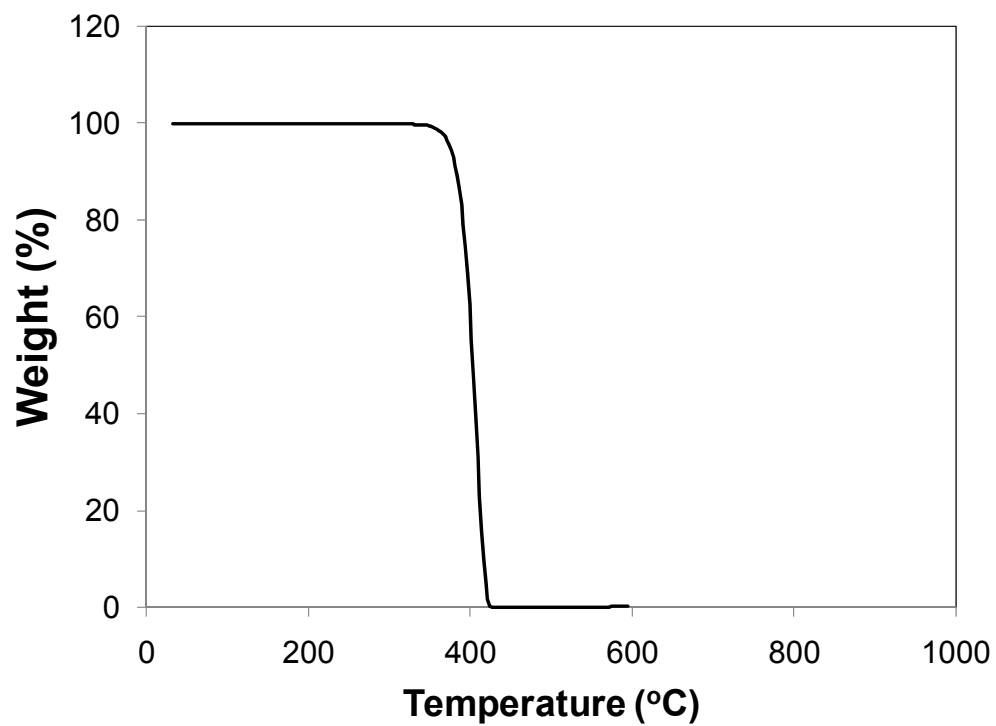


Figure F.17: C(100) in air

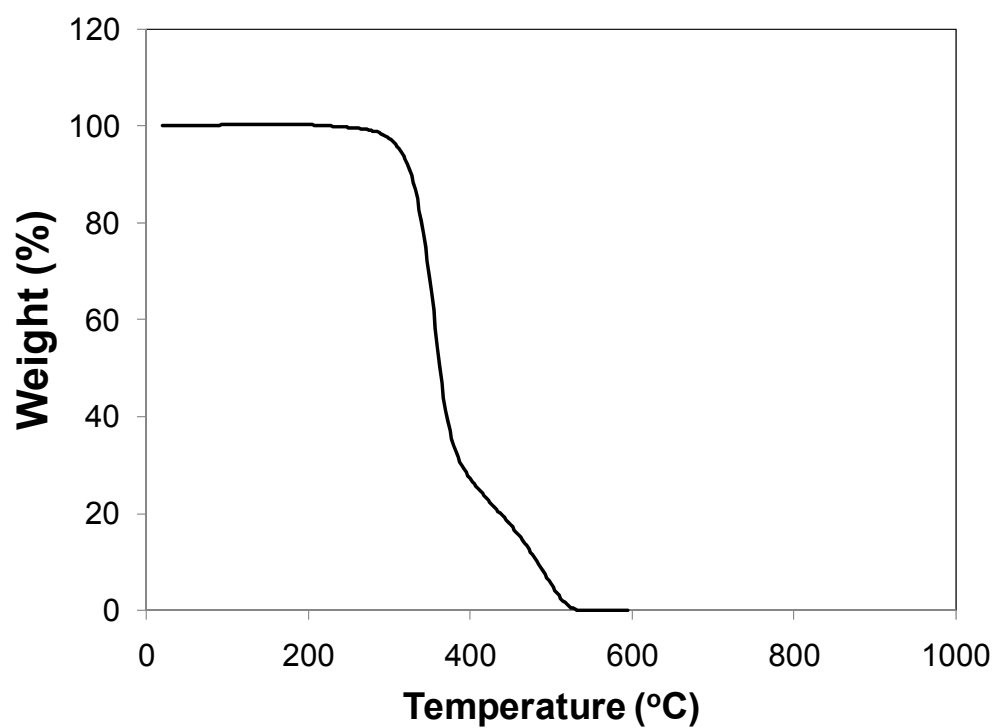


Figure F.18: CVS(46-52-02) in air

Appendix G: X-ray Photoelectron Spectroscopy (XPS) Spectra

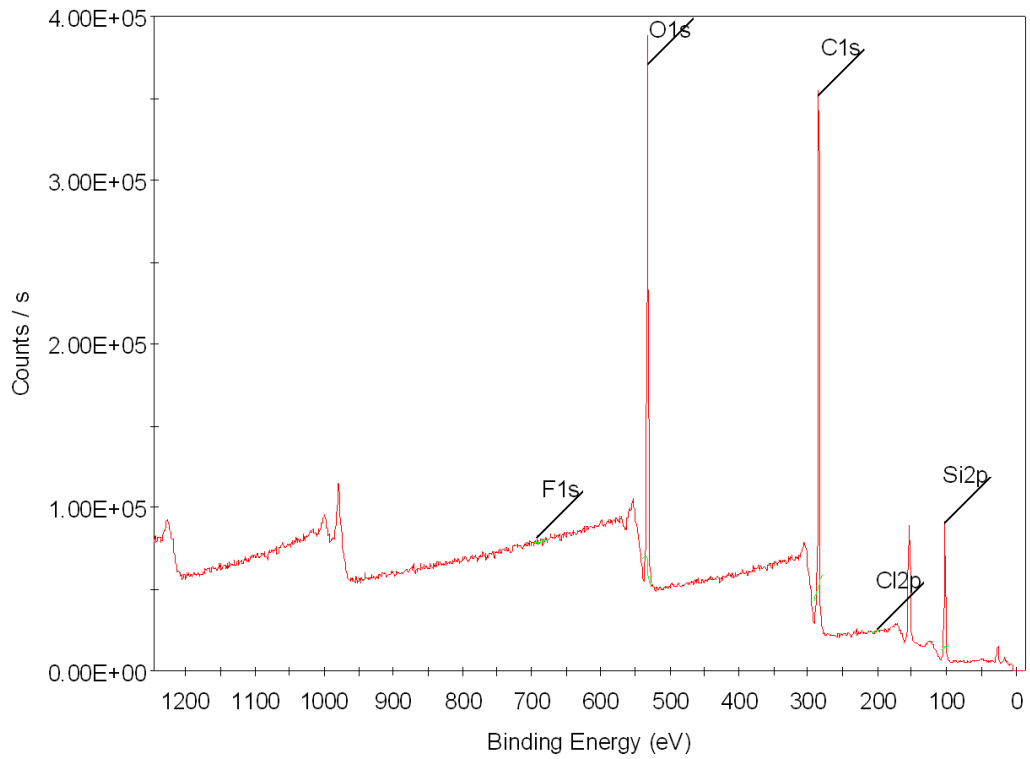


Figure G.1: CS(02-98) at 90° take-off angle

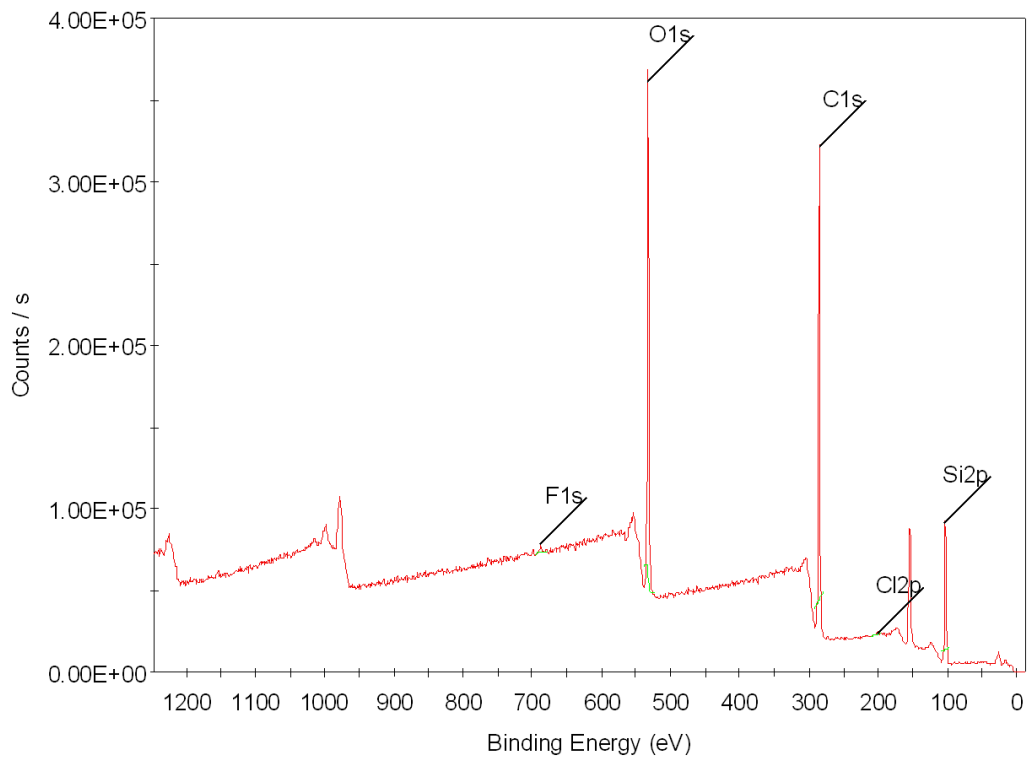


Figure G.2: CS(10-90) at 90° take-off angle

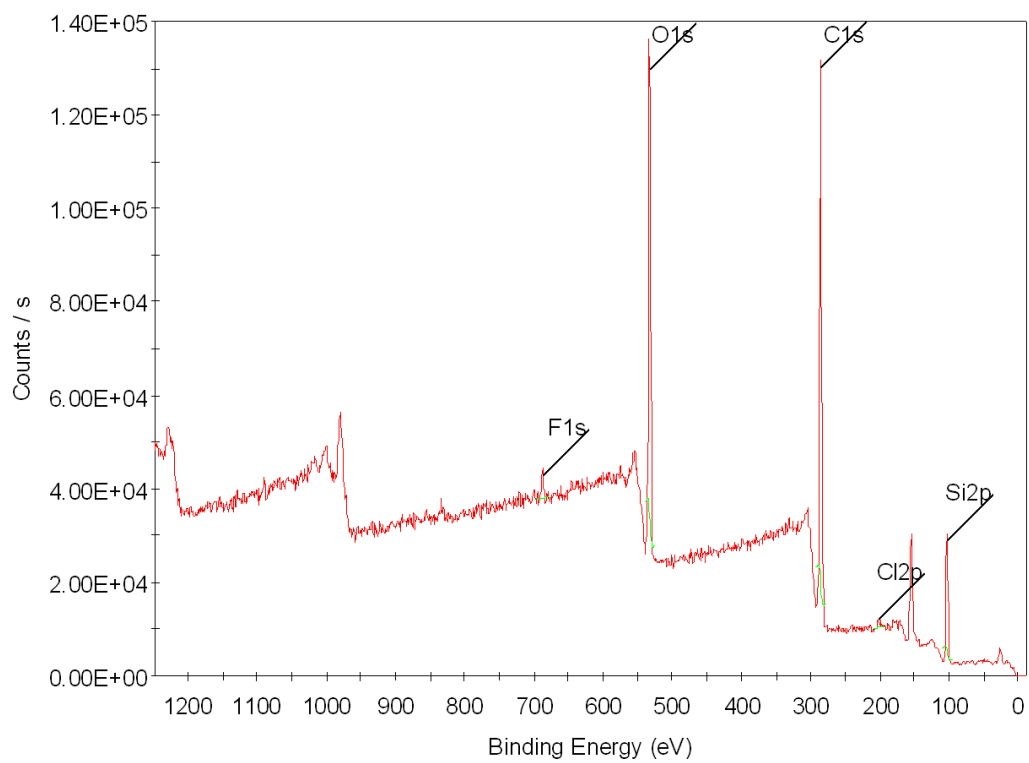


Figure G.3: CS(20-80) at 90° take-off angle

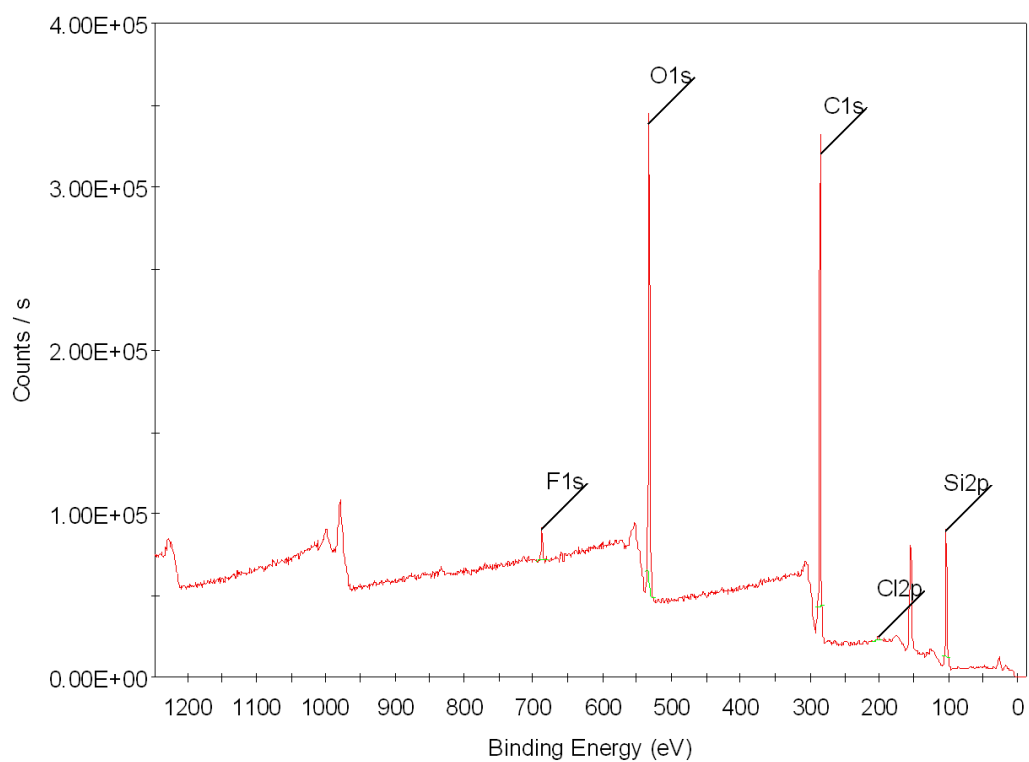


Figure G.4: CS(33-67) at 90° take-off angle

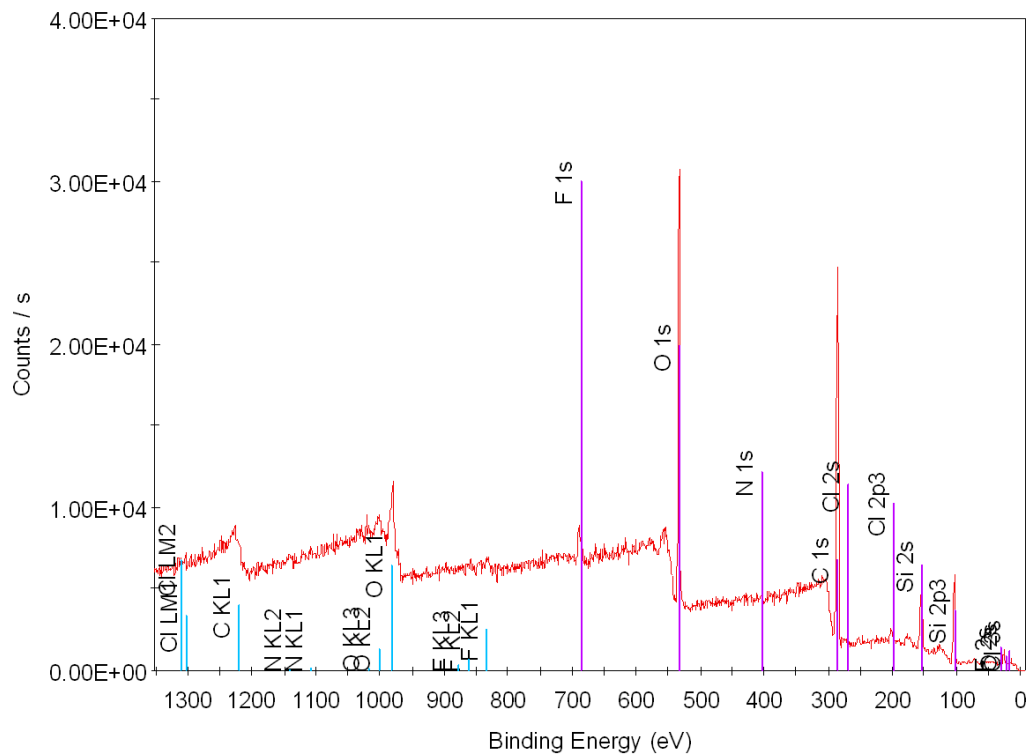


Figure G.5: CS(33-67) char prepared at 300 °C, 90° take-off angle

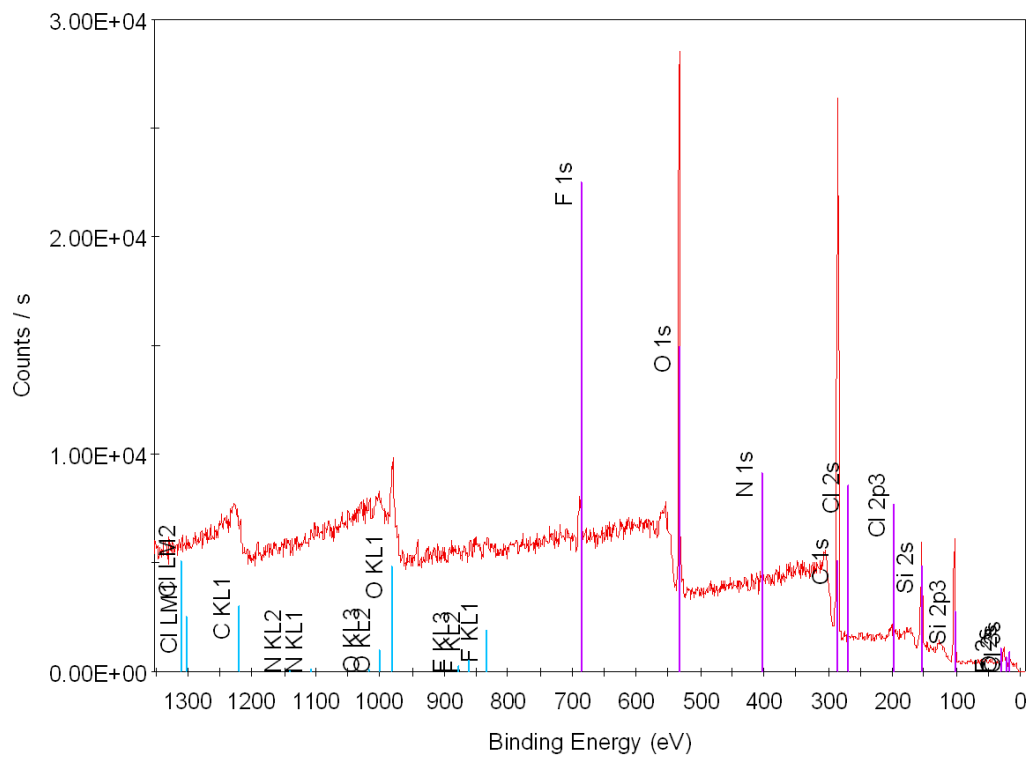


Figure G.6: CS(33-67) char prepared at 380 °C, 90° take-off angle

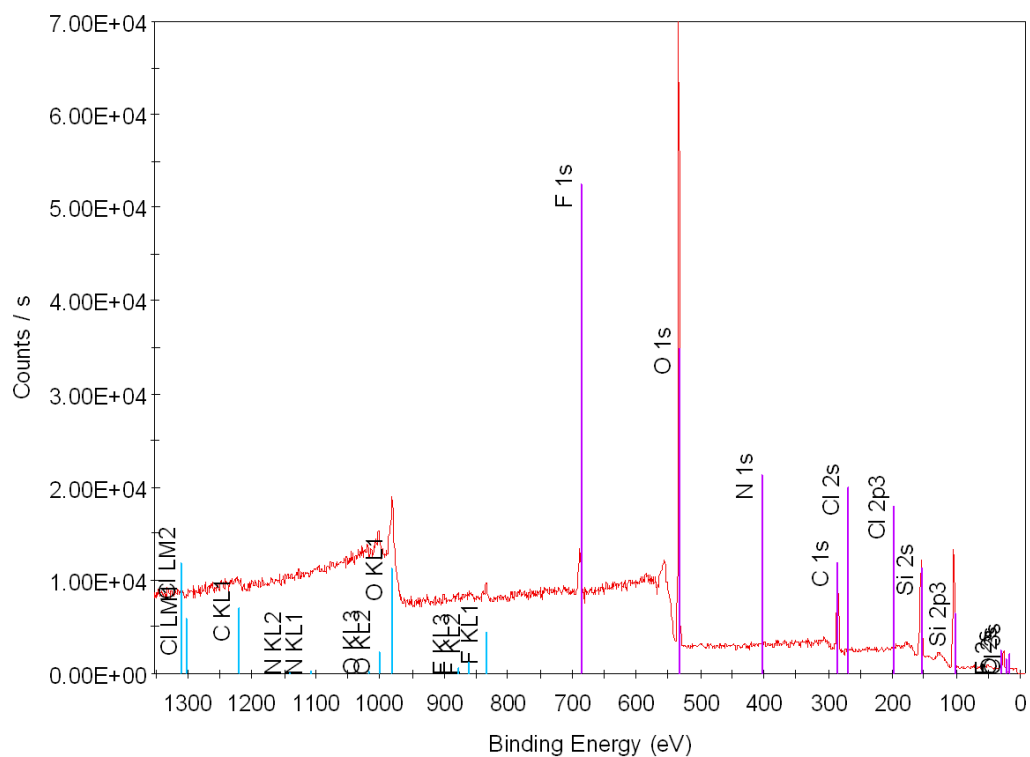


Figure G.7: CS(33-67) char prepared at 460 °C, 90° take-off angle

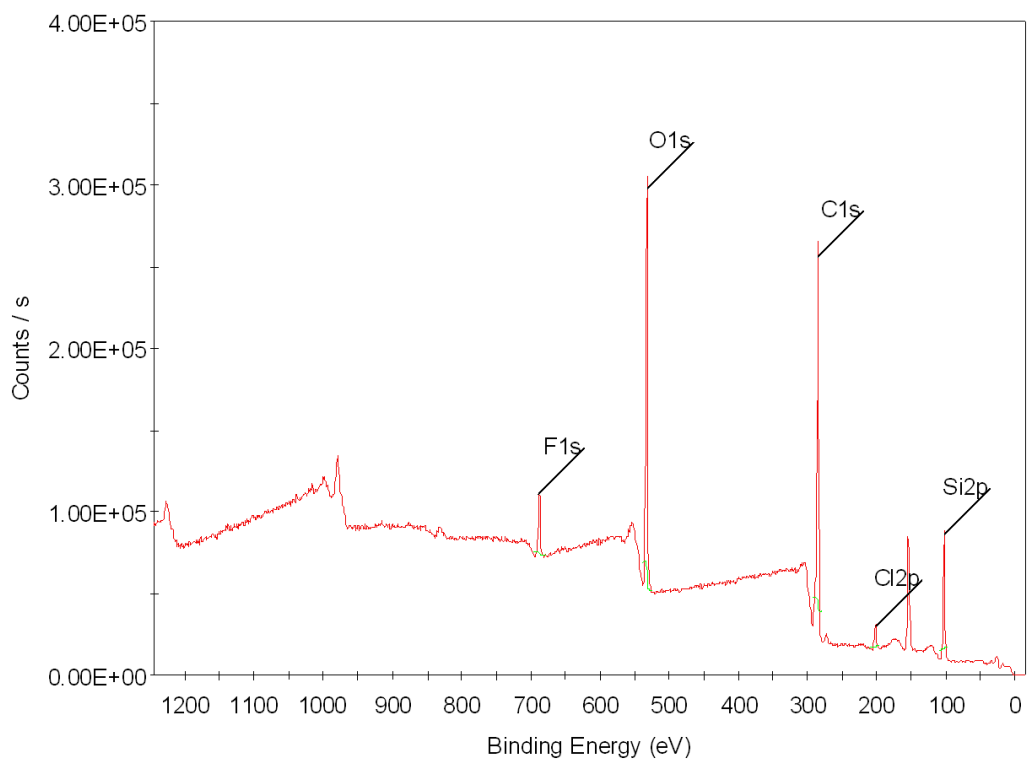


Figure G.8: CVS(40-59-01) at 90° take-off angle

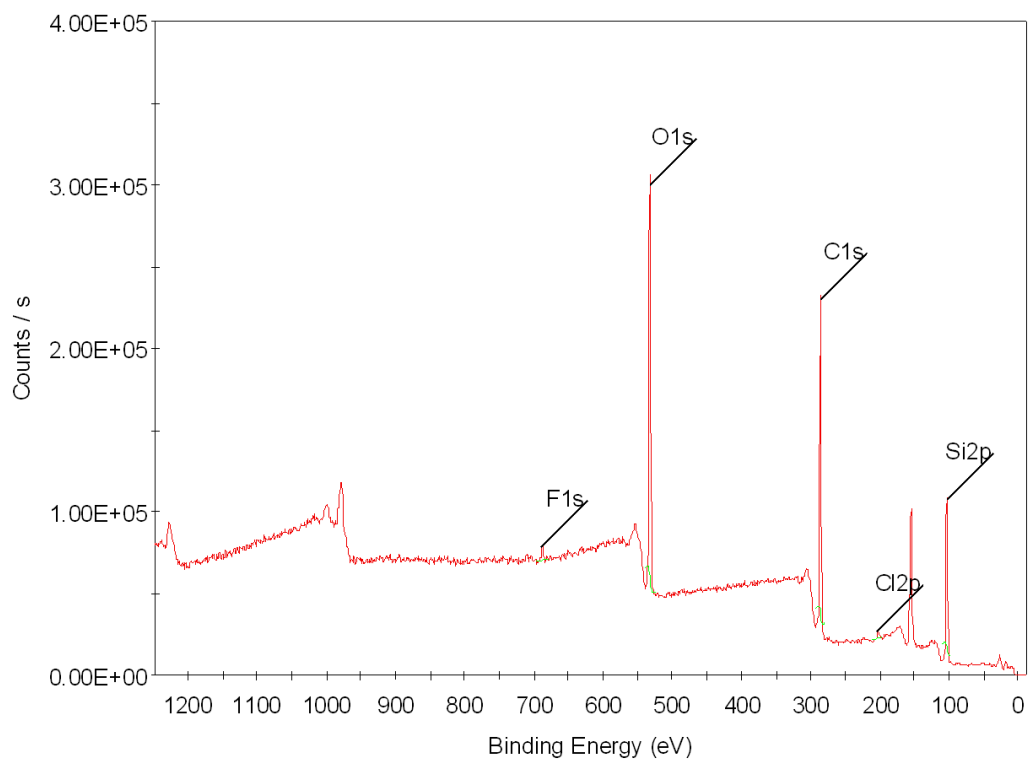


Figure G.9: CVS(46-52-02) at 90° take-off angle

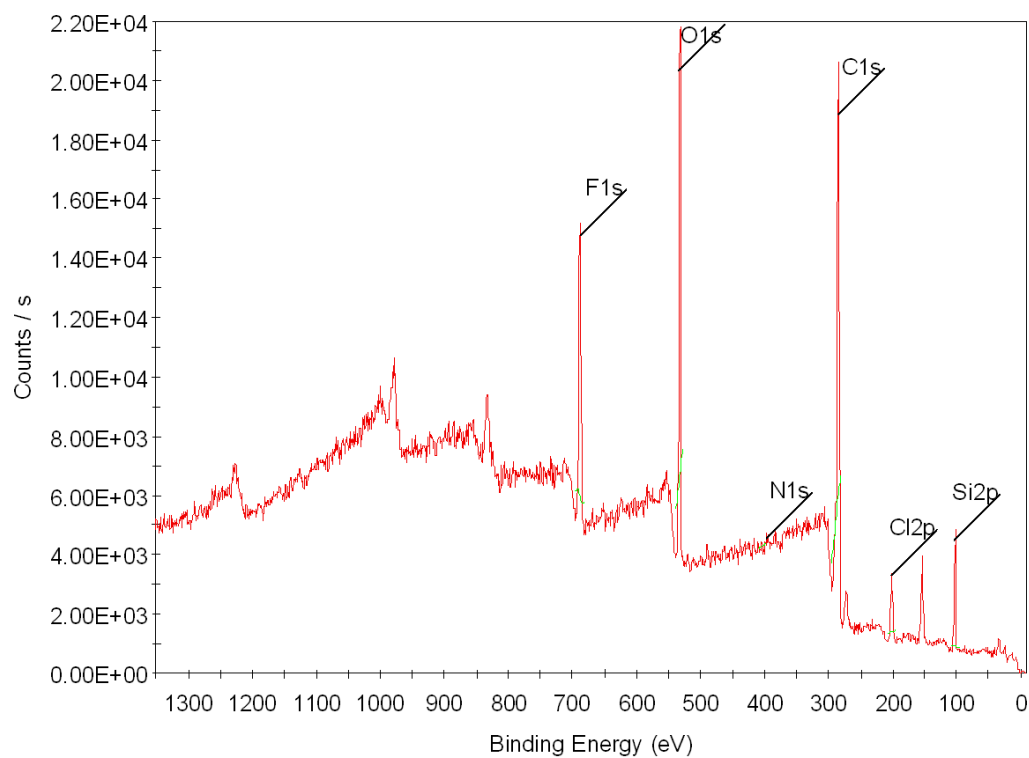


Figure G.10: CVS(46-52-02) char prepared at 300 °C, 90° take-off angle

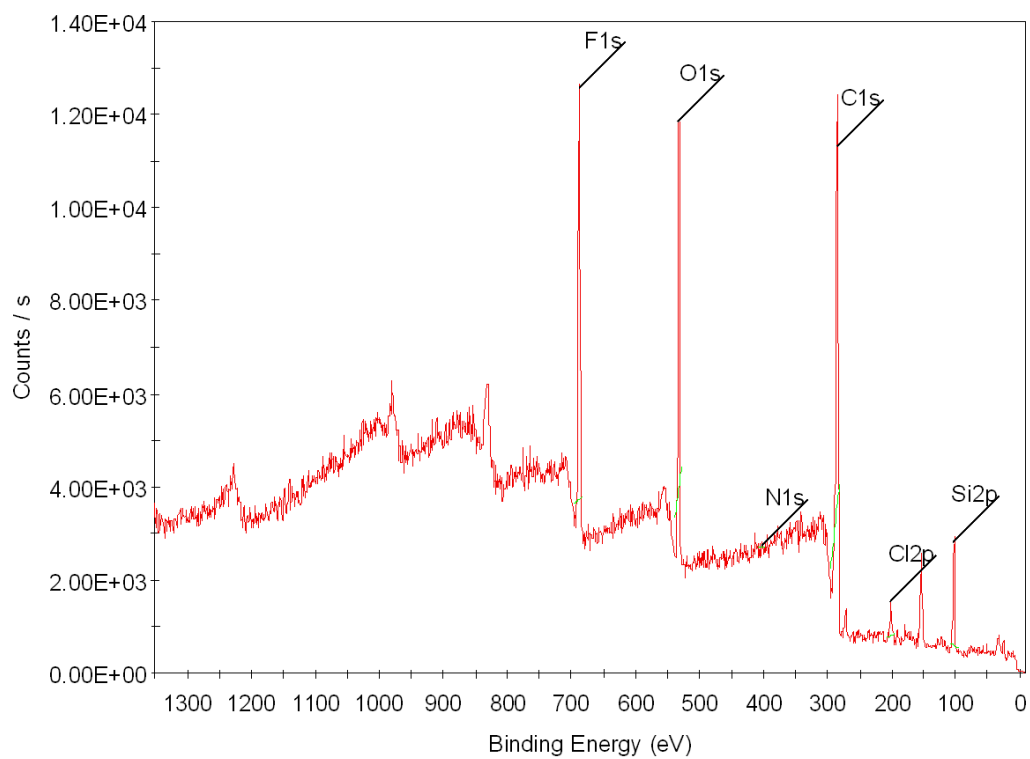


Figure G.11: CVS(46-52-02) char prepared at 375 °C, 90° take-off angle

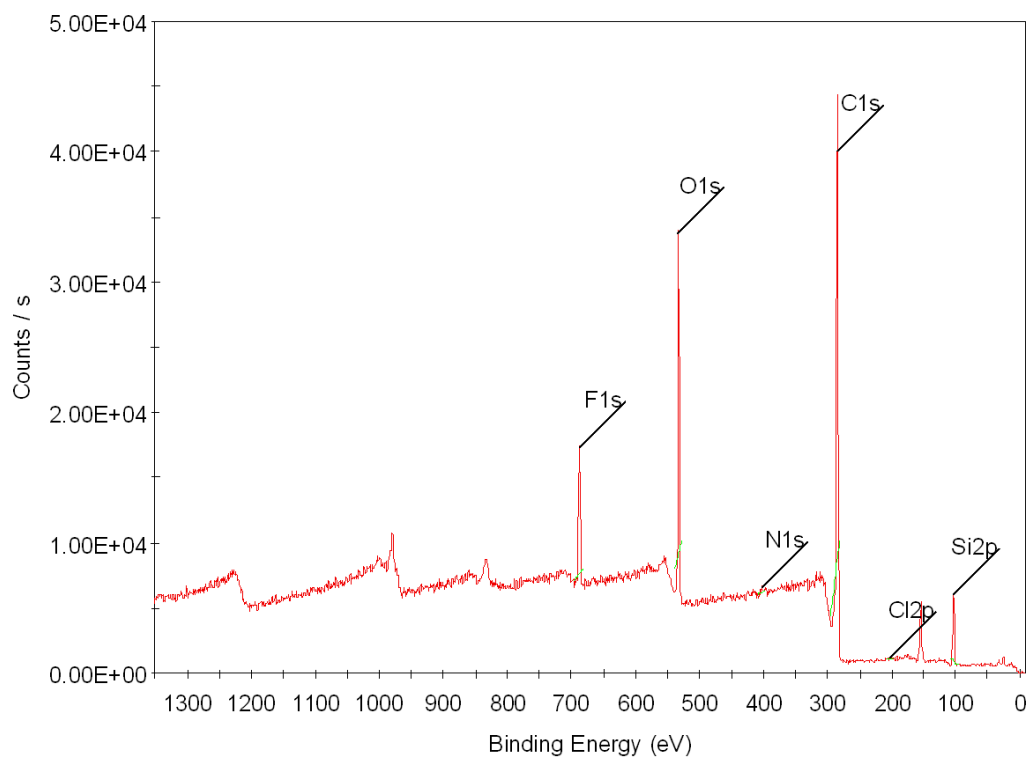


Figure G.12: CVS(46-52-02) char prepared at 400 °C, 90° take-off angle